

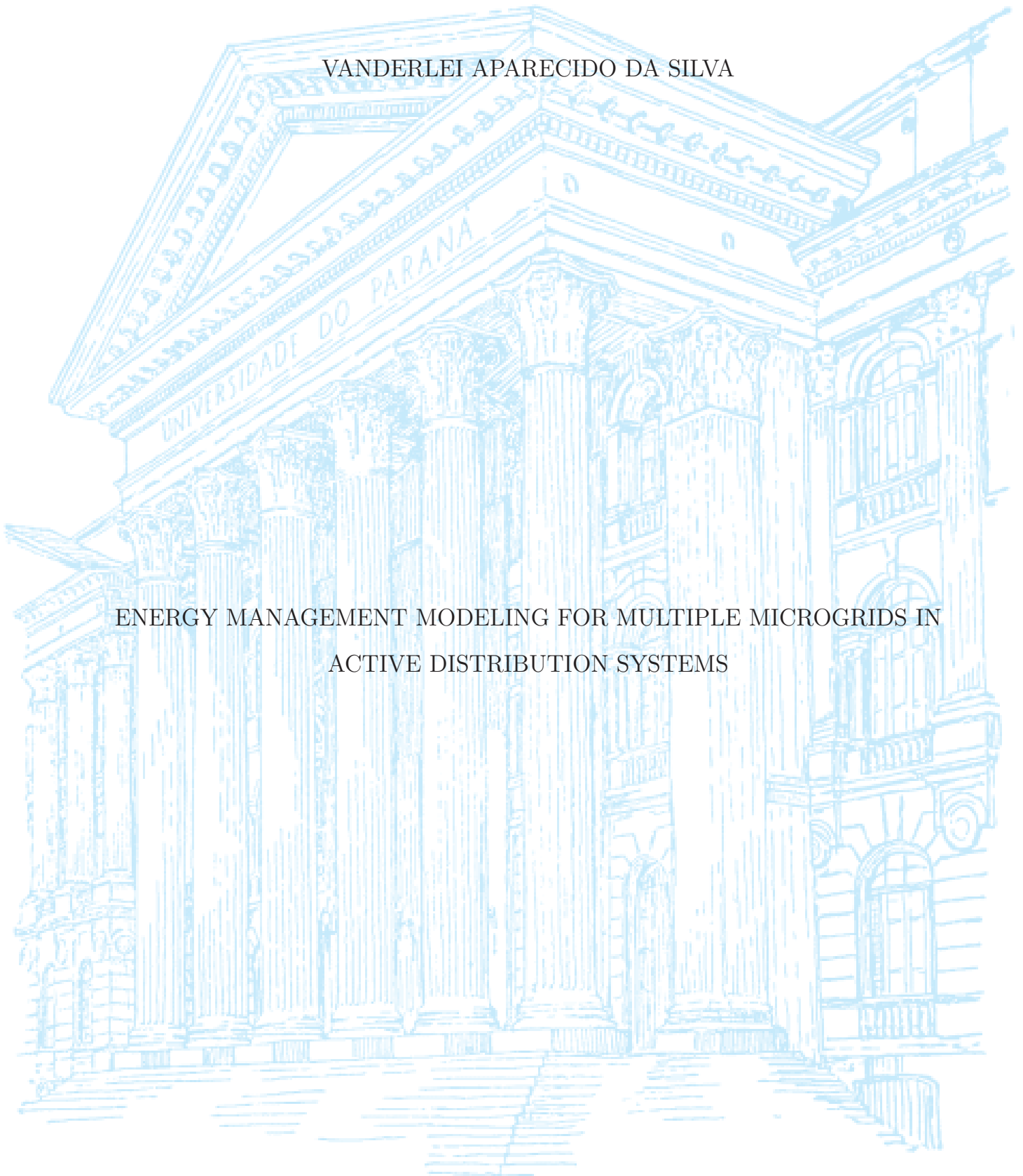
UNIVERSIDADE FEDERAL DO PARANÁ

VANDERLEI APARECIDO DA SILVA

ENERGY MANAGEMENT MODELING FOR MULTIPLE MICROGRIDS IN  
ACTIVE DISTRIBUTION SYSTEMS

CURITIBA

2022



VANDERLEI APARECIDO DA SILVA

ENERGY MANAGEMENT MODELING FOR MULTIPLE MICROGRIDS IN  
ACTIVE DISTRIBUTION SYSTEMS

Tese apresentada ao Programa de Pós-Graduação em Engenharia Elétrica, área de concentração Sistemas de Energia, do Setor de Tecnologia da Universidade Federal do Paraná, como requisito parcial para a obtenção do grau de Doutor em Engenharia Elétrica.

Orientador: Prof. Dr. Alexandre Rasi Aoki  
Coorientador: Ph.D. Germano Lambert-Torres

CURITIBA

2022

DADOS INTERNACIONAIS DE CATALOGAÇÃO NA PUBLICAÇÃO (CIP)  
UNIVERSIDADE FEDERAL DO PARANÁ  
SISTEMA DE BIBLIOTECAS – BIBLIOTECA DE CIÊNCIA E TECNOLOGIA

Silva, Vanderlei Aparecido da  
Energy management modeling for multiple microgrids in active distribution systems / Vanderlei Aparecido da Silva. – Curitiba, 2022.  
1 recurso on-line : PDF.

Tese (Doutorado) - Universidade Federal do Paraná, Setor de Tecnologia, Programa de Pós-Graduação em Engenharia Elétrica.

Orientador: Alexandre Rasi Aoki  
Coorientador: Germano Lambert-Torres

1. Redes elétricas. 2. Energia elétrica – Distribuição. 3. Sistemas de energia fotovoltaica. I. Universidade Federal do Paraná. II. Programa de Pós-Graduação em Engenharia Elétrica. III. Aoki, Alexandre Rasi. IV. Lambert-Torres, Germano. V. Título.

Bibliotecário: Elias Barbosa da Silva CRB-9/1894



MINISTÉRIO DA EDUCAÇÃO  
SETOR DE TECNOLOGIA  
UNIVERSIDADE FEDERAL DO PARANÁ  
PRÓ-REITORIA DE PESQUISA E PÓS-GRADUAÇÃO  
PROGRAMA DE PÓS-GRADUAÇÃO ENGENHARIA  
ELÉTRICA - 40001016043P4

## TERMO DE APROVAÇÃO

Os membros da Banca Examinadora designada pelo Colegiado do Programa de Pós-Graduação ENGENHARIA ELÉTRICA da Universidade Federal do Paraná foram convocados para realizar a arguição da tese de Doutorado de **VANDERLEI APARECIDO DA SILVA** intitulada: **Energy management modeling for multiple microgrids in active distribution systems**, sob orientação do Prof. Dr. ALEXANDRE RASI AOKI, que após terem inquirido o aluno e realizada a avaliação do trabalho, são de parecer pela sua APROVAÇÃO no rito de defesa.

A outorga do título de doutor está sujeita à homologação pelo colegiado, ao atendimento de todas as indicações e correções solicitadas pela banca e ao pleno atendimento das demandas regimentais do Programa de Pós-Graduação.

CURITIBA, 26 de Maio de 2022.

Assinatura Eletrônica  
27/05/2022 14:53:50.0  
ALEXANDRE RASI AOKI  
Presidente da Banca Examinadora

Assinatura Eletrônica  
29/05/2022 15:30:56.0  
THELMA SOLANGE PIAZZA FERNANDES  
Avaliador Interno (UNIVERSIDADE FEDERAL DO PARANÁ)

Assinatura Eletrônica  
03/06/2022 13:35:50.0  
LUIZ ANTONIO DE SOUZA RIBEIRO  
Avaliador Externo (UNIVERSIDADE FEDERAL DO MARANHÃO)

Assinatura Eletrônica  
08/06/2022 11:54:09.0  
LUIZ CARLOS PEREIRA DA SILVA  
Avaliador Externo (UNIVERSIDADE ESTADUAL DE CAMPINAS-  
DSEE/FEEC)

*I dedicate this work to my parents,  
who were my first educators and supporters,  
and to my wife and son, who unconditionally  
supported me on this 4-year journey.*

*Without their support,  
I would never have been successful in this endeavor.*

## ACKNOWLEDGEMENTS

I thank the Creator of everything for awakening in my life the vocation for science, illuminating my thoughts, and guiding my decisions to carry out this work, a result of a lot of dedication.

I would like to thank my family members for their support, especially my mother and father, for their efforts to educate their children. It worked.

To my wife and son, my sincere gratitude for their companionship, patience, attention, and support given during this special period of my life. I hope to be able to return so much affection and dedication.

A special thanks to Prof. Dr. Alexandre Rasi Aoki, who generously invested his time in this project, competently guided my activities, wisely led the technical discussions, and patiently understood the difficulties I had along this way.

I thank the Federal University of Paraná, as an institution and the professors and collaborators, for supporting me as a student and researcher.

I also thank the Federal University of Paraná Foundation for the Development of Science, Technology, and Culture – FUNPAR, Companhia Paranaense de Energia - Copel, and Gnarus Institute for the financial support during the work.

Finally, I would like to thank all the people who have passed through my life and somehow contributed to making this work possible.

*“It’s not about getting there first, it’s about getting there well.”*  
*(Unknown)*

*“Whoever acknowledges me before others, I will also acknowledge before my Father  
in heaven.”*  
*(Jesus Christ, by Matthew, 10:32)*

## RESUMO

Este estudo aborda a modelagem de gerenciamento de energia em sistemas ativos de distribuição com múltiplas microrredes. Duas contribuições principais podem ser destacadas neste trabalho: o desenvolvimento de uma metodologia para regulação de tensão em alimentador utilizando ajuste de carga em multimicrorredes e o desenvolvimento de uma metodologia para modelar detalhadamente a otimização da operação do dia seguinte de microrredes. A pesquisa foi conduzida de forma a modelar primeiramente uma única microrrede com objetivo de otimizar a operação de seus recursos distribuídos de energia, para na sequência modelar um alimentador de distribuição contendo diversas destas microrredes. Embora existam diversos trabalhos publicados em literatura sobre o tema otimização de operação de microrredes, havia algumas lacunas de pesquisa ainda não preenchidas, como a modelagem de ilhamento programado, deslocamento de cargas de ciclo contínuo, corte de geração fotovoltaica, e modelagem detalhada do sistema de armazenamento de energia (SAE), as quais estão abordadas neste trabalho. A pesquisa foi realizada com a modelagem de uma microrrede contendo um sistema fotovoltaico, um SAE por baterias e cargas controláveis, contando ainda com a possibilidade de comprar e vender energia para o operador do sistema de distribuição e para outras microrredes. A partir do modelo matemático, a programação linear inteira mista foi utilizada para a resolução do problema de otimização com objetivo de minimizar os custos de operação da microrrede. Um conjunto de simulações foi realizado utilizando a Tarifa Branca brasileira para compor o modelo de mercado. Além de validar modelo matemático proposto, os resultados mostraram a relevância do SAE na redução de custos de operação da microrrede e deram origem a uma publicação em revista científica. Adicionalmente, foi realizado um estudo para analisar o impacto das microrredes no desempenho da operação da rede de distribuição. Esse estudo resultou no desenvolvimento de uma metodologia para regulação trifásica de tensão em alimentadores por meio de ajuste de cargas em multimicrorredes. Neste ajuste, a carga da multimicrorrede vista pelo sistema de distribuição pode ser positiva ou negativa, o que corresponde ao modo carga de operação da multimicrorrede ou ao modo fonte, respectivamente. Tomando como base o modelo IEEE de 13 barras, a metodologia foi avaliada em um alimentador trifásico de distribuição altamente carregado e desequilibrado contendo quatro microrredes agrupadas como multimicrorredes. A plataforma de simulação proposta neste trabalho utiliza um algoritmo de regulação de tensão que toma decisões baseadas nos resultados do fluxo de potência trifásico do alimentador. Os resultados de simulação validaram a metodologia proposta, mostraram a interação que pode haver entre o operador do sistema de distribuição e o operador da multimicrorrede, evidenciando assim sua viabilidade em implementações práticas. Os resultados também evidenciaram de forma quantitativa o impacto das microrredes no perfil de tensão do alimentador e como elas podem contribuir para melhorar este perfil na prática. Finalmente, os resultados destacam alguns indicadores de performance de operação do alimentador sob teste, os quais carregam informações que futuramente podem ser endereçadas na regulamentação sobre a prestação de serviços ancilares de regulação de tensão por multimicrorredes.

**Palavras-chave:** multimicrorredes; modelagem de microrrede; regulação de tensão em alimentador; prestação de serviço ancilar; programação linear inteira mista.



## ABSTRACT

This study addresses the modeling of energy management in active distribution systems with multiple microgrids. Two main contributions can be emphasized in this work: a methodology for voltage regulation in a feeder using load adjustment in multi-microgrids (MMG) and a methodology to model, in detail, the problem of optimal day-ahead scheduling of microgrids. The research was conducted to first model a single microgrid to optimize the operation of its distributed energy resources (DER), and then model a distribution feeder containing a number of these microgrids. Although there are several works published in the literature on the topic of optimal scheduling of microgrids, some research gaps in the science have not yet been filled, such as the modeling of scheduled intentional islanding, continuous cycle shiftable loads, photovoltaic (PV) generation curtailment, and the modeling of a battery energy storage system (BESS) in detail, which are addressed in this work. This research was carried out with the modeling of a microgrid with a PV system, BESS, and controllable loads as DERs, with the possibility of buying and selling energy to the distribution system operator (DSO) and other microgrids. From the mathematical model, mixed-integer linear programming (MILP) was used to solve the optimization problem to minimize microgrid operating costs. Simulations were performed using the Brazilian White Tariff to compose the market model. In addition to validating the proposed mathematical model, the results show the relevance of BESS in reducing microgrid operating costs and gave rise to a publication in a scientific journal. Additionally, a study was carried out to analyze the impact of microgrids on the performance of the distribution network operation, which resulted in the development of a methodology for three-phase voltage regulation in feeders through load adjustment in MMG. In this methodology, the multi-microgrid load seen by the distribution system can be positive or negative, which corresponds to the MMG load mode or supply mode of operation, respectively. Based on the IEEE 13-bus model, this methodology was performed in a highly loaded and unbalanced three-phase distribution feeder containing four microgrids grouped as MMG. The simulation platform presented in this work uses a voltage regulation algorithm that makes decisions based on the results of a three-phase power flow of the feeder. The simulation results validate the proposed methodology and show the interaction between the DSO and the MMG operator, thus evidencing its feasibility in practical implementations. Results also show quantitatively the impact of microgrids on the voltage profile of the feeder and how they can contribute to improving this profile in practice. Finally, the results highlight some operating performance indicators of the feeder under test, which carry information that in the future may be addressed in a regulatory framework on the ancillary service provision of voltage regulation by MMGs.

**Keywords:** multi-microgrids; microgrid modeling; feeder voltage regulation; ancillary service provision; mixed-integer linear programming.

## LIST OF ILLUSTRATIONS

Figure 2.1 – Distribution voltage level for connecting distributed generation in Brazil.	44
Figure 2.2 – Energy storage technologies.	48
Figure 2.3 – Capacity degradation for a 68Ah lithium-ion battery cell (6,000 cycle life).	49
Figure 2.4 – The round trip concept for batteries.	50
Figure 2.5 – Diagram of connecting a BESS to an electrical system bus.	51
Figure 2.6 – Schematic diagram of a microgrid supervisory control.	52
Figure 2.7 – A simplified distribution network diagram for microgrid protection analysis purposes from the point of view of selectivity.	59
Figure 2.8 – Microgrid schematic diagrams.	65
Figure 2.9 – Multi-Microgrids layouts.	66
Figure 3.1 – Schematic diagram of the MG day-ahead EMS model addressed in the present work, showing its relationship with the input and output data and its interaction with the real-time EMS; CD, ED, FD, LD, PD, and TD stand for cost, estimated, forecasted, limit, price, and technical data, respectively.	87
Figure 3.2 – Schematic diagram of the MG model used in the MILP problem; $st^{(t)}$ -type decision variables are virtual disconnectors and $P^{(t)}$ -type are real powers. Also, $\hat{P}$ -type variables represent forecasted values.	89
Figure 3.3 – Clarifying the nomenclature of BESS used throughout the present study. The definitions of SOC and DOD are following the IEEE Std 2030.2.1™ (IEEE, 2019).	96
Figure 3.4 – Exponential approximation curves for state of health, where $SOH_{tsh} = 0.8$ and $L_{cyc} = 6000$ .	103
Figure 3.5 – Visual abstract on the work of Zhao et al. (2018).	108
Figure 3.6 – A case study of operation cost in a distribution network with three MGs for increasing levels of uncertainty in RES (WT and PV): approaches with and without MMG.	109
Figure 3.7 – Visual abstract on the work of Zhang et al. (2018).	110
Figure 4.1 – Three-phase schematic diagram of an MGs with BESS, PVS, and delta-connected load.	113
Figure 4.2 – Voltage regulation methodology flowchart illustrating the interaction between the DSO and the MMG operator.	116
Figure 4.3 – Schematic diagram of a feeder based on the IEEE 13-bus with four MGs in an MMG environment.	118

Figure 4.4 – Flowchart for day-ahead applications of the load adjustment procedure to voltage regulation on a feeder with MMG. . . . .	128
Figure 4.5 – Flowchart for real-time applications of the load adjustment procedure to voltage regulation on a feeder with MMG. . . . .	132
Figure 5.1 – Regions of MG operation represented by the normalized energy bill. . .	137
Figure 5.2 – Block diagram of the simulation platform including the inter-process communication between Matlab and OpenDSS. . . . .	139
Figure 5.3 – Schematic diagram of the IEEE 13-bus test feeder. . . . .	140
Figure 5.5 – IEEE 13 Node Test Feeder adapted to include the MMG. . . . .	142
Figure 5.6 – An example of a Matlab output report frame with identification of fields.	144
Figure 6.1 – Results of simulation 1. . . . .	147
Figure 6.2 – Results of simulation 2. . . . .	148
Figure 6.3 – Results of simulation 3. . . . .	150
Figure 6.4 – Normalized energy bill for a sequence of simulations with increasing values of microgrid self-sufficiency; curves for BESS rated capacity ( $E_r$ ) from 12% to 30% of the average daily PV system capacity ( $E_{pv}$ ); $\bar{P}_{pcc} = 800$ kW; $E_{load} = 2400$ kWh; $E_{pv} := 2400 MG_{ss}$ kWh. . . . .	151
Figure 6.5 – Three-phase voltage profile evolution along the feeder in simulation 1. .	155
Figure 6.6 – Output report frames for the five iterations in simulation 1. . . . .	156
Figure 6.7 – Final result report frames for the simulation 1. . . . .	157
Figure 6.8 – Three-phase voltage profile evolution along the feeder in simulation 2. .	159
Figure 6.9 – Final result report frames for the simulation 2. . . . .	160
Figure 6.10–Three-phase voltage profile evolution along the feeder in simulation 3. .	162
Figure 6.11–Output report frames for the three iterations in simulation 3. . . . .	163
Figure 6.12–Final result report frames for simulation 3. . . . .	164
Figure 6.13–Three-phase voltage profile evolution along the feeder in simulation 4. .	165
Figure 6.14–Output report frames for the two iterations in simulation 4. . . . .	166
Figure 6.15–Final result report frames for simulation 4. . . . .	166
Figure A.1 – Graphical output from a simulation with the <code>intlingprog</code> function. . .	193
Figure B.1 – Defining the searches parameters: research axes and its keywords . . .	194
Figure B.2 – Flowchart representing the Ensslin’s raw set of papers filtering; (a) Selecting papers and authors by representativeness; (b) Selecting both recent papers and those whose authors have representativeness . . . . .	198
Figure B.3 – Axes of research and its keywords . . . . .	199
Figure A.1 – Datasheet of a BESS for commercial and industrial applications. . . . .	202
Figure A.2 – Datasheet of a power converter for grid applications with battery energy storage. . . . .	203
Figure A.3 – Datasheet of ESS solution for solar farm and microgrid application. . .	204

Figure B.4–PVS800-57 central inverter for 100, 250, and 500 kW solar PV power plants; technical datasheet part 1. . . . .	205
Figure B.5–PVS800-57 central inverter for 100, 250, and 500 kW solar PV power plants; technical datasheet part 2. . . . .	206
Figure B.6–PVS800-57B central inverter for 1,645, and 1,732 kW solar PV power plants; technical datasheet part 1. . . . .	207
Figure B.7–PVS800-57B central inverter for 1,645, and 1,732 kW solar PV power plants; technical datasheet part 2. . . . .	208

## LIST OF FRAMEWORKS

Framework 2.1 – An explanation matrix for selectivity analysis purposes based on the microgrid operational condition combined with the fault locations from Figure 2.7. . . . .	61
---	----

## LIST OF TABLES

Table 3.1 – State variables for the model, in which the value 1 means state enabled and 0 disabled. . . . .	88
Table 3.2 – Power variables for the model. . . . .	90
Table 3.3 – Input variables for the model. . . . .	90
Table 3.4 – State parameters. . . . .	92
Table 3.5 – Power parameters of the MILP problem. . . . .	93
Table 3.6 – Values of energy storage system efficiency for three battery technologies. . . . .	95
Table 3.7 – Summary of the equations, organized by features, required to build the matrices and vectors of constraints of the MILP problem; $\mathbf{0}$ is a $N \times 1$ vector of zeros. . . . .	102
Table 3.8 – A list of equivalency among symbols; n.a. stands for not available. . . . .	107
Table 5.1 – The Brazilian White Tariff; average time blocks were computed from 104 companies data; average prices were calculated from the 11 major energy distributors in Brazil, weighted by the number of customers of each company. . . . .	136
Table 5.2 – Load definitions; n.a. and unch. stand for “not applicable” and “unchanged”, respectively. . . . .	143
Table 5.3 – Matlab report field description. . . . .	145
Table 6.1 – Simulation results for setting $w_{drop}$ values. . . . .	153
Table 6.2 – Intermediate and final values of MG load adjustment factors in simulation 1. . . . .	158
Table 6.3 – MMG load adjustment and feeder operation performance indicators; n.c. and unch. stand for “do not care” and “unchanged”, respectively. . . . .	168
Table A.1 – Identifying the reasons why the algorithm stopped. . . . .	190
Table A.2 – Information about the optimization process. . . . .	191
Table A.3 – A short list of options to set up the solving algorithm. . . . .	192
Table B.1 – Number of matched results for each query. . . . .	195
Table B.2 – The main publishers and the number of general and selected titles . . . . .	196
Table B.3 – Results from the classification step. . . . .	196

## LIST OF ABBREVIATIONS AND ACRONYMS

e.g.	stands for <i>exempli gratia</i> in Latin, which means “for example”
etc.	stands for <i>et cetera</i> in Latin, which means “and so forth”
i.e.	stands for <i>id est</i> in Latin, which means “that is”
Iter.	stands for iteration
n.a.	stands for not available or not applicable
n.c.	stands for do not care
Orig.	stands for original
p.u.	stands for per unit
unch.	stands for unchangeable
Sim.	stands for simulation
Std.	stands for standard
AC	Alternating current
ADN	Active distribution network
ANEEL	Agência Nacional de Energia Elétrica
BESS	Battery energy storage system
BMS	Battery management system
CAES	Compressed air energy storage
CAISO	California Independent System Operator
CCG	Constraint and column generation
CD	Cost data
CIGRE	Conseil International des Grandes Réseaux Électriques
CL	Controllable loads
COM	Component object model

DAS	Day-ahead scheduling
DC	Direct current
DCL	Directly controlled load
DE	Diesel engine
DER	Distributed energy resources
DG	Distributed generation
DLC	Double layer capacitor
DMS	Distribution management system
DN	Distribution network
DNA	Distribution network applications
DOD	Depth of discharge
DR	Distributed resources
DOI	Digital object identifier
DSO	Distribution system operator
ED	Estimated data
EMS	Energy management system
EPE	Empresa de Pesquisa Energética
EPS	Electric power system
ESS	Energy storage system
FD	Forecasted data
FEM	Free energy market
GSIM	Grid of series interconnected microgrids
HIF	High impedance fault
HV	High voltage
HVD	High voltage of distribution
HVDC	High voltage direct current



IEC	International Electrotechnical Commission
IED	Intelligent electronic device
IEEE	Institute of Electrical and Electronics Engineers
ILP	Integer linear programming
IMG	Independent microgrids
ISO	Independent system operator
ISO	International Organization for Standardization
KCL	Kirchhoff's current law
LB	Lower bound
LD	Limit data
LG	Single line-to-ground (fault)
LL	Line-to-line (fault)
LLG	Double line-to-ground (fault)
LLL	Line-to-line-to-line (fault)
LLLG	Three-phase-to-ground (fault)
LP	Linear programming
LS	Load shedding
LSP	Level of source penetration
LTC	Load tap change
LV	Low voltage
LVD	Low voltage of distribution
MAS	Multi-Agent system
MG	Microgrid
MGCC	Microgrid central controller
MILP	Mixed-integer linear programming
MMG	Multi-microgrids

MPC	Model predictive control
MPPT	Maximum power point tracking
MPSC	Mixed parallel-series connection
MT	Micro turbine
MTG	Micro turbine generator
MV	Medium voltage
MVD	Medium voltage of distribution
O&M	Operation and maintenance
ONS	Operador Nacional do Sistema Elétrico
PCC	Point of common coupling
PCM	Parallel connected microgrids
PD	Price data
pdf	Probability density function
PF	Power flow
PI	Proportional and integral
PID	Proportional, integral, and derivative
PLC	Programmable logic controller
PoP	Publish or Perish
PRODIST	Procedimentos de Distribuição
PV	Photovoltaic
PVC	Photovoltaic curtailment
PVS	Photovoltaic system
RES	Renewable energy sources
RTE	Round trip efficiency
RTO	Regional transmission organization
SAE	Sistema de armazenamento de energia

SCADA	Supervisory, control and data acquisition
SE	System engineering
SMES	Superconducting magnetic energy storage
SOC	State of charge
SOH	State of health
SoS	System of systems
SoSE	System of systems engineering
STC	Standard test conditions
TD	Technical data
ToU	Time-of-use
U.S. DOE	United States Department of Energy
UB	Upper bound
UMG	Unified microgrids
USD	United States Dollar
VPP	Virtual power plants
VRE	Variable renewable energy
VSI	Voltage-source inverter
WG C6.22	CIGRE Working Group C6.22
WT	Wind turbine
WTC	Wind turbine curtailment

## LIST OF SYMBOLS

### Conventions and Definitions

	lowercase bold symbols are vectors, as in $\mathbf{x}$ and $\beta$
	uppercase bold symbols are matrices, as in $\mathbf{A}$ and $\mathbf{\Pi}$
$(a, b)$	is an ordered pair $a, b$ ; $(a, b) = (c, d)$ if and only if $a = c$ and $b = d$
$\max\{ \}$	is an operator that returns the largest value of a vector
$\underset{\mathbf{x}}{\text{minimize}} \mathbf{f}^T \mathbf{x}$	means finding a vector $\mathbf{x}$ that minimizes $\mathbf{f}^T \mathbf{x}$
$\min_{\mathbf{x}} f(\mathbf{x})$	means finding an argument $\mathbf{x}$ that minimizes $f(\mathbf{x})$
$\mathbf{A}^T$	is the transpose of matrix $\mathbf{A}$
$\mathbf{U} * \mathbf{V}$	the symbol $*$ represents the Hadamard product between two matrices, in this example, $\mathbf{U}$ and $\mathbf{V}$ , also known as the element-wise product
$\{x_1, \dots, x_n\}$	is a set with elements $x_1, \dots, x_n$
$a := b$	$a$ is by definition equal to $b$
$a \approx b$	$a$ is approximately $b$
$a \cong b$	$a$ is approximately equal to $b$
$p \implies q$	$p$ implies $q$
<b>Sets</b>	
$\mathbb{Z}$	is the set of integers
$\mathbb{S}_M$	is the set of MGs in the optimization problem
$\mathbb{U}_{in}$	is the set of MGs included in the MMG voltage regulation procedure
$\mathbb{U}_{mg}$	is the set of MGs in the MMG voltage regulation methodology
$\mathbb{U}_{out}$	is the set of MGs excluded from the MMG voltage regulation procedure
$\mathbb{R}$	is the set of real numbers
$\mathbb{S}_N$	is the set of discrete-time integers

## Modifiers

$(x)_i$	this modifier relates the quantity $x$ within the parentheses to a bus, node, line, or phase $i$
$\dot{I}^*$	the complex conjugate modifier is a superscript star
$\dot{V}$	the phasor modifier is an over-symbol dot
$\overline{A}$	overline is the upper bound modifier
$\underline{A}$	underline is the lower bound modifier
$ Z $	is the absolute value of a real or complex number $Z$
$\hat{A}$	widehat is the forecasted modifier
$I\angle\theta$	is the polar notation of a phasor or complex number with absolute value $I$ and angle $\theta$
$V'$	the modifier for the voltage regulation procedure post-perform quantities is an apostrophe symbol

## Matrix and Vectors

$[x_1, \dots, x_n]$	is a row vector with columns separated by commas;
$[x_1; \dots; x_n]$	is a column vector with rows separated by semicolons; all vectors are column vectors by default; row vectors must be declared explicitly
$\mathbf{0}$	is a $N \times 1$ vector of zeros
$\mathbf{0}^m$	is a $mN \times 1$ vector of zeros; $\{m \in \mathbb{Z} \mid m \geq 1\}$ ; $\mathbf{0}^1 = \mathbf{0}$
$\mathbf{1}$	is a $N \times 1$ vector of ones
$\mathbf{1}x$	is the $N \times 1$ vector of $x$ elements
$\mathbf{1}^m$	is a $mN \times 1$ vector of ones; $\{m \in \mathbb{Z} \mid m \geq 1\}$ ; $\mathbf{1}^1 = \mathbf{1}$
$\mathbf{1}^m x$	is the $mN \times 1$ vector of $x$ elements
$\dot{\mathbf{i}}_{loads}$	represents the vector of current phasors for the sum of other loads
$\dot{\mathbf{i}}_{mg(j)}$	represents the vector of current phasors for the $j$ -th MG
$\dot{\mathbf{i}}_{mmg}$	represents the sum of the MG current vector phasors in a MMG
$\dot{\mathbf{i}}_{sn}$	represents the vector of current phasors on the line $sn$

$\dot{\mathbf{V}}_{\text{diff}}$	is the three-phase vector that represents the vector of voltage difference phasors across a line	
$\dot{\mathbf{V}}_n$	represents the vector of voltage phasors on the $n$ -th bus	
$\dot{\mathbf{V}}_{rg60}$	represents the source voltage phasor in the IEEE 13 bus test feeder	
$\alpha$	is the vector for selecting the bound of uncertainty	
$\beta$	is the vector for enabling the uncertainty	
$\mathbf{A}$	is the matrix of linear inequality constraints	
$\mathbf{A}_{eq}$	is the matrix of linear equality constraints	
$\mathbf{b}$	is the vector of linear inequality constraints	
$\mathbf{b}_{eq}$	is the vector of linear equality constraints	
$\mathbf{f}$	is the parameters vector the optimization problem	
$\mathbf{f}_p$	is the price vector of the optimization problem	\$/kWh
$\mathbf{f}_{st}$	is the cost vector of the optimization problem	\$
$\mathbf{J}_P$	is the sensitivity matrix for real power	
$\mathbf{J}_Q$	is the sensitivity matrix for reactive power	
$\mathbf{l}_b$	is the vector of lower bounds	
$\mathbf{M}_{drop}$	is matrix of intermediate load adjustment factors	
$\mathbf{S}_{mg(j)}$	is the vector of apparent powers to the $j$ -th MG	
$\mathbf{S}_{mmg}$	is the matrix of apparent powers of microgrids	
$\mathbf{S}_{mmg}^{(k)}$	is the matrix of apparent powers of microgrids at the $k$ -th iteration	
$\mathbf{u}_b$	is the vector of upper bounds	
$\mathbf{V}_{drop}^{loads}$	is the three-phase vector that represents the contribution of other loads to the voltage drop on a bus	
$\mathbf{V}_{drop}^{mmg}$	is the three-phase vector that represents MMG contribution to the voltage drop on a bus	
$\mathbf{V}_{drop_n}$	represents the vector of voltage drop on the $n$ -th bus	
$\mathbf{x}$	is the decision vector of the optimization problem	

$\mathbf{x}_p$	is the power decision vector of the optimization problem	kW
$\mathbf{x}_{st}$	is the state decision vector of the optimization problem	
$\mathbf{Z}_{share}^{n,i}$	is the sum of the impedance matrices of the line segments shared between bus $n$ and MG( $i$ )	
$\mathbf{Z}_{sn}$	represents the impedance matrix of the line segment $sn$	
$\{\mathbf{1}x^{(j)}\}$	is a vector with elements $[\mathbf{1}x_{j_1}; \dots; \mathbf{1}x_{j_m}]; \{j_k \in \mathbb{Z} \mid j_k \geq 1\}$	
$\{x^{(j,t)}\}$	is a vector with elements $[x_{j_1,t_1}; \dots; x_{j_1,t_n}; \dots; x_{j_m,t_1}; \dots; x_{j_m,t_n}]; \{t_i \in \mathbb{Z} \mid t_i \geq 0\}$ , and $\{j_k \in \mathbb{Z} \mid j_k \geq 1\}$	
$\{x^{(t)}\}$	is a vector with elements $[x_{t_1}; \dots; x_{t_n}]; \{t_i \in \mathbb{Z} \mid t_i \geq 0\}$	

### Greek Letters Symbols

$\alpha(t)$	is the variable for selecting the bound of uncertainty at time $t$	
$\beta(t)$	is the variable for enabling the uncertainty at time $t$	
$\Delta\bar{P}$	is the upper bound of uncertainty	kW
$\Delta P$	is the lower bound of uncertainty	kW
$\delta_{Vmin}$	is the condition of minimum voltage difference between $V_{drop}^{mmg}$ and $V_{vio}$	
$\Delta P_k$	represents the real power variation in the $k$ -th bus	kW
$\Delta P_{mmg}$	represents the amount of real power variation in the MMG load adjustment procedure	kW
$\Delta Q_k$	represents the reactive power variation in the $k$ -th bus	kvar
$\Delta Q_{mmg}$	represents the amount of reactive power variation in the MMG load adjustment procedure	kvar
$\Delta t$	is the discrete-time resolution; $\{\Delta t \in \mathbb{Q} \mid \Delta t > 0\}$	h
$\Delta V_k$	represents the voltage variation in the $k$ -th bus	V
$\eta_{bat}$	is the is the battery packs charge and discharge efficiency	
$\eta_{bess}$	is the BESS charge and discharge efficiency	
$\eta_{chr}$	is the battery packs charge efficiency	
$\eta_{conv}$	is the BESS converter efficiency	

$\eta_{dch}$	is the battery packs discharge efficiency	
$\eta_{rte}$	is the battery round trip efficiency	
$\eta_{sto}$	is the battery packs storage efficiency	
$\eta_{tfr}$	is the BESS coupling transformer efficiency	
$\kappa_{pv}$	is the annual degradation rate of a PVS	%/year
$\lambda_{reg}$	is the generation capacity of a geographic region	kWh/year per kW
$\Pi$	is the uncertainty set	
$\gamma_{int}$	is the factor of interruptible loads	
$\gamma_{shd}$	is the factor of load shedding	

### Latin Letters Symbols

$\dot{I}_p$	represents the p-phase current phasor on a line along the feeder	A
$\dot{I}_{der_p}$	represents the p-phase current phasor on the MG DER bus	A
$\dot{I}_{load_p}$	represents the p-phase current phasor on the MG load	A
$\dot{I}_{mg_p}$	represents the p-phase current phasor on the MG PPC bus	A
$\dot{V}_p$	represents the p-phase voltage phasor on a bus along the feeder	V
BRL	is the ISO code for the Brazilian Real	
D-I	represents a constant current delta-connected load	
D-PQ	represents a constant power delta-connected load	
D-Z	represents a constant impedance delta-connected load	
Y-I	represents a constant current wye-connected load	
Y-PQ	represents a constant power wye-connected load	
Y-Z	represents a constant impedance wye-connected load	
$AR_{net}$	represents a network automatic recloser	
$AR_{sub}$	represents a substation automatic recloser	
$b_\pi$	represents the level (budget) of uncertainty	
$CB$	represents a circuit breaker	



$C_{cap,bess}$	is the cost of capital for the BESS	\$
$C_{cap,pv}$	is the cost of capital for a PVS	\$
$C_{pv}$	is the daily cost of PVS availability	\$
$C_{year}$	is the annual generation cost of a PVS	\$
$c_{chr}$	is an MG fixed cost for charging the battery	\$
$c_{dch}$	is an MG fixed cost for discharging the battery	\$
$c_{int}$	is an MG fixed cost for disconnecting interruptible loads	\$
$c_{pur_{\mu}}$	is an MG fixed cost of service when purchasing energy from another MG	\$
$c_{pur_g}$	is an MG fixed cost of service when purchasing energy from the grid	\$
$c_{sel_{\mu}}$	is an MG fixed cost of service when selling energy to another MG	\$
$c_{sel_g}$	is an MG fixed cost of service when selling energy to the grid	\$
$c_{shd}$	is an MG fixed cost for disconnecting (shedding) loads	\$
$c_{shf}$	is an MG fixed cost for disconnecting shiftable loads	\$
$DOD$	is the battery depth of discharge	
$DOD_r$	is the battery rated depth of discharge	
$E_{\eta}$	is the normalized daily electric bill	
$E_{avl}$	is the BESS available energy	kWh
$E_{bill}$	is the MG daily energy bill	\$
$E_{load}$	is the amount of daily energy load of a microgrid	kWh
$E_{pv}$	is the amount of daily energy generation of a PVS	kWh
$E_{pvc}$	is the amount of daily PV generation curtailment in a microgrid	kWh
$E_r$	is the BESS rated capacity	kWh
$E_{shd}$	is the amount of daily load shedding in a microgrid	kWh
$E_{sto}$	is the BESS stored energy	kWh
$E_{year}$	is the annual amount of energy generated by a PVS	kWh/year
$FS_w$	represents a fuse-switch	

$f(\mathbf{x})$	is an objective function whose solution is the vector $\mathbf{x}$	\$
$F_{in}$	represents a internal fault (inside the MG)	
$F_{out}$	represents a external fault (outside the MG)	
$k_e$	is the factor of non-linearity of the SOH family curves	
$k_{drop}^{in}$	is the load adjustment factor to the MGs $\in \mathbb{U}_{in}$	
$k_{drop}^{mg(j)}$	is the load adjustment factor to the $j$ -th MG	
$k_{drop}^{mmg}$	is the MMG load adjustment factor	
$k_{drop}^{out}$	is the load adjustment factor to the MGs $\in \mathbb{U}_{out}$	
$L_{cyc}$	is the cycle life of a BESS	cycles
$L_{E,bess}$	is the energy life of a BESS	kWh
$L_{spv}$	is the lifespan of a SPV	years
$MG_{ss}$	is the MG self-sufficiency	
$MG_j$	is the $j$ -th MG in a multiple MGs environment	
$M$	is the number of MGs in a multiple MGs environment	
$N_b$	represents the number of bus in a feeder	
$N_{iter}$	represents the number of iterations in the voltage regulation procedure	
$N$	is the number of time slots in the optimization problem	
$n.p$	represents the $p$ -th phase of the $n$ -th node	
$n_{cyc}$	is an independent variable to represent the current cycle of a BESS	
$PCC_j$	is the point of common coupling of the $j$ -th MG in a multiple MGs environment	
$P$	is the real power	kW
$p_{bess}$	is the cost each kWh for charging or discharging the battery	\$/kWh
$P_{chr}$	is the battery charge power	kW
$p_{chr}$	is the cost each kWh for charging the battery	\$/kWh
$P_{dch}$	is the battery discharge power	kW

$p_{dch}$	is the cost each kWh for discharging the battery	\$/kWh
$P_{int}$	is the amount of interruptible load	kW
$p_{int}$	is the cost of each kWh of interruptible load disconnected	\$/kWh
$P_{load}$	is the total load curve	kW
$p_{out}$	is the off-peak energy price	\$/kWh
$p_{peak}$	is the on-peak energy price	\$/kWh
$P_{pv}$	is the output power of a PV power plant	kW
$P_{pvc}$	is the amount PV output power curtailment	kW
$p_{pvc}$	is the cost of each kWh of PV output power curtailment	\$/kWh
$P_r$	is the BESS rated power	kW
$p_{ref}$	is the reference energy price	\$/kWh
$p_{reg}$	is the local cost per kW of a installed PVS	\$/kWh
$P_{shd}$	is the amount of load shedding	kW
$p_{shd}$	is the cost of each kWh of load disconnected (shedding)	\$/kWh
$P_{shf}$	is the amount of shiftable load	kW
$p_{shf}$	is the cost of each kWh of shiftable load disconnected	\$/kWh
$P_{wt}$	is the output power of a WT power plant	kW
$p_{wt}$	is the cost of operation and maintenance of a WT power plant	\$/kWh
$P_{wtc}$	is the amount WT output power curtailment	kW
$p_{wtc}$	is the cost of each kWh of WT output power curtailment	\$/kWh
$P_{mg(j)}$	represent the real power to the $j$ -th MG	kW
$P_{mmg}$	represent the sum of MG real powers in a MMG	kW
$P_{sto}$	is the battery storage power	kW
$P_{pur}$	is the power injected by the main grid into the MG	kW
$P_{pur_{\mu}}$	is the power injected by the main grid into the MG, when trading with another MG	kW

$p_{pur_{\mu}}$	is the is the purchase price of energy, when trading with another MG	\$/kWh
$P_{pur_g}$	is the power injected by the main grid into the MG, when trading with the grid	kW
$p_{pur_g}$	is the is the purchase price of energy, when trading with the grid	\$/kWh
$P_{sel}$	is the power injected by the MG into the main grid	kW
$P_{sel_{\mu}}$	is the power injected by the MG into the main grid, when trading with another MG	kW
$p_{sel_{\mu}}$	is the is the sale price of energy, when trading with another MG	\$/kWh
$P_{sel_g}$	is the power injected by the MG into the main grid, when trading with the grid	kW
$p_{sel_g}$	is the is the sale price of energy, when trading with the grid	\$/kWh
$Q_{mg(j)}$	represent the reactive power to the $j$ -th MG	kvar
$Q_{mmg}$	represent the sum of MG reactive powers in a MMG	kvar
$RTE$	is the battery pack round trip efficiency	
$R_{bill}$	is the reference daily electric bill	\$
$R_{min}$	is the minimum representativeness	cites/year
$R_{paper}$	is the representativeness of the current paper	cites/year
$SOC$	is the battery state of charge	
$SOH$	is the battery state of health	
$SOH_{exp}$	is a function that represents the SOH exponential family curves	
$SOH_{tsh}$	is the battery state of health threshold	
$st_{chr}$	is the state of charge permission for the battery: $(1, 0) = (\text{enabled}, \text{disabled})$	
$st_{con}$	is the status of MG connection with the grid: $(1, 0) = (\text{enabled}, \text{disabled})$	
$st_{dch}$	is the state of discharge permission for the battery: $(1, 0) = (\text{enabled}, \text{disabled})$	
$st_{int}$	is the connection state of interruptible loads: $(1, 0) = (\text{enabled}, \text{disabled})$	
$st_{pv}$	is the connection state of the PVS $(1, 0) = (\text{enabled}, \text{disabled})$	

$st_{shd}$	is the enable state of load shedding for the MG: $(1, 0) = (\text{enabled}, \text{disabled})$	
$st_{shf}$	is the connection state of shiftable loads: $(1, 0) = (\text{enabled}, \text{disabled})$	
$st_{pur_{\mu}}$	is the state of purchasing transaction when trading with another MG: $(1, 0) = (\text{enabled}, \text{disabled})$	
$st_{pur_g}$	is the state of purchasing transaction when trading with the grid: $(1, 0) = (\text{enabled}, \text{disabled})$	
$st_{sel_{\mu}}$	is the state of sale transaction when trading with another MG: $(1, 0) = (\text{enabled}, \text{disabled})$	
$st_{sel_g}$	is the state of sale transaction when trading with the grid: $(1, 0) = (\text{enabled}, \text{disabled})$	
$S$	represent the apparent power	kVA
$s_a$	is the number of rows of matrix $\mathbf{A}$	
$s_e$	is the number of rows of matrix $\mathbf{A}_{eq}$	
$S_{mg(j)}$	represent the apparent power to the $j$ -th MG	kVA
$s_p$	is the number of lines of vector $\mathbf{x}_p$	
$s_{st}$	is the number of lines of vector $\mathbf{x}_{st}$	
$S_w$	is a load switch	
$s_x$	is the number of rows of vector $\mathbf{x}$	
$t$	is the discrete-time in the optimization problem; $\{t \in \mathbb{Z} \mid t \geq 0\}$	
$T_{int}$	is the maximum discrete-time to disconnect loads	
$T_{isl}$	is the discrete-time period of islanding; $\{T_{isl} \in \mathbb{Z} \mid 0 \leq T_{isl} \leq N\}$	
$T_{shf}$	is the cycle period of shiftable loads	
$V_{base}$	represents the base voltage of a system	V
$V_{drop}$	represents the voltage drop on a phase of a bus along the feeder	V
$V_{drop}^{mg(j)}$	represents the contribution of the $j$ -th MG in MMG to the voltage drop on a bus along the feeder	V
$V_{drop}^{mmg}$	represents the MMG contribution to the voltage drop on a bus along the feeder	V

$V_{vio}$	represents the voltage violation on a bus along the feeder	V
$w_{drop}$	is a weight applied to $k_{drop}^{in}$ in the first iteration if necessary	

### Other Symbols

$\bar{P}_{int}$	is the upper bound for interruptible loads	kW
$\bar{P}_{pcc}$	is the upper bound for real power on the MG PCC bus	kW
$\bar{P}_{shd}$	is the upper bound for shedding loads	kW
$\bar{P}_{shf}$	is the power magnitude of shiftable loads	kW
$\overline{SOC}$	is the upper bound for the battery state of charge	
LiFePO <sub>4</sub>	is the lithium iron phoshate battery technology	
$\underline{SOC}$	is the lower bound for the battery state of charge	
$\hat{P}$	is the forecasted power	kW
$\hat{P}_{load}$	is the forecasted load curve	kW
$\hat{P}_{pv}$	is the forecasted output power of a PV power plant	kW
$\hat{P}_{wt}$	is the forecasted output power of a WT power plant	kW
$\hat{P}_{\pi}$	is the forecasted power plus uncertainty	kW

# CONTENTS

<b>1</b>	<b>Introduction</b>	<b>34</b>
1.1	Scientific Question and Hypothesis Formulation	36
1.1.1	Scientific Question	36
1.1.2	Hypothesis	36
1.1.3	Experimental Tests	36
1.2	Objectives	37
1.3	Scientific Contributions of this Thesis	37
1.4	Document Structure	38
<b>2</b>	<b>Fundamentals</b>	<b>40</b>
2.1	Distributed Energy Resources	42
2.1.1	Distributed Generation	42
2.1.1.1	Renewables Penetration Level	43
2.1.1.2	Self-Sufficiency in MG	45
2.1.2	Energy Storage	45
2.1.2.1	Battery Management System	51
2.1.3	Controllable Loads	52
2.2	IEEE Std 1547™ Series of Interconnection Standards	53
2.3	Microgrid Control	54
2.4	Microgrid Protection	57
2.5	Multi-Microgrids	63
2.5.1	MMG as System of Systems	67
2.5.2	Community Microgrids	68
2.5.3	Uncertainty Set For Forecasted Quantities	69
2.6	Literature Review	70
2.6.1	Literature Reveiw on Operation and Control of Microgrids	70
2.6.2	Literature Review on Multi-Microgrids	78
2.7	Final Considerations	82
<b>3</b>	<b>Optimal Day-Ahead Scheduling of Microgrids</b>	<b>83</b>
3.1	Introduction	83
3.2	Microgrid Energy Management System	86

3.3	Microgrid Modeling Methodology . . . . .	88
3.3.1	Objective Function . . . . .	91
3.3.2	Energy and Power Exchanges . . . . .	92
3.3.3	Power Balance . . . . .	94
3.3.4	Battery Energy Storage System . . . . .	94
3.3.5	Directly Controllable Loads and Load Shedding . . . . .	98
3.3.6	PV System . . . . .	99
3.3.7	Matrix Formulation . . . . .	100
3.4	Cost Estimation Methodology . . . . .	101
3.4.1	BESS Costs . . . . .	101
3.4.2	PV Costs . . . . .	104
3.4.3	Other Costs . . . . .	105
3.5	MMG Energy Management Modeling . . . . .	106
3.6	Final Considerations . . . . .	111
<b>4</b>	<b>MMG as Active Element in Feeder Voltage Regulation . . . . .</b>	<b>112</b>
4.1	Background Information on DN Voltage Control with MGs . . . . .	113
4.2	Overview of the Proposed Methodology . . . . .	115
4.3	Development of the Proposed Methodology . . . . .	117
4.4	Cases of MMG Voltage Drop . . . . .	122
4.4.1	Voltage Drop Case 1: $V_{drop}^{mmg} > V_{vio}$ . . . . .	122
4.4.2	Voltage Drop Case 2: $V_{drop}^{mmg} \leq 0$ . . . . .	124
4.4.3	Voltage Drop Case 3: $0 < V_{drop}^{mmg} < V_{vio}$ . . . . .	125
4.4.4	Voltage Drop Case 4: $V_{drop}^{mmg} = V_{vio}$ . . . . .	126
4.5	Methods to Perform the Proposed Voltage Regulation Procedure . . . . .	127
4.5.1	Method for Day-Ahead Applications . . . . .	127
4.5.2	Method for Real-Time Applications . . . . .	131
4.6	Final Considerations . . . . .	133
<b>5</b>	<b>Simulation Methods . . . . .</b>	<b>135</b>
5.1	Simulation Method for Optimal Day-Ahead Scheduling of MGs . . . . .	135
5.1.1	Normalized Energy Bill . . . . .	137
5.1.2	Simulation Cases . . . . .	138
5.2	Simulation Method for Feeder Voltage Regulation . . . . .	138
5.2.1	Simulation Platform . . . . .	138
5.2.2	Distribution Feeder Model . . . . .	139



5.2.3	Simulation Cases . . . . .	141
5.2.4	Matlab Reports . . . . .	144
<b>6</b>	<b>Results and Discussion . . . . .</b>	<b>146</b>
6.1	Optimal Day-Ahead Scheduling of MGs . . . . .	146
6.1.1	Simulation Results . . . . .	146
6.1.2	Discussion . . . . .	151
6.2	Feeder Voltage Regulation . . . . .	153
6.2.1	Simulation Results . . . . .	153
6.2.1.1	Voltage Drop Case 1 . . . . .	154
6.2.1.2	Voltage Drop Case 2 . . . . .	159
6.2.1.3	Voltage Drop Case 3 . . . . .	160
6.2.1.4	Voltage Drop Case 4 . . . . .	163
6.2.1.5	Feeder Operation Performance Indicators . . . . .	167
6.2.2	Discussion . . . . .	170
<b>7</b>	<b>Conclusions and Final Considerations . . . . .</b>	<b>173</b>
7.1	Conclusions . . . . .	173
7.2	Scientific Contributions . . . . .	174
7.3	Future Works . . . . .	175
7.4	Scientific Production . . . . .	176
	<b>REFERENCES . . . . .</b>	<b>178</b>
	 <b>Appendix . . . . .</b>	 <b>187</b>
	<b>Appendix A Linear Programming . . . . .</b>	<b>188</b>
A.1	Introduction . . . . .	188
A.2	Mixed-Integer Linear Programming with Matlab . . . . .	189
	<b>Appendix B Literature Review Methodology . . . . .</b>	<b>194</b>
B.1	Literature Review on MG Operation and Control . . . . .	194
B.2	Literature Review on Multi-Microgrids . . . . .	197
	<b>Appendix C Repository . . . . .</b>	<b>200</b>

<b>Annex</b>	<b>201</b>
<b>Annex A BESS Technical Data . . . . .</b>	<b>202</b>
<b>Annex B Central Inverter for Solar PV Power Plants Technical Data . . . . .</b>	<b>205</b>

# 1 Introduction

Microgrids (MG) have attracted the attention of researchers, government officials, and electric power companies because of the values and services it can add to the grid. In general, the term microgrid is associated with renewable energy sources (RES), reduction of greenhouse gases, resilience, and reliability. All of them are well-known advantages that an MG can offer (HEDERMAN, 2014; MARNAY et al., 2015a). On the other hand, an energy distribution system containing MGs (or distributed energy resources, DER) presents new challenges concerning its operation and protection. Protection schemes previously used in distribution networks (DN) may not be suitable for systems with MGs (MEMON; KAUHANIEMI, 2015; GOPALAN; SREERAM; IU, 2014). Also, the effects of the increasing penetration level of RES and the coordination of multiple energy resources are new issues in the operation of current systems (KROPOSKI et al., 2017; ALAM; CHAKRABARTI; GHOSH, 2019). According to Alam, Chakrabarti and Ghosh (2019), in a literature review on networked microgrids, there is a growing interest in researching how to coordinate and manage all these new features in the distribution network.

An energy distribution system capable of actively managing and coordinating distributed energy resources connected to its distribution network jointly with its conventional infrastructure has been called an active distribution network (ADN) in the literature (REPO et al., 2017; KOUTSOUKIS et al., 2017). Such systems can supervise and control DERs and microgrids at some level to, for example, perform voltage control on a feeder, request active and reactive energy support (ancillary services), enable islanding of an operation area, request support in a recombination of loads during outages, among other reasons. Thus, given the reality of DERs connected to current distribution networks, distribution system operators are facing the challenge of transitioning from a conventional to an active distribution network.

The operation of microgrids according to the purposes of an ADN must take into account both optimizing the internal use of its resources and making them available to achieve some common objectives in the distribution network. The joint operation of several independent microgrids with one or more goals in common gives rise to a multi-microgrid system. Motivations to form an MMG can be technical and economical, such as minimizing operating costs, improving the system reliability, and providing ancillary services to the distribution system operator (DSO).

Although the multi-microgrids subject is recent in research, a project is underway, sponsored by the U.S. Department of Energy, to integrate two microgrids in the city of Chicago: the Bronzeville community microgrid and the Illinois Institute of Technology microgrid campus (SHAHIDEHPOUR et al., 2017; MICROGRID KNOWLEDGE, 2022). The

project aims to reduce the outage time of critical loads, improve the grid's overall operation and efficiency, and reduce local emissions in the Chicago community.

Thus, optimizing the operation of a single microgrid is the first step towards optimizing an MMG. Optimally dispatching a microgrid over a day means getting the highest revenue at the lowest cost, or equivalently, minimizing a daily energy bill. Revenues may come from the sale of energy produced with its own resources or from the provision of ancillary services to the distribution system operator. On the other hand, the term costs comprises the cost of operating, maintaining, and administrating an MG, also called operating cost, and the cost of investing in long-term assets, such as solar panels and batteries, also called capital cost. On the other hand, optimizing the operation of an MMG depends on the individual optimization interests, the joint interests in the group, and the constraints and interests of the DSO.

When a distribution system contains more than one microgrid in the same operating area, they can be operated in at least three different ways:

- as an independent microgrids (IMG) system, where each microgrid has operational autonomy, and the group has no common objective.
- as a multi-microgrids (MMG) system, where each microgrid has operational independence, but the group has at least one common and collaborative goal. An MMG fits, by definition, a system of systems (SoS).
- as a unified microgrids (UMG) system, where the group of microgrids are operated as if they were a monolithic system with a unique objective;

In all three cases, there is a group of microgrids whose level of integration ranges from entirely independent to fully associated. Moreover, all cases represent practical situations that can occur in future energy distribution systems.

An energy distribution system, in which all microgrids assets belong to a single entity, such as the distribution system operator, can be an example of UMG system. In that case, the DSO could optimize the day-ahead dispatch by having all the distributed energy resources (DER) at its disposal. It could formulate the optimization problem trying to minimize the daily costs of a single system, containing a group of MGs and DERs, having the distribution network operational limits among the constraints. Or it could use DERs to adjust the voltage profile of the DN, relieve the overload in transformers and distribution lines, decrease losses in conductors, and recompose loads in power outages with more efficiency.

However, if each MG is installed in the DN by private initiative, then it is natural that each microgrid, in a group, can belong to different entities. Thus, the primary interest is to minimize each MG daily energy bill in an attempt to reduce the payback period on capital investments. In such a case, adjusting the voltage profile, relieving overload,

decreasing losses, and so on, may be characterized as ancillary services provided by the MG operator, with the possibility of remuneration by the DSO. This scenario can give rise to an MMG system if there is any level of association among the MGs. Otherwise, it may give rise to an IMG system.

According to Maier (1998), an SoS, by definition, presents higher costs than a monolithic system due to its inherent redundancy. The term costs means system group costs. As a direct application of this concept, an MMG system can present higher costs than a UMG. On the other hand, according to (ZHAO et al., 2018), an MMG system may present lower costs than an IMG, in the sense that there is no collaboration between MGs in the latter.

The present study addresses how to model the energy management of multi-microgrids in active distribution systems.

## 1.1 Scientific Question and Hypothesis Formulation

### 1.1.1 Scientific Question

How does an association of multiple heterogeneous and independent microgrids as a group, while subject to operating restrictions of a distribution system, affect the operating performance of a distribution network?

In such a question, variables to be experimentally measured are technical performance indicators, and the microgrids' distributed energy resources are variables to be changed.

### 1.1.2 Hypothesis

- i. A microgrid operator should not consider the distribution network an unrestricted source of resources to optimize its operating costs;
- ii. Microgrids operating in groups (MMG) have technical advantages that override the advantages of individual operation (IMG) in a scenario with operating restrictions;

If the hypotheses are confirmed, the results should point to the SoS modeling of multiple microgrids as a feasible option for some practical cases where energy distribution systems do not have full control over the MGs' assets in their operating area.

### 1.1.3 Experimental Tests

A distribution feeder containing a group of microgrids will be mathematically modeled on a simulation platform so that performance indicators of a distribution network

can be experimentally measured. Experiments are carried out in Matlab and OpenDSS software based on an analytical modeling technique developed in the present work.

## 1.2 Objectives

The main objective is to develop a methodology to model the operation and control of a power distribution system containing a group of microgrids and, thus, investigate how this group affects the performance of the distribution network.

Specific objectives are

1. To analyze microgrid and multiple microgrid modeling techniques;
2. To develop a modeling technique to solve microgrids optimized day-ahead scheduling problems;
3. To develop a voltage regulation technique in feeders through load adjustment in MMG;
4. To validate the proposed models through computer simulations;
5. To analyze simulation results according to the scientific hypothesis.

## 1.3 Scientific Contributions of this Thesis

The main contributions of this work are:

1. Detailed mathematical modeling of a battery energy storage system (BESS) for microgrid operation optimization purposes by
  - presenting a practical methodology to compute the BESS availability cost;
  - modeling of a BESS system considering battery, converter, and transformer useful values of efficiencies;
  - modeling of the BESS state of charge as a non-recursive constraint to the MILP problem.
2. Modeling of scheduled intentional islanding in a microgrid operation with the possibility of curtailment and load shedding;
3. Modeling of non-interruptible shiftable loads (continuous cycle) when participating in demand response programs;

4. Presenting a practical methodology to compute the availability cost of solar photovoltaic (PV) systems.
5. Development and validation of a methodology for voltage regulation in unbalanced three-phase feeder circuits through the adjustment of MMG loads.

The methodology presented in Chapter 3 and its respective results presented in Section 6.1 gave rise to the paper (SILVA; AOKI; LAMBERT-TORRES, 2020) published in the scientific journal *Energies*. Contributions cited in items 1 to 4 are clarified in that paper and this thesis. In addition, the methodology presented in Chapter 4 and its respective results presented in Section 6.2 will also be published in a scientific paper, which is about to be submitted to a scientific journal. The contribution cited in item 5 originates from these results.

## 1.4 Document Structure

Chapter 1 presents a brief introduction to the subject of this thesis and an explanation of the scientific question and hypothesis. Then, the general and specific objectives are presented, followed by the scientific contributions of this doctorate.

Chapter 2 introduces some fundamentals on DER, MG, and MMG. It also addresses an overview of the interconnection of distributed resources (DR) with the electric power system (EPS) by presenting the IEEE 1547 standard. This chapter also includes a literature review on the operation and control of microgrids and multi-microgrids.

The mathematical modeling of an optimal day-ahead energy dispatch of microgrids is the subject of Chapter 3. It brings a literature review on this subject before presenting, in detail, the mathematical modeling of distributed energy resources and the transactions carried out with the distribution system operator and other microgrids, as addressed in the first three sections of the published paper. At the end of the chapter there is an explanation of two MMG models found in the literature.

Chapter 4 addresses the methodology developed in this work for including MMG as active element in feeder voltage regulation. A mathematical development is presented in order to support a voltage control strategy through microgrid load adjustment. The problem is demonstrated through four cases of MMG contribution to the voltage drop on the bus under violation, called MMG voltage drop cases. For each there is a different voltage control strategy. Next, two methods for performing the voltage regulation procedure were presented, one for day-ahead applications, another for real-time. Some considerations about this methodology are made at the end of the chapter, including a background information on distribution network voltage control with microgrids.

Chapter 5 presents the simulation methods used in this work to validate the methodologies presented in Chapters 3 and 4. Section 5.1 presents a simulation method

for optimal day-ahead scheduling of MGs, which is a reproduction of the Section 4 of the published paper. Next, the simulation method for feeder voltage regulation is presented.

Simulation results are presented in Chapter 6 for both methodologies of Chapters 3 and 4, and are followed by a discussion about them. Results and discussion for optimal day-ahead scheduling of MGs simulations are a reproduction of those presented in the published paper.

Chapter 7 presents some conclusions about the work carried out in this doctorate and the objectives achieved. A list of subjects that may be addressed in future works is presented in the final paragraphs.

In Appendix A, it is possible to find an overview of linear programming (LP) using Matlab, which is the method used in this work for microgrid optimization. Appendix B.1 and Appendix B.2 present the methodology used in the literature review. Appendix C presents repository hyperlinks of Matlab files used to produce the simulation results of this work.

To conclude, Annexes A and B illustrate some technical data from manufacturers.



## 2 Fundamentals

In 2011, the Microgrid Exchange Group, in a report to the United States Department of Energy (U.S. DOE), defined microgrid as “a group of interconnected loads and distributed energy resources within clearly defined electrical boundaries that acts as a single controllable entity with respect to the grid. A microgrid can connect and disconnect from the grid to enable it to operate in both grid-connected or island-mode” (TON; SMITH, 2012; SMITH; TON, 2013).

In 2012, the Microgrid Evolution Roadmap, a CIGRE (Conseil International des Grandes Réseaux Électriques) working group (WG C6.22), defined microgrid as “electricity distribution systems containing loads and distributed energy resources, (such as distributed generators, storage devices, or controllable loads) that can be operated in a controlled, coordinated way either while connected to the main power network or while islanded” (MARNAY et al., 2015a, p. 139). Although there is no mention on the distributed generation (DG) technology to be used, Marnay et al. (2015a) states the term generation encompasses all possible types of sources, whether renewable or not. Besides, the term storage device includes electrical, electrochemical, mechanical and heat storage technology.

These are the main definitions of microgrid in literature, which have been widely used in several works on the subject (JIMÉNEZ-ESTÉVEZ et al., 2014; MANZ et al., 2014; MARNAY et al., 2015a; PARHIZI et al., 2015). They emphasize three requirements regarding a microgrid:

- i. it must contain loads and distributed energy resources;
- ii. it must be controllable;
- iii. it must be able to operate in both grid-connected or islanded mode.

These requirements highlight the importance of control for a microgrid. What differentiates a microgrid from a distribution system with distributed energy resources spread along the network is that the former must be controllable. Thus, the main system can view it as a controlled and coordinated unit (STRBAC et al., 2015). Also, the requirements allow inferring that a microgrid must have an energy management system (EMS) to manage its distributed energy resources, and to interact with its controllers.

Microgrids have potential benefits for consumers and utilities. They can (HED-ERMAN, 2014; MARNAY et al., 2015a):

- improve energy efficiency;

- reduce greenhouse gases emission;
- improve system reliability;
- improve system resilience;
- defer capital investment in capacity;
- provide ancillary services;
- provide power to remote or isolated communities;
- enable customers to engage in transactive energy markets.

Microgrids can increase the penetration of renewable energies into the grid, helping to improve energy efficiency by reducing losses in the power system as a whole while reducing greenhouse gases emission. This alignment with climate and energy policies around the world brings additional value to microgrid projects (LORUBIO; SCHLOSSER, 2014). Furthermore, microgrids can help the power system improve its ability to deliver electricity in quantity and quality demanded by users (reliability) because of its distributed energy resources. Additionally, microgrids can help reduce the magnitude and duration of disruptive events in the electrical system which can range from a simple fault in the main system causing a power outage to even a more serious event as an earthquake (resilience).

For utilities, microgrids are an option to defer capital investments in assets, such as transformers and distribution lines, to meet circuits that require additional capacity due to localized load growth (HEDERMAN, 2014). Also, microgrids can take advantage of the control on distributed generation, energy storage, and controllable loads to provide some ancillary services to the main grid such as frequency and voltage control, reactive power, spinning reserve, and operational reserve.

Microgrids also are an option to provide power to remote or isolated communities, as it happens in northern Canada. According to Arriaga, Nasr and Rutherford (2017), “the remote and dispersed nature of Canada’s off-grid communities in addition to specific geography and climate pose a real barrier to the provision of energy services”. Historically, the technology employed in those microgrids has been diesel generator with fuel storage. However, due to this barriers, the transportation and storage of fuel have been a challenge for those communities, and local residents have faced technological, social, environmental, and economic issues. In recent years, however, solar photovoltaic, wind, hydro and energy storage technologies in combination with diesel generating (hybrid systems) has been successfully employed in some microgrids of that region and thus helping to decrease their dependence on fossil fuel (ARRIAGA; NASR; RUTHERFORD, 2017).

Finally, a microgrid can still be an agent of a new transactive energy paradigm. According to Vaahedi et al. (2017), when in grid-connected mode, a microgrid could participate in retail, wholesale, and bilateral markets; it could also engage in bilateral trades with other microgrids, prosumers, and consumers. In this scenario, the transactions are performed by the microgrid, distributed energy resources, and demand response assets operators.

A microgrid can typically be composed of up to four distinct elements:

- i. distributed generation;
- ii. energy storage systems (ESS);
- iii. controllable loads;
- iv. noncontrollable loads.

The first three elements fit the concept of distributed energy resources, while the latter concerns conventional loads.

## 2.1 Distributed Energy Resources

### 2.1.1 Distributed Generation

Distributed generation is the term used to designate the generation of energy geographically closest to points of consumption, usually connected to a power distribution system. The supply of power with power plants directly connected to the distribution system can bring several benefits to the electric power system as a whole. It can help to relieve the transmission system; can reduce local overloads of transformers and transmission lines; can smooth peaks in load curves, and can increase system reliability. This has an impact on the planning of power systems, since the investment in building new centralized power plants units, new transmission lines, and new power substations can be avoided or delayed, as well as the investment in acquiring new power transformers.

According to the national energy agency of Brazil, named *Agência Nacional de Energia Elétrica* (ANEEL), DG comprises “power plants of any power, with installations connected directly to the distribution system or through consumer facilities, which are authorized to operate connected or not to the distribution system and dispatched or not by the ONS” (AGÊNCIA NACIONAL DE ENERGIA ELÉTRICA, 2018, p. 29, our translation), in which ONS (*Operador Nacional do Sistema Elétrico*) stands for national electric system operator.

The energy source used in the DG can be either renewable as wind, solar, and biopower, or non-renewable as fossil fuel. In addition, distributed generation units can

be dispatchable and non-dispatchable. The former are those whose energy source can be considered relatively constant over time, such as fossil fuel and small hydropower plants. The latter are those whose energy source naturally varies over time, such as wind and solar energy.

Concerning the connection mode, distributed generation can be either directly connected to the distribution network or connected through inverters. The former is called directly connected or directly coupled DG (MEMON; KAUHANIEMI, 2015), and the last converter-based or inverter-based DG (IEEE, 2011). As examples, a genset is directly coupled, and a solar PV is inverter-based.

The connection voltage level for DG depends on the regulatory framework of each country. In Brazil, ANEEL establishes voltage level ranges for distribution systems as (AGÊNCIA NACIONAL DE ENERGIA ELÉTRICA, 2018, p. 55):

- HVD – High Voltage of Distribution:  $69 \text{ kV} \leq \text{HVD} < 230 \text{ kV}$ ;
- MVD – Medium Voltage of Distribution:  $1 \text{ kV} < \text{MVD} < 69 \text{ kV}$ ;
- LVD – Low Voltage of Distribution:  $\text{LVD} \leq 1 \text{ kV}$ .

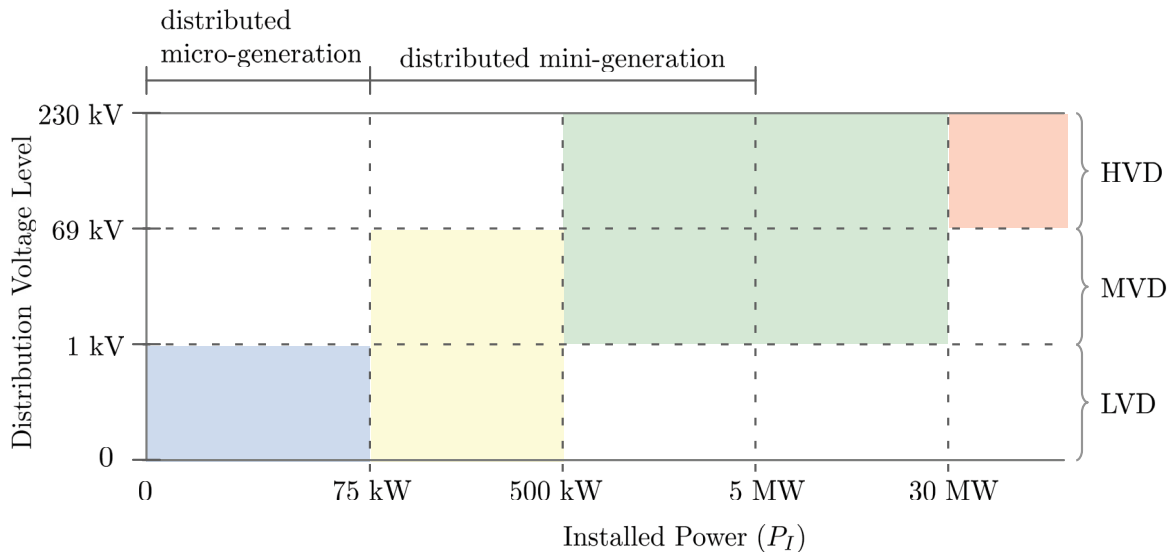
and the connection voltage level for DG depends on the installed capacity ( $P_I$ ) of each power plant unity (AGÊNCIA NACIONAL DE ENERGIA ELÉTRICA, 2017, p. 37) as shown in Figure 2.1; the higher the power, the higher the connection voltage level. Also, ANEEL assigns a particular name to distributed generation installed in consumer units, namely micro-generation for  $P_I$  below 75 kW and mini-generation for  $P_I$  between 75 kW and 5 MW, as illustrated in the figure.

#### 2.1.1.1 Renewables Penetration Level

The annual level of source penetration (LSP) is the amount of energy produced by a source as a fraction of the amount provided by a whole system annually (KROPOSKI et al., 2017); energy values are typically in GWh. While the energy mix contains information on available energy sources and their respective capacities, the annual LSP informs how those energy sources were applied over time. Instantaneous LSP, on the other hand, is the amount of power provided by a source as a fraction of the power supplied by an entire system, in real-time (KROPOSKI et al., 2017); values are typically in GW.

In the context of variable renewable energy (VRE), the terms “annual LSP” and “instantaneous LSP” are often used in technical literature to evaluate its impact on the interconnected system. The former is used to verify the evolution of a VRE over the years on an annual basis. The VRE instantaneous penetration has a direct impact on the power system stability and therefore some countries usually limit its level, as happens in Ireland, where it is limited to 55%. Also, countries such as Denmark, Ireland, and Germany have VRE annual penetrations of more than 20% (KROPOSKI et al., 2017).

Figure 2.1 – Distribution voltage level for connecting distributed generation in Brazil.



Source: The author (2022).

The increasing penetration of VRE in the power system, represented mainly by solar PV and small wind turbines (WT), brings two main concerns: one regarding its invisibility to the system operator and another about its intermittent characteristic. Usually, distributed generation units cannot receive dispatch commands from the system operator. The main system sees DG as a decrease in load, and DG is often not visible from the system operating point of view. However, if a significant portion of DG goes off-line in response to a systemic frequency or voltage disturbance, then the bulk power system can experience a cascade blackout if it is unprepared (EXETER ASSOCIATES, INC. AND GE ENERGY, 2012, p. 28). Also, in a quadrennial report requested by the United States government to the Institute of Electrical and Electronics Engineers (IEEE), researchers stand that for low levels of penetration of VRE, their variation and uncertainty is not a serious problem (HEDERMAN, 2014, p. 8). With some changes in planning and operating procedures (HEDERMAN, 2014, p. 9) the main grid can accommodate a certain amount of intermittent DG penetration (around 30% of the generated annual energy) regardless of whether or not energy storage is available. This is because the variation and uncertainty presented by the intermittent DG are equivalent to the characteristic behavior of the loads in the bulk power system, which is already prepared for this (HEDERMAN, 2014). Historically, the power system has been designed, controlled and operated to compensate up to a certain level of load variation by means of a respective variation in the output of generation (MANZ et al., 2014).

In Brazil, according to Empresa de Pesquisa Energética (EPE) (EPE, 2021), there

was a total energy generation of 621251 GWh in 2020, of which 57051 GWh is from wind generation and 10748 GWh from solar generation. Thus, there was an annual penetration of 9.18% for wind generation and 1.73% for solar. Although in Brazil the VRE penetration level is around 10%, it reaches high values in some countries around the world, such as Denmark with 42% (2015), EirGrid/Ireland with 22% (2016), Portugal with 23% (2015), South Australia with 35% (2016), California independent system operator (CAISO) with 27% (2016) (BLOOM et al., 2017). That recommendation of 30% made by IEEE report has been successfully exceeded by some countries and is close to being by others.

### 2.1.1.2 Self-Sufficiency in MG

Self-Sufficiency in energy is the ratio of the energy produced and consumed by an entity, analyzed throughout time. For a microgrid, self-sufficiency ( $MG_{ss}$ ) indicates the degree of independence to the main grid, as illustrated by Equation 2.1. Independence occurs for values greater than or equal to 1.

$$MG_{ss} := \frac{\text{energy produced by the MG}}{\text{energy consumed by the MG}} \quad (2.1)$$

For a microgrid with VRE, both energy produced and consumed varies from day to day, from month to month and from season to season. Thus, the degree of self-sufficiency of a microgrid can be better assessed if it is taken over a year. On the other hand, in addition to the annual value, daily and monthly values can be useful to help design a microgrid. In the present research, daily self-sufficiency is a parameter of simulation to establish the proportion between solar generation and the load of a microgrid, for example.

## 2.1.2 Energy Storage

Energy storage and VRE sources can be considered complementary elements in microgrids. Together they can address the challenge of islanded operation mode. Fitzgerald et al. (2015) cited 13 services that battery energy storage system can provide, grouped according to stakeholders. Independent system operator (ISO) and regional transmission organization (RTO) services are:

- i. energy arbitrage or price arbitrage: the practice of purchasing electricity from the main grid when it is cheap, and storing it for later use when grid electricity is expensive;
- ii. spinning reserve: a reserve of generation that is instantaneously available;

- iii. non-spinning reserve: a reserve of generation that is available within a short period of time (typically units of minutes), but not instantaneously available;
- iv. frequency regulation: a set of actions to maintain the frequency in a previously established range to meet legal requirements;
- v. voltage support: a set of actions to maintain the voltage level in a previously established range to meet legal requirements, as well as quality and reliability requirements;
- vi. black start: a support to restore large power plants without relying on the external grid energy;

Utility services are:

- vii. resource adequacy: it enables a utility to invest in energy storage to reduce the need for new generation capacity rather than investing in new generation itself, in order to minimize the risk of investment in that area;
- viii. distribution/transmission deferral: “delaying, reducing the size of, or entirely avoiding utility investments in distribution/transmission system upgrades; necessary to meet projected load growth on specific regions of the grid” (FITZGERALD et al., 2015);
- ix. utilities asset relief: transmission system relief; local overloads relief of transformers, transmission lines and distribution lines;

Finally, customer services are:

- x. time-of-use bill management: the practice of making use (behind-the-meter) of energy which was stored during periods of lower rates to minimizing electricity purchase from the main grid when time-of-use rates are higher;
- xi. increased PV self-consumption: maximize the consumption of electricity generated by behind-the-meter photovoltaic systems;
- xii. demand charge reduction: demand charge management;
- xiii. backup power: backup power for residential customers.

In addition to providing the primary services for which it was designed (the main reason for its acquisition), an energy storage system, when inside a microgrid, can also offer additional (secondary) services that add value to the system and decrease its payback. Typical primary services of BESS in microgrid can be energy arbitrage, increased PV self-consumption, and demand reduction. Also, a microgrid can provide ancillary services



such as spinning reserve, frequency regulation, and voltage support. Its storage capacity, when added to that of others BESS, can assist in these ancillary services. Moreover, it can be financially rewarded for this, provided that service is adequately regulated.

Services that energy storage provides are in two main groups, namely energy and power applications Manz, Piwko and Miller (2012). The former are those that demand a continuous supply of energy over long periods of time, typically hours. The latter are those that require rapid injection and absorption of energy over short periods of time. Among examples of energy applications are (MANZ et al., 2014): energy arbitrage, utilities asset relief and time-of-use bill management. On the other hand, examples of power applications include (MANZ; PIWKO; MILLER, 2012): frequency regulation, voltage support and spinning and non-spinning reserve.

Typically, an energy storage system is bounded by its rated power ( $P_r$ ), and rated capacity ( $E_r$ ). The former determines how much power can flow into or out of the system at any time. The latter is the measure of how much electricity the system can deliver or absorb over the one-hour period. It provides information on the amount of energy that can be stored. Both are manufacturer's specifications.  $P_r$  is also referred as nominal output power (see Annex A).

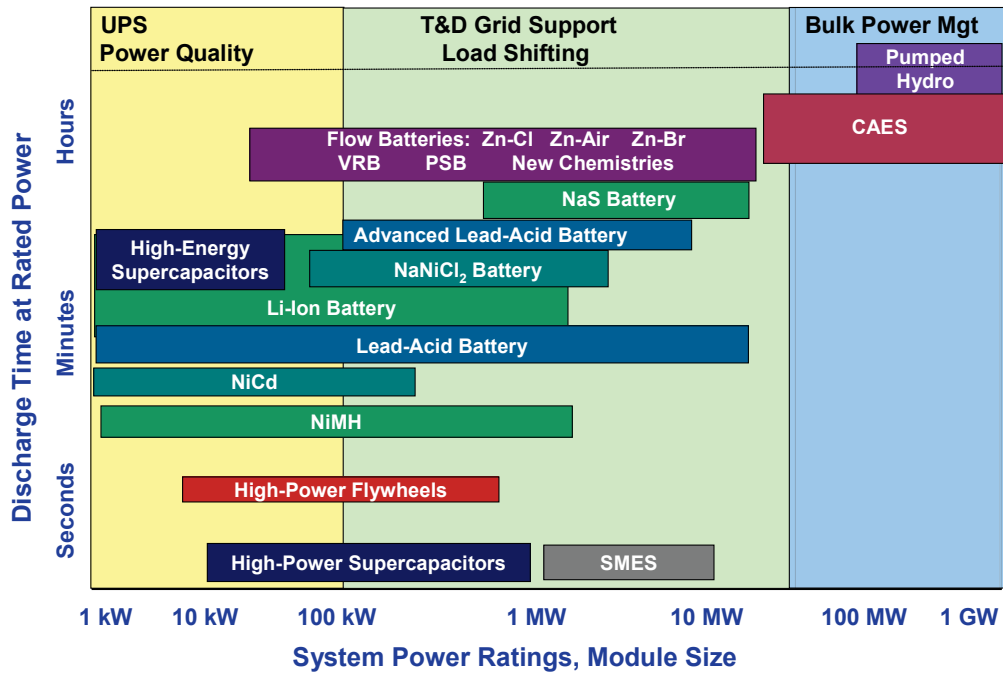
There is a relation between these two quantities named power-to-energy ratio, which is defined as  $P_r/E_r$  (typically in MW/MW·h or kW/kW·h). For example, one application that require 10 MW of power availability for a time interval of up to 12 min demands a power-to-energy ratio of 10 MW/2 MW·h. The power-to-energy ratio can determine if an energy storage technology is a power or energy application. Storage technologies with  $P_r/E_r$  of about 2 or greater are well suited to power applications. On the other hand, those with  $P_r/E_r$  of about 1/2 or smaller are well suited to energy applications (MANZ; PIWKO; MILLER, 2012).

There are several forms of storage energy such as electrochemical, electrical, magnetic, kinetic, hydraulics and compressed air. There are also a wide variety of technologies capable of making them feasible in the electric power system such as batteries, supercapacitors, superconducting magnetic energy storage (SMES), flywheels, pumped hydro systems and compressed air energy storage (CAES) (BOICEA, 2014) as illustrated in Figure 2.2. However, the technology of choice in the present study will be battery only. That is why it is being widely used in power systems, and has a wide power range from 1 kW to more than 10 MW, as shown in the figure. That power range is enough to cover microgrids' applications as a whole.

In a BESS, battery rated capacity refers to the manufacturer's specified capacity, and available capacity refers to the actual energy storage capability (CADE ELECTRONICS INC., 2019). When the battery is new, they are the same. However, over time and as the battery is used, an inactive part appears, which is permanently lost. As a result, the battery capacity fades. Figure 2.3 shows a curve of capacity degradation versus the



Figure 2.2 – Energy storage technologies.



Source: Sandia National Laboratories (2013, p. 29).

number of cycles, provided by a manufacturer (SAMSUNG SDI, 2016), for a 68Ah lithium-ion battery cell designed for electrical grid applications. Note that this battery loses 20% of its capacity around 6000 usage cycles. According to this curve, degradation is not a linear function of the number of cycles of use.

In a battery, state of charge (SOC) is the stored energy as a fraction of the available capacity, i.e.,

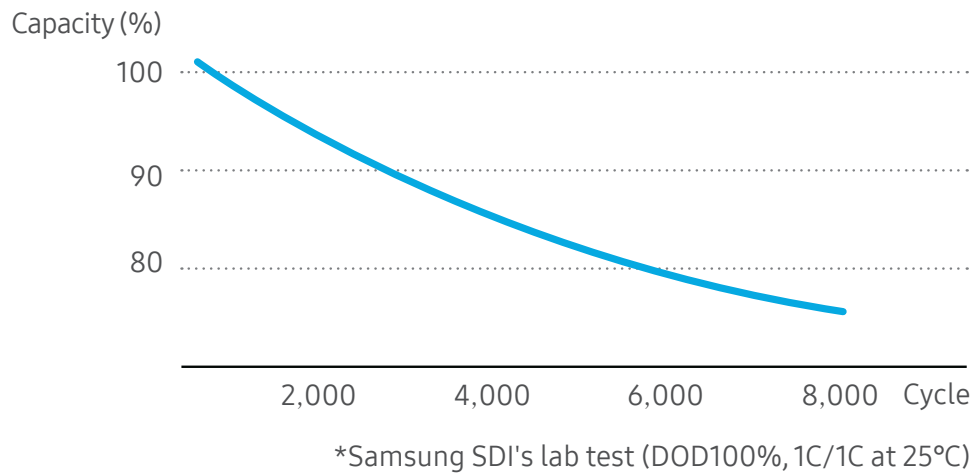
$$SOC = \frac{\text{stored energy}}{\text{available capacity}} \quad (2.2)$$

Also, state of health (SOH) is the ratio between the available and rated capacity (LAWDER et al., 2014),

$$SOH = \frac{\text{available capacity}}{\text{rated capacity}} \quad (2.3)$$

Battery end-of-life happens when the SOH falls below a threshold for a given application. Additionally, the cycle count and expiration date can also determine the end-of-life (CADE ELECTRONICS INC., 2019). IEEE Std 2030.2.1™ defines cycle life as “the number of cycles after which electricity storage becomes inoperable or unusable for a given electric power system application” (IEEE, 2019). The battery whose curve is illustrated in Figure 2.3 has a 6,000 cycle life, which means reaching 80% of its capacity ( $SOH = 0.80$ ).

Figure 2.3 – Capacity degradation for a 68Ah lithium-ion battery cell (6,000 cycle life).



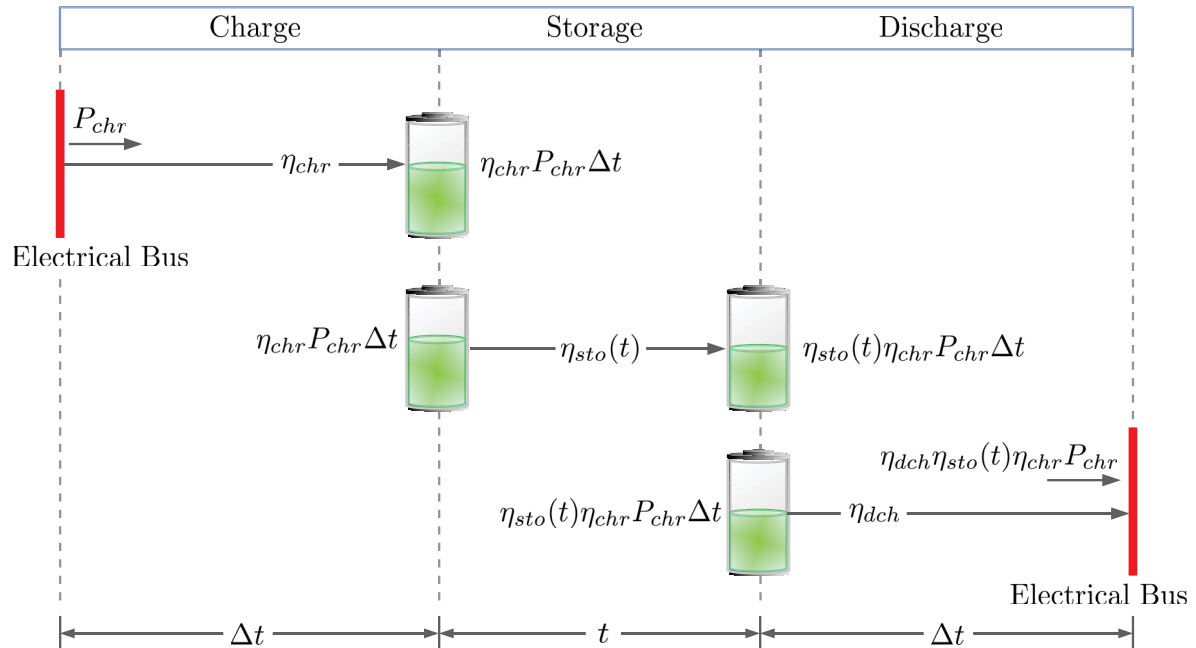
Source: SAMSUNG SDI (2016).

For batteries, depth of discharge (DOD) and state of charge are complementary quantities, i.e.,  $DOD = 1 - SOC$ . According to Sandia National Laboratories (2013), the battery life is a function of DOD. The deeper the discharges are, the shorter the battery life will be. Thus, battery manufacturers specify the cycle life for a rated depth of discharge (SANDIA NATIONAL LABORATORIES, 2013). For example, (ALPHAESS, 2019) (see Annex A) presents a lithium iron phosphate battery for energy storage system of 6,000 cycle life at a rated DOD of 0.90. On the other hand, Figure 2.3 (another manufacturer) illustrates a lithium-ion battery of 6,000 cycles for a DOD of 1.00 (as subtitle information). Therefore, the rated DOD can be a lower bound ( $\underline{SOC}$ ) for the SOC so that the cycle life can be achieved. Furthermore, according to Lawder et al. (2014), operating at a full state of charge can be dangerous for a battery. Therefore, an upper bound ( $\overline{SOC}$ ) of SOC can be established for daily operations to prevent this situation.

In storage systems, the process of converting energy from one form to another, and then recovering it in its original way is named round trip (RODRIGUES et al., 2014). Thus, for batteries, it is the process of convert electrical energy into chemical and, after into electrical again. Knowing the efficiency of this process is relevant to model the operation of a storage system over time. Figure 2.4 presents the concept of round trip efficiency (RTE) addressing the stages of charge, discharge, and storage. The charging process occurs during  $\Delta t$  hours with a constant power input  $P_{chr}$  and efficiency  $\eta_{chr}$ . During the storage period, the battery loses charge. Thus, at this stage, the efficiency  $\eta_{sto}(t)$  depends on the storage time  $t$ . The discharge stage has the same time window of charging, an efficiency  $\eta_{dch}$ , and a power weighted by the efficiency of the three stages.

Therefore, defining the energy that leaves the electric bus in the charge stage

Figure 2.4 – The round trip concept for batteries.



Source: The author (2022).

as energy input, and energy recovered as the energy that reaches the electric bus in the discharge stage, the round trip efficiency is

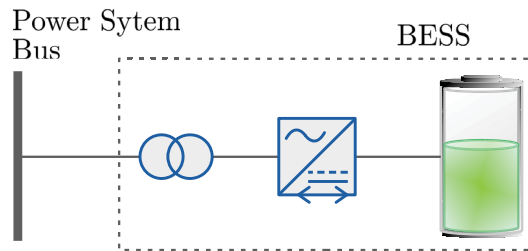
$$RTE = \frac{\text{energy recovered}}{\text{energy input}} = \frac{\eta_{chr} \eta_{sto}(t) \eta_{dch} P_{chr} \Delta t}{P_{chr} \Delta t} \quad (2.4)$$

$$\implies RTE = \eta_{chr} \eta_{sto}(t) \eta_{dch}$$

Storage efficiency is critical in systems that need additional energy to maintain its charge. The SMES (superconducting magnetic energy storage) technology, for example, needs energy for cooling the system at around  $-270$  °C, which reduces its  $\eta_{sto}$  (RODRIGUES et al., 2014). On the other hand, batteries can present a high  $\eta_{sto}$ . According to Palizban and Kauhaniemi (2016), lithium-ion batteries can present a energy loss of 5% per month. Divya and Østergaard (2009) stands that lead-acid technology has a self-discharge of 2-5% per month, and lithium-ion 1% per month. A self-discharge of 1, 2, or 5% per month implies a per hour storage efficiency of 0.988862, 0.995613, or 0.997818, respectively. Thus, for batteries,  $\eta_{sto} \approx 1$  in Equation 2.4 can be a good approximation. Moreover, in practical applications is usually to consider  $\eta_{chr} \approx \eta_{dch} = \eta_{bat}$ , which results in,  $\eta_{bat} \approx \sqrt{RTE}$ .

Connecting a battery system to an electrical bus requires a power converter, as shown in Figure 2.5. Furthermore, depending on the power bus voltage level, this connec-

Figure 2.5 – Diagram of connecting a BESS to an electrical system bus.



Source: The author (2022).

tion may demand a coupling transformer. In Brazil, as shown in Figure 2.1, BESS with rated power greater than 75 kW can be connected in MVD, and those with rated power greater than 500 kW must be connected in MVD. These cases require a coupling transformer. However, the converter and transformer impact the round trip efficiency. Thus, the overall charging and discharging efficiency of the BESS will be  $\eta_{bess} = \eta_{bat} \eta_{conv} \eta_{tfr}$ , where  $\eta_{conv}$  is the efficiency of one direction of the converter, whether charging or discharging, and  $\eta_{tfr}$  the transformer efficiency. If there is no transformer,  $\eta_{tfr} = 1$ .

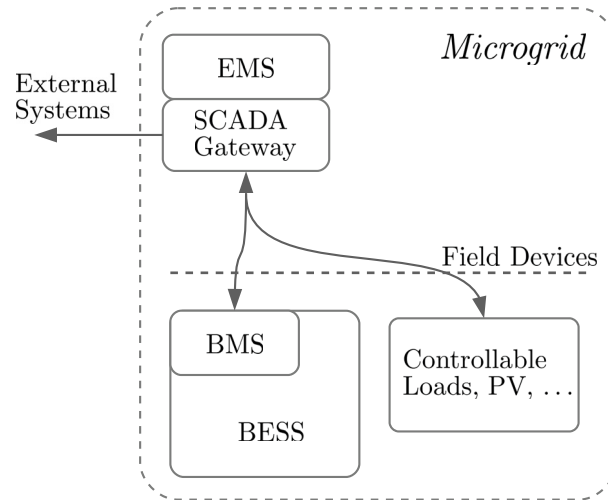
As an example, Figure A.2 (Annex A) illustrates a data-sheet of a converter for battery energy storage applications. According to the manufacturer (ABB, 2017), the efficiency of the converter is higher than 97%, and the joint efficiency of the converter and transformer is greater than 94%.

### 2.1.2.1 Battery Management System

A BESS needs a battery management system (BMS) to monitor and control the battery pack in real-time. It is responsible for estimating the SOC and SOH of the system and acting to minimize the temperature gradient and battery degradation, providing battery safety and longevity. It has voltage, current, and temperature as measured variables and current as a manipulation variable (LAWDER et al., 2014). Also, according to IEEE Std 2019.2.1™ (IEEE, 2019), BMS should provide reliable protection for battery packs (overvoltage, overcurrent, overtemperature, etc.).

Figure 2.6 shows what can be a schematic diagram example of a microgrid supervisory control. BMS typically passes the information on the status of BESS (such as SOH, SOC, temperature alarm, etc.) to the EMS and receives control signals from it (charging and discharging power), through the SCADA (supervisory, control and data acquisition) gateway.

Figure 2.6 – Schematic diagram of a microgrid supervisory control.



Source: The author (2022).

### 2.1.3 Controllable Loads

Controllable loads (CL) can play a fundamental role in microgrids. They can be used as a resource to control the microgrid frequency in emergency cases (fast response) (REBOURS et al., 2007), and to achieve an optimized operating point of the microgrid. In addition, controllable loads, energy storage and distributed generation can together give more resiliency to the main grid in disturbance events.

Regarding control, domestic loads can be classified as (OLIVAL; MADUREIRA; MATOS, 2017; SOARES; GOMES; ANTUNES, 2012):

- noncontrollable loads: loads that can not participate in any type of automatic demand response actions, because it can cause discomfort to the consumer if they were switched off or shifted;
- interruptible loads: domestic loads that “can be switched off for short period of time without compromise the quality of service and consumer habits” (OLIVAL; MADUREIRA; MATOS, 2017);
- shiftable loads: loads whose working cycle can be anticipated or postponed during a day. For example, they can be shifted from peak hours to periods with high distributed generation levels, with no relevant impact on the consumer habits.

Therefore, interruptible and shiftable loads are controllable. Daily, the microgrid controller has to decide when, where, how much, and for how long it should connect (or disconnect) controllable loads.

Siebert (2013) presents two models of demand response: incentive-based and price-based. In the former, the consumer responds to requests or actions from the utility or microgrid operator. Already in the latter, the customer makes his own decision to participate, influenced by the price of electric energy. The concept of controllable loads fits the incentive-based demand response definition. Direct load control, interruptible/curtailable load, emergency demand response, and ancillary service market are examples of incentive-based demand response programs quoted in (SIEBERT, 2013; VARDAKAS; ZORBA; VERIKOUKIS, 2015). The microgrid controller can manage them as interruptible or shiftable loads, as defined in (OLIVAL; MADUREIRA; MATOS, 2017; SOARES; GOMES; ANTUNES, 2012).

According to Vardakas, Zorba and Verikoukis (2015), incentive-based demand response programs are more suitable for industrial consumers. However, for microgrids, the participation of residential consumers can have an equivalent impact on that programs, although a microgrid can also have industrial consumers.

Finally, throughout the present research, it can be more appropriate to use the term controllable loads and not the term demand response. The latter addresses more elements than the present study intends to cover.

## 2.2 IEEE Std 1547™ Series of Interconnection Standards

The interconnection of distributed resources with the electric power system has been the subject of the IEEE Standard 1547™ series of interconnection standards. They are guidelines on the interconnection and interoperability specifications, and requirements for distributed resources. Also, they address questions about the operation, control, protection, maintenance, design, information exchange, and monitoring of DR. Such standards are, by extension, applicable to microgrids because they must have distributed resources. According to IEEE Standard 1547.4 (IEEE, 2011), the terms DR islanded systems and microgrids are equivalent. However, it is worth mentioning that such standards have been developed for interconnecting DERs in general, and microgrids are a specific case of DER interconnection.

The IEEE 1547-2018 defines two cases of DER islanding (IEEE, 2018):

- 1) Unintentional islanding: when a DER energizes an EPS island area unintentionally, i.e., an area for which the DER was not designed.
- 2) Intentional islanding: when a DER provides power to an EPS island area for which it was designed and prepared previously. It also referred by the IEEE (2018) as microgrid operation.

- a) Scheduled intentional islands are formed by manual action or other operating dispatch means, e.g., energy management systems.
- b) Unscheduled intentional islands are formed by action of protection relay when it detect abnormal conditions at the interconnection point.

This definition can be extended to microgrids by analogy. A microgrid can participate in unintentional islanding when an event in the main system (e.g. a fault) causes an interruption of power supply to an area of the EPS in which the microgrid is located. Then, microgrid starts to supply power for the whole islanded area, meeting a demand for which it was not designed. Scheduled intentional islanding can occur when the distribution system operator, or the microgrid operator, act at the point of common coupling (PCC) disconnecting the microgrid from the main system. Finally, unscheduled intentional islanding can occur when the microgrid protection or control devices detect some abnormality condition (e.g. an external fault or a deviation of frequency) in the main system and perform the disconnection of it, preserving the power quality within the microgrid area.

## 2.3 Microgrid Control

A microgrid control scheme should meet some basic requirements; it has to

- allow operation of a microgrid in both connected and islanded mode;
- perform smooth transition (with no loss of load) between the two operating modes;
- provide amplitude and frequency voltage within a desired range of values;
- share the total load between parallel generation units;
- ensure voltage and frequency stability;
- control the power flow between the microgrid and main grid;
- perform scheduled and unscheduled intentional islanding;
- manage controllable loads;
- manage the charge and discharge of energy storage systems.

Antoniadou-Plytaria et al. (2017) and Yazdanian and Mehrizi-Sani (2014) classify control schemes based on their communication characteristics:

- centralized control: the controller is located at a central coordinator that receives measurements from local meter devices (e.g., smart meters) scattered across the grid, and use them to solve the control problem. Then, the resulting set-points are communicated to the intelligent electronic devices (IED) at the DG units;
- decentralized control: the controllers are intelligent electronic devices and there is no communication among them. They only use local measurements to solve the control problem. Decentralized control is also known as local control (ANTONIADOU-PLYTARIA et al., 2017);
- distributed control: there is no central coordinator and the IEDs are in communication only with their neighbors. Thus, together they can reach the goals that have been set by the grid operator or the end-user.

In microgrids, the generation units can be scattered over a wide geographic area (GUERRERO et al., 2013). Thus, the requirement of communication between the generating units and the central controller can be a drawback for centralized control schemes. Other issues such as the need to redesign the controller when there is a change in a unit; computation burden, and common point of failure (central controller) are additional drawbacks of this control scheme (YAZDANIAN; MEHRIZI-SANI, 2014).

Decentralized control presents fast response to variations in DG and is not affected by communication failures (ANTONIADOU-PLYTARIA et al., 2017). On the other hand, stability on a global scale is a critical issue when each interface is controlled based only on local measurement (GUERRERO et al., 2013). Yazdanian and Mehrizi-Sani (2014) cites a real case that shows if each subsystem tries to guarantee its own stability, then the overall stability can be affected.

Distributed control approach provides plug and play capability and make possible a self-organized power grid (ANTONIADOU-PLYTARIA et al., 2017). It makes possible to decompose a large problem into several smaller problems using less computational burden. In a microgrid environment with several generation units and various control strategies, the distributed control approach can make a difference to a workable solution (YAZDANIAN; MEHRIZI-SANI, 2014).

The European Network of Transmission System Operators for Electricity (2009) organizes its control actions in a hierarchical classification within its synchronous area. They are performed in three different levels named as primary, secondary and tertiary. Each one has its own characteristics and qualities, but all depend on each other. This classification has been used successfully in large interconnected systems, with the assumptions of large synchronous machines with high inertia and inductive networks. On the other hand, there is no inertia in the sources of distributed generation connected to the distribution network. Besides, the assumption of purely inductive networks is not suitable



to model microgrids (GUERRERO et al., 2013). Hence, the hierarchical classification has been adopted for microgrids, but taking into account the differences between systems.

In a microgrid, each distributed generation and energy storage system unit is connected to the distribution network through a voltage-source inverter (VSI), and all units are in parallel. Primary control is the local control on each VSI. With the fastest response, this control level responds to the systems dynamics and it is responsible for stabilizing the system voltage and frequency at a stationary value (set points). Output power control, power sharing, and islanding detection are also assignment of this control level (YAZDANIAN; MEHRIZI-SANI, 2014). Primary control requires no communication and it is based on local measurements only. Droop control has been the preferred choice to apply at this level in scientific literature.

The secondary control can be used to compensate the frequency and amplitude deviations (long-term) after every change of load or generation inside the microgrid. Voltage frequency and amplitude of a microgrid without secondary control are load-dependent (GUERRERO et al., 2013). This control level provides the set points for the primary control (YAZDANIAN; MEHRIZI-SANI, 2014).

The tertiary control is the slowest one and provides long-term set points based on the microgrid status. It can manage the power flow when in grid-connected mode based on market signals and other system requirements. Besides, it can be used to manage multiple microgrids, forming a cluster (YAZDANIAN; MEHRIZI-SANI, 2014; GUERRERO et al., 2013). This control level can be considered part of the host grid.

The primary control level is essentially a decentralized control scheme due to its two main characteristics: lack of communication and use of local measurements only. On the other hand, the secondary and tertiary levels can be either centralized or distributed. According to Yazdanian and Mehrizi-Sani (2014), research works on secondary and tertiary control have moved from centralized to distributed control, mainly due to the high dependence of the communication link presented by the centralized schemes.

Yazdanian and Mehrizi-Sani (2014) pointed out four distributed control techniques that have been verified in research on microgrids:

- distributed model predictive control has been used to control reactive in unbalanced microgrids, adjust the voltage and reactive power set points to achieve a smooth voltage profile and reduce computational burden;
- consensus-based techniques have been used to solve distributed optimization problems and offer a flexible formulation that promises extendability and scalability;
- agent-based techniques have been used to state estimation in power systems, to address the limited knowledge of agent, achieve power balancing, and maintain voltage within the required limits;

- decomposition-based techniques, which is based on decomposing the original optimization problem into a number of sub-problems that are solved iteratively until convergence.

More recently, Mahmoud, Alyazidi and Abouheaf (2017) pointed out intelligent and adaptive techniques for microgrids control, which are reproduced here with application examples:

- particle swarm optimization has been used to power flow control and to provide optimized placement of DGs.
- fuzzy logic control combined with distributed control systems has been used to control load frequency, voltage, and power sharing in microgrids.
- neural networks have been used to control battery system in microgrid to eliminate load fluctuations.
- adaptive PI/PID controller with neural networks have been used to control voltage and frequency in distributed secondary control.
- adaptive sliding mode controller has been used to solve voltage and frequency fluctuations and the changes in customer demands.
- reinforcement learning has been used to handle load fluctuations in microgrids.

## 2.4 Microgrid Protection

The main objective of system protection is to provide quickly isolation of an area affected by a fault, so that the rest of the system remains as possible as intact or has minimized impact. To meet this goal, a system protection project must take into account five elements (BLACKBURN; DOMIN, 2006):

- i. Reliability: the ability of the protection system to perform correctly when required and to avoid unnecessary operation;
- ii. Selectivity: maximum continuity of service with minimum system disconnection;
- iii. Speed of operation: clearing a fault as rapidly as possible;
- iv. Simplicity: the ability to find out a minimum solution that meets the protection objectives;
- v. Economics: meet the protection objectives at a minimal cost.

Although a microgrid presents features of both generation and distribution of energy, its protection requirements are not fully met by the direct application of the conventional schemes of these two areas. Considered as an integral part of the distribution system, a microgrid may demand more elaborate protection techniques than those for conventional distribution networks. Its power generation units may respond to fault events differently than the conventional ones. Additionally, DGs can impact the protection performance already existing in a distribution system. These issues have motivated a number of scientific researches on microgrid protection (MEMON; KAUHANIEMI, 2015; GOPALAN; SREERAM; IU, 2014). Basically, the question is how to achieve the five project goals (already mentioned) in order to provide complete protection for microgrids during both grid-connected and islanded mode.

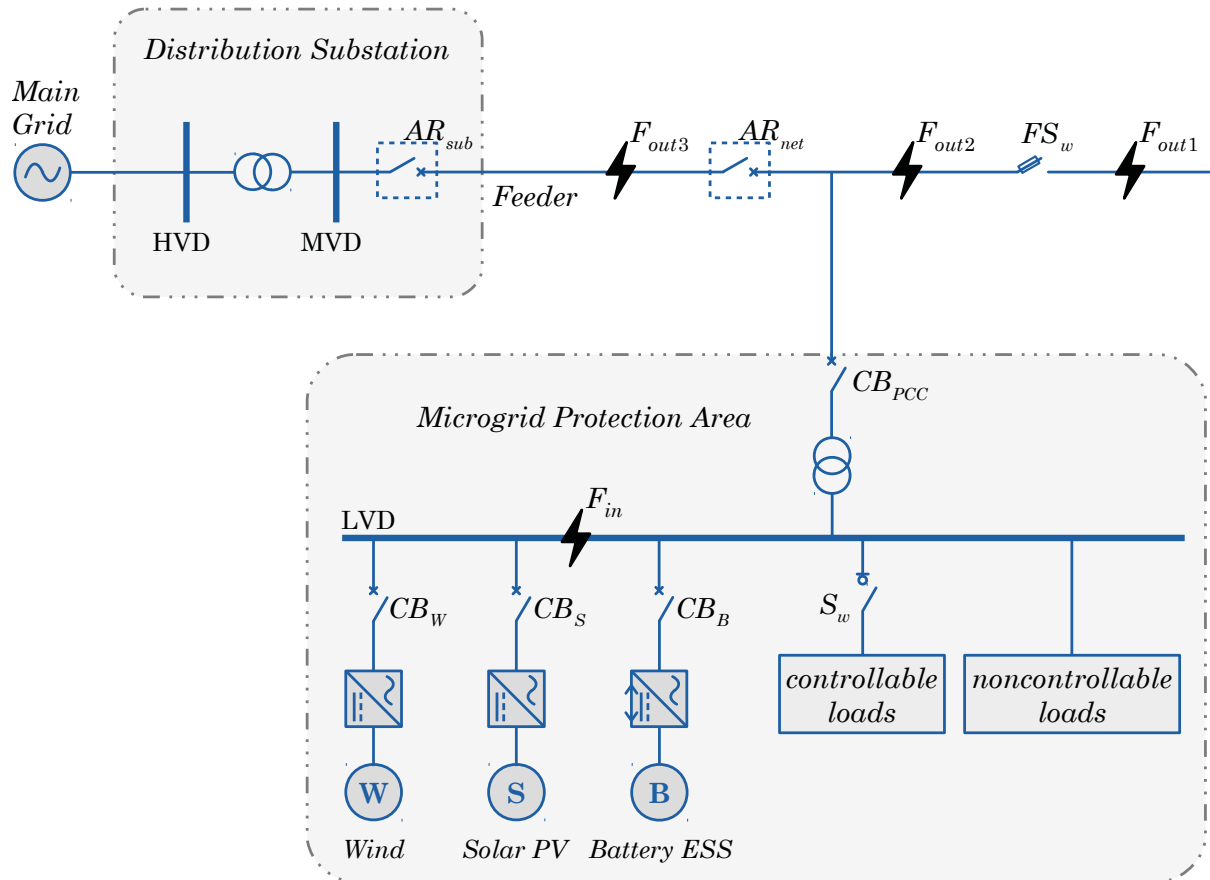
According to Gopalan, Sreeram and Iu (2014), a microgrid protection project needs to address the medium voltage (MV) side of the microgrid area, distributed generation, energy storage, and distribution transformers protection. Also, the authors stand that connecting DG to the power grid can impose some challenges regarding reliability and selectivity:

- The coordination between overcurrent protection devices is hampered by the bi-directional nature of the power flow within the distribution system;
- The IEEE Standard 1547.7 recommends that all DGs be disconnected in the event of a fault in the distribution system. However, such an action could affect the system reliability as the penetration of DGs increases;
- When the microgrid is islanded, the low fault current values (due to the limited contribution from the VSIs) may be insufficient to activate the overcurrent relays.

According to IEEE (2014a, p 46), inverter-based DRs are current limited under fault conditions and present low fault current contribution compared to rotating machines. The short-circuit current is generally limited to 1 or 1.2 times its load-carrying capability (IEEE, 2011, p 23). Active control methods used to protect semi-conductor switching devices in inverters (IEEE, 2014a) limit the fault current. Therefore, it is unlikely that selectivity (coordination of protective devices) can be established since the other protection devices usually trip at approximately 2 times their respective load rating (IEEE, 2011).

Consider a simplified distribution network diagram for microgrid protection analysis purposes as illustrated in Figure 2.7, where  $F_{out}$  represents a fault outside the microgrid area;  $F_{in}$  a fault inside the microgrid area;  $AR_{sub}$  and  $AR_{net}$  automatic circuit reclosers located at the distribution substation and along the distribution network, respectively;  $FS_w$  a fuse-switch;  $CB_{PCC}$  a point of common coupling circuit breaker;  $CB_W$  and  $CB_S$  inverter-based DG representative circuit breakers;  $CB_B$  a battery energy storage system representative circuit breaker; and lastly,  $S_w$  a controllable loads representative

Figure 2.7 – A simplified distribution network diagram for microgrid protection analysis purposes from the point of view of selectivity.



Source: The author (2022).

switch. An analysis from the selectivity point of view addressing external and internal fault cases and considering both the intentional islanding and the interconnected condition is shown in Framework 2.1. This framework matrix exposes some issues regarding the impact of the MG on the distribution system protection, the choice of conventional overcurrent to microgrid protection, and the unintentional islanding cases.

The impact of this illustrative MG on the distribution system protection and operation is emphasized by the comparison between the interconnected and islanded condition Framework 2.1 rows. The intentional islanding condition can represent by analogy a (conventional) distribution system with the absence of MGs. In this example, the distribution system protection project should take into account the coordination with the MG and the bidirectional power flow added by the DRs to achieve selectivity and reliability. In addition, there are indications that the MG needs, in addition to synchronization, a permission signal to connect to the main system. For example, MG should not connect to main system during the execution of an reclosing cycle of  $AR_{net}$  or  $AR_{sub}$ .

During an external fault event like  $F_{out1}$ ,  $F_{out2}$  or  $F_{out3}$ , an unintentional islanding condition can happen, where the microgrid starts to supply power to a distribution network area, including the  $F_{out}$  one. Although, central inverters manufacturers can provide individual built-in anti-islanding protection, as illustrated in the Annex B, when inverter-based DR are inside a microgrid area as Figure 2.7 indicates, according to the selectivity protection criteria, is desirable that the protection scheme only acts on  $CB_{PCC}$ , disconnecting the MG from the main grid while keeping DG and energy storage system supplying power to the microgrid. Thus, the primary anti-islanding protection should act only on  $CB_{PCC}$  and the built-in anti-island protection of each central inverter should act as backup protection. Finally, the IEEE Standard 1547 (IEEE, 2003) establishes DR systems must be able to detect an unintentional islanding condition and must disconnect (trip) from the system in no more than two seconds of the island formation. Considering that the automatic reclosers present in the distribution system usually have cycles with auto-reclose times longer than 2 seconds and they must be coordinated with the downstream fuses (fuse saving scheme), then complying with this IEEE standard requirement may mean disconnecting the MG for any fault event, temporary or not. This can become a reliability problem for the power system as DR penetration increases, besides to increasing the number of openings and synchronization of the PCC circuit breaker. However, the automatic reclosing has been considered in the latest version of the standard (IEEE, 2018, p. 65) by extending this time up to 5 seconds.

For the  $\{F_{out}, \text{Interconnected}\}$  set of cases, the choice of conventional overcurrent protection at  $CB_{PCC}$  seems not to be adequate to achieve the protection objectives of reliability and selectivity. On the other hand, the action of clearing the fault is mostly attributed to the DSO. Then, the resulting absence of a main source after the DSO action can activate the anti-island protection by isolating the microgrid. As a consequence, both the MG would be dependent on a successful action of the DSO, as well as would be subject to the performance times of it. Finally, more sophisticated protection techniques have been recommended in the case of intentional islanding with internal fault (MEMON; KAUHANIEMI, 2015; GOPALAN; SREERAM; IU, 2014) for the reasons already mentioned.

Framework 2.1 – An explanation matrix for selectivity analysis purposes based on the microgrid operational condition combined with the fault locations from Figure 2.7.

		Fault Location		
		$F_{out1}$	$F_{out2}$	$F_{out3}$
Microgrid Operational Condition	Intentional Islanding	<p><b>Primary protection:</b> a trip signal can be sent to the <math>CB_W</math>, <math>CB_S</math>, and <math>CB_B</math> breakers to clear the fault. <b>Backup protection:</b> built-in central inverters protection. <b>Obs.:</b> the low fault current value of the inverter-based DRs may be insufficient to activate the traditional distribution overcurrent relays.</p>	<p><b>Primary protection:</b> trip on <math>FS_w</math> with MG interconnection allowed. <b>Backup protection:</b> relay at <math>AR_{net}</math> set to trip and the MG interconnection is denied.</p>	<p><b>Primary protection:</b> relay at <math>AR_{net}</math> is set to trip and the MG interconnection is denied. <b>Backup protection:</b> relay at <math>AR_{sub}</math> is set to trip and the MG interconnection keep denied;</p>
	Interconnected	<p><b>Primary protection:</b> relay at <math>CB_{PCC}</math> is set to trip and a trip signal can be sent to the <math>CB_W</math>, <math>CB_S</math>, and <math>CB_B</math> to clear the fault. <b>Backup protection:</b> relay at <math>AR_{net}</math> is set to trip. <b>Obs.:</b> the fault current contribution from the main grid on the PCC is high enough to sensitize the overcurrent protection.</p>	<p><b>Primary protection:</b> trip on <math>FS_w</math> and the MG may keep interconnected. <b>Backup protection:</b> relays at <math>AR_{net}</math> and <math>CB_{PCC}</math> are set to trip (unscheduled intentional islanding). <b>Obs.:</b> the fault current contribution from the microgrid on the PCC may not be high enough to sensitize the conventional overcurrent protection and an unintentional islanding can happen.</p>	<p><b>Primary protection:</b> relays at <math>AR_{sub}</math> and <math>AR_{net}</math> are set to trip. <b>Backup protection:</b> protection at <math>CB_{PCC}</math> (unscheduled intentional islanding) or substation internal protection is set to trip. <b>Obs.:</b> the fault current contribution from the microgrid on the PCC may not be high enough to sensitize the conventional overcurrent protection and an unintentional islanding can happen.</p>

Source: The author (2022).

Protection projects need to consider both the protection coordination strategy and the protection scheme. The former is necessary to coordinate the operations of primary and backup protection schemes. The latter refers to the method used to detect a fault and send a trip signal to the circuit breakers. In order to address the MG protection issues, several coordination strategies and protection schemes have been proposed in the scientific literature (MEMON; KAUHANIEMI, 2015; GOPALAN; SREERAM; IU, 2014). According to Gopalan, Sreeram and Iu (2014, p. 227), communication-based and time grading are the two main coordination strategies for use in MG. Faster fault clearing times are achieved if communication is employed as a coordination strategy, but the failure or availability lack of it can cause a reliability issue. On the other hand, time grading is more reliable by not using communication; however, it presents a slower operating speed. It should be emphasized that slow speed response of protective devices can cause a loss of MG stability due to faults on the main grid or within MG protection area; the sensitivity of the DG to a voltage dip caused by a fault event may compromise the MG stability (MEMON; KAUHANIEMI, 2015).

Some features can be relevant in the choice of the protection scheme to MG, such as topology: radial or ring; DG connection mode: directly coupled and/or inverter-based; operating mode: islanded and/or interconnected; type of faults: LLL (line-to-line-to-line), LLLG (line-to-line-to-line-to-ground), LL (line-to-line), LLG (line-to-line-to-ground), LG (line-to-ground) and HIF (high impedance fault); and load unbalance. Memon and Kauhaniemi (2015) have reviewed available solutions to microgrid protection schemes considering both modes of operating:

- Adaptive protection: a microgrid central controller (MGCC) updates the protection settings according to the microgrid operational mode by using a communication link. This scheme is based on numerical directional overcurrent relays with directional interlocking.
- Differential protection: a scheme based on the principle of differential current. Different techniques such as relays of overcurrent, synchronized phasor measurement, or overcurrent combined with under voltage protection, have been proposed. All of these techniques use communication link.
- Distance protection: an admittance-based scheme in which each relay has three protection zones. It is capable of detecting fault currents even with lower magnitudes (considering inverter-based DG).
- Pattern recognition schemes: a differential energy-based protection scheme using a modified S-transform. The differential energy is obtained by means of a time-frequency analysis of fault currents at both ends of the faulted line and used as an indicator for fault patterns recognition in the MG.



- Current traveling waves: a scheme that use the changing in the frequency of the power voltage signals at local bus bar to detect a fault, as well as current traveling waves to find the fault location.

The results in (MEMON; KAUHANIEMI, 2015, p. 28) have shown some features about the schemes:

- The use of the overcurrent technique is usually related to the presence of directly coupled DG since it presents a relevant contribution to the fault current. This is the case in the adaptive directional overcurrent protection and in the differential schemes;
- Load unbalance is a feature present in microgrids that can be an issue for the differential protection scheme. On the other hand, the current traveling waves protection scheme is immune to load unbalance, as well as it can allow plug-and-play generators and both modes of operating;
- The most of the protection schemes address some types of faults and ignore some others. Only the pattern recognition based scheme addresses all the fault types;
- In addition, HIF is also an issue to be solved in most of the protection schemes, as in the distance and the adaptive protection ones;
- In all of the presented protection schemes, communication dependence is a factor to be considered.

## 2.5 Multi-Microgrids

When a group (at least two) of multiple microgrids can be operated and controlled by the system operator in a coordinated way, where is possible to take advantage of an existing electrical connection between such microgrids, or between them and the main grid, or a mix of both, such a group has been called multi-microgrid systems (ZHAO et al., 2018), or microgrid cluster (BULLICH-MASSAGUÉ et al., 2018; HAN et al., 2018), or even networked microgrids (ALAM; CHAKRABARTI; GHOSH, 2019; GAO et al., 2018). The advantages of MMG go beyond the well-known advantages of individual microgrids since the association of multiple microgrids can result in additional benefits. Microgrids belonging to an MMG can provide support to each other in the occurrence of contingencies. Hence, when operated in a coordinated way with the distribution management system (DMS), an MMG can improve the operational stability and efficiency of a distribution system, and increase its reliability and resilience (BULLICH-MASSAGUÉ et al., 2018; ZHAO et al., 2018; ALAM; CHAKRABARTI; GHOSH, 2019).



The operator of an MMG system may be the distribution system operator, or an Independent System Operator, i.e., an entity authorized by a federal regulatory agency to operate and control such a regional area of the grid (independent of commercial interests), or even the owner of the MMG (probably with commercial interests). Each MG can have an operator, just as MMG has one, and all of them must work in coordination with the distribution system operator. However, an energy management system, whose real-time decisions are made automatically and free from human intervention, can perform the operation of a single MG and an MMG.

Figure 2.8a shows a schematic diagram of an MG which contain distributed generation, controllable and uncontrollable loads, energy storage, and intelligent metering devices, all distributed across multiple buses. The power flow within the MG can be bidirectional because there are two distinct points of connection to the external network and also the distributed generations. In addition, the figure shows a bus for control signals and another for measurement, both connected to a microgrid control center. Hence, this MG has a centralized control considering communication aspects.

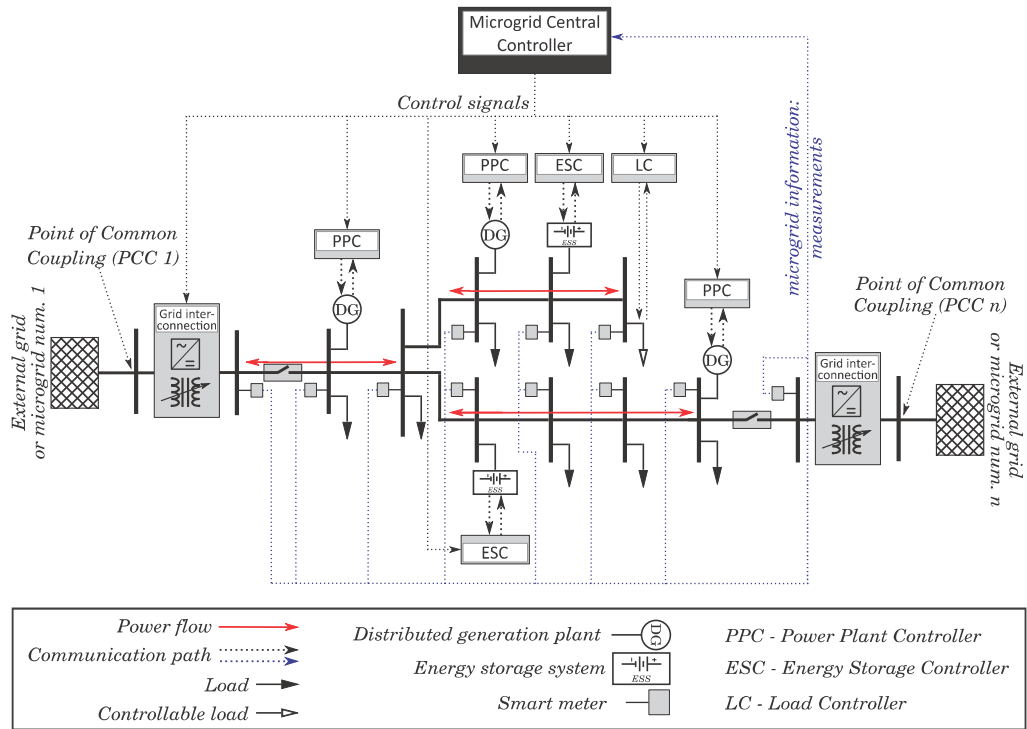
However, in the modeling of distribution systems involving MMG, it may not be necessary to represent an MG with this high level of detail. In fact, it may be more appropriate to represent it by an equivalent schematic diagram containing a single controllable bus, as shown in the Figure 2.8b.

The idea is to represent the microgrid as a single controllable entity (BULLICH-MASSAGUÉ et al., 2018), which can both generate energy to the external grid or consume energy from it, depending on the control signals of an external entity and its current generation capacity and consumption. That was the technique used by Bullich-Massagué et al. (2018) to propose three types of MMG layouts and to analyze them without concern for the internal details of each MG unit, as illustrated in Figure 2.9.

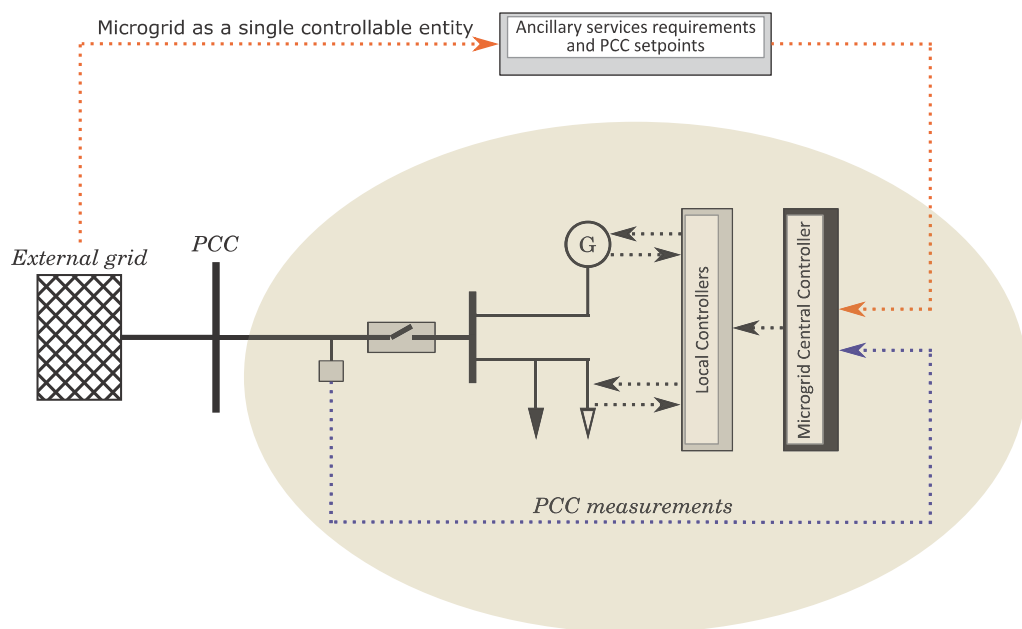
In those layouts, MGs may be interconnected directly with one another, or through the external network, or a mix of both. Each MG can operate in low voltage of distribution or medium voltage of distribution. In addition, a single MMG can have both MGs in LVD and MVD, including the possibility of direct interconnection between them.

In the layout illustrated in Figure 2.9a with parallel connected microgrids (PCM), all MGs are connected to the external network through a single point of common coupling. Thus, any power flow between MG must necessarily pass through the external network. In this type of configuration, there must be an external energy management system that sends control signals to each MG regarding the dispatch of energy at its respective PCC. The objectives of this control can among others be to improve the voltage profile in the external network, minimize losses in the external network, relieve distribution lines, or even maintain power supply in the whole MMG in case of loss of the external main source. In the latter case, an MG that is not self-sufficient in power supply can benefit from another that has an excess of available generation. From a commercial point of view,

Figure 2.8 – Microgrid schematic diagrams.



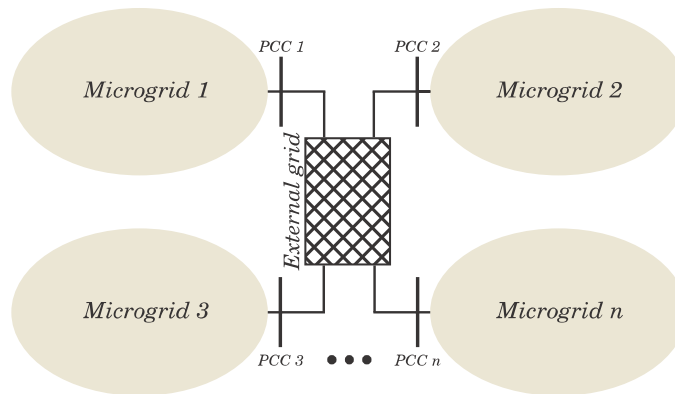
(a) An MG with the indication of control and measurement signals, and power flow.



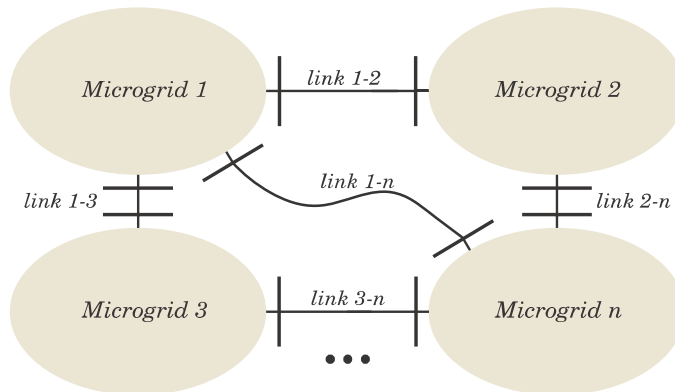
(b) An equivalent schematic diagram of an MG as single controllable bus.

Source: Bullich-Massagué et al. (2018)

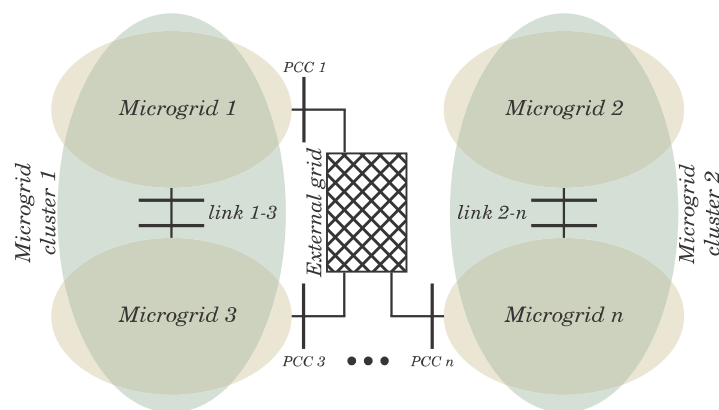
Figure 2.9 – Multi-Microgrids layouts.



(a) Parallel Connected Microgrids - PCM



(b) Grid of Series Interconnected Microgrids - GSIM



(c) Mixed Parallel-Series Connection - MPSC

Source: Bullich-Massagué et al. (2018)

there may be energy transaction between internal elements of a single microgrid of the group, between microgrids, and between elements of different microgrids, provided that there is a regulatory framework available.

Figure 2.9b shows an MMG layout in which the MGs form a grid of series interconnected microgrids (GSIM). Such an MMG architecture does not have interconnection with an external grid. That absence of the main grid brings some additional challenges to the MMG, among which are the self-sufficiency in power supply; EMS capable of controlling the voltage and frequency of the grid as a whole, besides controlling the power dispatch of each MG; inertia enough to ensure the stability of the grid as a whole. Although each MG has at least two PCCs, each one must be oversized, because if the power flow in a distribution line is interrupted (contingency), then the power flow in a PCC can increase considerably. One additional advantage of the GSIM architecture lies in its reliability since it supports N-1 contingencies, i.e., it can maintain its stability and power supply even with the loss of one distribution line (named link in the figure), provided that the MMG was designed considering this requirement.

The third and last architecture proposed by Bullich-Massagué et al. (2018) and presented in Figure 2.9c is the mixed parallel-series connection (MPSC), which combines features of the two previous architectures. From the PCM architecture, it inherits the good characteristic of being connected to a main grid, and from the GSIM architecture, it inherits the good characteristic of forming clusters of MGs that can operate independently of the main grid (disconnected) in case of contingency. However, the control of this type of MMG must be more sophisticated because at least three operating states are possible: the normal state where all the distribution lines are in their normal operating state; the contingency state with formation of MG clusters, and the contingency state with the islanded operation of one or more MG.

### 2.5.1 MMG as System of Systems

According to Maier (1998) a system of systems is a group of collaboratively integrated systems that have two additional properties:

- i) Elements with operational independence: each element (system) must be able to operate individually in the event of the dismemberment of the group;
- ii) Elements with independent management: the elements of the group must continually operate with management and goals of their own, which must be independent of those in the group.

Jamshidi (2008) analyzed and discussed several definitions of SoS in the literature to propose its own: “systems of systems are large-scale integrated systems that are

heterogeneous and independently operable on their own, but are networked together for a common goal”, which can be cost, performance, robustness, and so on.

One of the challenges faced by SoS theory lies in how to apply traditional systems engineering (SE) concepts such as analysis, control, estimation, design, modeling, controllability, observability, stability, filtering, and simulation in SoS (JAMSHIDI, 2008). This issue should be addressed by SoS engineering (SoSE), which according to (ISO; IEC; IEEE, 2019) “is the process of planning, analyzing, organizing, and integrating the capabilities of a mix of existing and new systems into a system-of-systems capability that is greater than the sum of the capabilities of the constituent parts”.

An MMG system fits the SoS definition, since each MG must collaborate with the group, but must also be able to operate individually in the event of a dismemberment of the group (for example a communication breakdown between the MMG and MGs controllers, or the occurrence of an MG intentional islanding), and must also have its own operational objectives (for example maximizing the profit of the MG subject to that restrictions imposed by MMG’s control). As a consequence, works involving MMG systems can make use of SoSE theory and take benefit from its development in the various fields of science.

According to Maier (1998), a system that meets both SoS criteria will necessarily be more costly compared to a monolithic system, because of its inherent redundancy. For example, in an MMG environment, if each MG tries to optimize its dispatch to reduce internal losses while the MMG tries to optimize the dispatch of each MG to reduce the losses of its distribution lines, then the result will not be as effective as if the optimization problem were solved in a unique and global way (a monolithic system).

However, there are situations where the MMG approach may be the difference between a solution being feasible or not. Bullich-Massagué et al. (2018) cite an example of MMG application in which there is an incentive for the installation of renewable DG that will result in a large growth of DG facilities in the assets of MVD and LVD. In that case, the control system of the DSO would not be prepared to absorb as many additional generation units. Consequently, the operation of the distribution network could be compromised. On the other hand, if MGs were created so that all DGs and loads within an MG could be managed as a single entity, then the DSO would be able to integrate such MGs into its control system without major problems. That is an example, which could be a real one, of a solution that becomes feasible due to the MMG system approach.

## 2.5.2 Community Microgrids

Clean Coalition (2015) defines a community microgrid as “a coordinated local grid area served by one or more distribution substations and supported by high penetrations

of local renewables and other distributed energy resources, such as energy storage and demand response”. Regarding its magnitude, a community microgrid can typically encompass the whole operating area of one or more feeders, i.e., an entire community, with high RES penetration and unlimited capacity to meet priority loads. A community microgrid has as its main motivation to benefit a local community economically, environmentally, and socially, in addition to increasing its resilience (GUI; DIESENDORF; MACGILL, 2017; CLEAN COALITION, 2015). It may comprise prosumers, prosumer-community groups, virtual power plants (VPP) and microgrids (GUI; DIESENDORF; MACGILL, 2017).

Regarding the control and operating structure, an energy management system that is capable of absorbing the large amount of DERs, VPPs, prosumers, and consumers, present in a community microgrid can be of high complexity. For each new element (DER) added to a community microgrid, a change to the entire network control and operating design must be required. One option to reduce this complexity is to divide such community microgrid into smaller microgrids that can be handled as a single entity. Thus, the MMG system approach can be used provided that the original objectives of a community microgrid are maintained.

### 2.5.3 Uncertainty Set For Forecasted Quantities

When an optimization problem involves data with some level of uncertainty, such as forecasted data or those with errors in the measurement process, the optimal solution additionally becomes a function of the uncertainties. Moreover, if such uncertainties impact the solution significantly, then they should be considered in the formulation of the problem. According to Ben-Tal et al. (1998), some methods have been proposed in the scientific literature to solve an optimization problem with uncertainty. Stochastic programming, for example, considers uncertainty as a random perturbation applied to the data (measured or forecasted), which requires determining the probability density function (pdf) of the uncertainty. As a consequence, the constraints are satisfied from a certain probability, as well as the optimal result.

Another method, proposed by Ben-Tal et al. (1998), improved in (BEN-TAL et al., 2004) and called adjustable robust optimization, assumes that an uncertain data belongs to an uncertainty set  $\Pi$ , with well-defined limits. In this case, the disturbance, although unknown, is limited. A solution satisfying the constraints for any perturbation in the admissible region  $\Pi$  is called robust solution. Thus, this method first seeks to maximize the uncertainty (worst case among robust solutions) and then minimize the objective function, which leads to a conservative but guaranteed solution. More recently, (ZHAO et al., 2018), (ZHANG et al., 2018), and (GAO et al., 2018) have used the adjustable robust optimization to solve a day-ahead scheduling problem in an MMG system, when considering uncertainties in the PV and WT output forecasted power. Gao et al. (2018)

also considers uncertainty in the forecasted load curve.

Consider a random perturbation for a power data ranging from an upper bound  $\Delta\bar{P}$  and a lower bound  $\Delta\underline{P}$ , which is added to a forecasted power  $\hat{P}$  to give a level of uncertainty to the resulting power  $P_\pi(t)$ , as illustrated in Equation 2.5.

$$P_\pi(t) = \underbrace{\hat{P}(t)}_{\text{forecast}} + \underbrace{\beta(t)(\Delta\bar{P}(t)\alpha(t) - \Delta\underline{P}(t)(1 - \alpha(t)))}_{\text{uncertainty}} \quad (2.5)$$

In this equation,  $\beta(t) \in \{0, 1\}$  has the function of enabling the uncertainty at the instant  $t$ , and  $\alpha \in \{0, 1\}$  the function of selecting the bound of uncertainty:  $\alpha = 0$  selects  $\Delta\underline{P}$  and  $\alpha = 1$ ,  $\Delta\bar{P}$ .

In this case, the vectors  $\alpha \in \{0, 1\}^N$  and  $\beta \in \{0, 1\}^N$  define the uncertainty set  $\Pi$  according to the Equation 2.6,

$$\Pi = \left\{ \alpha; \beta \left| \begin{array}{l} \alpha(t); \beta(t) \in \{0, 1\}, \quad \text{for } t = \{1, 2, \dots, N\} \\ \sum_{t=1}^N \beta(t) \leq b_\pi, \quad \{b_\pi \in \mathbb{Z} \mid 0 \leq b_\pi \leq N\} \end{array} \right. \right\} \quad (2.6)$$

where  $b_\pi$  is used to control the level of uncertainty from absent ( $b_\pi = 0$ ) until maximal ( $b_\pi = N$ ). This parameter is known as the budget of uncertainty and used in practice to control the conservative level of the model (ZHANG et al., 2018). A value of  $b_\pi = 7$ , for example, means that uncertainty can be added to the  $\hat{P}(t)$  only up to seven intervals of time.

## 2.6 Literature Review

### 2.6.1 Literature Review on Operation and Control of Microgrids

This section presents a literature review on operation and control of microgrids. Appendix B.1 shows in details the method used to select the scientific articles used in this review.

Mahmoud, Alyazidi and Abouheaf (2017) present a literature review on adaptive intelligent methods that have been applied to microgrid control systems. The authors state that although the PI/PID controllers are reliable and robust, their performance is highly dependent on the gain values. When the operating point of a system may change over time and thus require changes in the gain values (as in microgrid applications), from the authors' point of view, a self-tuning PI/PID controller could be used to overcome this drawback. In addition, authors state that model predictive control (MPC) has been used to eliminate the tracking error and steady-state error.



Antoniadou-Plytaria et al. (2017) present a review of control schemes applied to smart distribution networks with decentralized or distributed coordination among controllers. Authors address a classification of control schemes based on communication, namely: local, centralized, distributed, and decentralized control. From the authors' standpoint, distributed and decentralized are robust and flexible control schemes and can work even in a limited and low bandwidth communication environment, which is attractive for microgrid applications.

Han et al. (2017) present an overview of different strategies of active and reactive power sharing in hierarchical controlled microgrids. From the authors' point of view, when in islanded operation mode, if the conventional droop control scheme is adopted, the active and reactive power sharing can be an issue for a microgrid due to the influence of impedance mismatch of the distributed generation as well as the different power ratings of the generation units. As an alternative to the  $P$ - $f$  and  $Q$ - $V$  conventional droop control under resistive networks (as in low voltage microgrids), the authors presents some  $P$ - $V$  and  $Q$ - $f$  control schemes to share active and reactive power. In addition, to address the problem of reactive power sharing under nonlinear and unbalanced load conditions (secondary control), the authors analyze some algorithms based on intelligent techniques as multi-agent systems (MAS) and graph theory.

Han et al. (2016) present a critical analysis on various approaches to power sharing control schemes. From the authors' perspective, control techniques can be classified according to communication among controllers into concentrated, master/slave, and distributed. Particularly, the first and the last have a similar definition to that pointed by others authors, as Antoniadou-Plytaria et al. (2017). According to (HAN et al., 2017; HAN et al., 2016; EID et al., 2016), low voltage microgrid presents line impedance mainly resistive which can cause some troubles to the conventional droop control. Thus, the authors present some alternatives droop control schemes that are able to control voltage and frequency considering both the effects of active and reactive power jointly, or adding a virtual impedance in the loop control in order to avoid the active and reactive power coupling. The authors also present comparative tables among various control methods and conclude that it is difficult for a single control scheme to overcome all drawback for all applications. In addition, they also conclude that multi-agent control and hierarchical control are trending in research of microgrid technologies, and as a consequence, communication systems are becoming a key factor to make theses applications feasible.

Eid et al. (2016) suggest to characterize microgrids under 5 different aspects, such as AC or DC microgrid. It is emphasized that under the aspect of control they suggest to classify it in either centralized or decentralized. However, such decentralized control corresponds to the distributed control pointed out by other authors, as (ANTONIADOU-PLYTARIA et al., 2017; HAN et al., 2017; HAN et al., 2016). As a main contribution, the authors present a list of several different microgrid control objectives with a brief descrip-



tion of their respective problems and solutions, as well as their bibliographic references.

LI and NEJABATKHAH (2014) present an overview of interfacing converter topologies, energy management schemes, and ancillary services in microgrids. Authors point out that distributed generation with DC output power, as solar PV and fuel cell, is usually connected to local AC loads (AC bus) through either a single-stage converter (DC/AC) or double-stage (traditional solution) converter (DC/DC, DC/AC). According to the authors, the DC/DC stage (in double-stage topology) is a technique used commonly with PV solar systems to maximize power extraction (maximum power point tracking (MPPT) control), as well as make the DC voltage level suitable for the next stage. However, from the authors' standpoint, the single-stage topology is becoming more popular due to its greater efficiency, at the cost of less flexibility of control and a limited operating range. On the other hand, AC distributed generation, like a wind turbine, is typically connected to local AC loads by means of either a double-stage converter (AC/DC, DC/AC) or a multi-stage converter (AC/DC, DC/DC, DC/AC). In the double-stage topology, the AC/DC converter is used to control the DC bus voltage, which is the same function as a DC/DC converter in a multi-stage topology. In addition, according to the authors, the use of a multi-stage topology can be more cost effective although less efficient. LI and NEJABATKHAH (2014) also present a classification of energy management schemes in a microgrid, namely: centralized, decentralized, and communication-less control. Authors' definition to decentralized and communication-less control corresponds to the distributed and decentralized control definition in Antoniadou-Plytaria et al. (2017), respectively. Finally, regarding ancillary services authors pointed out once a distributed generation system does not operate at full capacity all the time, then it is also able to provide ancillary services for the electric grid. Two of them are emphasized in the article: compensation of grid voltage unbalance (due to unbalanced loads) and mitigation of system harmonics. From the authors' standpoint, through a suitable control scheme, the DG interfacing converters could be used to mitigate both voltage unbalance and system harmonics.

Tayab et al. (2017) present a literature review of droop control techniques applied microgrids. As in the other articles surveyed, the authors describe the conventional droop control and point out its disadvantages. Among them is the difficulty of providing reactive power sharing when there is impedance mismatch between inverters. Thus, the authors present the technique of using a virtual impedance (only in the control loop) to compensate for such impedance mismatch and thus solve that problem. Authors also make reference to adaptive droop controls. The basic idea is to use the current value of reactive power to dynamically set a droop curve (in-memory three options) at run-time that is most suitable for that power range. Simulation results considering a single phase microgrid with two 5 kVA inverters were presented by the authors, considering conventional, virtual impedance and adaptive droop control. According to the authors, the results show that adaptive and

virtual impedance controls minimize the impedance mismatch effect by improving the sharing of reactive power when compared to the conventional control. On the other hand, the virtual impedance technique presented degradation in the voltage regulation, as well as an increase in the voltage value when in a no-load condition. In addition, the adaptive control technique resulted in worsening both active power sharing and harmonics.

Dorfler, Simpson-Porco and Bullo (2016) present a review of primary, secondary and tertiary control strategies for microgrids, as well as make an analogy with the application of this type of control to bulk power systems. Then, the authors present an analysis of the behavior of frequency and voltage in microgrids after a disconnection of the main system. Such microgrid was modeled using the IEEE 37 bus network distribution model. Three types of control were analyzed through simulation by the authors in that scenario: conventional droop control, decentralized secondary integral control, and distributed averaged PI control. According to the authors, the simulation results during the islanding condition show that while the droop controller stabilizes the frequency at a value below the nominal, thus presenting a steady-state error, the other ones present a better performance reaching a stable value with no deviations from the nominal value; but both with different levels of power injection. Regarding the voltage, authors show simulations results with a similar behavior for the three controllers, i.e., curves converging to a stable (constant) value and close to the nominal one (1 p.u.).

Yazdanian and Mehrizi-Sani (2014) provide a study on distributed control techniques for microgrids. In addition, they present a discussion about the relationships between hierarchical and distributed control. The authors come up with a list of disadvantages that could limit the application of conventional droop control in microgrids. Among them, the partial coupling between active and reactive power; the influence of the output impedance mismatch of the inverters on the reactive power sharing, and the poor performance in nonlinear load conditions due to harmonics, can be emphasized. On the other hand, the authors acknowledge the existence of several published works with techniques that seek to overcome such limitations, such as virtual impedance in the case of impedance mismatch and nonlinear power sharing in the case of nonlinear loads. With respect to the distributed control, authors suggest that, in case of microgrids with several generation units, such a technique could make feasible a control solution that would be unfeasible in the centralized control. According to the authors, the distributed control could also reduce communication costs, besides facilitating the insertion of new generating units in the existing system, which would not require a readjustment of control parameters of the entire system. Regarding the hierarchical control applied to microgrids, the authors present their viewpoint on primary, secondary and tertiary control, which is not different from that other author's ones presented here. However, it is possible to emphasize that they assign to the primary control the function of detecting the islanding condition in order to activate the switching of the controllers to the islanding mode. The

secondary control, in turn, is called energy management system by the authors and would be responsible for interfacing with the distribution management system. In addition, from the authors' standpoint, a secondary control could have additional control objectives as voltage profile and reduction of losses. Yazdanian and Mehrizi-Sani (2014) also state that within the control hierarchy for microgrids, the distributed control is located only in the secondary and tertiary layer, since the primary control is predominantly accomplished without communication among the controllers. Among the distributed control techniques cited by the authors are distributed model predictive control, consensus-based techniques and those based on intelligent agents. According to the authors, distributed MPC has been used to control reactive power and voltage in microgrids as well as to control voltage limits in multi-area power systems. The consensus-based technique, in turn, has been used for the optimum economic dispatch of generation units in microgrids, because of its ability to reach a global optimum through a consensus-based approach without the need for a centralizing unit. Another application cited for this technique is the primary frequency control for multi-terminal high voltage direct current (HVDC) systems. Finally, according to the authors, multi-agent systems strategy have been used for hierarchical distributed control of microgrids in order to maintain voltage within the limits and to maximize economic benefits of the microgrid, as well as for secondary voltage control and economic dispatch. At the end of the paper, there is a list of current challenges, of which two may be emphasized: more research efforts are needed in cybersecurity and stability analysis.

Guerrero et al. (2013) present a review of microgrid decentralized control methods, including stability analysis as well as hierarchical control. In the literature review on decentralized control, the authors pointed out the advantages and disadvantages of the well-known droop control as well as their improvements. Regarding stability, from the authors' point of view, a microgrid system can be considered stable if it reaches a steady-state in which all voltages in the system present both amplitudes and relative phase angle differences constants. Authors pointed out that systems formed by radial microgrids, with inductive line impedance, and with frequency and voltage controlled by droop controllers, can reach steady-state stability for small signals independent of the size of the microgrid. However, according to the authors, the small signal stability depends on the operating point, which in turn, changes with a change in frequency or voltage. The authors also comment further studies on small signal stability for microgrids which indicate that both the voltage and angle stability can be achieved whether the control of the generating units inverters presents actions fast enough. It must be emphasized that some references of real-time hardware simulation of microgrid controllers are presented by the authors as investigation cases of microgrid stability. At the end of the paper, some control equations for primary, secondary and tertiary control are presented and discussed by the authors.

Palizban and Kauhaniemi (2016) make a comparison of energy storage technologies regarding storage capacity, time of response, time of discharge, and lifetime, in order to help industry and researchers determine an optimum storage technology for a given application. In addition, the authors analyze the possibilities for integrating different types of energy storage systems. Among the several electrochemical storage technologies presented by the authors, two of them can be emphasized: lead-acid batteries present high performance and are the most economical options for microgrids; lithium-ion batteries have rapid charge capability, high energy density, are maintenance free, and present a very low energy loss of about 5% per month; but their performance decreases at high temperatures. Regarding mechanical storage, the flywheel energy storage present some good features as low maintenance, long life cycles, no carbon emission neither toxic components and a very fast response. On the other hand, it presents a self-discharge rate of 3 to 20% per hour. According to the authors, compressed air energy storage systems have typical capacities varying from 50 to 300 MW; present a very high response time, and are able to store energy for more than a year (very low losses). However, they are very expensive. With reference to electrical storage, the authors make comments about the double layer capacitor (DLC) and superconducting magnetic energy storage. The former presents a high energy storage capability (from 0.1 to 0.5 MWh), but with a self-discharge rate of 5 % per day. In the latter, the energy is stored in a cryogenically cooled superconductor coil. From the authors' point of view, potential applications for energy storage are energy arbitrage, peak shaving, ancillary services, load following, spinning reserve, voltage support, black start, frequency regulation, power quality, and power reliability. At the end of the paper, there is a table where the authors suggest energy storage technologies that are suitable, possible, and unsuitable, for each application aforementioned.

Rodrigues et al. (2014) make an analysis of ESS benefits and applications with emphasis on islanded systems. Authors make comments on the Santa Rita Jail Microgrid where a 2 MW lithium iron phosphate battery was installed to work with a local renewable energy generation. In order to emphasize the importance of operation and maintenance (O&M) of ESS (for providing reliability and long life-cycles), authors pointed out a use case of lead-acid batteries at Metlakatla Island, which were replaced after 12 years, but still presenting good conditions. For additional information, authors present a table with several real cases of application of ESS in islands system with peak demand sizing from dozens of kW up to 195 MW. In these systems, regardless of size, the use of wind, PV, and diesel generation jointly with battery energy storage constitute the absolute majority of cases. According to the table, in the larger power systems, the use of advanced lead-acid battery is predominate, while in the lower power systems, the lead-acid batteries is the usually choice. In addition, the table contains the indication of renewable penetration level for some cases, as well as information about the battery energy-ratings and specific applications considered in each project. Finally, there also is information on economic

data of the projects in the table, as the total investment, implementation cost, and cost of replacement for some cases. The case of Bonaire Island (Netherlands), serving 14,500 consumers with wind and biodiesel power generation, as well as battery energy storage, is one example. The peak demand and the installed capacity are 12 MW and 25 MW, respectively, in which 14 MW are of biodiesel and 11 MW of wind energy, reaching thus a renewable energy penetration level of 100 %. In this project, a nickel-based battery EES of 0.845 MWh was used. The total investment was \$60,000,000.

Fossati et al. (2015) suggest an optimal method for determining the size of a energy storage system in a microgrid. The system model analyzed consists of a wind turbine, a microturbine, a fuel cell, two diesel generators, and an ESS. In total, the microgrid has an installed power of 200 kW and is connected to the main system through a 45 kVA transformer. The power management system is centralized. The authors present a wind turbine model with parameters values based on a commercial one, and an ESS model considering constraints, losses in charge and discharge, and a lifetime model. They also model the capital cost, as well as operating and maintenance costs in the ESS. The problem was formulated in order to minimize the sum between the average cost of dispatch and cost of capital. The former is associated with the average cost (or profit) of the energy exchange between the microgrid and the main system considering a time interval of 1 year. For this, a unit commitment problem must be solved for each day of the year (365 times). An expert fuzzy system was used to determine if the battery should be discharged or charged and at what rate. The authors evaluated the method using two scenarios: a microgrid in islanding mode and in connected mode. According to the authors, the results indicate that the optimum size of ESS would be 300 kWh for the islanding mode and 400 kWh for the connected mode. In the former, the existence of the ESS in the microgrid leads to a saving of 3.2 % in the average operating cost. In the latter, the economy reaches 14.1 %.

Arghandeh et al. (2016) try to clarify the definition of resilience for power systems and suggest their own definition of that term for cyber-physical systems. According to the authors, although there are previous definitions in the literature on resilience in power systems, there also are disagreements between them. In this paper, the authors try to highlight the differences and similarities between the terms resilience, robustness, reliability, and stability in power systems. The definitions presented by the authors can be better understood if they are illustrated by some examples (of my free interpretation). A distribution network that contains one or more microgrids becomes more resilient because, in the face of a system disturbance, as a feeder outage, it has the ability to reduce the magnitude and duration of the disturbance due to the microgrids islanded mode. Indeed, the system partially keeps its functionality while interrupting the power delivery for some consumers and maintain it for others. However, specifically for that microgrid consumers, the system can be considered more reliable because it has the ability to maintain

its functionality with acceptable quality and at the amount needed even when such a disturbance occurs. In addition, a distribution system when designed to contain microgrids or distributed generation may be considered a more robust system as it has the ability to maintain its functionality of power delivery even in the face of a disturbance. However, such a robust system may not be reliable if there is not adequate control of that generation sources, in order to maintain the quality of service. Finally, when a disturbance in a distribution system causes a disconnection of a DG unit, the operating point of that system can change, which can lead to voltage or angle instability. If the system supports such a change (by an adequate control for example) while maintaining its stability with voltage and angle within the preset limits, then it can be considered more reliable. On the other hand, if that system finds a new stable operating point but violating voltage limits, then it cannot be considered reliable because of the quality of energy criteria. According to the authors, cyber-physical power systems are a combination of physical and software grid components. Physical grid components examples are sensors, transmission lines, transformers, IEDs, etc; software grid components examples are control, state estimation systems, etc. Cyber-physical vulnerabilities are related with cyber intrusions that can cause physical damages to grid components and services. Thus, the authors suggest a definition to cyber-physical resilience: “a resilient power system responds to cyber-physical disturbances in real-time or semi real-time, avoiding interruptions of critical services. A resilient power system alters its structure, loads, and resources in an agile way”.

Memon and Kauhaniemi (2015) present a review of protection schemes applied to microgrids, as well as, address the main issues on the subject. Among the challenges that microgrid protection face of, authors analyze the coordination and selectivity of a distribution system with DG, and the microgrid protection in both grid-connected and islanded mode. According to the authors, conventional protection schemes usually used in distribution systems are not suitable to overcome those challenges. Therefore, the authors analyze some alternatives protection schemes as the adaptive, differential, and distance ones. According to the authors' conclusions, in order to cover all types of fault events in an effective way, and ensure a minimum supply disruption to consumers, the research on protection schemes to microgrid needs more effort.

Gopalan, Sreeram and Iu (2014) present a literature review of coordination strategies and protection schemes to a microgrid. The authors point out some challenges to be overcome in the protection of microgrid, among them the bidirectional flow caused by the insertion of GD in the distribution system and the low level of fault current presented by the inverters used in such GD insertion. According to the authors, to overcome such challenges it is necessary to employ alternative techniques to the use of conventional over-current protection and coordination schemes in the current distribution systems. In this paper, authors make a review of some strategies for coordination of primary and backup protection, including the time grading and communication-based ones. Among the works



reviewed by Gopalan, Sreeram and Iu (2014), there is one that suggests a solution of integrated protection and control, once the availability of communication infrastructure must attend both protection and control needs (centralized solution in this case). According to the authors, protection schemes to microgrid as voltage-based, admittance relaying, adaptive techniques, and differential zone protection have been proposed in the literature as an alternative to the conventional overcurrent one. From the author's standpoint, adaptive protection has good features as fastness, selectivity, and reliable operation. In addition, this scheme can adapt to changes in the microgrid configuration. However, it depends on the communication link, whose failure can compromise the scheme. The differential zone is a good promise because it presents effectiveness and low cost, but no test has been performed yet. Finally, voltage-based schemes are a good alternative to zone protection because are effective in both internal and external ones. On the other hand, it does not consider both symmetrical and high impedance faults.

### 2.6.2 Literature Review on Multi-Microgrids

This section presents a literature review on multi-microgrids. Appendix B.2 shows in details the method used to select the scientific articles used in this review.

Bullich-Massagué et al. (2018) make an analysis of microgrid cluster architectures. The authors point out that although there are already studies in the literature on the operation, control, and management of multi-microgrids, none of them systematically approaches the types of multi-microgrids architectures. Then the authors propose to identify, classify and analyze some architectures of microgrid clusters. Three different types of layout (how the MG are interconnected), two types of line technology (AC or DC), as well as two types of interconnection technology (transformers or inverters), are identified by the authors. So the proposed architectures are compared in terms of cost, scalability, protection, reliability, stability, communication, and business model throughout the paper. The authors conclude that for existing installations (current grid) the PCM and MPSC layouts with AC line technology are more indicated. In addition, the MPSC was evaluated by the authors as the best layout option because it presents a higher level of scalability, reliability, and stability at a reasonable cost. On the other hand, for areas not yet electrified (in planning), the authors visualize an opportunity for studies and applications of unconventional transmission and interconnection technologies, considering the specific requirements of each project. As a final conclusion, the authors indicate the need to carry out case studies of multi-microgrids architectures, which were not identified by them in their literature review.

Alam, Chakrabarti and Ghosh (2019) present a literature review on networked microgrids, addressing its various control strategies, communication technologies, and energy management techniques. Also, they discuss the benefits and challenges of networked

MG and future perspectives. According the authors, “networked MGs is referred to the interconnection of two or more MGs with an ability to connect DN to exchange power among the MGs and/or the DN at the point of common coupling”. Thus, networked MG and MMG are just different names for define the same concept. However, authors report that to date, real-field implementation of networked MGs are still in development. The types of MMG architecture presented in this paper are similar to those shown in (BULLICH-MASSAGUÉ et al., 2018). Regarding control, the authors compare the techniques of hierarchical (centralized) and distributed control. The latter, in the view of the authors, presents high reliability and flexibility, as well as the possibility of plug and play connections. Moreover, according to the authors, the distributed technique shows a lower complexity than the hierarchical one. On the other hand, the authors consider the distributed method sub-optimal from operating costs standpoint. Regarding the operation, the authors classify the EMS system into two levels. There is an EMS in each MG (the first level) whose function is to control loads, generating units and storage, to maintain voltage and frequency within its nominal ranges. The second level of EMS has the purpose of controlling external loads and external distributed generation. At this level, the economic dispatch is performed, and set-points of P and Q are sent to each EMS of the first level. Also, the second level of EMS receives set-points from the main grid operator (upper level). Regarding the benefits, the authors point to better use of DERs because the nearest MG can incorporate them; a reduction in overall cost due to DERs; the use of electric vehicles within microgrids for energy backup (ancillary service); and an improvement in the resilience and reliability of the power system. On the other hand, they indicate several challenges to be overcome as, issues of power system stability due to high penetration of DERs with uncertainties; a difficulty of achieving protection elements coordination along the feeder due to topology changes during a day, seeking the best performance for the overall system.

Mengelkamp et al. (2018) present a framework to design of microgrid energy market in terms of required components for successful market operation. Also, they give an overview of blockchain technology applied to microgrid energy markets. Besides, they present an implemented case study of a blockchain-based microgrid energy market: the Brooklyn Microgrid. According to the author, there are seven fundamental components for designing such a market: 1) Microgrid setup, where must be clearly defined the objective, the definition of market participants, and the form of energy traded; 2) Grid connection points for balancing energy generation and demand within the microgrid; 3) A high-performing information system to connect all market participants, providing market platform, access, and monitoring. From the authors’ standpoint, a blockchain protocol based on smart contracts can meet these requirements. 4) A market mechanism (implemented on the information system platform) for matching buy and sell orders in real time throughout well-defined payment rules and bidding format. 5) Pricing mechanism



(implemented via market mechanism) to efficiently allocating energy supply and demand. 6) Energy management trading system to guarantee energy supply for the participants, and to make feasible a specific bidding strategy. 7) Regulation, which defines how this market fit the current legislative rules. According to the authors, the Brooklyn Microgrid matches (fully or partially addressed) six of the seven components. Component seven was not addressed because peer-to-peer local microgrid energy market was still not legalized for that region. Authors conclude that the blockchain protocol can successfully implement and operate a microgrid energy market. Also, the Brooklyn Microgrid energy market is operational, but its design needs to be further evaluated.

Zhao et al. (2018) propose an SoS approach to modeling the energy management of an MMG system. The authors state there are few works in the literature modeling power engineering systems as SoS, as well as few works on energy management for MMG systems. According to the authors, previous works have not considered the intrinsic uncertainty from RES. Then, as a scientific contribution, the authors propose to add this uncertainty to the MG model, and for that, they use the robust optimization methodology (BEN-TAL et al., 2004) to solve the linear programming problem. With the ultimate goal of reducing the operating costs of a distribution network, an optimization problem with uncertainties was presented in the article. In fact, there are two optimization problems that are solved iteratively in the method proposed. In the former, the DMS system treats each MG with a single entity and aims to reduce both the cost of energy exchange between MGs and between the distribution network and MGs. In the latter, each MG central controller has the objective of reducing both generation costs (PV, WT, diesel, ESS, load shedding) and purchase of energy from other MGs and the distribution network. For each time slot (a day is divided into 96 of them) an optimal solution should be found. For this, there is an interchange of intermediate solutions (integrated optimization) between the DMS and the central controllers until there is convergence to the optimal solution (a convergence tolerance is required). Through the results of a case study with 3 MGs that fit into the PCM architecture of Bullich-Massagué et al. (2018), the authors conclude that it may be more costly to operate a distribution network with each MG operating independently than in a collaborative way (MMG). In addition, the results showed that the higher the uncertainty in RES, the higher the cost of operation, whether for an MMG system or for MGs operating independently.

Han et al. (2018) present a bibliographic survey on distributed control and optimization in MG and MMG. According to the authors, the multi-agent system technique based on consensus protocols has been widely used and recognized in academia to enable the distributed control in MG and MMG. However, the authors present more than two hundred cites in their work, each one accompanied by only a brief comment. In addition, the text is wordy and superficial, with repetition of various concepts, which makes it difficult to read and understand unless the reader is willing to read directly the more than

200 citations presented.

Zhang et al. (2018) formulate the question of operating an MMG system as a unit commitment problem. The authors point out that a scenario in which the microgrids operate independently exchanging energy only with the DN presents a cost of operation superior to the scenario where the microgrids operate in a collaborative way. The coordinated operation approach, as called by the authors, allows the MGs to exchange energy with the DN and with the other MGs. The scenario consists of several homes connected to the DN, each containing a rooftop PV, controllable loads, conventional loads and an electric vehicle that behaves as a storage unit. According to the authors, each house constitutes a microgrid (named home MG) and the complete system is called residential MMG. Each home MG has a local controller/inverter. All local controllers are logically connected to a central controller, called Aggregator, whose task is to optimize the operation of the MMG considering the energy price set by the distribution system operator, the costs of each home MG, and the energy demand. Commercial energy transactions (cash) are made only through the Aggregator, either between a home MG and the DSO or between two home MGs. On the other hand, each home MG is directly connected to the DN through its local controller/inverter, which plays the additional role of PCC.

Gao et al. (2018) propose a decentralized energy management framework for MMG operation. The authors consider in their model dispatchable distributed generation (micro turbine generator, MTG), controllable loads, energy storage, photovoltaic and wind generation, and conventional loads. The model contemplates a PCM-type MMG architecture and also considers MTG, WT, PV, and ESS connected in the external network. The external grid and MGs are different entities with their own individual objectives, but with a common purpose: to reduce the overall cost of operation. The authors modeled the uncertainties of PV, WT and load forecast using the same method presented in (ZHANG et al., 2018; ZHAO et al., 2018), although Zhang et al. (2018) and Zhao et al. (2018) have not modeled load forecast uncertainty. The robust optimization problem is solved in two stages using the constraint and column generation (CCG) algorithm. Tests were performed on the IEEE 33-bus model modified with three MG. The results show the convergence of the algorithm used and the consequent optimization of MMG costs.

Li et al. (2019) present a fully distributed control method for MMG, in which the primary, secondary, and tertiary control are based on MAS. The objective of this method is to perform the power sharing in the generation units, to control the frequency and voltage within the microgrids, to make the power balance within the microgrids, as well as the power balance of the MMG system. According to this method, a two-layer model is needed to accomplish MMG control. The first layer (top layer) is an agent-based communication network, where the rules of network constructing are elaborated. This layer is divided into two subgraphs: one used to the inside MG control and another to the MMG control. The second layer models the point of common coupling of each

MG. Beyond to show a systematic method to derive a set of distribution control laws for agents, this paper also presents a guarantee of convergence of these laws through a proposition of two theorems. Among the main advantages pointed out by the authors is the method's capacity of fault tolerance of different types of agents. According to the authors, the results of simulations performed in Matlab/Simulink show that the objectives were achieved even with variations in the loads and environmental conditions, and with the occurrence of an agent fail.

## **2.7 Final Considerations**

Both literature reviews presented in the previous sections contributed to elaborating a theoretical basis on distributed energy resources, microgrids, and multi-microgrids described in this chapter. It helped to identify the main DERs considered in the literature, how they are defined, and where they are applied. Also, it contributed to finding the state of the art on microgrid control and protection. It enabled the definition of the main concepts about the operation, control, and protection of MGs, based on the most relevant works on this subject. In the end, some questions about multi-microgrids were clarified.

# 3 Optimal Day-Ahead Scheduling of Microgrids

The research carried out on optimal day-ahead scheduling of microgrids resulted in the publication of the paper (SILVA; AOKI; LAMBERT-TORRES, 2020). Thus, this chapter is a reproduction of the first three sections of that paper:

1. Introduction - in addition to contextualizing the topic, this section presents a bibliographic review on optimal day-ahead scheduling of microgrids and lists the paper contributions.
2. Microgrid Energy Management System - to contextualize and thus limit the scope of the problem to be addressed, this section presents an overview of an energy management system for microgrids considering the day-ahead and real-time modules;
3. Modeling Methodology - this section presents a microgrid mathematical model to address the optimal day-ahead scheduling problem.

Furthermore, at the end of this chapter some energy management modeling techniques in multi-microgrids are discussed.

## 3.1 Introduction

The introduction of distributed energy resources in the distribution system has brought several benefits to consumers, utilities, and society. These include increasing system reliability and resilience, reducing greenhouse gases, relieving distribution and transmission systems, reducing energy tariffs for consumers who also produce energy (referred to as prosumers in (FARUQUI; BOURBONNAIS, 2020)), and the possibility of forming an energy market in which consumers and prosumers can participate actively. However, it also came with some challenges as the need to readapt distribution systems (infrastructure, automation, protection, control, operating systems, planning) to receive these new resources and to deploy modern energy tariffs to meet the equity criterion (FARUQUI; BOURBONNAIS, 2020), finding a trade-off between encouraging renewable sources while avoiding cross-subsidization between consumers and prosumers. Microgrids, as part of this new active distribution system, experience the same benefits and challenges; however, they have an additional purpose: being economically efficient, producing energy at the lowest possible cost while eliminating or minimizing waste.

A microgrid can contain loads and distributed energy resources such as distributed generators, storage devices, and controllable loads, and must be operated in a controlled way whether or not connected to the main grid (MARNAY et al., 2015b). With such resources, a microgrid can provide ancillary services to the distribution system operator, perform energy arbitrage (store energy when the price is low to sell it or use it when the price is high), actively participate in energy markets, in addition to participating in distribution systems with multiple microgrids. However, to make these activities feasible, a microgrid must optimize the use of its resources, seeking economic efficiency. Due to the renewable energy sources and load forecasting features, the time horizon for this optimization is the day-ahead. On the other hand, markets whose energy prices can vary hourly may require optimization with an equivalent time horizon. Thus, day-ahead and intra-day optimal schedulings are requirements for microgrids to participate in current and future energy markets.

The optimal scheduling of microgrids with battery energy storage system, solar and/or wind generation has been studied in (RAMLI; BOUCHEKARA; ALGHAMDI, 2019; LEE et al., 2020; NGUYEN; CROW, 2016; ZHANG et al., 2018; EL-HENDAWI et al., 2018; WANG; ZHANG; DONG, 2020; KIM et al., 2020; ZHAO et al., 2018; PRUDHVIRAJ; KIRAN; PINDORIYA, 2020; ZHANG; WANG; WANG, 2015; LIU et al., 2017; KUMAR; SARAVANAN, 2019; NGUYEN et al., 2018; GAO et al., 2018; EBRAHIMI; AMJADY, 2019; ESMAEILI; ANVARI-MOGHADDAM; JADID, 2019; HUANG et al., 2017; BAZIAR; KAVOOSI-FARD; ZARE, 2013). Although these works address the modeling of solar photovoltaic systems for microgrids, none of them discusses modeling of PV curtailment in day-ahead scheduling (DAS). In addition, the costs related to the PV system can be modeled in the objective function by a fixed term, or by a term proportional to the power generated, or by a combination of them, depending on the methodology adopted to address such costs. The authors (EBRAHIMI; AMJADY, 2019; EL-HENDAWI et al., 2018; KUMAR; SARAVANAN, 2019) model these costs through a term proportional to the power generated. In (ESMAEILI; ANVARI-MOGHADDAM; JADID, 2019), these costs are modeled using a fixed term and another proportional to the power. Similar modeling is presented in (RAMLI; BOUCHEKARA; ALGHAMDI, 2019) with a fixed term and two others which are proportional to the power and the square of the power. However, all of these works do not present a methodology for calculating costs related to the PV system. As a consequence, in the simulations presented in those works, the authors consider such costs as known values.

Regarding the modeling of battery energy storage systems, most authors present simplified modeling that considers only upper and lower limits for charging and discharging power and for the state of charge, as in (LIU et al., 2017; KUMAR; SARAVANAN, 2019; EL-HENDAWI et al., 2018; NGUYEN; CROW, 2016; RAMLI; BOUCHEKARA; ALGHAMDI, 2019). Others present a recursive equation for the BESS state of charge but without clarifying how to transform such a recursive equation into a constraint of an optimization problem,

as in (ZHAO et al., 2018; ZHANG et al., 2018; GAO et al., 2018; BAZIAR; KAVOOSI-FARD; ZARE, 2013; NGUYEN; CROW, 2016; LEE et al., 2020). The authors in (HUANG et al., 2017) address the modeling of BESS costs considering the ratio between the cost of capital and the total number of cycles, however without considering the impacts of the depth of discharge and battery degradation. Finally, the authors in (ESMAEILI; ANVARI-MOGHADDAM; JADID, 2019) address the modeling of BESS costs considering the cost of battery degradation, for a given depth of discharge, an exponential relationship that depends on a function fitting to the curve provided by the manufacturer. However, they do not address the method for obtaining the curve parameters.

Demand response programs in microgrids have been investigated through modeling of directly controlled loads (DCL) in (KUMAR; SARAVANAN, 2019; NGUYEN et al., 2018; GAO et al., 2018; ALQUNUN; GUESMI; FARAH, 2020). Authors in (KUMAR; SARAVANAN, 2019; ALQUNUN; GUESMI; FARAH, 2020) use a discrete DCL model with load blocks to analyze the problem of microgrids optimization with demand response, which is equivalent to a model of interruptible loads per block. Authors in (GAO et al., 2018) present a similar approach but considering the load to be interrupted as a continuous variable. However, these works do not address the modeling of shiftable loads as an option for DCLs. In (NGUYEN et al., 2018), loads are classified as fixed and adjustable (DCL), including shiftable and curtailable (interruptible) loads. Both types of DCL are modeled only by an upper power limit. However, shiftable loads require more complete modeling due to their need for a continuous duty cycle, which was not addressed at that work.

Several studies address the problem of optimal DAS of microgrids by modeling uncertainties in load and generation forecasts. Authors in (EBRAHIMI; AMJADY, 2019; ZHAO et al., 2018; ZHANG et al., 2018; GAO et al., 2018) divide the optimization problem into levels or stages to deal with uncertainties in load, generation, and price forecast. Thus, an intermediate stage of optimization has the role of finding, in a set of bounded uncertainties, the condition that maximizes the cost of the microgrid (the worst case). Once such a condition has been defined, the next stage seeks to minimize the cost of the microgrid. Authors refer to this technique as robust optimization. In (ESMAEILI; ANVARI-MOGHADDAM; JADID, 2019), the authors model the uncertainties probabilistically, and in (HUANG et al., 2017), the authors propose the interval mathematics technique to solve the same problem. However, considering uncertainties in the optimization problem comes at a price because, in addition to increasing the complexity of the problem, it leads to a sub-optimal solution compared to the deterministic solution. It is what the authors in (BEN-TAL et al., 2004; BERTSIMAS; SIM, 2004) call the price of robustness in robust optimization. If on the one hand, there may be a mismatch between the forecasted and realized values as a deterministic solution is used, on the other hand, such a mismatch may even increase in solutions such as robust optimization. That is because in such a technique there is no correlation between the uncertainty considered in the day-ahead

problem and that which should actually happen in the intra-day. These are the main reasons why the present study addresses this problem in a deterministic way, which has the advantage of simplicity and low implementation complexity.

Linear programming is the most used technique among the works consulted in the present literature review to solve the problem of DAS optimization for microgrids (GAO et al., 2018; ZHAO et al., 2018; ZHANG et al., 2018; LIU et al., 2017; NGUYEN et al., 2018; ALQUNUN; GUESMI; FARAH, 2020). Furthermore, in an extensive literature review carried out in (NOSRATABADI; HOOSHMAND; GHOLIPOUR, 2017), it was found that mixed-integer linear programming (MILP) is the most appropriate approach for solving the scheduling problem for microgrids and virtual power plants. These works support the choice for linear programming in the present study, without prejudice to the mathematical modeling of the elements here presented.

The optimal dispatch of distributed energy resources in distribution systems and microgrids is of economic interest to the entities that operate these systems. Although there are some works published in the literature on the subject, there also are some gaps in the mathematical modeling that this work seeks to fill. For example, no previous work was found that formulated the day-ahead problem considering scheduled intentional islanding, as defined by the IEEE Std. 1547-2018 (IEEE, 2018). The same for the modeling of shiftable loads of continuous cycle and solar photovoltaic generation curtailment. Furthermore, there is no work in the present literature review that model in detail the BESS system and its cost of availability, maintaining the linearity of the problem.

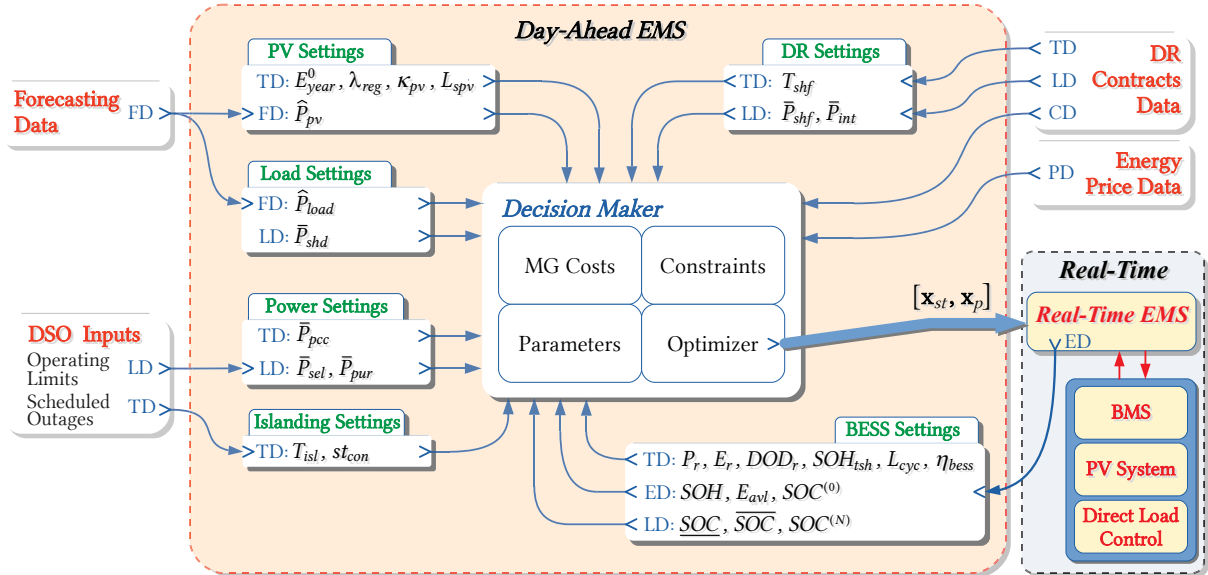
## 3.2 Microgrid Energy Management System

From a logical point of view, a microgrid EMS can be divided into day-ahead and real-time modules, as illustrated in Figure 3.1 (variables in this figure are defined in the next section). Furthermore, the day-ahead EMS requires some input modules to update their data daily. The forecasting data input module is responsible for the daily forecast of the microgrid generation and load curves, which can be based on historical data and weather forecasting. The DSO inputs represent information passed on by the distribution system operator, as scheduled outages and distribution network operational limits, which can be established by a power flow analysis of the distribution network region in which the microgrid is located. The DR contracts data module has the role of updating technical information about consumers who participate in demand response programs. Finally, the energy price module is responsible for updating the energy market prices for the next day.

The day-ahead EMS module must contain the microgrid settings data, the mathematical model of all the microgrid devices and the desired operating conditions, and an optimizer algorithm. The decision-maker block calculates costs that depend on settings



Figure 3.1 – Schematic diagram of the MG day-ahead EMS model addressed in the present work, showing its relationship with the input and output data and its interaction with the real-time EMS; CD, ED, FD, LD, PD, and TD stand for cost, estimated, forecasted, limit, price, and technical data, respectively.



Source: Silva, Aoki and Lambert-Torres (2020).

data and sets up the optimization problem with constraints and parameters for the optimizer. The output of this module is the optimal solution, which is formed by the states and powers that will be the operating setup for the real-time EMS module throughout the next day. Therefore, the day-ahead EMS module, as illustrated in Figure 3.1, defines and limits the scope of this work.

In addition to daily receiving the optimal operating condition from the day-ahead module, the real-time EMS module is updated with data from local and central controllers, electronic meters, and the battery management system in real-time. This module has the role of a real-time decision-maker as it must correct the deviations between the forecasted load and generation and the real-time acquisition data. Such a correction can be made, for example, considering a one-hour horizon. These data are then passed on to lower-level controllers. In addition, this module has the role of deciding the microgrid's operating strategy if the schedule received from the day-ahead module is broken, as can happen in the event of intentional unscheduled islanding (IEEE, 2018). Finally, this module can daily pass data estimated by the BMS to the day-ahead module, such as the current BESS capacity and state of health, as well as the state of charge expected to the end of the day. It will be the initial state of charge in the day-ahead module. Real-time EMS modeling is outside the scope of this work.



### 3.3 Microgrid Modeling Methodology

Figure 3.2 illustrates a schematic diagram of the microgrid reference model for the MILP problem addressed in the present study. The model comprises integer (binary) and real decision variables. The former ( $st^{(t)}$  type) has the function of virtual disconnect switches, and the latter ( $P^{(t)}$  type) represents the active powers of each element of the model. Variables of type  $\hat{P}$  represent forecasted values, which are input variables for the model. Features of the model include: solar PV system, battery energy storage system, directly controllable loads, conventional loads, load shedding, energy transactions with the external grid, and the possibility of islanding. As this model requires a large number of decision variables, they are described in Table 3.1 and Table 3.2. Table 3.3 presents some input variables of the model in Figure 3.2.

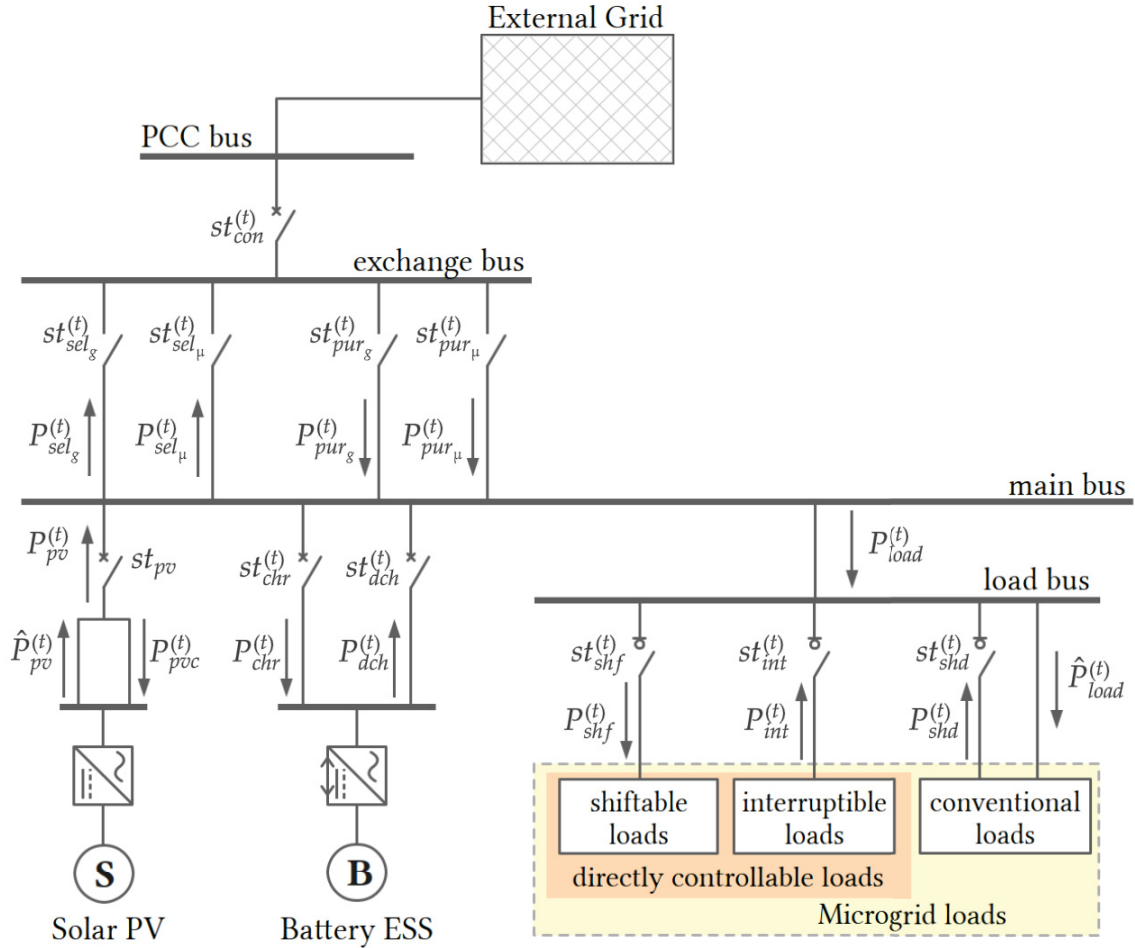
Table 3.1 – State variables for the model, in which the value 1 means state enabled and 0 disabled.

State Variables	Description
$st_{pur_g}^{(t)}, st_{pur_\mu}^{(j,t)}$	represent the state of purchasing transaction at time $t$ ; index $g$ stands for trading with the main grid and $\mu$ trading with the $j$ -th microgrid;
$st_{sel_g}^{(t)}, st_{sel_\mu}^{(j,t)}$	represent the status of energy sale transaction at time $t$ ; index $g$ stands for trading with the main grid and $\mu$ trading with the $j$ -th microgrid;
$st_{chr}^{(t)}, st_{dch}^{(t)}$	represent the state of charge and discharge of the battery, at time $t$ , respectively;
$st_{int}^{(t)}, st_{shf}^{(t)}$	represent the connection state of interruptible and shiftable loads, respectively.
$st_{shd}^{(t)}$	represents the activation state of the load shedding resource.

Source: Silva, Aoki and Lambert-Torres (2020).

Some elements in the model do not necessarily correspond to a real device present in the microgrid. The energy transacted with the external grid pass through virtual disconnectors (in practice, they are not required). Creating these branches connected to the exchange bus allows the model to identify the agents that are exchanging energy with the microgrid, in addition to quantifying that energy. In fact, such transaction can be a contractual obligation only, since all the energy that enters and leaves the

Figure 3.2 – Schematic diagram of the MG model used in the MILP problem;  $st^{(t)}$ -type decision variables are virtual disconnectors and  $P^{(t)}$ -type are real powers. Also,  $\hat{P}$ -type variables represent forecasted values.



Source: Silva, Aoki and Lambert-Torres (2020).

microgrid through the point of common coupling bus has a single source or destination: the external grid. Furthermore, in practical applications, the BESS is connected to the main bus through a single branch, and a battery management system is responsible for controlling the charge and discharge operations. On the other hand, without loss of generality, modeling charging and discharging by different branches (see Figure 3.2) may be more suitable for mathematical programming purposes.

In the MG model of Figure 3.2, DCL are loads in a demand response program that the MG operator can remotely disconnect or cycle upon contractual agreement and notification (FEDERAL ENERGY REGULATORY COMMISSION - U.S. DEPARTMENT OF ENERGY, 2012). Furthermore called flexible loads, they can be interruptible or shiftable. The former are loads subject to curtailment or interruption under system contingencies,

Table 3.2 – Power variables for the model.

<b>Power Variables (kW)</b>	<b>Description</b>
$P_{pur_g}^{(t)}, P_{pur_\mu}^{(j,t)}$	are the powers injected by the main grid into the microgrid ( <i>pur</i> index) through the <i>PCC</i> , at time $t$ . The index $g$ stands for trading with the main grid and $\mu$ trading with the $j$ -th microgrid;
$P_{sel_g}^{(t)}, P_{sel_\mu}^{(j,t)}$	are the powers injected by the microgrid into the main grid ( <i>sel</i> index) through the <i>PCC</i> , at time $t$ . The index $g$ stands for trading with the main grid and $\mu$ trading with the $j$ -th microgrid;
$P_{chr}^{(t)}, P_{dch}^{(t)}$	are the battery charging and discharging power, respectively.
$P_{pvc}^{(t)}, P_{shd}^{(t)}$	are the amount of PV output power curtailment and load shedding, respectively.
$P_{int}^{(t)}, P_{shf}^{(t)}$	are the amount of interruptible and shiftable loads, respectively.

Source: Silva, Aoki and Lambert-Torres (2020).

Table 3.3 – Input variables for the model.

<b>Non-Decision Variables</b>	<b>Description</b>
$\hat{P}_{load}^{(t)}, \hat{P}_{pv}^{(t)}$	are the day-ahead forecasted load and PV output power curves, respectively (kW).
$st_{con}^{(t)}, st_{pv}$	are the microgrid and PV system state of connection, respectively; state 0 means disconnected and 1 connected.

Source: Silva, Aoki and Lambert-Torres (2020).

as air conditioners and water heaters (DENG et al., 2015). The latter are continuous cycle loads that can be shifted in time as washers and dryers. On the other hand, when the microgrid operator needs to disconnect non-flexible loads, the conventional ones in Figure 3.2, due to a contingency or generation shortage, it must use the load shedding resource. As this type of load is not participating in a demand response program, there is a penalty associated with such a disconnection.

As a day-ahead scheduling is made up of a 24-hours time horizon, then the time

slot for the model can be defined as,

$$\Delta t = \frac{24}{N} \text{ (h)}, \quad \text{for } N \in \mathbb{Z}, N \geq 1 \quad (3.1)$$

where  $N$  represents the number of time slots. In addition, throughout this work, the independent variable  $t \in \mathbb{S}_N$  represents the discrete-time of the model, where  $\mathbb{S}_N = \{k \in \mathbb{Z} \mid 1 \leq k \leq N\}$

The rate of change of the physical quantities handled by the model at each time slot should guide the choice of  $\Delta t$ . It should be small enough to capture significant changes in the forecasted load and solar generation curves, for example. On the other hand, it must be large enough to meet the time requirements of microgrid's tertiary control. Typical values for  $\Delta t$  are from 1/4 h (KIM et al., 2020; ZHAO et al., 2018; ZHANG; WANG; WANG, 2015) to 1 h (ZHANG et al., 2018; GAO et al., 2018; LI; ROCHE; MIRAOU, 2017). However, 1/4 h may be a more appropriate time slot when the problem involves controllable loads, as it can better adjust to load cycles.

### 3.3.1 Objective Function

Consider a daily MG energy bill ( $E_{bill}$ ) made up of the difference between daily costs and revenue, such that positive  $E_{bill}$  values indicate an amount to be paid, and negative, an amount to be received or converted into energy credits, i.e.,

$$E_{bill} := - \underbrace{\Delta t \sum_{t=1}^N P_{sel}^{(t)} p_{sel}^{(t)}}_{\text{revenue}} + \underbrace{\Delta t \sum_{t=1}^N P_{pur}^{(t)} p_{pur}^{(t)}}_{\text{costs}} + \{\text{MG costs}\} \quad (\$) \quad (3.2)$$

where  $p_{pur}$  and  $p_{sel}$  are the purchase and sale prices of energy, respectively. Although it is usual in other studies to name  $E_{bill}$  a daily operating cost, Equation 3.2 shows its value does not always represent a cost. Therefore, optimizing the dispatch of a microgrid consists of minimizing its daily energy bill; and, the optimization problem can be formulated as

$$\begin{aligned} \min_{\mathbf{x}} E_{bill}(\mathbf{x}) = & C_{pv} + \sum_{t=1}^N \left( st_{pur_g}^{(t)} c_{pur_g} + st_{sel_g}^{(t)} c_{sel_g} + \sum_{j=1}^M \left( st_{pur_\mu}^{(j,t)} c_{pur_\mu} + st_{sel_\mu}^{(j,t)} c_{sel_\mu} \right) + \right. \\ & st_{shd}^{(t)} c_{shd} + st_{int}^{(t)} c_{int} + st_{shf}^{(t)} c_{shf} + st_{chr}^{(t)} c_{chr} + st_{dch}^{(t)} c_{dch} + \Delta t \left( P_{pvc}^{(t)} p_{pvc}^{(t)} + \right. \\ & P_{chr}^{(t)} p_{chr} + P_{dch}^{(t)} p_{dch} + P_{shd}^{(t)} p_{shd} + P_{int}^{(t)} p_{int} + P_{shf}^{(t)} p_{shf} + \\ & \left. \left. P_{pur_g}^{(t)} p_{pur_g}^{(t)} - P_{sel_g}^{(t)} p_{sel_g}^{(t)} + \sum_{j=1}^M \left( P_{pur_\mu}^{(j,t)} p_{pur_\mu}^{(j,t)} - P_{sel_\mu}^{(j,t)} p_{sel_\mu}^{(j,t)} \right) \right) \right) \end{aligned} \quad (3.3)$$

where  $\mathbf{x}$ , the vector of decision variables, is a feasible solution to the problem; and  $M$  is the number of external MGs with whom the microgrid carries out energy transactions.

The linear objective function in Equation 3.3 is a sum of products. Those of type  $\{st \times c\}$ , whose variables are shown in Tables 3.1 and 3.4, represent fixed costs of energy transaction and operating DERs such as BESS, load shedding, and controllable loads. Products of type  $\Delta t\{P \times p\}$ , whose variables are described in Tables 3.2 and 3.5, represent the revenues and expenses with the amount of energy transacted and the costs to operate each kWh of the DERs.

Table 3.4 – State parameters.

State parameters (\$)	Description
$c_{sel_g}, c_{sel_\mu}$	are fixed costs of service when selling energy to the grid or to the $j$ -th microgrid.
$c_{pur_g}, c_{pur_\mu}$	are fixed costs of service when purchasing energy from the grid or from the $j$ -th microgrid.
$c_{chr}, c_{dch}$	represent a fixed cost for charging and discharging the battery, respectively;
$c_{int}, c_{shf}$	represent a fixed cost for disconnecting interruptible loads, and for connecting shiftable loads, respectively;
$c_{shd}, C_{pv}$	represent a fixed cost for disconnecting load (shedding), and the availability cost of the PV system, respectively;

Source: Silva, Aoki and Lambert-Torres (2020).

### 3.3.2 Energy and Power Exchanges

Regarding the energy transaction, there must be a logical constraint to deny that the microgrid can buy and sell energy simultaneously, that is,

$$0 \leq st_{pur_g}^{(t)} + st_{sel_g}^{(t)} + \sum_{j=1}^M st_{pur_\mu}^{(j,t)} + st_{sel_\mu}^{(j,t)} \leq st_{con}^{(t)}, \quad \forall t \in \mathbb{S}_N \quad (3.4)$$

However, if energy market rules allow the purchase of energy from two or more entities simultaneously, then this constraint can be decomposed into constraints that consider each term individually. The same goes for a market logic of simultaneous selling.

Table 3.5 – Power parameters of the MILP problem.

Power paramet. (\$/kWh)	Description
$p_{sel_g}^{(t)}, p_{sel_\mu}^{(j,t)}$	are the sale prices of energy, at time $t$ , when trading with the grid ( $g$ index) or with the $j$ -th microgrid ( $\mu$ index);
$p_{pur_g}^{(t)}, p_{pur_\mu}^{(j,t)}$	are the purchase prices of energy, at time $t$ , when trading with the grid ( $g$ index) or with the $j$ -th microgrid ( $\mu$ index);
$p_{chr}, p_{dch}$	are the cost of each kWh for charging and discharging the battery, at time $t$ , respectively.
$p_{pvc}^{(t)}, p_{shd}^{(t)}$	are the cost of each kWh of PV output power curtailment and load disconnected (shedding), at time $t$ , respectively.
$p_{int}^{(t)}, p_{shf}^{(t)}$	are the cost of each kWh to disconnect interruptible loads and to connect shiftable loads, at time $t$ , respectively.

Source: Silva, Aoki and Lambert-Torres (2020).

According to Equation 3.4, to insert a condition of islanding into the schedule, it is enough to make  $st_{con} = 0$  during the desired period of islanding,  $T_{isl} \in \mathbb{S}_N$ , and  $st_{con} = 1$ , otherwise. In fact,  $st_{con} = 0$  means that the microgrid can be either indeed operating in islanded mode (the real disconnect switch is open, e.g., due to a scheduled maintenance outage planned by the DSO) or connected but without exchanging power with the grid (see Equation 3.5). Furthermore, if the microgrid cannot sell energy to the main grid (e.g., due to contractual restrictions with the DSO), then it is enough to make,  $st_{sel_g}^{(t)} = st_{sel_\mu}^{(j,t)} = 0, \forall t \in \mathbb{S}_N, \forall j \in \mathbb{S}_M$ , where  $\mathbb{S}_M = \{k \in \mathbb{Z} \mid 1 \leq k \leq M\}$  is the set of external microgrids.

Regarding the power exchange, some technical features as line capacity, PCC sizing, or contracted limits can restrain the power exchange ( $P_{pur}$  and  $P_{sel}$ ) between the microgrid and the main grid or external microgrids (ZHANG et al., 2018). Furthermore, if a state variable  $st_{pur}$  or  $st_{sel}$  is zero, then the respective power  $P_{pur}$  or  $P_{sel}$  must be zero, i.e.,

$$0 \leq P_{pur_g}^{(t)} \leq st_{pur_g}^{(t)} \bar{P}_{pur_g}, \quad \forall t \in \mathbb{S}_N \quad (3.5a)$$

$$0 \leq P_{sel_g}^{(t)} \leq st_{sel_g}^{(t)} \bar{P}_{sel_g}, \quad \forall t \in \mathbb{S}_N \quad (3.5b)$$

$$\begin{aligned} 0 &\leq P_{pur_\mu}^{(1,t)} \leq st_{pur_\mu}^{(1,t)} \bar{P}_{pur_\mu}^{(1)}, & \forall t \in \mathbb{S}_N \\ &\vdots & \\ 0 &\leq P_{pur_\mu}^{(M,t)} \leq st_{pur_\mu}^{(M,t)} \bar{P}_{pur_\mu}^{(M)}, & \forall t \in \mathbb{S}_N \end{aligned} \quad (3.5c)$$

$$\begin{aligned}
0 &\leq P_{sel_\mu}^{(1,t)} \leq st_{sel_\mu}^{(1,t)} \bar{P}_{sel_\mu}^{(1)}, & \forall t \in \mathbb{S}_N \\
&\vdots & \\
0 &\leq P_{sel_\mu}^{(M,t)} \leq st_{sel_\mu}^{(M,t)} \bar{P}_{sel_\mu}^{(M)}, & \forall t \in \mathbb{S}_N
\end{aligned} \tag{3.5d}$$

where  $\bar{P}_{pur}$  and  $\bar{P}_{sel}$  are individual upper limits imposed by external entities (index  $\mu$  for MGs, and  $g$  for the main grid). Besides, a power flow analysis considering the MG exchange bus as a node in the external grid can result in a constraint of physical upper limit  $\bar{P}_{pcc}$  for the point of common coupling,

$$P_{pur_g}^{(t)} + \sum_{j=1}^M P_{pur_\mu}^{(j,t)} \leq \bar{P}_{pcc}, \quad \forall t \in \mathbb{S}_N \tag{3.6a}$$

$$P_{sel_g}^{(t)} + \sum_{j=1}^M P_{sel_\mu}^{(j,t)} \leq \bar{P}_{pcc}, \quad \forall t \in \mathbb{S}_N \tag{3.6b}$$

### 3.3.3 Power Balance

To satisfy the power balance at a given time  $t$ , the sum of the energy generated, imported and exported must equal the microgrid demand. Assuming the total load power is given by (see Figure 3.2)

$$P_{load}^{(t)} = \hat{P}_{load}^{(t)} - P_{shd}^{(t)} - P_{int}^{(t)} + P_{shf}^{(t)}, \quad \forall t \in \mathbb{S}_N \tag{3.7}$$

then, the power balance equation is given by

$$\begin{aligned}
P_{int}^{(t)} + P_{shd}^{(t)} + P_{dch}^{(t)} + P_{pur_g}^{(t)} + \hat{P}_{pv}^{(t)} st_{pv} + \sum_{j=1}^M P_{pur_\mu}^{(j,t)} = \\
P_{chr}^{(t)} + P_{sel_g}^{(t)} + P_{pvc}^{(t)} + P_{shf}^{(t)} + \hat{P}_{load}^{(t)} + \sum_{j=1}^M P_{sel_\mu}^{(j,t)}, \quad \forall t \in \mathbb{S}_N
\end{aligned} \tag{3.8}$$

where  $\hat{P}_{load}^{(t)}$  and  $\hat{P}_{pv}^{(t)}$  are the forecasted load and PV output curves in kW.

### 3.3.4 Battery Energy Storage System

A battery energy storage system for power system applications can comprise a coupling transformer, a converter system, and a battery pack. The efficiency of each one ( $\eta_{trf}$ ,  $\eta_{conv}$ , and  $\eta_{bat}$ , respectively) impacts the overall BESS efficiency as

$$\eta_{bess} = \eta_{trf} \eta_{conv} \eta_{bat} \tag{3.9}$$

which is valid for both charging and discharging operations, once in practical applications, it is usual to consider the charge and discharge efficiency ( $\eta_{bat}$ ) are the same. In this case,

$\eta_{bat} = \sqrt{\eta_{rte}}$ , where  $\eta_{rte}$  is the round trip efficiency. The storage efficiency ( $\eta_{sto}$ ) could also make up the value of  $\eta_{bat}$ ; however, batteries present high  $\eta_{sto}$ . The lead-acid technology, for example, can achieve a self-discharge of 2%–5% per month, and lithium-ion 1% per month (DIVYA; ØSTERGAARD, 2009). Therefore, the storage efficiency can be neglected in models with a time horizon of a day.

According to the authors in (RODRIGUES et al., 2014), higher technologies lithium-ion batteries can achieve an  $\eta_{rte}$  of 95%, which implies an  $\eta_{bat}$  of 0.9747. On the other hand, authors in (PALIZBAN; KAUHANIEMI, 2016) stand lead-acid and lithium-ion technologies can achieve a round trip efficiency of 85% and 90%, respectively, which leads to the values of 0.9220 and 0.9487 for  $\eta_{bat}$ . In addition, according to data in (ATLANTIC CLEAN ENERGY SUPPLY LLC, 2019), a battery manufactured with the  $\text{LiFePO}_4$  technology can achieve an  $\eta_{bat}$  of 0.9747. Regarding the efficiency of converters and transformers, manufacturing data (ABB, 2017) for systems from 500 kW to 5000 kW show that each can be greater than 97%. Table 3.6 presents a summary of these efficiency values for three battery technologies, and the respective  $\eta_{bess}$  calculated from Equation 3.9.

Table 3.6 – Values of energy storage system efficiency for three battery technologies.

Battery Technology	Coupling Transformer	Efficiency			
		$\eta_{trf}$	$\eta_{conv}$	$\eta_{bat}$	$\eta_{bess}$
Lead-acid	no	–	> 0.97	0.9220	0.8943
	yes	> 0.97	> 0.97	0.9220	0.8675
Lithium-ion	no	–	> 0.97	0.9487	0.9202
	yes	> 0.97	> 0.97	0.9487	0.8926
LiFePO <sub>4</sub> , and Lithium-ion of higher technology	no	–	> 0.97	0.9747	0.9454
	yes	> 0.97	> 0.97	0.9747	0.9170

Source: Silva, Aoki and Lambert-Torres (2020).

The IEEE Std 2030.2.1<sup>TM</sup> (IEEE, 2019) presents the main concepts related to BESS engineering. Some of them are illustrated in Figure 3.3. According to the standard, state of charge is “the degree to which a BESS is charged relative to the maximum possible amount of energy that can be stored by the system”, and depth of discharge is “the degree to which a BESS is discharged relative to the maximum possible amount of energy that



can be discharged by the system”. Thus, let  $E_{avl}$  be the BESS available capacity (the maximum possible amount of energy..., kWh), then

$$SOC = \frac{E_{sto}}{E_{avl}} \quad (3.10)$$

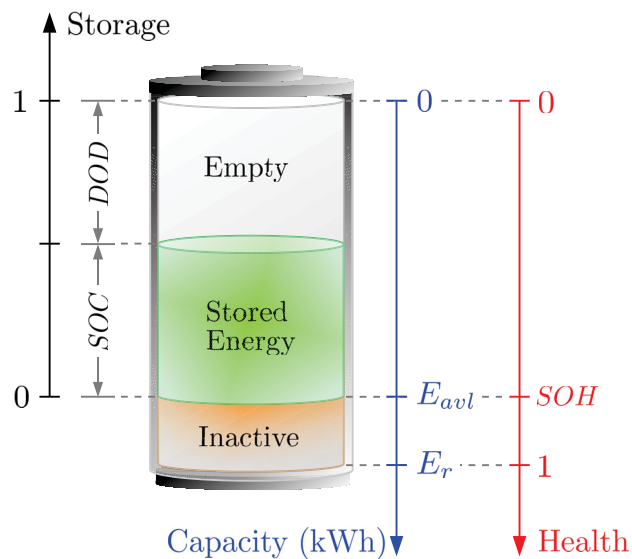
and  $DOD = 1 - SOC$ ; where  $E_{sto}$  is the stored energy.

Furthermore, the ratio of available capacity to rated capacity ( $E_r$ ) defines the battery state of health,

$$SOH = \frac{E_{avl}}{E_r} \quad (3.11)$$

Therefore, the amount of stored energy during the BESS operation is  $E_{sto} = SOC SOH E_r$ . In real life systems, a battery management system can estimate the battery state of health at run time.

Figure 3.3 – Clarifying the nomenclature of BESS used throughout the present study. The definitions of SOC and DOD are following the IEEE Std 2030.2.1™ (IEEE, 2019).



Source: Silva, Aoki and Lambert-Torres (2020).

As the state of charge is a constraint in the optimization problem, Equation 3.10 needs to be rewritten to illustrate the dynamics of charging and discharging the battery. Adopting the main bus as the reference point, the next state of charge can be computed

from the previous one as

$$\begin{aligned} SOC^{(t)} E_{avl} &= SOC^{(t-1)} E_{avl} + \eta_{bess} P_{chr}^{(t)} \Delta t - \frac{1}{\eta_{bess}} P_{dch}^{(t)} \Delta t \\ \implies SOC^{(t)} &= SOC^{(t-1)} + \frac{\eta_{bess} \Delta t}{E_{avl}} P_{chr}^{(t)} - \frac{\Delta t}{\eta_{bess} E_{avl}} P_{dch}^{(t)}, \quad \forall t \in \mathbb{S}_N \end{aligned} \quad (3.12)$$

Although Equation 3.12 is recursive, it can also be written directly, bringing up the initial state of charge  $SOC^{(0)}$ , i.e.,

$$SOC^{(t)} = SOC^{(0)} + \sum_{k=1}^t \left( \frac{\eta_{bess} \Delta t}{E_{avl}} P_{chr}^{(k)} - \frac{\Delta t}{\eta_{bess} E_{avl}} P_{dch}^{(k)} \right), \quad \forall t \in \mathbb{S}_N \quad (3.13)$$

Furthermore, the SOC may vary within a limited range with maximal ( $\overline{SOC}$ ) and minimal ( $\underline{SOC}$ ) values,

$$\underline{SOC} \leq SOC^{(t)} \leq \overline{SOC}, \quad \forall t \in \mathbb{S}_N \quad (3.14)$$

As manufacturers usually define the battery cycle life ( $L_{cyc}$ ) at a rated depth of discharge ( $DOD_r$ ), then it can be useful to consider  $\underline{SOC} = 1 - DOD_r$ , if the goal is to reach the amount of  $L_{cyc}$  cycles.

Finally, the substitution of Equation 3.13 in Equation 3.14 results in  $N$  MILP constraints for SOC, bringing out the decision variables  $P_{chr}$  and  $P_{dch}$ ,

$$\underline{SOC} - SOC^{(0)} \leq \sum_{k=1}^t \left( \frac{\eta_{bess} \Delta t}{E_{avl}} P_{chr}^{(k)} - \frac{\Delta t}{\eta_{bess} E_{avl}} P_{dch}^{(k)} \right) \leq \overline{SOC} - SOC^{(0)}, \quad \forall t \in \mathbb{S}_N \quad (3.15)$$

Furthermore, by setting  $t = N$  in Equation 3.13, it is possible to add an equality constraint to set the desired final state of charge  $SOC^{(N)}$ , that is,

$$\sum_{k=1}^N \left( \frac{\eta_{bess} \Delta t}{E_{avl}} P_{chr}^{(k)} - \frac{\Delta t}{\eta_{bess} E_{avl}} P_{dch}^{(k)} \right) = SOC^{(N)} - SOC^{(0)} \quad (3.16)$$

However, to make a more balanced economic analysis, at the end of an  $N$  period, the state of charge should return to its initial value, as in (ZHAO et al., 2018), which can be reached by setting  $SOC^{(N)} = SOC^{(0)}$  in Equation 3.16.

The state variables for charging and discharging are binary, i.e.,  $\{st_{chr}, st_{dch}\} \in \{0, 1\}$ . As the system cannot perform charging and discharging operations at the same time, then

$$0 \leq st_{chr}^{(t)} + st_{dch}^{(t)} \leq 1, \quad \forall t \in \mathbb{S}_N \quad (3.17)$$

When a state variable disables operation of charging or discharging, naturally,

the respective power decision variable must be forced to zero. Otherwise, the power is limited by the BESS rated power ( $P_r$ ). Then, for all  $t \in \mathbb{S}_N$ ,

$$0 \leq P_{chr}^{(t)} \leq st_{chr}^{(t)} P_r \quad (3.18a)$$

$$0 \leq P_{dch}^{(t)} \leq st_{dch}^{(t)} P_r \quad (3.18b)$$

### 3.3.5 Directly Controllable Loads and Load Shedding

The state variable of load shedding is an integer of bounds  $0 \leq st_{shd}^{(t)} \leq 1, \forall t \in \mathbb{S}_N$ , and the amount of load shedding is bounded by  $\bar{P}_{shd}^{(t)}$ ,

$$0 \leq P_{shd}^{(t)} \leq st_{shd}^{(t)} \bar{P}_{shd}^{(t)}, \quad \forall t \in \mathbb{S}_N \quad (3.19)$$

Typically,  $\bar{P}_{shd}^{(t)} = \gamma_{shd} \hat{P}_{load}^{(t)}$ , as in (ZHAO et al., 2018), where  $\{\gamma_{shd} \in \mathbb{R} \mid 0 \leq \gamma_{shd} \leq 1\}$  is a factor of shedding.

Since the optimizer algorithm could schedule load shedding to avoid buying energy when it is more expensive, it may be of interest to refuse this type of operation. For example, it may be useful to allow disconnecting the load only during islanding condition, which requires that

$$0 \leq st_{shd}^{(t)} \leq 1 - st_{con}^{(t)}, \quad \forall t \in \mathbb{S}_N \quad (3.20)$$

In the model of directly controllable loads illustrated in Figure 3.2, the amount of interruptible loads  $P_{int}^{(t)}$ , included in the forecasted daily load  $\hat{P}_{load}^{(t)}$ , is available for the optimizer algorithm to decide if it is necessary to disconnect it and when to do it. On the other hand, the amount of shiftable loads  $P_{shf}^{(t)}$  has different requirements, and the optimizer must connect this load block optimally throughout the day and ensure that it has a continuous cycle.

The state variables for interruptible and shiftable loads are integers such that  $0 \leq st_{int}^{(t)} \leq 1$  and  $0 \leq st_{shf}^{(t)} \leq 1, \forall t \in \mathbb{S}_N$ , respectively. Now assuming that, according to the demand response program, the period of time that the MG operator can keep interruptible loads disconnected from the system is limited to  $T_{int} \in \mathbb{S}_N$ , thus,

$$\sum_{t=1}^N st_{int}^{(t)} \leq T_{int} \quad (3.21)$$

Furthermore, the amount of interruptible loads is bounded by  $\bar{P}_{int}^{(t)}$ , i.e.,

$$0 \leq P_{int}^{(t)} \leq st_{int}^{(t)} \bar{P}_{int}^{(t)}, \quad \forall t \in \mathbb{S}_N \quad (3.22)$$

In fact,  $\bar{P}_{int}^{(t)}$  can vary throughout the day according to the characteristics of the interruptible load group available for the demand response program. Hence, in this

work, interruptible loads are modeled as a fraction of the forecasted load, such that  $\bar{P}_{int}^{(t)} = \gamma_{int} \hat{P}_{load}^{(t)}$ , where  $\{\gamma_{int} \in \mathbb{R} \mid 0 \leq \gamma_{int} \leq 1\}$ .

Assuming the block of shiftable loads has a cycle of period  $T_{shf} \in \mathbb{S}_N$  and magnitude  $\bar{P}_{shf}$ , then Equations (3.23)–(3.25) are constraints required for power and time of connection,

$$0 \leq P_{shf}^{(t)}, \quad \forall t \in \mathbb{S}_N \quad (3.23)$$

$$P_{shf}^{(t)} - st_{shf}^{(t)} \bar{P}_{shf} = 0, \quad \forall t \in \mathbb{S}_N \quad (3.24)$$

$$\sum_{t=1}^N st_{shf}^{(t)} = T_{shf} \quad (3.25)$$

However, to meet the continuous load cycle requirement, thus avoiding a sequence of turning the load on and off throughout the day, an additional restriction is required, which is

$$\begin{aligned} &\text{for } k = 1, 2, \dots, N - T_{shf} \\ &\quad \text{for } n = 0, 1, \dots, N - k - T_{shf} \\ &\quad \quad st_{shf}^{(k)} + st_{shf}^{(k+T_{shf}+n)} \leq 1 \\ &\quad \text{end} \\ &\text{end} \end{aligned} \quad (3.26)$$

Algebraically, Equation 3.26 intends to ensure the time distance between any two enabled states is less than one period of load cycle  $T_{shf}$ . In this equation, a pseudocode technique was adopted as a mathematical resource to represent the inequality restrictions in a compact and readable way.

To add other blocks of shiftable loads with different magnitudes, periods, and states to the model, consider add to the problem the set of variables  $\{P_{shf}^{(r,t)}, T_{shf}^{(r)}, st_{shf}^{(r,t)}\}$  for the  $r$ -th load block, which must meet the constraints of Equations (3.23)–(3.26) for each  $r$ . However, the computational cost can be high, since the number of restrictions per load block is  $N + 1 + (N - T_{shf})(N - T_{shf} + 1)/2$ . For example, each block of two hours of shiftable loads requires 4013 constraints in the MILP problem ( $\Delta t = 1/4$  h).

### 3.3.6 PV System

In a DAS problem, the PV output power variable is usually equal to the forecasted value for the next day. However, there can be conditions in which the microgrid has surplus generation but is unable to transfer energy to the grid (technical restrictions or islanding condition) or to the battery (SOC is at the upper limit, or the battery is out of service for maintenance). In such a situation there must be generation curtailment  $P_{pvc}^{(t)}$  to satisfy the power balance restriction. In addition,  $P_{pvc}^{(t)}$  must be limited by the amount of generation

expected for the next day. Such requirements result in the restriction of Equation 3.27 for the PV system.

$$0 \leq P_{pvc}^{(t)} \leq \widehat{P}_{pv}^{(t)} st_{pv}, \quad \forall t \in \mathbb{S}_N \quad (3.27)$$

The input variable  $st_{pv}$  must be set equal to zero if the PV system is out of service for maintenance; otherwise, it must be equal to 1. In fact, according to the modeling assumed in Equation 3.3, the daily cost of the PV System  $C_{pv}$  remains for all days of the year, even when the condition  $st_{pv} = 0$  is valid (for some days of the year). According to the authors in (NEHME et al., 2017), solar panels suffer degradation mainly due to climatic and environmental conditions. Therefore, in this modeling, the degradation of the PV system is assumed to be a continuous process that occurs even if it is turned off.

### 3.3.7 Matrix Formulation

Formulating the optimization problem in matrix notation may be more useful for performing it in computer algorithms. To this end, the solution vector can be split into a state vector  $\mathbf{x}_{st}$  and a power vector  $\mathbf{x}_p$ , i.e.,  $\mathbf{x} = [\mathbf{x}_{st}; \mathbf{x}_p]$ , where,

$$\mathbf{x}_{st} = \left[ 1; \{st_{pur_g}^{(t)}\}; \{st_{sel_g}^{(t)}\}; \{st_{pur_\mu}^{(j,t)}\}; \{st_{sel_\mu}^{(j,t)}\}; \{st_{shd}^{(t)}\}; \{st_{int}^{(t)}\}; \{st_{shf}^{(t)}\}; \{st_{chr}^{(t)}\}; \{st_{dch}^{(t)}\} \right] \quad (3.28a)$$

$$\mathbf{x}_p = \left[ \{P_{pvc}^{(t)}\}; \{P_{chr}^{(t)}\}; \{P_{dch}^{(t)}\}; \{P_{shd}^{(t)}\}; \{P_{int}^{(t)}\}; \{P_{shf}^{(t)}\}; \{P_{pur_g}^{(t)}\}; \{P_{sel_g}^{(t)}\}; \{P_{pur_\mu}^{(j,t)}\}; \{P_{sel_\mu}^{(j,t)}\} \right] \quad (3.28b)$$

Elements inside braces are row vectors; those with index  $(t)$  are  $N \times 1$  vectors, and with index  $(j, t)$ , are  $NM \times 1$  vectors, i.e., a chain of vectors with index  $(t)$ ; e.g.,  $\{st_{sel_\mu}^{(j,t)}\} = [\{st_{sel_\mu}^{(1,t)}\}; \dots; \{st_{sel_\mu}^{(M,t)}\}]$ . Elements in the state vector are integers (binaries) and in the power vector, real numbers. Furthermore, as  $E_{bill}(\mathbf{x})$  and the constraints are linear functions, the model fits a MILP problem. Furthermore,  $\mathbf{x}_{st}$  and  $\mathbf{x}_p$  are  $(N(2M+7)+1) \times 1$  and  $2N(M+4) \times 1$  vectors; therefore, the solution vector has  $N(4M+15)+1$  variables. As an example, a scenario with one external MG and  $\Delta t = 1/4$  h ( $M = 1$  and  $N = 96$ ) requires a MILP problem with 1,825 decision variables, of which 865 are integers and 960 real numbers.

Similarly, the parameters presented in Tables 3.4 and 3.5 can be grouped into a vector, i.e.,

$$\mathbf{f} = [\mathbf{f}_{st}; \mathbf{f}_p] \quad (3.29)$$

where

$$\mathbf{f}_{st} = \left[ C_{pv}; \mathbf{1}_{C_{pur_g}}; \mathbf{1}_{C_{sel_g}}; \{\mathbf{1}_{C_{pur_\mu}}^{(j)}\}; \{\mathbf{1}_{C_{sel_\mu}}^{(j)}\}; \mathbf{1}_{C_{shd}}; \mathbf{1}_{C_{int}}; \mathbf{1}_{C_{shf}}; \mathbf{1}_{C_{chr}}; \mathbf{1}_{C_{dch}} \right] \quad (3.30a)$$

$$\mathbf{f}_p = \left[ \{p_{pvc}^{(t)}\}; \mathbf{1}p_{chr}; \mathbf{1}p_{dch}; \{p_{shd}^{(t)}\}; \{p_{int}^{(t)}\}; \{p_{shf}^{(t)}\}; \{p_{pur_g}^{(t)}\}; -\{p_{sel_g}^{(t)}\}; \{p_{pur_\mu}^{(j,t)}\}; -\{p_{sel_\mu}^{(j,t)}\} \right] \Delta t \quad (3.30b)$$

where  $\mathbf{1}$  is a  $N \times 1$  vector of ones; also, by definition  $\{\mathbf{1}c_{pur_\mu}^{(j)}\} := [\{\mathbf{1}c_{pur_\mu}^{(1)}\}; \dots; \{\mathbf{1}c_{pur_\mu}^{(M)}\}]$  and  $\{\mathbf{1}c_{sel_\mu}^{(j)}\} := [\{\mathbf{1}c_{sel_\mu}^{(1)}\}; \dots; \{\mathbf{1}c_{sel_\mu}^{(M)}\}]$ . The same notation rule for vectors used in  $\mathbf{x}_{st}$  can be applied to the elements in Equation 3.30a and Equation 3.30b.

Finally, the MILP problem written in matrix notation is

$$\begin{aligned} & \underset{\mathbf{x}}{\text{minimize}} && \mathbf{f}^T \mathbf{x} \\ & \text{subject to} && \begin{cases} \mathbf{A}\mathbf{x} \leq \mathbf{b} \\ \mathbf{A}_{eq}\mathbf{x} = \mathbf{b}_{eq} \\ \mathbf{l}_b \leq \mathbf{x} \leq \mathbf{u}_b \\ \mathbf{x}_{st} \in \mathbb{Z} \end{cases} \end{aligned} \quad (3.31)$$

where  $\mathbf{A}$  and  $\mathbf{b}$  are the matrix and vector of linear inequality constraints, respectively;  $\mathbf{A}_{eq}$  and  $\mathbf{b}_{eq}$  are the matrix and vector of linear equality constraints, respectively; and  $\mathbf{l}_b$  and  $\mathbf{u}_b$  are the vectors of lower and upper bounds, respectively. Table 3.7 identifies the equations required to define and create the matrices and vectors of constraints.

## 3.4 Cost Estimation Methodology

### 3.4.1 BESS Costs

The calculation of the availability cost of a BESS ( $p_{bess}$ ) in \$/kWh requires estimating the total charge and discharge energy of the battery over its lifetime ( $L_{E,bess}$ ), and knowing its capital cost ( $C_{cap,bess}$ ), i.e.,

$$p_{bess} = C_{cap,bess} / L_{E,bess} \quad (\$/\text{kWh}) \quad (3.32)$$

Theoretically, the battery life ends when it reaches the SOH threshold ( $SOH_{tsh}$ ) for a given application. Thus, the curve SOH versus cycles ( $SOH(n_{cyc})$ ) can bring out the cycle life ( $L_{cyc}$ ) of the battery, since  $SOH(L_{cyc}) = SOH_{tsh}$ . Although it is possible to know the true  $SOH(n_{cyc})$  only in time of operation from the BMS estimates, the curve provided by the BESS manufacturer can be used for cost estimation purposes.

The IEEE Std 2030.2.1<sup>TM</sup> (IEEE, 2019) defines cycle as “the process of BESS discharging or charging from initial state of charge to the same state within a single discharge and charge”. A cycle can be full if it has  $DOD = 1$ , or partial if  $DOD < 1$  (WARNER, 2015). In a characterization testing, a battery manufacturer must determine how many full cycles (or partial cycles at a rated depth of discharge) the battery will achieve (WARNER, 2015), and then build the  $SOH(n_{cyc})$  curve. Therefore, the charge and discharge energy

Table 3.7 – Summary of the equations, organized by features, required to build the matrices and vectors of constraints of the MILP problem;  $\mathbf{0}$  is a  $N \times 1$  vector of zeros.

Features	Equations for A and b	Equations for A <sub>eq</sub> and b <sub>eq</sub>	Equations for l <sub>b</sub> and u <sub>b</sub>
State variables in general			$\mathbf{0} \leq \mathbf{x}_{st} \leq \mathbf{1}$
Energy exchange and islanding	(3.4)		(3.4)
Power exchange	(3.5), (3.6)		(3.5)
Power balance		(3.8)	
BESS, state variables	(3.17)		(3.17)
BESS, power variables	(3.15), (3.18)	(3.16)	(3.18)
Load shedding, state variable			(3.20)
Load shedding, power variable	(3.19)		(3.19)
Interruptible load, state variable	(3.22), (3.21)		
Interruptible load, power variable	(3.22)		(3.22)
Shiftable load, state variable	(3.26)	(3.24), (3.25)	
Shiftable load, power variable		(3.24)	(3.23), (3.24)
PV output power curtailment		(3.27)	(3.27)

Source: Silva, Aoki and Lambert-Torres (2020).

in a manufacturer's test cycle is  $2E_{avl}DOD_r$ , or similarly,  $2SOH(n_{cyc})E_rDOD_r$ . As a consequence, a lower bound on the battery charge and discharge energy over its lifetime can be

$$L_{E,bess} \geq 2E_rDOD_r \int_0^{L_{cyc}} SOH(n_{cyc}) dn_{cyc} \quad (3.33)$$

as long as during the BESS operation, the condition  $DOD(n_{cyc}) \leq DOD_r$  is satisfied. Equation 3.33 is a lower limit because it considers that charging and discharging operations whose  $DOD$  is less than  $DOD_r$ , as it happens under real-world conditions, prolong battery life as pointed out by authors in (XU et al., 2018). In addition, calculating the integral of that equation requires knowing an analytical  $SOH(n_{cyc})$  function that fits the empirical curve from the manufacturer. For lithium-ion batteries, an exponentially decreasing relationship between the state of health and the number of cycles can approximate a real  $SOH(n_{cyc})$ . Thus, consider the base function  $y(x) = e^{-x}$ . Applying the

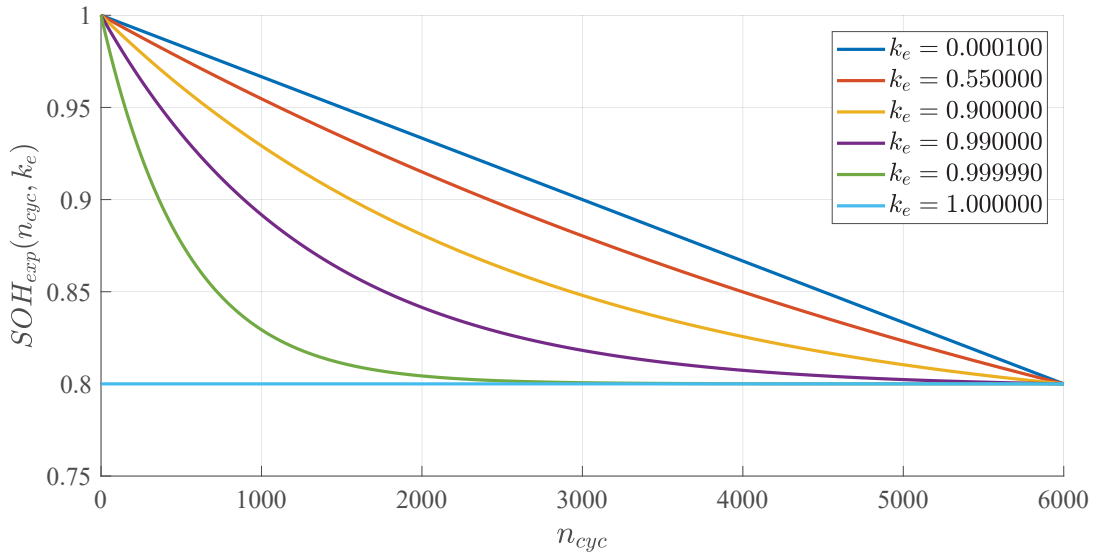
expansion technique on the x-axis, and compression and displacement on the y-axis, this function can be adjusted to the desired exponential  $SOH_{exp}(n_{cyc})$ , i.e.,

$$SOH_{exp}(n_{cyc}, k_e) = k_1 e^{-n_{cyc}/k_3} + k_2, \quad n_{cyc} \geq 0 \quad (3.34)$$

where  $k_1 = (1 - SOH_{tsh})/k_e$ ,  $k_2 = 1 - k_1$ ,  $k_3 = -L_{cyc}/\ln(1 - k_e)$ , and  $k_e \in \mathbb{R}$ ,  $0 < k_e \leq 1$ , is a factor of non-linearity. Note that  $SOH_{exp}(0, k_e) = 1$ , and  $SOH_{exp}(L_{cyc}, k_e) = SOH_{tsh}$ .

It is possible to show (through limits calculation) that Equation 3.34 is a family of curves between a linear approximation for SOH and the line  $SOH_{tsh}$ , for  $k_e$  ranging from 0 to 1, respectively, as illustrated in Figure 3.4. In fact, the non-linearity factor allows a fine adjustment to the SOH curve of interest, as the one provided by the manufacturer. As an example, data in (SAMSUNG SDI, 2016) show  $SOH(n_{cyc})$  curve of a Lithium-ion BESS of 6000 cycle life, and  $SOH_{tsh}$  of 0.8, which fits  $SOH_{exp}(n_{cyc}, k_e)$  for  $k_e \cong 0.55$ .

Figure 3.4 – Exponential approximation curves for state of health, where  $SOH_{tsh} = 0.8$  and  $L_{cyc} = 6000$ .



Source: Silva, Aoki and Lambert-Torres (2020).

Now, applying Equation 3.34 in (3.33),

$$L_{E,bess} \geq 2E_r DOD_r L_{cyc} \left( \frac{SOH_{tsh} - 1}{\ln(1 - k_e)} + \frac{SOH_{tsh} - 1}{k_e} + 1 \right) \quad (\text{kWh}) \quad (3.35)$$

As an example, consider a  $\text{LiFePO}_4$  BESS of 140 kW/280 kWh,  $SOH_{tsh}$  of 0.8, 6000 cycle life at  $DOD_r$  of 0.90,  $\eta_{bess}$  of 0.92 (according to Table 3.6), where the cost



of capital  $C_{cap,bess}$  is 91,000 USD (real market data). Thus, using Equation 3.35 and Equation 3.32, and assuming  $k_e = 0.55$ , the result is  $L_{E,bess} \geq 2,681,776$  kWh, and  $p_{bess} \leq 0.0339$  USD/kWh, respectively.

As  $p_{bess}$  represents the cost of charging and discharging each kWh at the battery cells node, then the BESS powers in the objective function, whose reference is the main (bus) node, must be weighted by the efficiency of BESS, which is similar to consider

$$\begin{aligned} \text{cost of charging: } \Delta t P_{sto} p_{bess} &= \Delta t P_{chr} \eta_{bess} p_{bess} = \Delta t P_{chr} p_{chr}, \\ &\implies p_{chr} = \eta_{bess} p_{bess} \end{aligned} \quad (3.36a)$$

$$\begin{aligned} \text{cost of discharging: } \Delta t P_{sto} p_{bess} &= \Delta t \frac{P_{dch}}{\eta_{bess}} p_{bess} = \Delta t P_{dch} p_{dch}, \\ &\implies p_{dch} = \frac{1}{\eta_{bess}} p_{bess} \end{aligned} \quad (3.36b)$$

where  $\Delta t P_{sto}$  is the portion of energy from  $\Delta t P_{chr}$  that was stored.

Finally, in energy arbitrage applications, a microgrid can purchase energy during an off-peak period, at a price  $p_{out}$  (\$/kWh), and store it for use during an on-peak period, when the energy is more expensive ( $p_{peak}$ ). Thus, the unit cost of energy after the storage process must be less than the on-peak price, i.e.,

$$\Delta t (P_{pur} p_{out} + P_{chr} p_{chr} + P_{dch} p_{dch}) < \Delta t P_{dch} p_{peak} \quad (3.37)$$

Now, making  $P_{pur} = P_{chr} = P_{dch} / \eta_{bess}^2$  in Equation 3.37, and using Equation 3.36a and Equation 3.36b,

$$\frac{1}{\eta_{bess}^2} p_{out} + \frac{2}{\eta_{bess}} p_{bess} < p_{peak}, \quad \implies p_{bess} < \frac{1}{2} \eta_{bess} \left( p_{peak} - \frac{1}{\eta_{bess}^2} p_{out} \right) \quad (3.38)$$

If this relationship is not satisfied, the optimizer algorithm may decide not to use the storage system to perform energy arbitrage.

### 3.4.2 PV Costs

The capacity of solar photovoltaic generation can vary considerably according to the region where the solar panels are installed. For example, according to data in (NREL, 2020), the region of Curitiba (Brazil) has a generation capacity  $\lambda_{reg}$  of about 1261.57 kWh/year per kW, at standard test conditions (STC), of solar panel (tilt 24°, azimuth 0°), while the New York City has  $\lambda_{reg} = 1360.49$  (tilt 37°, azimuth 180°), considering system losses of 14% and inverter efficiency of 96% in both cases. As a consequence, given an annual amount of energy  $E_{year}^0$  (kWh/year) to be generated by a PV system, its capital cost  $C_{cap,pv}$  depends on the region of installation due to the local price and

generation capacity, i.e.,

$$C_{cap,pv} = \frac{E_{year}^0}{\lambda_{reg}} p_{reg}, \quad (\$) \quad (3.39)$$

where  $p_{reg}$  (\$/kW) is the local cost per kW of a installed PV system.

A PV system with an annual degradation rate of  $\kappa_{pv}$  (%/year) should produce, in the  $n$ -th year, throughout its lifespan  $L_{spv}$  (years), an annual amount of energy of,

$$E_{year}^{(n)} = E_{year}^0 \left(1 - \frac{\kappa_{pv}}{100}n\right), \quad (\text{kWh}), \quad \text{for } n = 0, 1, \dots, L_{spv} - 1 \quad (3.40)$$

Similarly, the annual cost of generation, in the  $n$ -th year, can be proportional to the annual degradation, and by consequence, to the yearly energy generated, that is,

$$C_{year}^{(n)} = C_{year}^0 \left(1 - \frac{\kappa_{pv}}{100}n\right), \quad (\$), \quad \text{for } n = 0, 1, \dots, L_{spv} - 1 \quad (3.41)$$

required that

$$C_{cap,pv} = \sum_{n=0}^{L_{spv}-1} C_{year}^0 \left(1 - \frac{\kappa_{pv}}{100}n\right) = C_{year}^0 L_{spv} \left(1 - \kappa_{pv} \frac{L_{spv} - 1}{200}\right) \quad (3.42)$$

Now, applying Equation 3.42 in Equation 3.39 to obtain the value of  $C_{year}^0$  and then using the result in Equation 3.41, results in

$$C_{year}^{(n)} = \frac{(E_{year}^0/\lambda_{reg})p_{reg}}{L_{spv}(1 - (\kappa_{pv}/200)(L_{spv} - 1))} \left(1 - \frac{\kappa_{pv}}{100}n\right), \quad (\$), \quad \text{for } n = 0, 1, \dots, L_{spv} - 1 \quad (3.43)$$

For application in the day-ahead optimization model, the cost values must be daily. Thus, assuming an average daily cost of generation  $C_{pv}^{(n)} = C_{year}^{(n)}/365$  and an average daily capacity of generation  $E_{pv} = E_{year}^0/365$  in Equation 3.43 results in,

$$C_{pv}^{(n)} = \frac{(E_{pv}/\lambda_{reg})p_{reg}}{L_{spv}(1 - (\kappa_{pv}/200)(L_{spv} - 1))} \left(1 - \frac{\kappa_{pv}}{100}n\right), \quad (\$), \quad \text{for } n = 0, 1, \dots, L_{spv} - 1 \quad (3.44)$$

Authors in (JORDAN; KURTZ, 2012) summarized photovoltaic degradation rates using field tests reported in the literature. Results show an average degradation rate of 0.8%/year, which can be a practical value for  $\kappa_{pv}$ . Furthermore, manufacturers usually offer a 25-year standard solar panel warranty, which can be a practical value for  $L_{spv}$ .

### 3.4.3 Other Costs

Costs in Table 3.4 are related to the operating states of the virtual disconnect switches, whereas those in Table 3.5 are related to the amount of energy for each operation. When participating in a free energy market, a microgrid may incur third-party service

costs due to energy purchase and sale operations, which can be modeled by  $c_{pur}$  and  $c_{sel}$ . On the other hand, the market prices are covered in the model by  $p_{pur}$  and  $p_{sel}$ . Furthermore, in the present model,  $c_{shd}$  represents a penalty, imposed by the regulatory agency, for each operation of load disconnection performed by the microgrid, while it lasts. On the other hand,  $p_{shd}$  may represent a penalty due to the amount of disconnected load.

Finally, according to the modeling in the present study, if a cost does not apply to a given approach, it can be set zero.

### 3.5 MMG Energy Management Modeling

An MG operator can either purchase, offer, or store energy, or even curtail it, depending on the costs involved in all these processes at each instant of time. However, such decisions can depend on other MG operator's decisions. As a consequence, it may be necessary to jointly decide how energy transactions occur, to minimize the overall cost of operation and maintenance while respecting the DN physical limits, as well as limits from contracts between agents (when applicable). Therefore, it may be important to address this issue from the MMG perspective.

According to the methodology presented in Zhao et al. (2018), and in Zhang et al. (2018), such a multi-microgrid scenario can be modeled jointly by an objective function that minimizes the MMG costs and by another that minimizes the costs of each MG individually. However, as the result of the first impacts the second and vice versa, then it is necessary to use appropriate methods for solving this problem, with the overall objective to achieve the least cost as a whole.

Table 3.8 presents a list of equivalence between the nomenclature used in the present work so far, which should be taken as reference, and that adopted in (ZHANG et al., 2018) and (ZHAO et al., 2018). It allows comparing the modeling of the present study with the other two ones and identifying which resources each one is addressing. Zhang et al. (2018) do not address (in that table, n.a. stands for not available) wind generation and load shedding. Zhao et al. (2018) and Zhang et al. (2018) do not address generation curtailment and controllable loads. Finally, the present research and (ZHANG et al., 2018) do not address diesel generation.

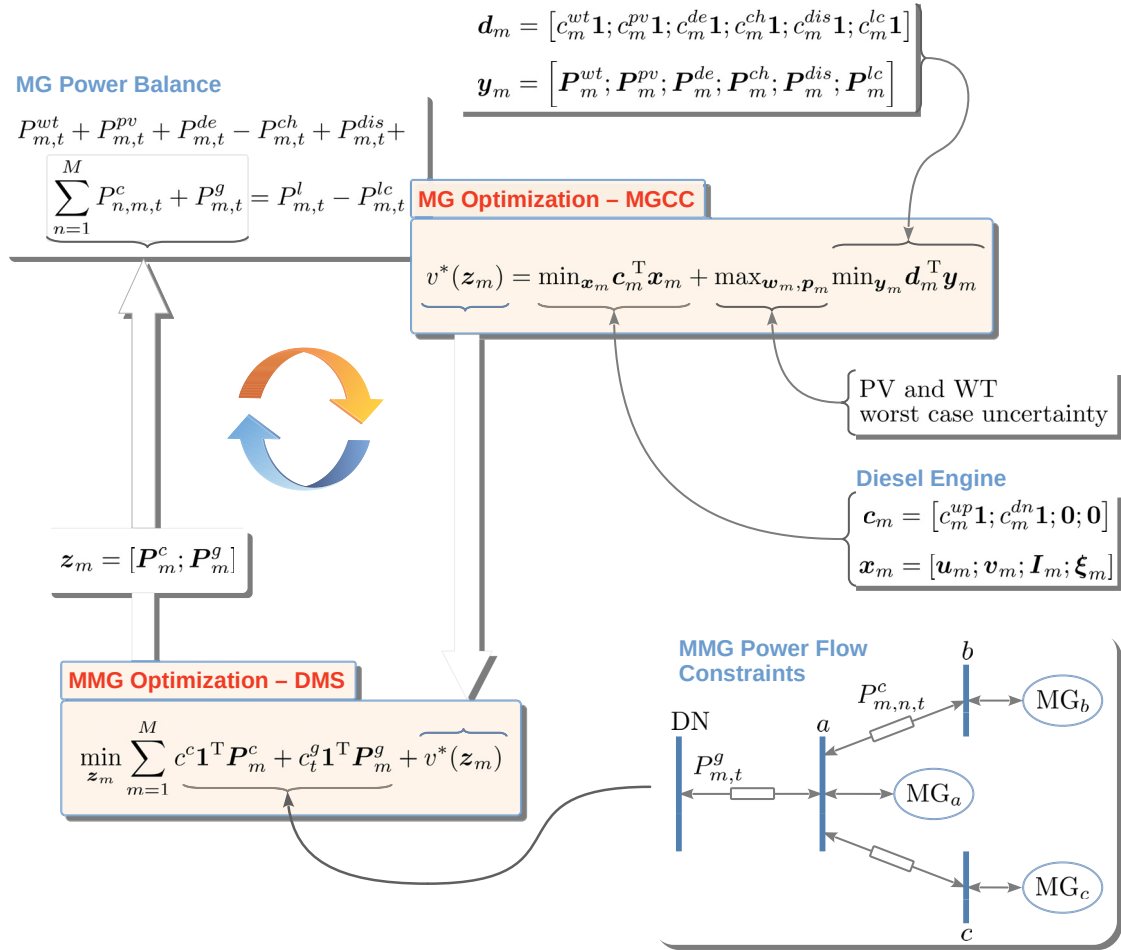
Figure 3.5 presents a graphical abstract, here elaborated, on the work of (ZHAO et al., 2018). The authors present an SoS approach to energy management in an MMG system, whose goal is to minimize costs with distribution network operation. Each MG is an independently managed system containing an MGCC responsible for optimizing your daily dispatch. However, the MG group must operate collaboratively to minimize the cost of an MMG while obeying the physical limits of DN. A DMS is responsible for playing the role of an MMG optimizer.

Table 3.8 – A list of equivalency among symbols; n.a. stands for not available.

	Present work		(ZHANG et al., 2018)		(ZHAO et al., 2018)	
Power variables	$P_{sel_g}^{(i,t)}$	$P_{sel_\mu}^{(i,j,t)}$	$p_{gs}(j, t)$	$p_{ms}(i, j, t)$	$P_{m,t}^g$	$P_{n,m,t}^c$
	$P_{pur_g}^{(i,t)}$	$P_{pur_\mu}^{(i,j,t)}$	$p_{gb}(j, t)$	$p_{mb}(i, j, t)$	$P_{m,t}^g$	$P_{n,m,t}^c$
	$P_{pv}^{(i,t)}$	$P_{wt}^{(i,t)}$	$p_{pv}(i, t)$	n.a.	$P_{m,t}^{pv}$	$P_{m,t}^{wt}$
	$P_{pvc}^{(i,t)}$	$P_{wtc}^{(i,t)}$	n.a.	n.a.	n.a.	n.a.
	$P_{chr}^{(i,t)}$	$P_{dch}^{(i,t)}$	$p_{ec}(i, t)$	$p_{ed}(i, t)$	$P_{m,t}^{ch}$	$P_{m,t}^{dis}$
	$P_{shd}^{(i,t)}$	n.a.	n.a.	n.a.	$P_{m,t}^{lc}$	n.a.
	n.a.		n.a.		$P_{m,t}^{de}$	
Price parameters	$p_{sel_g}^{(i,t)}$	$p_{sel_\mu}^{(i,t)}$	$c_{gs}(t)$	$c_m(t)$	$c_t^g$	$c^c$
	$p_{pur_g}^{(i,t)}$	$p_{pur_\mu}^{(i,t)}$	$c_{gb}(t)$	$c_m(t)$	$c_t^g$	$c^c$
	$p_{pv}^{(i)}$	$p_{wt}^{(i)}$	$C_{pv}(i)$	n.a.	$C_m^{pv}$	$C_m^{wt}$
	$p_{pvc}^{(i,t)}$	$p_{wtc}^{(i,t)}$	n.a.	n.a.	n.a.	n.a.
	$p_{chr}^{(i)}$	$p_{dch}^{(i)}$	$C_{ev}(i)$	$C_{ev}(i)$	$C_m^{ch}$	$C_m^{dis}$
	$p_{shd}^{(i,t)}$	n.a.	n.a.	n.a.	$C_m^{lc}$	n.a.
	n.a.		n.a.		$C_m^{de}$	
State variables	$st_{sel_g}^{(i,t)}$	$st_{sel_\mu}^{(i,j,t)}$	$v(i, t)$	$s(i, j, t)$	n.a.	n.a.
	$st_{pur_g}^{(i,t)}$	$st_{pur_\mu}^{(i,j,t)}$	$u(i, t)$	$r(i, j, t)$	n.a.	n.a.
	$st_{chr}^{(i,t)}$	$st_{dch}^{(i,t)}$	$z(i, t)$	$w(i, t)$	$\xi_{m,t}$	$1 - \xi_{m,t}$
	$st_{shd}^{(i,t)}$	n.a.	n.a.	n.a.	n.a.	n.a.
	n.a.	n.a.	n.a.	n.a.	$u_{m,t}$	$v_{m,t}$
	n.a.		n.a.		$I_{m,t}$	
Cost parameters	$c_{sel_g}$	$c_{sel_\mu}^{(i)}$	$b_{ser}$	$a_{ser}$	n.a.	n.a.
	$c_{pur_g}$	$c_{pur_\mu}^{(i)}$	$b_{ser}$	$a_{ser}$	n.a.	n.a.
	$c_{chr}$	$c_{dch}$	n.a.	n.a.	n.a.	n.a.
	$c_{shd}$	n.a.	n.a.	n.a.	n.a.	n.a.
	n.a.	n.a.	n.a.	n.a.	$C_m^{up}$	$C_m^{dn}$
Forecasted values	$\hat{P}_{pv}^{(i,t)}$	$\hat{P}_{wt}^{(i,t)}$	$P_{pv}^f(i, t)$	n.a.	$P_{m,t}^{pvf}$	$P_{m,t}^{wtf}$
	$\hat{P}_{load}^{(i,t)}$		$P_l(i, t)$		$P_{m,t}^l$	
Bounds	$\bar{P}_{sel_g}$	$\bar{P}_{sel_\mu}(i)$	$P_{gs}^{max}$	$P_m^{max}$	n.a.	n.a.
	$\bar{P}_{pur_g}$	$\bar{P}_{pur_\mu}(i)$	$P_{gb}^{max}$	$P_m^{max}$	n.a.	n.a.
	$P_r^{(i)}$	$P_r^{(i)}$	$P_{ec}^{max}(i)$	$P_{ed}^{max}(i)$	$P_{m,t}^{ch-max}$	$P_{m,t}^{dis-max}$
	$\underline{SOC}^{(i)}$	$\overline{SOC}^{(i)}$	$SOC_{ev}^{min}(i)$	$SOC_{ev}^{max}(i)$	$E_m^{min}$	$E_m^{max}$
	$E_r^{(i)}$	$SOC^{(i,t)}$	$Cap_{ev}(i)$	$SOC_{ev}^{(i,t)}$	n.a.	$E_{m,t}$
Others	$(i, j, t)$	$N, M, \Delta t$	$(i, j, t)$	$T, G, \Delta_T$	$(m, n, t)$	$N, M, \Delta t$
	$\eta_{bess}$	$\eta_{bess}$	$\eta_{ec}$	$\eta_{ed}$		

Source: The author (2022).

Figure 3.5 – Visual abstract on the work of Zhao et al. (2018).



Source: The author (2022).

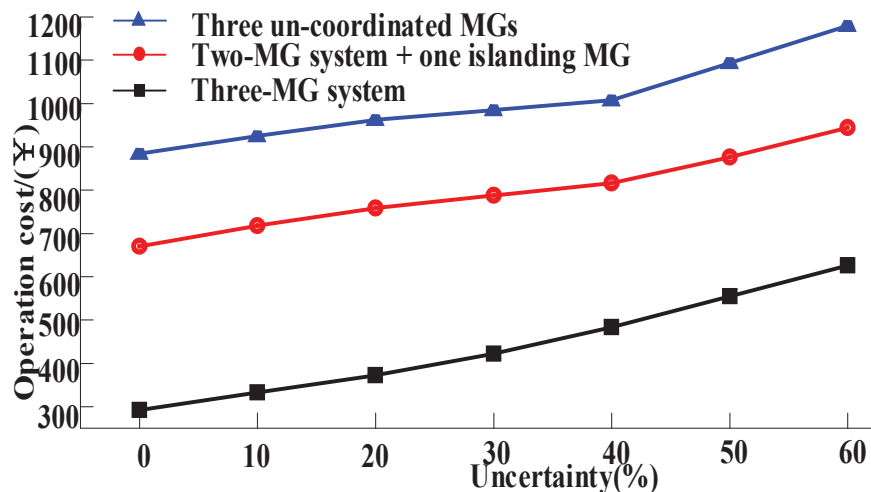
The objective function in DMS seeks to minimize the costs of buying and selling energy for the entire group of MGs. In the MGCC, the objective function try to minimize the costs of diesel generation ( $\min_{x_m}$ ), in addition to minimizing the costs with DERs ( $\min_{y_m}$ ) considering uncertainties in the PV and WT forecasted curves. Once the degree of uncertainty is defined, the algorithm in MGCC search for the worst case of cost ( $\max_{w_m, p_m}$ ), fixing the PV and WT curves for the minimization algorithm.

Performing this problem requires an interaction between the DMS and MGCC algorithms to obtain an ideal solution for both. It begins with a power flow analysis of the MMG DN area, considering the topology illustrated in Figure 3.5. From this analysis, a initial feasible vector  $z_m$  (active powers) is obtained. Then, DMS passes on the information to MGCC, and waits for  $v^*(z_m)$  to continue its optimization process. Upon receiving  $z_m$ , MGCC uses it in the power balance constraint to perform its optimization.

Next, the optimal cost  $v^*(z_m)$  for the current iteration, obtained by MGCC, is passed on to the DMS that makes up its first feasible solution. The procedure is repeated until the DMS algorithm reaches the specified tolerance range for convergence.

Authors consider a scenario for test in which 3 MGs are interconnected to a DN forming an MMG system of PCM architecture. However, only one MG is self-sufficient in energy over an entire day. In the end, the optimal cost of operation by MG and the total cost of the DN are obtained. In order to compare the approach of a DN with MGs operating independently and a DN with an MMG system, the authors present a case study considering these two scenarios, and a third as a combination of both. The results are reproduced in Figure 3.6 and show that MMG system approach can be less costly. Finally, since the authors consider the uncertainty in renewable energy resources (WT and PV) in modeling the problem, it was possible to analyze its impact on operating costs, as also illustrated by the Figure 3.6, i.e., the higher the level of uncertainty the higher the operating costs, independent of the scenario considered.

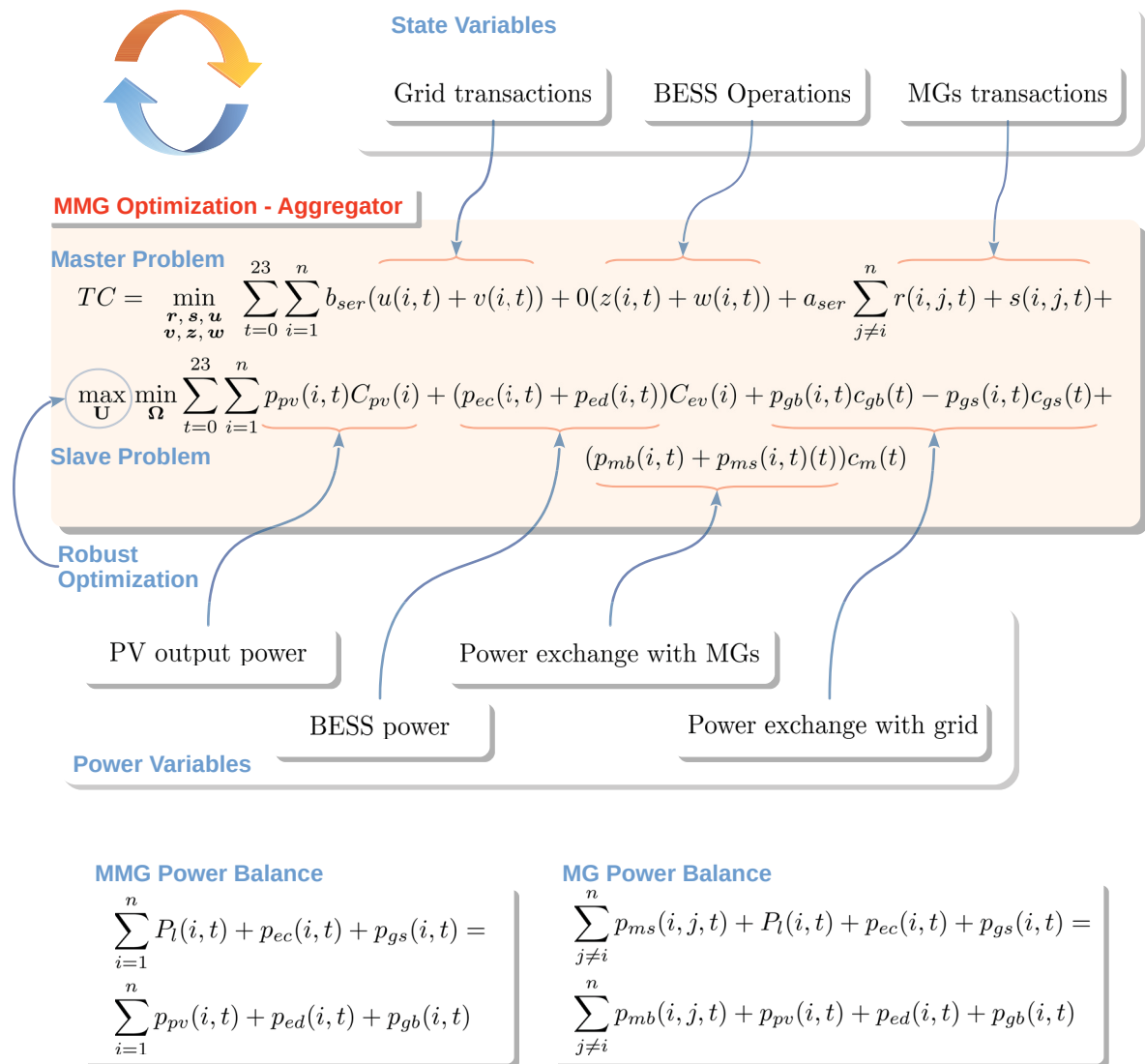
Figure 3.6 – A case study of operation cost in a distribution network with three MGs for increasing levels of uncertainty in RES (WT and PV): approaches with and without MMG.



Source: Zhao et al. (2018)

Figure 3.7 presents a graphical abstract, elaborated here, on the work of (ZHANG et al., 2018). In the MMG environment that the authors present, each MG is a residence containing PV rooftop, electric vehicle (which plays the role of energy storage system), and domestic loads. An agent called aggregator operates the MG group and has the

Figure 3.7 – Visual abstract on the work of Zhang et al. (2018).



Source: The author (2022).

function of managing transactions between MGs, and transactions with the main grid. He is also responsible for the optimization of the MMG.

The authors divide the problem into a master and a slave problem to solve it iteratively, as in Zhao et al. (2018). Thus, there are no two independent optimization problems as the formulation (transcribed from the article) of Figure 3.7 suggests.

When comparing a cooperative environment MMG, with transactions between MGs, with another without those transactions, the authors conclude that the former presents a reduction in the cost of operation and in the number of transactions.

## 3.6 Final Considerations

This chapter presents detailed modeling of the optimal dispatch of microgrids with a battery energy storage system; a PV system with the possibility of curtailment; demand response through directly controllable loads, such as the shiftable and interruptible ones; and the option of considering scheduled intentional islanding events with the possibility of performing load shedding when necessary.

The battery storage system is modeled according to the IEEE Std 2030.2.1-2019. Details of this modeling are presented, considering aspects such as the efficiency of the whole BESS, and state of charge as a non-recursive constraint. Furthermore, the ranges of some practical values for the model parameters are presented. In cost modeling, an exponential equation for the battery state of health is presented in order to fit a possible BESS manufacturing data curve. The costs of BESS storage, charging, and discharging are then presented as a function of the SOH threshold, rated depth of discharge, cycle life, and the battery capacity.

In the cost modeling of the PV system, factors such as annual degradation of the photovoltaic panels, the lifespan of PV panels, and the solar generation capacity from the region of installation are considered. The methodology adopted in the modeling gave rise to a problem of mixed-integer linear programming.

Finally, some MMG energy management models are presented and analyzed.



## 4 MMG as Active Element in Feeder Voltage Regulation

This chapter presents a methodology developed in this work for including MMG as active element in feeder voltage regulation.

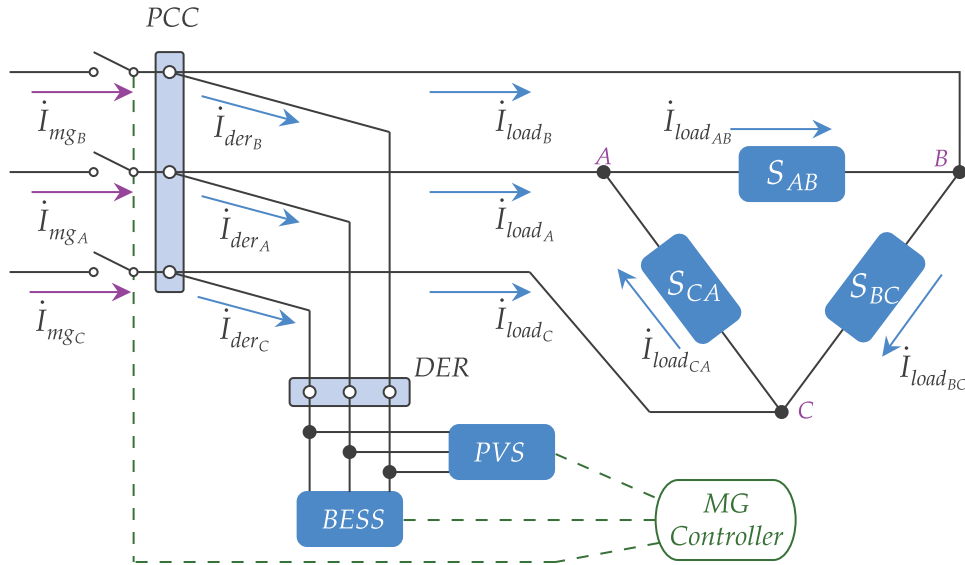
A measured or calculated condition where the voltage at a power system node is outside the acceptable operating standards limits constitutes a voltage violation. In a distribution network, a voltage violation can occur in line sections of a distribution feeder during its real-time operation. The voltage drop, and therefore the voltage violation, depends on the loads connected along the feeder, which are time-varying, the distance between the connection points and the substation, the impedance of the distribution line cables, and the mutual inductance between phases. As the loads connected along the feeder vary, there is a need for voltage regulation in order to prevent violations from occurring. Common methods of voltage regulation are the application of voltage regulators, load tap change transformers (LTC), and shunt capacitors (KERSTING, 2002).

The increasing penetration of MGs and DERs in today's distribution systems can impact voltage drop on feeders. On the one hand, increasing loads from MGs and energy storage systems operating in load mode can worsen the voltage profile of the feeder. On the other hand, distributed generation systems, energy storage systems operating in supply mode, and controllable loads can help to improve it and prevent a voltage violation from occurring. For example, an MG can use its distributed energy resources to control the power flow at the PCC bus and thus contribute to the feeder voltage regulation.

Figure 4.1 illustrates a three-phase schematic diagram of an MG with BESS, solar photovoltaic system (PVS), and a delta-connected load. The MG controller can use BESS as a resource to control the power injection on the MG PCC bus. Thus, when the BESS is in supply mode, the distribution network starts to see a reduction in the MG load without the actual connected load being effectively reduced. The controller can even make this load negative, which means reversing the power flow in the MG PCC bus. Also, it can utilize the controllable loads resource (when available) to effectively reduce the MG load for a period of time needed to assist in voltage regulation.

This concept can be extended to multiple MGs on a feeder, operating as an MMG, which is the subject of the methodology developed in this work and presented in this chapter. The basic idea is to take advantage of the MMG's operating flexibility due to its DERs to improve the voltage profile per phase of a three-phase distribution feeder and, consequently, minimize or avoid a voltage violation in that area of the distribution network.

Figure 4.1 – Three-phase schematic diagram of an MGs with BESS, PVS, and delta-connected load.



Source: The author (2022).

The following section presents a narrative review of the literature on voltage control in distribution networks using distributed energy resources in microgrids, preceded by a brief mathematical background on voltage sensitivity matrices. Some relevant and recent works on this subject indicate the trends, advantages, and results of methods currently explored in the literature.

## 4.1 Background Information on DN Voltage Control with MGs

In recently published works, voltage sensitivity analysis has been the preferred methodology to solve the voltage control problem in distribution networks, such as (WANG et al., 2018; DOU et al., 2018; PAPPALARDO; CALDERARO; GALDI, 2022). Equation 4.1 shows the voltage sensitivity matrix equation for a distribution network with  $N_B$  buses, where  $\Delta V_k$  is the voltage variation in the  $k$ -th bus due to the real  $\Delta P$  and reactive  $\Delta Q$  power variation in the other buses;  $\mathbf{J}_P$  and  $\mathbf{J}_Q$  are the sensitivity matrices for real and reactive powers, respectively, and their elements are the sensitivity coefficients.

$$\begin{aligned}
\begin{bmatrix} \Delta V_1 \\ \Delta V_2 \\ \vdots \\ \Delta V_k \\ \vdots \\ \Delta V_{N_b} \end{bmatrix} &= \underbrace{\begin{bmatrix} \frac{\partial V_1}{\partial P_1} & \frac{\partial V_1}{\partial P_2} & \cdots & \frac{\partial V_1}{\partial P_k} & \cdots & \frac{\partial V_1}{\partial P_{N_b}} \\ \frac{\partial V_2}{\partial P_1} & \frac{\partial V_2}{\partial P_2} & \cdots & \frac{\partial V_2}{\partial P_k} & \cdots & \frac{\partial V_2}{\partial P_{N_b}} \\ \vdots & \vdots & \ddots & \vdots & \ddots & \vdots \\ \frac{\partial V_k}{\partial P_1} & \frac{\partial V_k}{\partial P_2} & \cdots & \frac{\partial V_k}{\partial P_k} & \cdots & \frac{\partial V_k}{\partial P_{N_b}} \\ \vdots & \vdots & \ddots & \vdots & \ddots & \vdots \\ \frac{\partial V_{N_b}}{\partial P_1} & \frac{\partial V_{N_b}}{\partial P_2} & \cdots & \frac{\partial V_{N_b}}{\partial P_k} & \cdots & \frac{\partial V_{N_b}}{\partial P_{N_b}} \end{bmatrix}}_{\mathbf{J}_P} \begin{bmatrix} \Delta P_1 \\ \Delta P_2 \\ \vdots \\ \Delta P_k \\ \vdots \\ \Delta P_{N_b} \end{bmatrix} + \\
&\underbrace{\begin{bmatrix} \frac{\partial V_1}{\partial Q_1} & \frac{\partial V_1}{\partial Q_2} & \cdots & \frac{\partial V_1}{\partial Q_k} & \cdots & \frac{\partial V_1}{\partial Q_{N_b}} \\ \frac{\partial V_2}{\partial Q_1} & \frac{\partial V_2}{\partial Q_2} & \cdots & \frac{\partial V_2}{\partial Q_k} & \cdots & \frac{\partial V_2}{\partial Q_{N_b}} \\ \vdots & \vdots & \ddots & \vdots & \ddots & \vdots \\ \frac{\partial V_k}{\partial Q_1} & \frac{\partial V_k}{\partial Q_2} & \cdots & \frac{\partial V_k}{\partial Q_k} & \cdots & \frac{\partial V_k}{\partial Q_{N_b}} \\ \vdots & \vdots & \ddots & \vdots & \ddots & \vdots \\ \frac{\partial V_{N_b}}{\partial Q_1} & \frac{\partial V_{N_b}}{\partial Q_2} & \cdots & \frac{\partial V_{N_b}}{\partial Q_k} & \cdots & \frac{\partial V_{N_b}}{\partial Q_{N_b}} \end{bmatrix}}_{\mathbf{J}_Q} \begin{bmatrix} \Delta Q_1 \\ \Delta Q_2 \\ \vdots \\ \Delta Q_k \\ \vdots \\ \Delta Q_{N_b} \end{bmatrix}
\end{aligned} \tag{4.1}$$

Thus, the voltage variation on the  $k$ -th bus is a single element in the voltage variation vector from Equation 4.1, which can be calculated by

$$\Delta V_k = \sum_{i=1}^{N_b} \frac{\partial V_k}{\partial P_i} \Delta P_i + \frac{\partial V_k}{\partial Q_i} \Delta Q_i \tag{4.2}$$

Note that the sensitivity coefficients are partial derivatives of voltage functions as  $V_k(P_1, P_2, \dots, P_k, \dots, P_{N_b})$  and  $V_k(Q_1, Q_2, \dots, Q_k, \dots, Q_{N_b})$ . However, as power injections are nonlinear functions of voltages (ZHOU; BIALEK, 2008), sensitivity matrices changes with operating conditions. Hence, for each distribution network operating point, there is a new sensitivity matrix. Also, distribution networks are typically unbalanced three-phase systems, which requires an equivalent Equation 4.1 for each phase, in addition to consider the cross-sensitivity coefficients to represent the voltage variation in one phase due to power changes in the other two.

Since sensitivity matrices establish a direct relationship between power variations throughout the feeder and voltage variation in a bar, there is interest in computing or estimating these matrices to solve the voltage control problem. Wang et al. (2018) presents an optimal voltage regulation method for a distribution network with MMG. Each MG participates in voltage control as an ancillary service provider while minimizing operating costs. According to the authors, sensitivity analysis is a common voltage control method that usually obtain the sensitivity matrices through a Jacobin matrix computing, which could require massive communication and calculation. Thus, they propose to use a multi-agent system to calculate such matrices in a distribution network using only local

and neighborhood measurements (decentralized approach) to solve the voltage control problem. The modified IEEE 33 Bus test feeder is used to simulate and validate the proposed method. Since this is a balanced feeder, simulations are performed on an equivalent single-phase circuit model. The results show that microgrids improve the voltage profile of the distribution network and avoid possible voltage violations at the feeder for a day of operation.

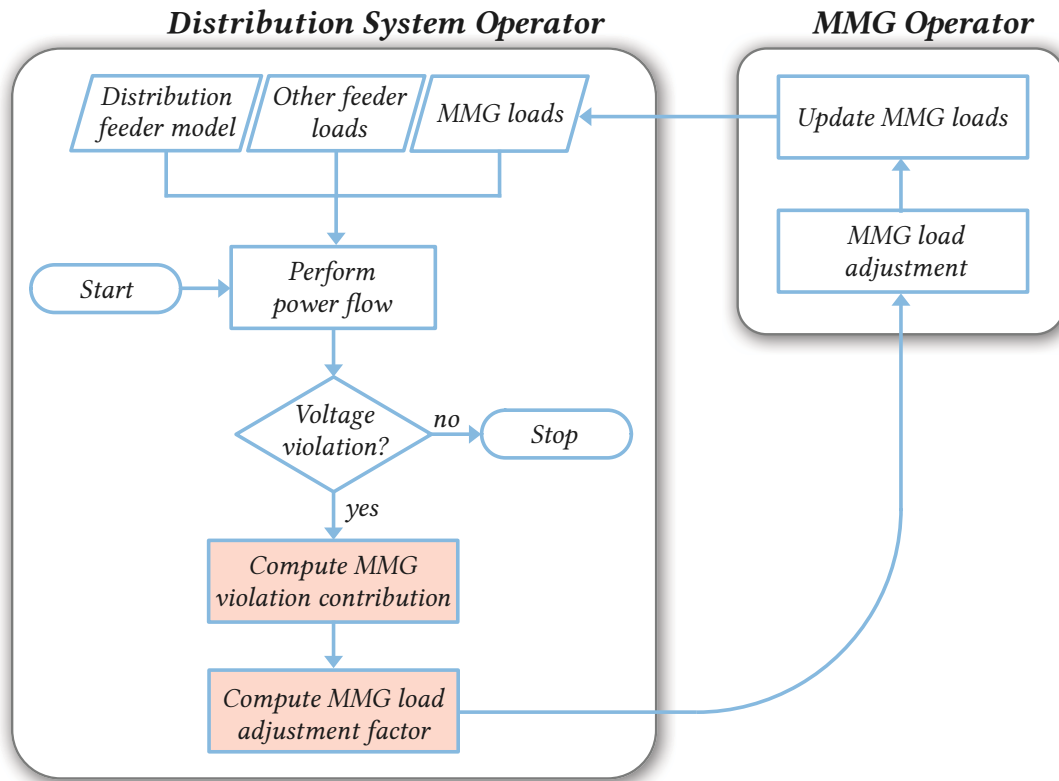
Dou et al. (2018) also presents a distributed voltage control strategy to an active distribution network containing multi-microgrids. As in Wang et al. (2018), the authors propose a control strategy in which each MG negotiates resources with its MG neighbor. In addition, they calculate the voltage sensitivity of a node from the Jacobian inverse matrix calculated during the power flow performing, as the method presented in (ZHOU; BIALEK, 2008). The simulations of this paper are performed in a single-phase distribution network equivalent model, proposed by the authors, in which the feeder presents only microgrids (three) as loads. The paper presents results which suggest that the proposed control may correct voltage deviations in the microgrids buses.

Pappalardo, Calderaro and Galdi (2022) present a voltage control method for distribution network with MGs that is also based on sensitivity analysis. In this paper, the method used to calculate the sensitivity coefficients, developed by the authors, makes possible to calculate the sensitivity matrix for both radial and mesh networks. The control strategy presented by the authors to correct a voltage violation is to use the reactive power of the distributed generation unity that has the highest sensitivity coefficient for the bus where the violation occurred. If the energy resource of this unit is not sufficient to fully correct the violation, then the distributed generation that has the second-highest coefficient is triggered, and so on. With this strategy, only one coefficient in Equation 4.2 is used at a time, making possible to compute  $\Delta Q_i$  directly from the coefficient considered. The authors perform simulations in two different circuits (with 40 buses and 41 buses) containing conventional generators, PV, and wind generation. Both circuits are modeled as a single-phase equivalent circuit. The results presented in that work show the proposed voltage regulation strategy can maintain the voltage of the distribution network within the operating limits.

## 4.2 Overview of the Proposed Methodology

Figure 4.2 illustrates a flowchart that describes the interaction between the DSO and MMG operator as an overview of this methodology. To check for voltage violation on a feeder at any time, the DSO needs to perform a three-phase power flow (PF) on that feeder, which is the initial task of that procedure in the figure. The electrical modeling of the feeder and the loads connected to it (MMG loads and other feeder loads) are input

Figure 4.2 – Voltage regulation methodology flowchart illustrating the interaction between the DSO and the MMG operator.



Source: The author (2022).

parameters for the PF algorithm. After performing the PF, it is possible to check if there is any violation. If not, the procedure ends. Otherwise, the next step is to calculate the MMG's contribution, in volts, to that violation. In addition, it is necessary to compute the MMG load adjustment factors that should result in a violation-free condition. The colored background blocks in the flowchart represent these last two tasks. As a next step, the DSO must send these factors to the MMG operator, who must use them to change the setpoints of its MG controllers and thus fulfill the DSO requirement. As a result, the load verified in each MG PCC bus should be updated. Therefore, the next PF performed by the DSO should result in a voltage profile within acceptable limits for operation, which ends the procedure.

This procedure can be applied to both real-time operation and day-ahead scheduling. The latter is the one that most resembles the flowchart shown in Figure 4.2. In it, the load blocks at the inputs of the PF block become load profiles for the next day. Initially, the MMG operator sends to the DSO the desired load profile of each MG for the next day, as a result of an optimization process. Then, the DSO checks for violation points

and sends load adjustment factors to the MMG operator. As a next step, a new round of MGs optimization is performed, now with the operating constraints imposed by the DSO, which results in an MMG updated load profile that is sent to the DSO. This procedure is repeated until the day-ahead schedule is violation-free.

In real-time operation, voltage violations are verified from the feeder voltage profile, which can be measured, estimated, or a mix of both. Consequently, the DSO does not necessarily perform PF to verify them. Therefore, the procedure begins after the DSO identify a violation. Then, from measurements of current on each MGG PCC bus, voltage on the substation bus, the violation voltage magnitude, and information from the feeder model, the DSO can calculate in volts each MG's contribution to such a violation. The load adjustment factor is then computed and sent to the MMG operator. In real-time, the MMG operator adjusts the setpoint of the MG controllers to perform the load reduction imposed by the DSO. Theoretically, after the action of the controllers, the DSO operation system should identify in real-time the elimination of that violation.

In real-time operation and day-ahead scheduling, the calculation of both the MMG violation contribution and the load adjustment factor are crucial tasks for the procedure here presented. Therefore, the following sections describe them in detail.

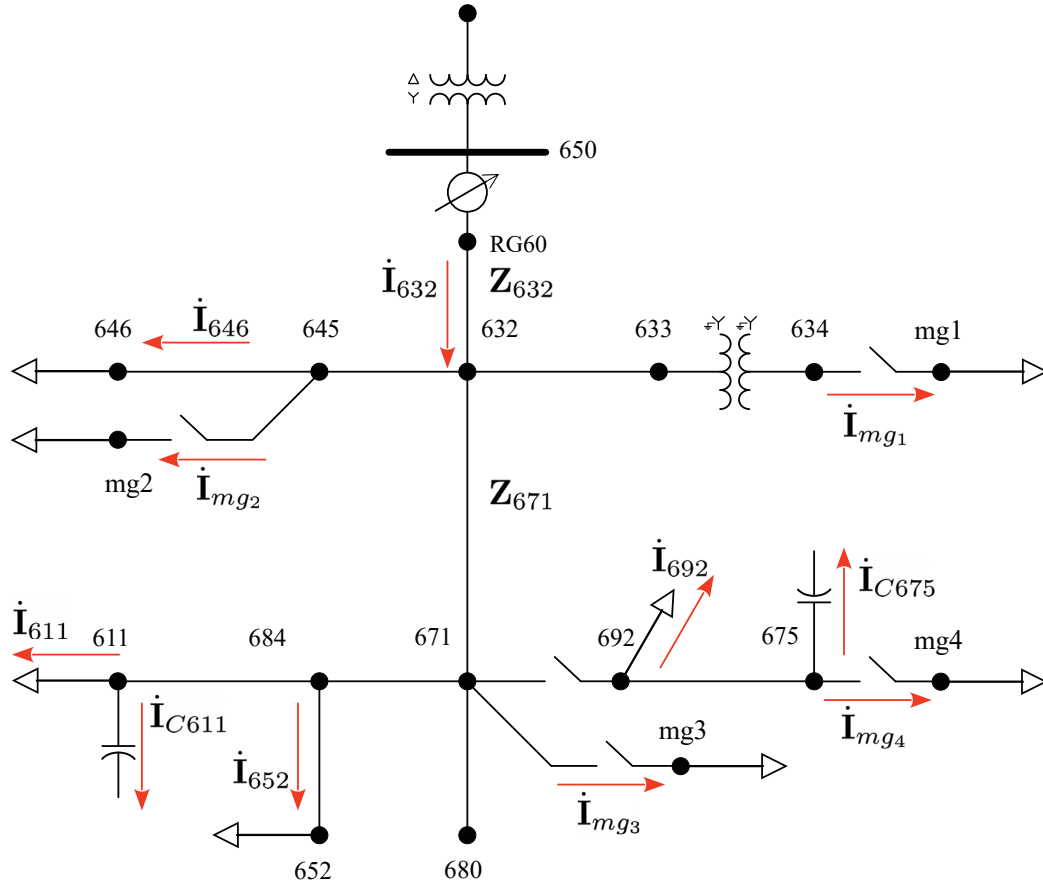
### 4.3 Development of the Proposed Methodology

Figure 4.3 shows a schematic diagram of a feeder adapted from the IEEE 13-bus with four MGs in an MMG environment, which is the reference circuit adopted for the development presented in this work. However, this methodology is not restricted to that circuit specifically, and as will be seen in this chapter, it can be applied to other radial feeder circuits of distribution networks.

Regarding the nomenclature, the phases of a three-phase system are represented in this work by the letters  $a$ ,  $b$ , and  $c$ , or numbers 1, 2, and 3, as long as the relation  $(a, b, c) = (1, 2, 3)$  is observed for the positive sequence of phasors ( $[0^\circ, -120^\circ, 120^\circ]$ ). In addition, the definition for the terms node and bus used throughout this text is in accordance with the standard IEEE Recommended Practice for Electric Power Distribution System Analysis (IEEE, 2014b) i.e.,

- node is “a single electrical connection point for power system conductors. One or more nodes may be collected into a bus.” (IEEE, 2014b);
- bus is “a grouping of electrical connection points consisting of one or more nodes, incorporating one or more phases, and possibly including neutral conductors.” (IEEE, 2014b).

Figure 4.3 – Schematic diagram of a feeder based on the IEEE 13-bus with four MGs in an MMG environment.



Source: Adapted from Kersting (2001).

Therefore, the  $p$ -th phase of the  $n$ -th bus is referred in this work as the connection point (node)  $n.p$ ; as for example, node  $632.a$  or  $632.1$ .

Now, consider the feeder illustrated in Figure 4.3. The relationship between the voltages of two consecutive buses connected by a line  $sn$  (from bus  $s$  to bus  $n$ ) is given by

$$\begin{bmatrix} \dot{V}_a \\ \dot{V}_b \\ \dot{V}_c \end{bmatrix}_n = \begin{bmatrix} \dot{V}_a \\ \dot{V}_b \\ \dot{V}_c \end{bmatrix}_s - \begin{bmatrix} Z_{aa} & Z_{ab} & Z_{ac} \\ Z_{ba} & Z_{bb} & Z_{bc} \\ Z_{ca} & Z_{cb} & Z_{cc} \end{bmatrix}_{sn} \times \begin{bmatrix} \dot{I}_a \\ \dot{I}_b \\ \dot{I}_c \end{bmatrix}_{sn} \quad (4.3)$$

which in matrix notation is

$$\dot{\mathbf{V}}_n = \dot{\mathbf{V}}_s - \mathbf{Z}_{sn} \dot{\mathbf{I}}_{sn} \quad (4.4)$$

where  $\dot{\mathbf{V}}_n$  and  $\dot{\mathbf{V}}_s$  are  $3 \times 1$  vectors of voltage phasors on the bus  $n$  and  $s$ , respectively;  $\mathbf{Z}_{sn}$  and  $\dot{\mathbf{I}}_{sn}$  are the  $3 \times 3$  impedance matrix and the  $3 \times 1$  vector of current phasors of

the line  $sn$ , respectively. Throughout this chapter, impedance matrices, and current and voltage phasor vectors have this default shape unless otherwise noted.

On the other hand, the voltage drop verified on a bus  $n$  located downstream of a bus  $s$  is given by (KERSTING, 2002)

$$\begin{aligned}\mathbf{V}_{drop_n} &:= \left| \dot{\mathbf{V}}_s \right| - \left| \dot{\mathbf{V}}_n \right| \\ &= \left| \dot{\mathbf{V}}_s \right| - \left| \dot{\mathbf{V}}_s - \mathbf{Z}_{sn} \dot{\mathbf{I}}_{sn} \right|\end{aligned}\quad (4.5)$$

which by phase is

$$\left( V_{drop_a} \right)_n = \left| \left( \dot{V}_a \right)_s \right| - \left| \left( \dot{V}_a \right)_s - \left( Z_{aa} \dot{I}_a + Z_{ab} \dot{I}_b + Z_{ac} \dot{I}_c \right)_{sn} \right| \quad (4.6a)$$

$$\left( V_{drop_b} \right)_n = \left| \left( \dot{V}_b \right)_s \right| - \left| \left( \dot{V}_b \right)_s - \left( Z_{ba} \dot{I}_a + Z_{bb} \dot{I}_b + Z_{bc} \dot{I}_c \right)_{sn} \right| \quad (4.6b)$$

$$\left( V_{drop_c} \right)_n = \left| \left( \dot{V}_c \right)_s \right| - \left| \left( \dot{V}_c \right)_s - \left( Z_{ca} \dot{I}_a + Z_{cb} \dot{I}_b + Z_{cc} \dot{I}_c \right)_{sn} \right| \quad (4.6c)$$

Also, consider the line rg60632 (from bus rg60 to 632). The voltage difference  $\dot{\mathbf{V}}_{diff632}$  across this line can be calculated by Equation 4.4, which is

$$\dot{\mathbf{V}}_{diff632} = \dot{\mathbf{V}}_{rg60} - \dot{\mathbf{V}}_{632} = \mathbf{Z}_{632} \dot{\mathbf{I}}_{632} \quad (4.7)$$

where  $\mathbf{Z}_{632}$  and  $\dot{\mathbf{I}}_{632}$  are the impedance matrix and vector of current phasors of the line rg60632, respectively.

The contribution of the MMG to the voltage difference on this line can be emphasized by applying the Kirchhoff's current law (KCL) to the bus 632, i.e.

$$\dot{\mathbf{V}}_{diff632} = \mathbf{Z}_{632} \left( \dot{\mathbf{I}}_{loads} + \dot{\mathbf{I}}_{mmg} \right) \quad (4.8)$$

where  $\dot{\mathbf{I}}_{mmg} = \dot{\mathbf{I}}_{mg1} + \dot{\mathbf{I}}_{mg2} + \dot{\mathbf{I}}_{mg3} + \dot{\mathbf{I}}_{mg4}$ , and  $\dot{\mathbf{I}}_{loads}$  is the sum of all other load currents, excluding the  $\dot{\mathbf{I}}_{mmg}$ .

An equivalent procedure can be adopted to calculate the voltage drop across this line (voltage drop verified on bus 632) using Equation 4.5

$$\begin{aligned}\mathbf{V}_{drop_{632}} &:= \left| \dot{\mathbf{V}}_{rg60} \right| - \left| \dot{\mathbf{V}}_{632} \right| \\ &= \left| \dot{\mathbf{V}}_{rg60} \right| - \left| \dot{\mathbf{V}}_{rg60} - \mathbf{Z}_{632} \dot{\mathbf{I}}_{loads} - \mathbf{Z}_{632} \dot{\mathbf{I}}_{mmg} \right|\end{aligned}\quad (4.9)$$

In Equation 4.8,  $\dot{\mathbf{V}}_{diff}$  is a linear sum of terms formed by all currents in that line segment, in which it is possible to isolate the contribution of the MMG. On the other hand, this procedure is not possible for  $\mathbf{V}_{drop}$  in (4.9), since the modulus is a non-linear function. However, according to Kersting (2002), the voltage drop across a distribution



line is approximately equal to the real part of  $\dot{\mathbf{V}}_{\text{diff}}$ , i.e.

$$\mathbf{V}_{\text{drop}_{632}} \cong \text{Re} \left\{ \mathbf{Z}_{632} \dot{\mathbf{I}}_{\text{loads}} + \mathbf{Z}_{632} \dot{\mathbf{I}}_{\text{mmg}} \right\} \quad (4.10)$$

This equation shows that the relationship between the voltage drop in the line and the currents through the same line is approximately linear. Therefore, the superposition theorem can be applied to this result, i.e.

$$\mathbf{V}_{\text{drop}_{632}} \cong \mathbf{V}_{\text{drop}_{632}}^{\text{mmg}} + \mathbf{V}_{\text{drop}_{632}}^{\text{loads}} \quad (4.11)$$

where

$$\mathbf{V}_{\text{drop}_{632}}^{\text{mmg}} \cong \text{Re} \left\{ \mathbf{Z}_{632} \dot{\mathbf{I}}_{\text{mmg}} \right\} \quad (4.12a)$$

$$\mathbf{V}_{\text{drop}_{632}}^{\text{loads}} \cong \text{Re} \left\{ \mathbf{Z}_{632} \dot{\mathbf{I}}_{\text{loads}} \right\} \quad (4.12b)$$

and  $\mathbf{V}_{\text{drop}}^{\text{mmg}}$  is the MMG contribution to the voltage drop across the line and  $\mathbf{V}_{\text{drop}}^{\text{loads}}$  the contribution of other feeder loads.

According to Equation 4.12, decreasing the MMG load current by a factor ( $k_{\text{drop}}^{\text{mmg}} \in \mathbb{R}$ ),  $\mathbf{V}_{\text{drop}}^{\text{mmg}}$  should decrease by the same factor, i.e.

$$\begin{aligned} \mathbf{V}'_{\text{drop}_{632}}{}^{\text{mmg}} &\cong \text{Re} \left\{ \mathbf{Z}_{632} k_{\text{drop}}^{\text{mmg}} \dot{\mathbf{I}}_{\text{mmg}} \right\} \\ &= k_{\text{drop}}^{\text{mmg}} \text{Re} \left\{ \mathbf{Z}_{632} \dot{\mathbf{I}}_{\text{mmg}} \right\} \\ &= k_{\text{drop}}^{\text{mmg}} \mathbf{V}_{\text{drop}_{632}}^{\text{mmg}} \end{aligned} \quad (4.13)$$

In addition, for any load, if  $S = \dot{V} \dot{I}^* = P + jQ$  by phase, then

$$\begin{aligned} S' &= \dot{V} k_{\text{drop}}^{\text{mmg}} \dot{I}^* = k_{\text{drop}}^{\text{mmg}} S \\ &= k_{\text{drop}}^{\text{mmg}} (P + jQ) \end{aligned} \quad (4.14)$$

Equations 4.14, 4.13, and 4.11 show that weighting (by phase) an MG load by a factor  $k_{\text{drop}}^{\text{mmg}}$  impacts the voltage drop (of this phase) on the bus by approximately the same factor. Furthermore, according to (4.6), although such a factor is being applied to a single phase, the voltage drop of all three phases can be impacted.

According to the Agência Nacional de Energia Elétrica (2021), the minimum service voltage at connection points with a rated voltage greater than 1 kV and less than 69 kV is 0.93 pu. A violation happens if the voltage at some point of the distribution network falls below this threshold. Thus, the violation voltage on a node  $n.p$  can be

defined by:

$$(V_{vio})_{n,p} := 0.93V_{base} - |(\dot{V})_{n,p}| \quad (4.15)$$

where  $V_{base}$  is the base voltage. A positive value of  $V_{vio}$  indicates the magnitude of a violation, and a negative or zero value indicates the magnitude of voltage above the threshold (no violation).

Now, considering that the MMG can help to minimize or overcome a voltage violation in the DN, then a new MMG voltage drop  $V'_{drop}{}^{mmg}$  (by phase) needs to be achieved, i.e.,

$$(V'_{drop}{}^{mmg})_{n,p} = (V_{drop}{}^{mmg})_{n,p} - (V_{vio})_{n,p} \quad (4.16)$$

Thus, the MMG load adjustment factor can be computed from (4.13) and (4.16),

$$(k_{drop}{}^{mmg})_p = \left( \frac{V'_{drop}{}^{mmg}}{V_{drop}{}^{mmg}} \right)_{n,p} = \left( \frac{V_{drop}{}^{mmg} - V_{vio}}{V_{drop}{}^{mmg}} \right)_{n,p} \quad (4.17)$$

Knowing the value of  $k_{drop}{}^{mmg}$  allows setting a new adjustment for the load that the distribution system sees at each MG PCC bus, i.e.

$$\begin{aligned} (S'_{mg1})_p &\leq (k_{drop}{}^{mmg})_p (P_{mg1} + jQ_{mg1})_p \\ (S'_{mg2})_p &\leq (k_{drop}{}^{mmg})_p (P_{mg2} + jQ_{mg2})_p \\ (S'_{mg3})_p &\leq (k_{drop}{}^{mmg})_p (P_{mg3} + jQ_{mg3})_p \\ (S'_{mg4})_p &\leq (k_{drop}{}^{mmg})_p (P_{mg4} + jQ_{mg4})_p \end{aligned} \quad (4.18)$$

In fact, it will be seen later that each MG can have a different drop factor to achieve the same result.

To calculate  $V'_{drop}{}^{mmg}$  in (4.16) it is necessary to know the value of  $V_{drop}{}^{mmg}$  which is a composition of the contribution of each MG, i.e.

$$(V_{drop}{}^{mmg})_{n,p} = (V_{drop}{}^{mg1} + V_{drop}{}^{mg2} + V_{drop}{}^{mg3} + V_{drop}{}^{mg4})_{n,p} \quad (4.19)$$

and  $V_{drop}{}^{mg(i)}$ , the value of each MG contribution to the voltage drop on that bus  $n$ , phase  $p$ , can be extracted from the three-phase vector  $\mathbf{V}_{drop}{}^{mg(i)}$  calculated as

$$\begin{aligned} (\mathbf{V}_{drop}{}^{mg(i)})_n &:= |\dot{\mathbf{V}}_{rg60}| - |\dot{\mathbf{V}}_n| \\ &= |\dot{\mathbf{V}}_{rg60}| - |\dot{\mathbf{V}}_{rg60} - \mathbf{Z}_{share}^{n,i} \dot{\mathbf{I}}_{mg(i)}|, \quad \text{for } i = \{1, \dots, 4\} \end{aligned} \quad (4.20)$$

where  $\dot{\mathbf{V}}_{rg60}$  is the source voltage phasor vector (for the reference feeder it is the voltage on the bus RG60);  $\dot{\mathbf{I}}_{mg(i)}$  is the current phasor vector verified at the PCC of the MG( $i$ );

and  $\mathbf{Z}_{share}^{n,i}$  is the matrix formed by the sum of the impedance matrices of the lines shared between bus  $n$  and MG( $i$ ).

Although along the development of this methodology Equation 4.10 has been used to show an approximately linear relationship between the MG current and the voltage drop in a distribution network bus, in fact, in Equation 4.20 it was used the definition presented in Equation 4.5, which is not an approximation. The justification for this choice is that Equation 4.10 represents the motivation for formulating the methodology whereas Equation 4.5 represents how this procedure can actually be performed regarding the computation of the voltage drop, without the need for approximations.

Concerning power injection on the PCC bus, two operating modes for an MG are considered in this work:

- Load mode: when the main grid is injecting real power into the MG PCC bus. Thus if an MG is consuming power from the main grid, then it is in load mode. Sign convention: real power (load) with positive sign.
- Supply mode: when an MG is injecting real power into the PCC bus. Therefore, if an MG is supplying power to the main grid, through BESS and/or PVS for example, then it is in supply mode. Sign convention: real power (load) with negative sign.

Finally, some MGs can participate in the voltage regulation procedure by adjusting their loads and others cannot. Thus, consider the following definitions:

- $\mathbb{U}_{mg} = \{1, 2, 3, 4\}$  is the set of MGs in the MMG;
- $(\mathbb{U}_{in})_{n,p}$  is a subset of  $\mathbb{U}_{mg}$  with the MGs that are included in the voltage regulation procedure on bus  $n$ , phase  $p$ ;
- $(\mathbb{U}_{out})_{n,p}$  is a subset of  $\mathbb{U}_{mg}$  with the MGs that are excluded from the voltage regulation procedure on bus  $n$ , phase  $p$ ;
- $\mathbb{U}_{in} \cap \mathbb{U}_{out} = \emptyset$

## 4.4 Cases of MMG Voltage Drop

### 4.4.1 Voltage Drop Case 1: $V_{drop}^{mmg} > V_{vio}$

When the situation  $0 < V_{vio} < V_{drop}^{mmg}$  occurs, from Equation 4.17, the range of the MMG load adjustment factor is  $0 < k_{drop}^{mmg} < 1$ . Thus, there is a voltage violation on a node  $n.p$  and the MMG is actively contributing to that. But, it can minimize its impact on the distribution network by adjusting its load. In this case, the MMG can:

- i) decrease the load of those MGs in load mode;
- ii) increase the power injection of MGs that are in supply mode, if any.

Thus, the MMG operator can choose either strategy (i) alone, or (i) and (ii) together. There may be a cost difference between one option and another, which characterizes an optimization problem to the MMG operator to solve. However, such an optimization problem is outside the scope of this work. Therefore, strategy (i) alone will be adopted in this study to make the process simpler.

In this case, if any MG of the group is in supply mode, then it may have a  $V_{drop}^{mg} \leq 0$ , and for that reason, it should be left out of the procedure, which just means keeping your load unchanged ( $k_{drop}^{mg} = 1$ ). Therefore, the MG sets can be defined as

$$(\mathbb{U}_{in})_{n,p} = \begin{cases} \text{MGs that have } V_{drop}^{mg} > 0, \\ \text{and have one or more line shared with bus } n, \\ \text{and have the phase } p. \end{cases} \quad (4.21a)$$

$$(\mathbb{U}_{out})_{n,p} = \begin{cases} \text{MGs that have } V_{drop}^{mg} \leq 0, \\ \text{or do not have any line shared with bus } n, \\ \text{or do not have the phase } p. \end{cases} \quad (4.21b)$$

Thus, MMG load adjustment factor for each group can be computed by

$$\left(k_{drop}^{in}\right)_p = \left( \frac{V_{drop}^{mmg} - V_{vio} - \sum_{i \in \mathbb{U}_{out}} V_{drop}^{mg(i)}}{\sum_{i \in \mathbb{U}_{in}} V_{drop}^{mg(i)}} \right)_{n,p}, \quad \forall \text{ MG} \in \mathbb{U}_{in} \quad (4.22a)$$

$$\left(k_{drop}^{out}\right)_p = 1, \quad \forall \text{ MG} \in \mathbb{U}_{out} \quad (4.22b)$$

As an illustrative example, consider that:  $V_{vio} = 60 V$  and  $V_{drop}^{mmg} = 100 V = \underbrace{120 V}_{mg1} - \underbrace{50 V}_{mg2} + \underbrace{15 V}_{mg3} + \underbrace{15 V}_{mg4}$ .

Therefore, the MG sets are  $\mathbb{U}_{in} = \{1, 3, 4\}$  and  $\mathbb{U}_{out} = \{2\}$ . Thus,

$$k_{drop}^{in} = \frac{100 - 60 - (-50)}{150} = 0.6$$

where  $k_{drop}^{mg1} = k_{drop}^{mg3} = k_{drop}^{mg4} = k_{drop}^{in}$ , and  $k_{drop}^{mg2} = k_{drop}^{out}$ .

Thus, to overcome the voltage violation at the node  $n,p$ , the MG loads must be

adjusted by

$$(S'_{mg1})_p \leq (k_{drop}^{mg1})_p (P_{mg1} + jQ_{mg1})_p \quad (4.23a)$$

$$(S'_{mg2})_p \leq (k_{drop}^{mg2})_p (P_{mg2} + jQ_{mg2})_p \quad (4.23b)$$

$$(S'_{mg3})_p \leq (k_{drop}^{mg3})_p (P_{mg3} + jQ_{mg3})_p \quad (4.23c)$$

$$(S'_{mg4})_p \leq (k_{drop}^{mg4})_p (P_{mg4} + jQ_{mg4})_p \quad (4.23d)$$

which allows the real and reactive group powers of the MMG (before and after the procedure) to be defined by

$$(P_{mmg})_p := \sum_{i=1}^M (P_{mg(i)})_p \quad (4.24a)$$

$$(P'_{mmg})_p := \sum_{i=1}^M (k_{drop}^{mg(i)} P_{mg(i)})_p \quad (4.24b)$$

$$(Q_{mmg})_p := \sum_{i=1}^M (Q_{mg(i)})_p \quad (4.24c)$$

$$(Q'_{mmg})_p := \sum_{i=1}^M (k_{drop}^{mg(i)} Q_{mg(i)})_p \quad (4.24d)$$

Finally, the load adjustment of the MMG group can be defined as the difference in its load before and after the procedure, which results in

$$(\Delta P_{mmg})_p := (P_{mmg} - P'_{mmg})_p \quad (4.25a)$$

$$(\Delta Q_{mmg})_p := (Q_{mmg} - Q'_{mmg})_p \quad (4.25b)$$

This equation allows accounting for the load variation of the MMG, in kW and kvar per phase, necessary to overcome the voltage violation.

#### 4.4.2 Voltage Drop Case 2: $V_{drop}^{mmg} \leq 0$

When  $0 < V_{vio}$  and  $V_{drop}^{mmg} \leq 0$ , from Equation 4.17, the range of the MMG drop factor is  $1 < k_{drop}^{mmg} < \infty$ . Although there is a voltage violation on bus  $n$ , the MMG is already actively contributing to increasing the voltage on that bus, probably because it is in supply mode. But, if MMG has the capacity to further increase its contribution, then this could be an ancillary service. In this case, the MMG can:

- i) increase the power injection of MGs that are in supply mode;
- ii) decrease the load of those MGs in load mode, if any.

Thus, the MMG operator can choose either strategy (i) alone, or (i) and (ii) together. For the same reasons presented in case 1, strategy (i) alone will be adopted in this study.

In this case, if any MG of the group is in load mode, then it may have a  $V_{drop}^{mg} \geq 0$ , and for that reason, it should be left out of the procedure, which just means keeping your load unchanged ( $k_{drop}^{mg} = 1$ ). Therefore, the MG sets can be defined as

$$(\mathbb{U}_{in})_{n.p} = \begin{cases} \text{MGs that have } V_{drop}^{mg} < 0, \\ \text{and have one or more line shared with bus } n, \\ \text{and have the phase } p. \end{cases} \quad (4.26a)$$

$$(\mathbb{U}_{out})_{n.p} = \begin{cases} \text{MGs that have } V_{drop}^{mg} \geq 0, \\ \text{or do not have any line shared with bus } n, \\ \text{or do not have the phase } p. \end{cases} \quad (4.26b)$$

The MMG load adjustment factor for each group can be computed by Equation 4.22.

As an illustrative example, consider that:  $V_{vio} = 60 V$ , and  $V_{drop}^{mmg} = -30 V = \underbrace{-10 V}_{mg1} + \underbrace{20 V}_{mg2} - \underbrace{50 V}_{mg3} + \underbrace{10 V}_{mg4}$ .

Therefore, the MG sets are  $\mathbb{U}_{in} = \{1, 3\}$  and  $\mathbb{U}_{out} = \{2, 4\}$ . From Equation 4.22

$$k_{drop}^{in} = \frac{-30 - 60 - (20 + 10)}{-10 - 50} = 2.0$$

thus,  $k_{drop}^{mg1} = k_{drop}^{mg3} = k_{drop}^{in}$ , and  $k_{drop}^{mg2} = k_{drop}^{mg4} = k_{drop}^{out}$ . Therefore, to overcome the voltage violation at the node  $n.p$ , the MG loads must be adjusted by Equations 4.23.

#### 4.4.3 Voltage Drop Case 3: $0 < V_{drop}^{mmg} < V_{vio}$

When  $0 < V_{drop}^{mmg} < V_{vio}$  happens in a node  $n.p$ , from Equation 4.17, the range of the MMG drop factor is  $-\infty < k_{drop}^{mmg} < 0$ . In this case, there is a voltage violation at node  $n.p$  and the MMG is actively contributing to that, probably because it is in load mode. However, to overcome this voltage violation, the MMG has to switch from load mode to supply mode. Thus, in addition to canceling its contribution to the voltage drop, the MMG starts to effectively increase the voltage at that node. This action can characterize an ancillary service. Hence, the MMG operator can:

- i) decrease the load of those MG in load mode;
- ii) change the operating mode of MGs in load mode to supply mode, if necessary;
- iii) increase the power injection of MGs that are initially in supply mode, if any.

Thus, the MMG operator can choose either strategy (i) and (ii) together, or (i), (ii), and (iii) together. For the same reasons presented in case 1, strategy (i) and (ii) together will be adopted in this study. Therefore, the MGs sets  $\mathbb{U}_{in}$  and  $\mathbb{U}_{out}$  can be defined as in Equation 4.21. Also, the MMG load adjustment factor for each group can be computed by Equation 4.22.

As an illustrative example, consider that:  $V_{vio} = 60 V$ , and  $V_{drop}^{mmg} = 20 V = \underbrace{10 V}_{mg1} - \underbrace{20 V}_{mg2} + \underbrace{40 V}_{mg3} - \underbrace{10 V}_{mg4}$ .

Therefore, the MG sets are  $\mathbb{U}_{in} = \{1, 3\}$  and  $\mathbb{U}_{out} = \{2, 4\}$ . From Equation 4.22

$$k_{drop}^{in} = \frac{20 - 60 - (-20 - 10)}{10 + 40} = -0.2$$

thus,  $k_{drop}^{mg1} = k_{drop}^{mg3} = k_{drop}^{in}$ , and  $k_{drop}^{mg2} = k_{drop}^{mg4} = k_{drop}^{out}$ . Also, to overcome the voltage violation at the node  $n.p$ , the MG loads must be adjusted by Equations 4.23. As  $k_{drop}^{in}$  is negative, MG 1 and 3 should change their operating mode from load to supply, whereas MG 2 and 4 remain in supply mode.

#### 4.4.4 Voltage Drop Case 4: $V_{drop}^{mmg} = V_{vio}$

If the situation  $0 < V_{vio}$  and  $V_{drop}^{mmg} = V_{vio}$  occurs, the MMG drop factor is zero. There is a voltage violation on a node  $n.p$  and the MMG is actively contributing to that. In fact, this is a special occurrence that can be included in case 1. As a result, the procedures for calculating the MG sets and the MMG load adjustment factor are the same as in that case. It is a special case because if the MMG cancels out its contribution to the voltage drop at node  $n.p$  it is also canceling out the voltage violation at that node. Thus, from the point of view of the  $n.p$  node voltage, the MMG appears to be disconnected from the distribution network.

As an illustrative example, consider that:  $V_{vio} = 60 V$ , and  $V_{drop}^{mmg} = 60 V = \underbrace{-10 V}_{mg1} + \underbrace{30 V}_{mg2} + \underbrace{50 V}_{mg3} - \underbrace{10 V}_{mg4}$ .

Therefore, the MG sets are  $\mathbb{U}_{in} = \{2, 3\}$  and  $\mathbb{U}_{out} = \{1, 4\}$ .

Note that, from Equation 4.17

$$k_{drop}^{mmg} = \frac{60 - 60}{60} = 0.0$$

but, from Equation 4.22  $k_{drop}^{in}$  is not zero, i.e.

$$k_{drop}^{in} = \frac{60 - 60 - (-10 - 10)}{30 + 50} = 0.25$$

thus,  $k_{drop}^{mg2} = k_{drop}^{mg3} = k_{drop}^{in}$ , and  $k_{drop}^{mg1} = k_{drop}^{mg4} = k_{drop}^{out}$ . Also, to overcome the voltage violation at the node  $n.p$ , the MG loads must be adjusted by Equations 4.23. As  $k_{drop}^{in}$  is not zero, MG 2 and 3 should adjust their load by 0.25, whereas MG 1 and 4 keep their loads unchangeable. But, as  $k_{drop}^{mmg}$  is zero, from the  $n.p$  node point of view, the MMG appears to be disconnected from the distribution network.

## 4.5 Methods to Perform the Proposed Voltage Regulation Procedure

### 4.5.1 Method for Day-Ahead Applications

A typical day-ahead scheduling process requires load profiles with forecasted values for a day of operation, i.e., for  $t = \{1, \dots, N\}$ . Thus, the MMG operator must provide the DSO with the forecasted load profile on each MG PCC bus daily. Then, the DSO checks for any operational limit violations. If so, it may impose operational constraints on the MMG. Such verification must be performed for an entire day ( $\forall t$ ), and at the end, the DSO informs the MMG operator where the violations occurred, what are the operational restrictions and the adjustment requests. This is the concept presented in the flowchart of Figure 4.4. Although it is a procedure for a single value of  $t$ , it can be repeated for all  $t$  in a day-ahead scheduling process.

The MMG load (apparent power) present in the input and output of this procedure is defined as

$$\mathbf{S}_{mmg} := [\mathbf{S}_{mg(1)}, \mathbf{S}_{mg(2)}, \dots, \mathbf{S}_{mg(M)}] \quad (4.27)$$

where

$$\mathbf{S}_{mg(i)} := \begin{bmatrix} (S_{mg(i)})_a \\ (S_{mg(i)})_b \\ (S_{mg(i)})_c \end{bmatrix} \quad (4.28)$$

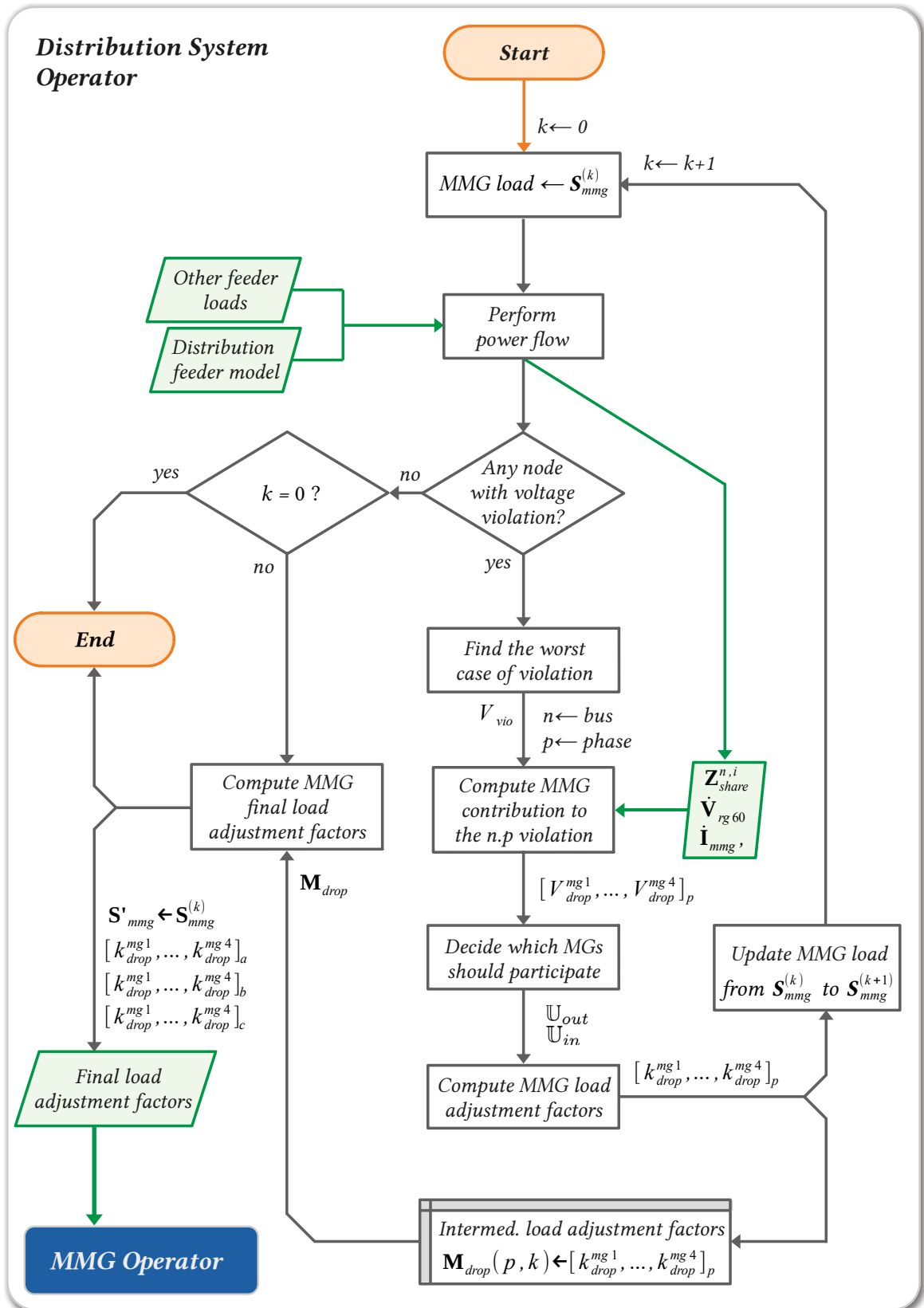
Therefore,  $\mathbf{S}_{mmg}^{(k)}$  is the MMG load at iteration  $k$ .

The following is a detailed description of the 10 main blocks in this flowchart.

1. “MMG load  $\leftarrow \mathbf{S}_{mmg}^{(k)}$ ” - The procedure starts with the subtask of assigning the current MMG load value  $\mathbf{S}_{mmg}^{(k)}$ . The initial load  $\mathbf{S}_{mmg}^{(0)}$  (iteration  $k = 0$ ) must be provided by the MMG operator.
2. “Perform power flow” - This block has the task of performing a three-phase power flow of the feeder, including as input parameters the three-phase model of that feeder and the loads connected to it (MMG and other feeder loads).



Figure 4.4 – Flowchart for day-ahead applications of the load adjustment procedure to voltage regulation on a feeder with MMG.



Source: The author (2022).

3. “Any node with voltage violation?” - The power flow subtask outputs voltage phasors on all phases and all buses of the feeder. Thus, through Equation 4.15, it is possible to verify which nodes present voltage violations.
4. “Find the worst case of violation” - After identifying the violation magnitudes and the respective nodes where they occurred, this subtask performs a search for the highest violation magnitude and passes the result to the next subtask.
5. “Compute MMG contribution to the  $n.p$  violation” - The contribution of each MG to the  $n.p$  violation must be calculated by Equation 4.20. Thus, this subtask must have as input, in addition to the identification of the node  $n.p$ , the current phasors of each MG, the source voltage phasor (bus  $rg60$ ), and the impedance matrix of the line segments shared between each MG and the bus  $n$ .
6. “Decide which MGs should participate” - The decision taken in this subtask is based on a strategy previously adopted by the MMG for the participation of each MG in the procedure. Thus, Equation 4.21 or Equation 4.26 can be used to define the sets  $\mathbb{U}_{in}$  and  $\mathbb{U}_{out}$ , which are the output parameters of this block.
7. “Compute MMG load adjustment factors” - In this subtask, Equation 4.22 must be used to calculate the load adjustment factors of the MMG, in iteration  $k$ . The voltage  $V_{drop}^{mmg}$ , required in this equation, can be computed by Equation 4.19.
8. “Update MMG load from  $\mathbf{S}_{mmg}^{(k)}$  to  $\mathbf{S}_{mmg}^{(k+1)}$ ” - In this subtask, loads of each MG (apparent power) are weighted by the factors calculated in the previous block, as defined in Equation 4.23, to update the MMG load vector  $\mathbf{S}_{mmg}$  to the next iteration.
9. “Intermed. load adjustment factors” - The intermediate factors calculated in the block 7 for each iteration must be stored so that the final factors are calculated at the end of the iterations. This block can save such factors in a matrix.
10. “Compute MMG final load adjustment factors” - After the algorithm has converged to an operating state without any violation verified by the power flow subtask, the final factors must be calculated and sent to the MMG operator. For each phase of each MG, the final factor is the result of the product of the intermediate factors saved in block 9. Thus, multiplying a final factor by the initial load of its respective MG must result in the load of the last iteration, i.e., the final load. This subtask performs such a product and makes the result available at the procedure output.

The procedure represented in Figure 4.4 is an iterative process that, when identifying a state of operating violation, seeks convergence to a violation-free state. In theory, Equation 4.22 can be used to calculate the load adjustment factors without the need for iterations. However, in practice, making this process iterative can be advantageous to

- i. avoid restrictions that are more severe than necessary, i.e., requesting a load adjustment greater than the minimum required to get out of the violation state. Although it is possible to calculate the contribution of each load to the violation, the sum of all individual contributions does not necessarily result in the total contribution since the Equation 4.11 is an approximation. The error inherent in this approximation can impact the adjustment factor, making it larger than necessary.
- ii. apply the procedure in all phases and manage the influence of one phase on another, since trying to improve the voltage profile of one phase can degrade the profile of another phase. This can be verified in the Equation 4.6, where a change in load current of one phase impacts the voltage drop of the other two phases.

Consider that an adequate load adjustment value is the minimum necessary for the system to transition from a state of operating violation in one or more phases to a violation-free state in all phases. However, according to Equation 4.22a, the greater the magnitude of the voltage violation ( $V_{vio}$ ) the smaller the value of  $k_{drop}$ . On the other hand, the smaller the value of  $k_{drop}$ , the greater the adjustment that must be performed on the MMG loads. Thus, during the implementation in a programming language of this procedure, it was empirically verified that the lower the value of  $k_{drop}$ , the more accentuated the deviation of the load adjustment from the adequate value. On the other hand, for  $k_{drop}$  values closer to 1 (above 0.9 for example) it was observed that this deviation is minimal. In other words, if the violation magnitude is high, an adjustment greater than necessary occurs, otherwise, the adjustment is adequate.

As a numerical solution to this issue, in the first iteration of this iterative process, a weight  $w_{drop} > 1$  can be applied to  $k_{drop}$ , if necessary, to transform a high-magnitude violation to low-magnitude and then, after the following iterations, result in convergence to an adequate load adjustment. Thus, for the first iteration, Equation 4.22a becomes

$$\left(k_{drop}^{in}\right)_p = w_{drop} \times \left( \frac{V_{drop}^{mmg} - V_{vio} - \sum_{i \in \mathbb{U}_{out}} V_{drop}^{mg(i)}}{\sum_{i \in \mathbb{U}_{in}} V_{drop}^{mg(i)}} \right)_{n.p}, \quad \forall \text{ MG} \in \mathbb{U}_{in} \quad (4.29)$$

It should be emphasized the final  $k_{drop}$  is the product of  $k_{drop}$  factors from each iteration. Assume that the final load adjustment factor for the  $p$ -phase of the  $i$ -th microgrid is  $\left(k_{drop}^{mg(i)}\right)_p$  and that  $\left(k_{drop(n)}^{mg(i)}\right)_p$  is the factor for the  $n$ -th of  $N_{iter}$  iterations. Thus,

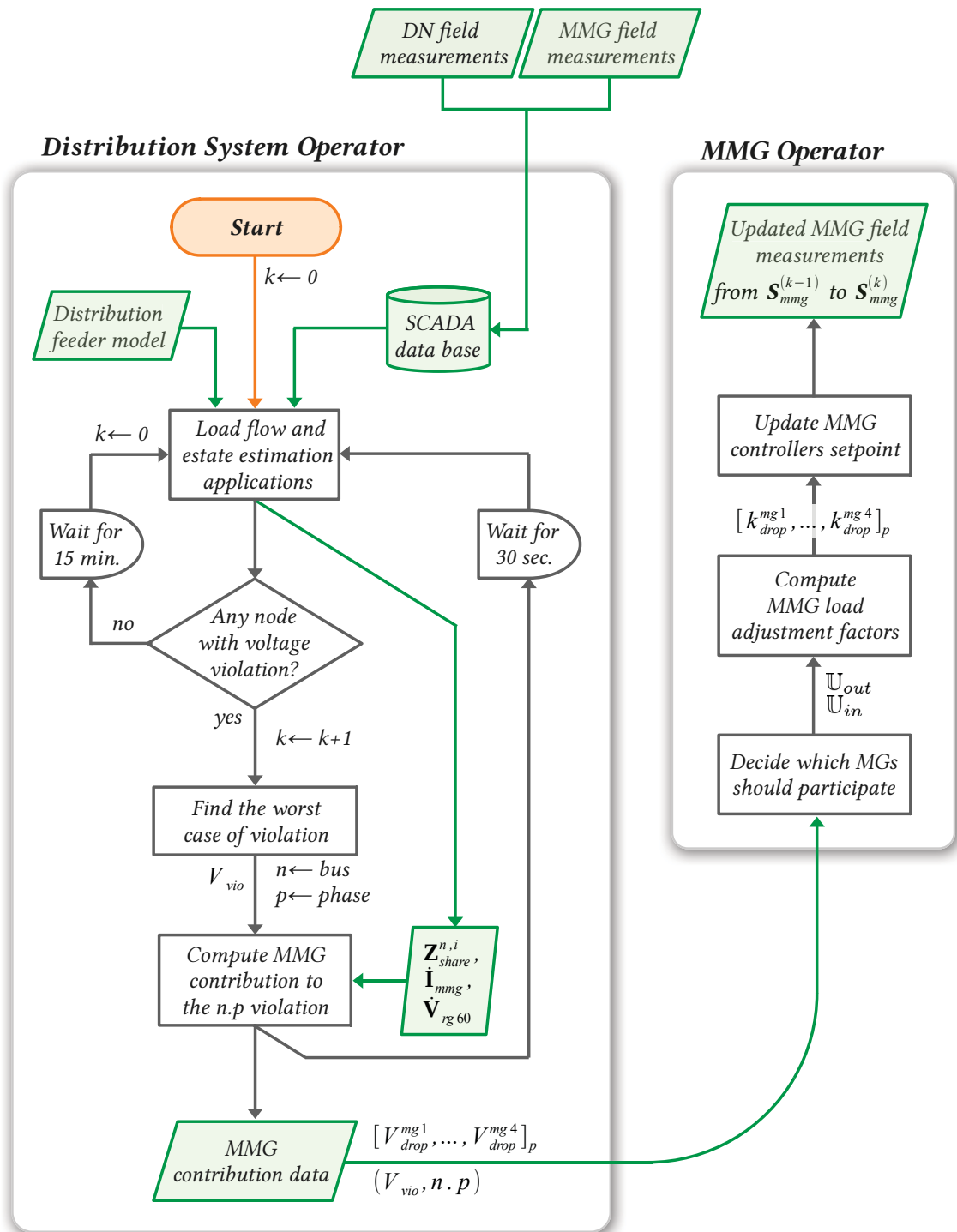
$$\left(k_{drop}^{mg(i)}\right)_p = \prod_{n=1}^{N_{iter}} \left(k_{drop(n)}^{mg(i)}\right)_p \quad (4.30)$$

## 4.5.2 Method for Real-Time Applications

Figure 4.5 illustrates a suggested flowchart to perform the load adjustment procedure for real-time voltage regulation. Every 15 minutes, the DSO process checks for any violations. If so, it initiates an interactive process with the MMG operator to adjust the MGs loads and thus, regulate the voltage on the feeder to reach a violation-free state. The following is a detailed description of the 9 main blocks in this flowchart. Blocks with no description have the same meaning presented in the day-ahead flowchart.

1. “Load flow and state estimation applications” - The procedure begins with the subtask of performing the three-phase power flow and state estimation based on the feeder model and real-time data from SCADA. This includes field measurements of the distribution network and MGs PCC buses. As output, this block must provide the voltage profile, the MG current phasors, the source voltage phasor, and the impedance matrix of the line segments shared between each MG as the bus  $n$ ;
2. “Any node with voltage violation?”;
3. “Wait for 15 min.” - Since there is no immediate action in the case of a violation-free state, the process can wait 15 minutes (or a time defined by the DSO) to perform the next iteration;
4. “Find the worst case of violation”;
5. “Compute MMG contribution to the  $n.p$  violation” - Although this subtask has the same function as in the day-ahead case, it also provides the MMG operator with the contribution data through real-time communication;
6. “Decide which MGs should participate” - The MMG operator has to define the sets  $\mathcal{U}_{in}$  and  $\mathcal{U}_{out}$  based on its own operating strategy, as illustrated by Equation 4.21 and Equation 4.26.
7. “Compute MMG load adjustment factors”;
8. “Update MMG controllers setpoint” - In this subtask, the MMG operator must decide which resources of each MG it should employ to respond to the DSO load adjustment request, such as BESS and controllable loads. Thus, the controllers of each MG must receive and perform a new adjustment setpoint;
9. “Wait for 30 sec.” - After calculating the contribution of the MMG in the block 5, the process must wait a minimum amount of time (30 sec. is a suggestion) for the requested changes to take effect in the distribution system. This delay must be enough for the MMG operator to receive the requested changes and perform

Figure 4.5 – Flowchart for real-time applications of the load adjustment procedure to voltage regulation on a feeder with MMG.



Source: The author (2022).

them in its controllers. Then the distribution system electrically responds to these changes so that the SCADA system can capture them through the acquisition of field

measurements. Thus, the process can proceed with the next iteration by performing the subtask in block 1 again.

In a real-time application, the distribution operating system can identify a violation through an event of limit violation from the SCADA system, or it can periodically check it (polling). Although the flowchart of Figure 4.5 is an example of the polling implementation, the main blocks of this flowchart keep the same in an event-driven case, changing only the way of identifying the violation.

Finally, this procedure could be even more detailed to handle cases in which the MMG does not have available resources to meet the adjustment request made by the DSO. Or even, it has resources to only partially fulfill the request. This issue would require actions such as employing traditional voltage regulation methods (voltage regulators, LTCs, and shunt capacitors) or even implementing a feeder load shedding plan. However, this approach has been well explored in other works and is beyond the scope of this one.

## 4.6 Final Considerations

In Brazil, ANEEL's Normative Resolution 697 (ANEEL, 2015) establishes the procedures for the provision and remuneration of ancillary services for centrally dispatched generating plants such as self-recovery, frequency control, and reactive supply. For the provision of the first two services, there is a fixed annual remuneration. On the other hand, for services such as reactive supply, the remuneration is variable and the value is proportional to the energy made available (Mvarh, MWh) for the provision of that service. However, this normative resolution does not deal with ancillary services provided by generating plants that are not centrally dispatched (distributed generation). In addition, there is no mention about the provision of ancillary services in the Electricity Distribution Procedures for the National Electric System (PRODIST) currently in force.

The methodology presented in this chapter may result in the MMG providing a voltage control/regulation ancillary service to the DSO. However, as there is still no legislation in force in Brazil to regulate this type of service, it is not possible to discuss its remuneration. On the other hand, due to the similarity with the ancillary service of reactive supply in the centralized generation, it is possible that in the future the voltage regulation service provided by an MMG may be classified as an ancillary service of variable remuneration, with a value proportional to the energy made available (kvarh, kWh) by the MMG. Backhaus et al. (2016) argues that coordinated energy management can be implemented using a networked microgrid (MMG) configuration and that the use of energy storage and common loads can be considered energy assets that participate in frequency/voltage regulation.

Regardless of how this type of service provision will be regulated in the future, the methodology presented in this chapter provides indicators that can be considered both in the decision to remunerate the ancillary service such as  $V_{drop}^{mmg}$ , as well as in the remuneration value composition as the energy made available by the MMG for the service provision.

## 5 Simulation Methods

This chapter presents the simulation methods used in this work to validate the methodologies presented in Chapters 3 and 4. Section 5.1 presents a simulation method for optimal day-ahead scheduling of MGs, which is a reproduction of the Section 4 of the paper (SILVA; AOKI; LAMBERT-TORRES, 2020), and Section 5.2 presents the simulation method for feeder voltage regulation.

### 5.1 Simulation Method for Optimal Day-Ahead Scheduling of MGs

All results of the present work were obtained through the implementation of the MG model, described in Section 3.3, in the MATLAB<sup>®</sup> software. The optimizer function `intlinprog()` was used to solve the MILP problem from Equation 3.31, subject to the constraints from Table 3.7. Furthermore, it was used a time resolution  $\Delta t$  of 1/4 h, and  $N = 96$  time slots.

The BESS is a 140 kW/280 kWh LiFePO<sub>4</sub> system with coupling transformer, where:  $\eta_{bess} = 0.92$  (see Table 3.6),  $DOD_r = 0.90$ ,  $SOH = 0.90$ ,  $L_{cyc} = 6000$  cycles,  $SOH_{tsh} = 0.80$ ,  $SOC^{(0)} = SOC^{(N)} = 0.40$ ,  $\overline{SOC} = 1$ ,  $\underline{SOC} = 1 - DOD_r$ , and  $k_e = 0.55$ . Furthermore, according to the example from Section 3.4.1,  $p_{bess} = 0.0339$  USD/kWh, and from Equation 3.36,  $p_{chr}$  and  $p_{dch}$  are 0.0312 and 0.0369 USD/kWh respectively.

The solar PV system is the same from Section 3.4.2, for the city of Curitiba, with:  $\lambda_{reg} = 1,261.57$  kWh/year per kW,  $L_{spv} = 25$  years,  $\kappa_{pv} = 0.8\%$ ,  $p_{reg} = 2,060$  USD (market price). The average daily PV generation  $E_{pv}$  was defined according to the daily load  $E_{load}$ , i.e.,  $E_{pv} := MG_{ss}E_{load}$ , where  $MG_{ss}$  is the microgrid self-sufficiency, and  $E_{load}$  is constant and equal to 2,400 kWh. Thus, the daily cost of the PV system for the first year of use ( $n = 0$ ), calculated from Equation 3.44 and used in the simulations of this work is a function of the  $MG_{ss}$ .  $C_{pv} = 173.40$  USD, for  $MG_{ss} = 1$ , was used in the first three simulation cases. Furthermore, the PV generation curve was retrieved from (PVOUTPUT.ORG, 2020), whose data are from a region in Africa and were collected on a sunny day of summer.

The load curve comes from field measurements of a group of middle-income residential consumers, which were collected during a business day (YAMAKAWA, 2007).

The Brazilian time-of-use tariff, named White Tariff, was used to set the prices used in the simulations of this work. In the Brazilian captive energy market, customers can only buy electricity from an agent authorized to do the distribution service, typically



the DSO. A regulatory agency (ANEEL) sets the price of energy, and the customer cannot negotiate it. However, the White Tariff allows customers to manage their consumption voluntarily according to the energy price. The regulated ToU (time-of-use) time blocks are on-peak, off-peak, and pre and post-peak. Each energy distribution company can set its time blocks according to the load demand in its operating area. Table 5.1 shows the time blocks with their respective average periods (AGÊNCIA NACIONAL DE ENERGIA ELÉTRICA, 2020). Furthermore, it presents the weighted average of rates charged in Brazil for the conventional and ToU tariff. They were calculated considering data from 11 major energy distributors in Brazil (AGÊNCIA NACIONAL DE ENERGIA ELÉTRICA, 2020), weighted by the number of customers of each company. In this table, ToU prices and time blocks define  $p_{pur_g}^{(t)}$  and  $p_{sel_g}^{(t)}$  (USD/kWh) used in this model. The conventional tariff was used as the reference price  $p_{ref}$  in Equation 5.1.

In load shedding simulations, it was adopted  $p_{shd} = 3p_{ref}$  (\$/kWh) as a penalty for the amount of disconnected load. Furthermore, in directly controllable loads simulations, it was adopted  $p_{int} = 2p_{ref}$  and  $p_{shf} = 0$ , with  $T_{int} = 4$  (one hour) and  $T_{shf} = 10$  (two hours and a half). All other costs whose values have not been mentioned have been set to zero.

Finally, although the model presented here is prepared to simulate external MGs supplying and acquiring energy from the microgrid, this feature was not explored in any simulation because it does not fit the adopted ToU tariff model.

Table 5.1 – The Brazilian White Tariff; average time blocks were computed from 104 companies data; average prices were calculated from the 11 major energy distributors in Brazil, weighted by the number of customers of each company.

Tariff	Average Time Blocks		Average Prices		Percentage Prices (%)
	Start Time	End Time	BRL/kWh	USD/kWh	
Conventional tariff	–	–	0.558	0.130	100
ToU, off-peak	00:00	17:00	0.466	0.109	84
ToU, pre-peak	17:00	18:00	0.679	0.158	122
ToU, on-peak	18:00	21:00	1.059	0.247	190
ToU, post-peak	21:00	22:00	0.679	0.158	122
ToU, off-peak	22:00	24:00	0.466	0.109	84

Source: Silva, Aoki and Lambert-Torres (2020).

### 5.1.1 Normalized Energy Bill

For results analysis purposes, it may be preferable to handle a normalized energy bill than to work with monetary values. To this end, consider a reference daily MG energy bill  $R_{bill}$  in which all distributed energy resources are turned off, that is,

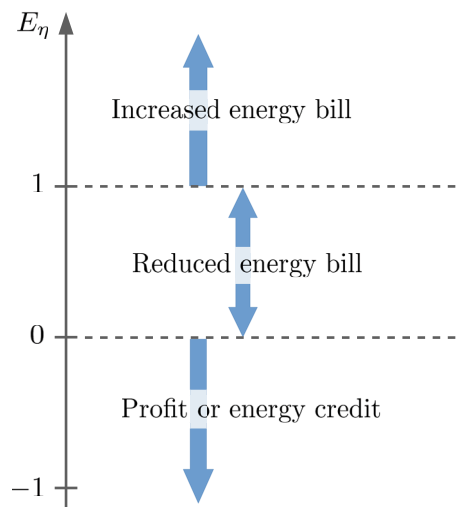
$$R_{bill} := \Delta t \sum_{t=1}^N P_{load}^{(t)} p_{ref}^{(t)} \quad (5.1)$$

where  $p_{ref}$  stands for a reference energy price. Therefore, the normalized energy bill is

$$E_{\eta} := \frac{E_{bill}}{R_{bill}} \quad (5.2)$$

$E_{\eta}$  can represent three distinct operating regions for an MG:  $E_{\eta} > 1$ ,  $0 \leq E_{\eta} \leq 1$ , and  $E_{\eta} < 0$ , as Figure 5.1 shows. In the first, there was a relative increase in the energy bill; as an example, a microgrid could operate in this region when it is connected to the main grid with generation off, BESS in operation, and the purchase price of energy is constant throughout the day. Naturally, such a region should be avoided. In the second, there was a relative reduction in the energy bill; a microgrid can operate in this region when in the first operating mode, however with energy prices favoring the practice of energy arbitrage. Finally, a microgrid can operate in the third region when in the previous operating modes, but with enough generation surplus to meet the load and still sell energy.

Figure 5.1 – Regions of MG operation represented by the normalized energy bill.



Source: Silva, Aoki and Lambert-Torres (2020).

### 5.1.2 Simulation Cases

1. Energy arbitrage as a result of the Brazilian White Tariff applied to a microgrid;
2. MG scheduled intentional islanding using the resources of interruptible loads and PV output curtailment; two islanding periods:  $T_{isl_1} = 13$ , from 02:00 to 05:15, and  $T_{isl_2} = 8$ , from 10:30 to 12:30;  $MG_{ss} = 1$ .
3. MG scheduled intentional islanding using the resources of interruptible loads, PV output curtailment, load shedding, and shiftable loads; two islanding periods:  $T_{isl_1} = 16$ , from 02:00 to 06:00, and  $T_{isl_2} = 8$ , from 10:30 to 12:30;  $MG_{ss} = 1$ .
4. The impact of the microgrid self-sufficiency on the normalized energy bill; limit for energy import and export:  $\bar{P}_{pcc} = 800$  kW; curves for  $E_r = 12, 16, 20$ , and 30% of  $E_{pv}$ .

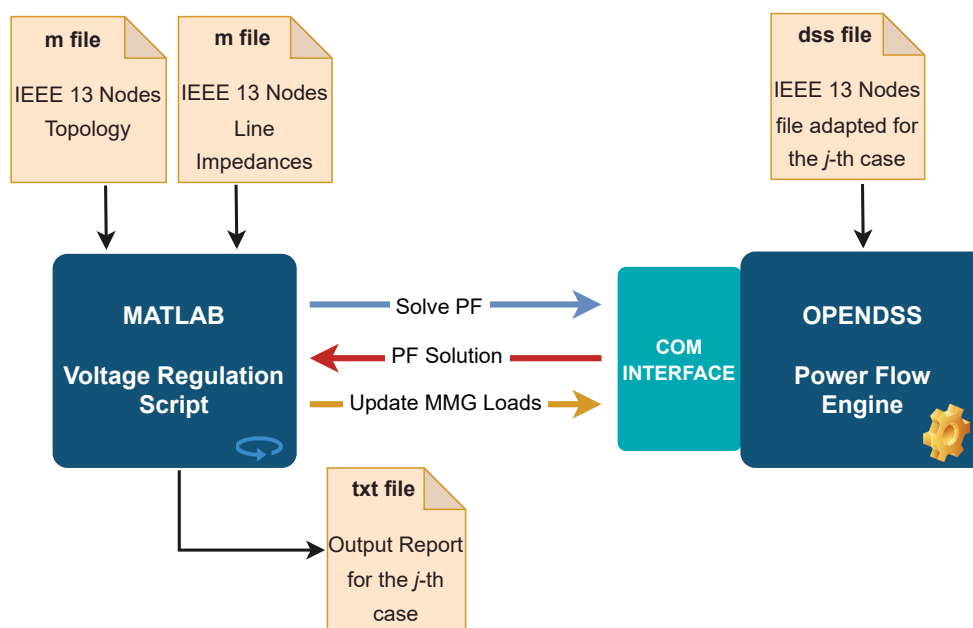
## 5.2 Simulation Method for Feeder Voltage Regulation

### 5.2.1 Simulation Platform

The simulations presented in this work perform the feeder voltage regulation flowchart, previously shown in Figure 4.4, using Matlab and OpenDSS software. A Matlab set of scripts performs all the subtasks from that flowchart iteratively, except for the power flow, which is an OpenDSS task. For each feeder circuit configuration adopted in simulation cases, the OpenDSS performs a three-phase power flow when demanded by a Matlab main script iteration. Figure 5.2 presents a block diagram that illustrates the inter-process communication between Matlab and OpenDSS adopted in the simulations of this work. The Component Object Model (COM) interface enables the communication between OpenDSS and external software such as Matlab, Python, and Microsoft Excel.

In the present work simulations, the Matlab main script sends commands to OpenDSSuses through COM interface objects, such as solving power flow (Solve PF) and getting the solution (PF Solution), or updating the MMG loads (Update MMG Loads), as illustrated in Figure 5.2. The topology and line impedances of the distribution feeder that will be simulated are inputs for the Matlab voltage regulation script. The output is a report file with simulation results. Although in this simulation platform there is an m file for line impedance, it can also be acquired through the COM interface, as this information is available in the dss file.

Figure 5.2 – Block diagram of the simulation platform including the inter-process communication between Matlab and OpenDSS.



Source: The author (2022).

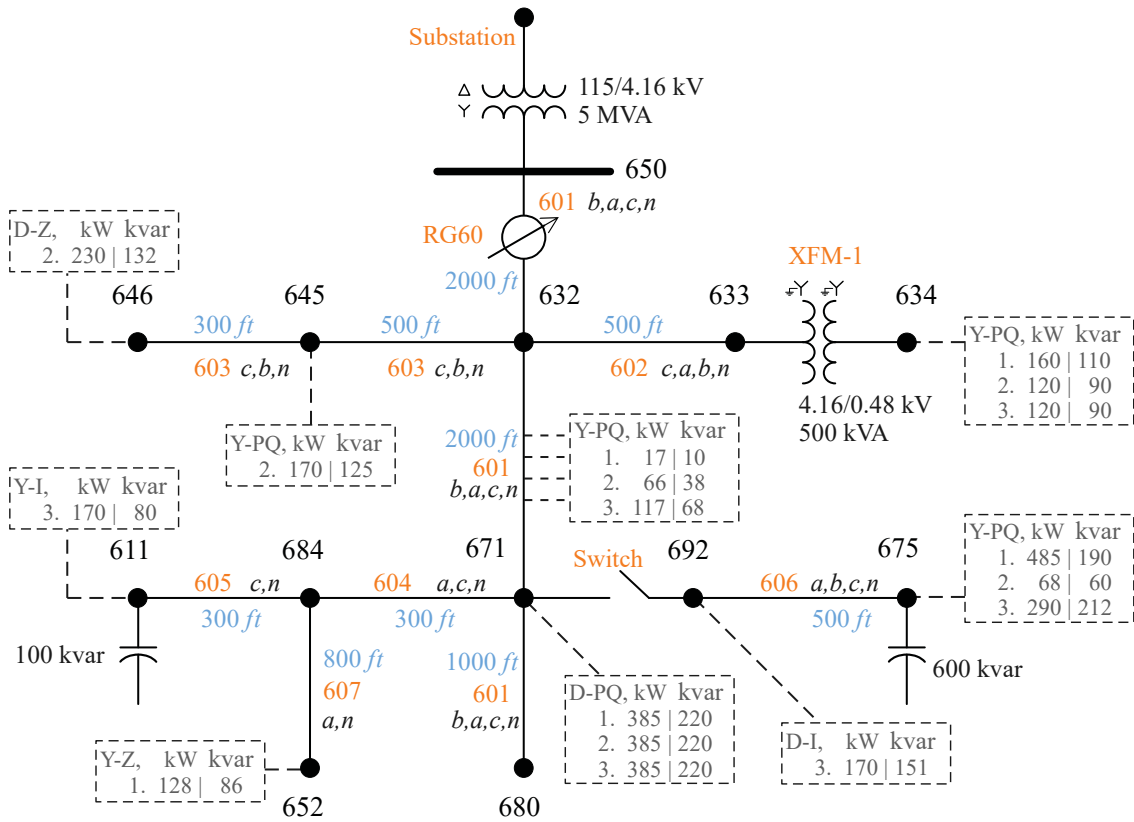
## 5.2.2 Distribution Feeder Model

The IEEE 13 Node Test Feeder is the distribution feeder model adopted in this work for voltage regulation simulations. It has a voltage regulator at the substation bus with three single-phase units connected in wye, overhead and underground lines with variety of phasing, shunt capacitor banks, in-line transformer, unbalanced spot and distributed loads, as illustrated in Figure 5.3. According to Kersting (2001), it is a small feeder that provides conditions for testing common features of distribution analysis software. Of these characteristics, three stand out that justify its choice for this work:

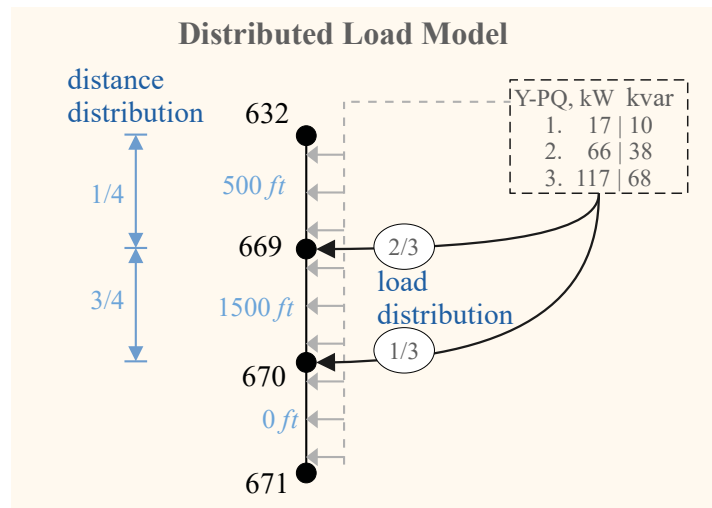
1. It is a small feeder, resulting in a more controlled and less complex simulation environment and thus allows a better analysis of the results.
2. The feeder is highly loaded. It is a realistic feature that can be intensified by inserting microgrids into the distribution network;
3. The circuit presents a high level of unbalance, a real condition that requires voltage regulation per phase.

Figure 5.3a presents the topology and configurations of the IEEE 13 Node Test Feeder, in its original form. Distances between buses are represented by light blue text;

Figure 5.3 – Schematic diagram of the IEEE 13-bus test feeder.



(a) Topology and configurations as originally proposed by the IEEE.



(a) Distributed load model adopted in this work between buses 632 and 671.

Source: The author (2022).

the identification number of configuration for each distribution line segment is represented by orange text; the phases for a line are represented by the letters a, b, c, and n, next to the segment and separated by a comma; the loads are represented by a dashed rectangle connected to a busbar; inside this rectangle are the real and reactive power values for each phase; moreover, loads connected in delta or wye are represented by the letters D or Y inside the rectangle, respectively; finally, the letters Z, I, and PQ identify constant impedance, constant current, and constant power loads, respectively.

The IEEE feeder model has a uniformly distributed load connected between the 632 and 671 buses. According to (KERSTING, 2002), to calculate both the voltage drop along the line and the power loss for uniformly distributed loads, one-third of the load should be placed at the end of the line, and two-thirds of the load placed in one-fourth of the upstream bus. Such a model is illustrated in Figure 5.4a and was used in the present work to compute PF in the OpenDSS. Note that buses 669 and 670 were added to the circuit topology to make the OpenDSS implementation feasible.

In this work, the IEEE 13 Nodes Test Feeder was adapted to enable the simulation of a multi-microgrid environment, as shown in Figure 5.5. Four new buses were inserted into the model in order to connect a microgrid to each one. Named mg1, mg2, mg3, and mg4, these buses are connected to existing buses through a connection switch that configures the point of common coupling. Initially, the loads on each microgrid were kept equal to the loads originally connected at each point. However, to build each simulation case, these values experienced changes in one or more phases.

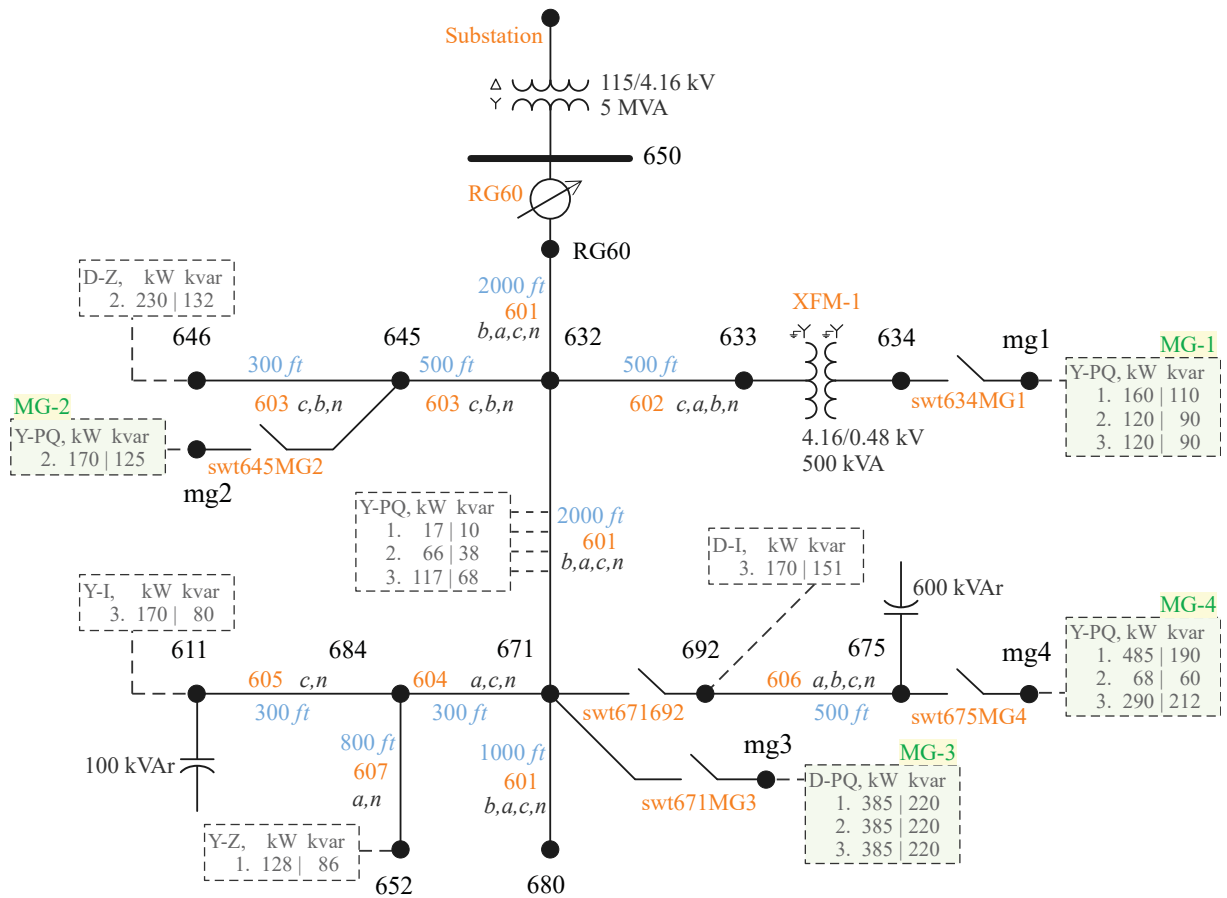
### 5.2.3 Simulation Cases

To validate the methodology presented in Chapter 4, four simulations cases were performed with Matlab and OpenDSS following the simulation platform and feeder model presented in the previous sections of this chapter. From 1 to 4, the simulations cases were designed to reproduce the voltage drop cases from 1 to 4 presented in Chapter 4, respectively. The entire simulation environment was maintained according to the model in Figure 5.5, except for the load values.

In the first three columns, Table 5.2 illustrates the original load values per phase, for each bus. In the last four columns are the changes introduced to compose the four simulation cases. In this table, “unch.” stands for unchangeable and “n.a.” not applicable. Negative real power values mean the MG is in supply mode. Negative reactive power values mean capacitive load. In all simulation cases, the voltage regulator control was kept off, with fixed tap on the three phases to present an output voltage of 1 p.u.

In simulation 1, the only change performed in the original model was a 10-times increase in the phase b load of MG4, as in Table 5.2. This must cause a voltage violation in this phase to make the statement  $V_{drop}^{mmg} > V_{vio}$  true, which is a necessary condition to

Figure 5.5 – IEEE 13 Node Test Feeder adapted to include the MMG.



Source: The author (2022).

simulate voltage drop case 1. In simulation 2, the condition  $V_{drop} \leq 0$  must be satisfied, which requires the MMG to be in supply mode and yet there is voltage violation across the feeder. Thus, it was necessary to make the loads of MG3 negative (supply mode), increase the loads of nodes 611.c and 646.b, and adjust the load of the mg4.c node. For simulation 3, the condition to be reached is  $0 < V_{drop}^{mmg} < V_{vio}$ , i.e., it is necessary to tune  $V_{drop}^{mmg}$  between the condition of simulation 1 and 2. Thus, MG3 was kept in supply mode, but mg4.c returned to its original load value, which should increase  $V_{drop}^{mmg}$  compared to simulation 2. In addition, there was a significant increase in distributed loads and nodes mg4.b and 652.a.

The simulation case 4 seeks to satisfy the condition  $V_{drop}^{mmg} = V_{vio}$ , which characterizes the voltage drop case 4. Thus, to numerically reach this condition, it was necessary to establish a condition of minimum voltage difference  $\delta_{V_{min}}$  between these two quantities,

Table 5.2 – Load definitions; n.a. and unch. stand for “not applicable” and “unchanged”, respectively.

Bus	Ph.	Orig. load (kW)+j(kvar)	Load change per simulation case (kW)+j(kvar)			
			Simulation 1	Simulation 2	Simulation 3	Simulation 4
mg1	a	160.0 + j110.0	unch.	unch.	unch.	unch.
	b	120.0 + j90.0	unch.	unch.	unch.	unch.
	c	120.0 + j90.0	unch.	unch.	unch.	unch.
mg2	a	n.a.	n.a.	n.a.	n.a.	n.a.
	b	170.0 + j125.0	unch.	unch.	unch.	unch.
	c	n.a.	n.a.	n.a.	n.a.	n.a.
mg3	a	385.0 + j220.0	unch.	-385.0 - j220.0	-385.0 - j220.0	unch.
	b	385.0 + j220.0	unch.	-385.0 - j220.0	-385.0 - j220.0	unch.
	c	385.0 + j220.0	unch.	-385.0 - j220.0	-385.0 - j220.0	unch.
mg4	a	485.0 + j190.0	unch.	unch.	unch.	194.0 + j76.0
	b	68.0 + j60.0	680.0 + j600.0	unch.	272.0 + j240.0	unch.
	c	290.0 + j212.0	unch.	145.0 + j106.0	unch.	232.0 + j169.6
669	a	12.0 + j7.0	unch.	unch.	96.0 + j56.0	36.0 + j21.0
	b	44.0 + j26.0	unch.	unch.	352.0 + j208.0	132.0 + j78.0
	c	78.0 + j46.0	unch.	unch.	624.0 + j368.0	234.0 + j138.0
670	a	5.0 + j3.0	unch.	unch.	40.0 + j24.0	15.0 + j9.0
	b	22.0 + j12.0	unch.	unch.	176.0 + j96.0	66.0 + j36.0
	c	39.0 + j22.0	unch.	unch.	312.0 + j176.0	117.0 + j66.0
611	c	170.0 + j80.0	unch.	510.0 + j240.0	unch.	431.26 + j202.9
646	b	230.0 + j132.0	unch.	690.0 + j396.0	unch.	unch.
652	a	128.0 + j86.0	unch.	unch.	512.0 + j344.0	unch.
692	c	170.0 + j151.0	unch.	unch.	unch.	unch.

Source: The author (2022).

i.e.,

$$\left| k_{drop}^{mmg} \right| = \left| \frac{V_{drop}^{mmg} - V_{vio}}{V_{drop}^{mmg}} \right| < \delta_{Vmin} \quad (5.3)$$

where  $\delta_{Vmin} = 0.01$  is the condition adopted in simulation. In this case, the load values for the simulation 4 were defined through several simulations observing the result of  $\left| k_{drop}^{mmg} \right|$



and adjusting the load values to reach the established condition. This procedure resulted in the load values for simulation 4 indicated in Table 5.2.

Finally, the values of the  $w_{drop}$  weight were empirically adjusted by performing several simulations using the same platform as in simulations 1 to 4. The method consists of defining a set of values for the model feeder loads so that  $k_{drop}^{in}$  assumes values within predetermined ranges and allows the adjustment of a fixed value of  $w_{drop}$  within that range.

### 5.2.4 Matlab Reports

One of the methods used to present results in the Chapter 6 is the Matlab output report from the simulation platform in Figure 5.2. The voltage regulation script produces a frame with a set of values by iteration for the phase under analysis and records them in the output report file, as illustrated in Figure 5.6. An output frame contains a set of fields whose values are recorded before and after an iteration of the procedure runs, as indicated by red right curly brackets in the figure. Table 5.3 presents a description of each field, and also makes a relationship with the notation used throughout the Chapter 4.

Figure 5.6 – An example of a Matlab output report frame with identification of fields.

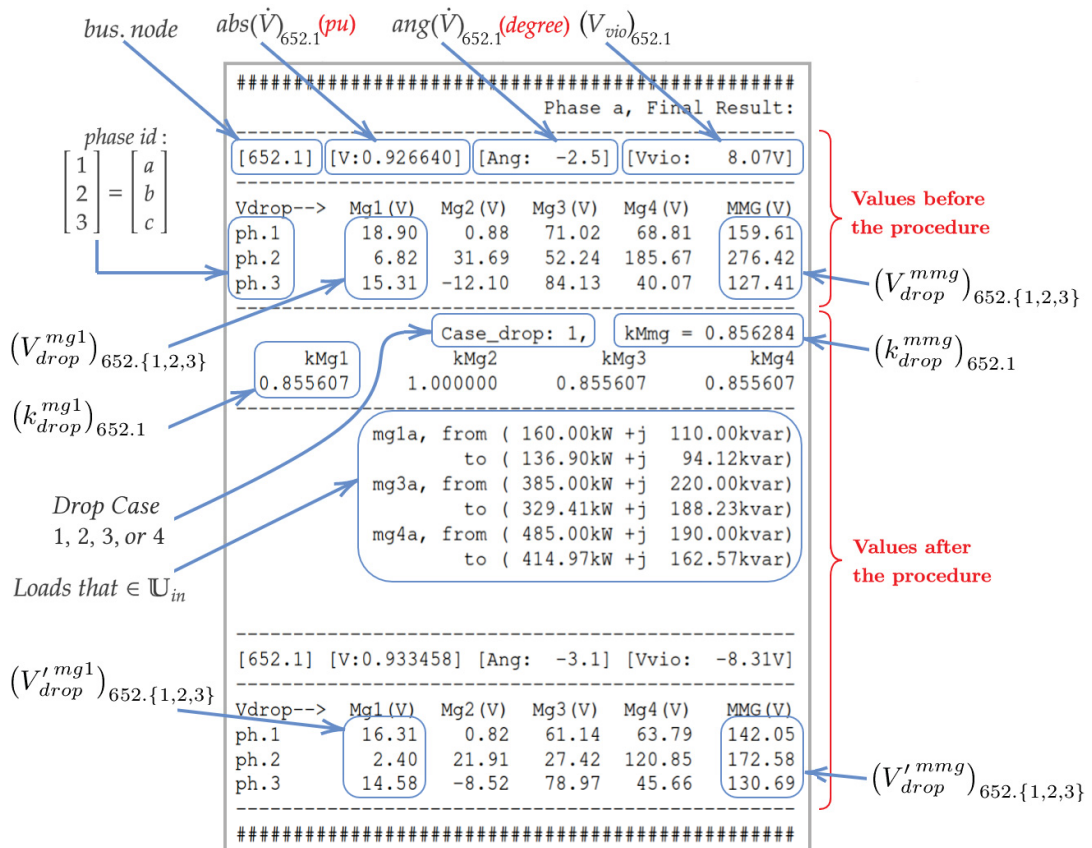


Table 5.3 – Matlab report field description.

Field Name	Notation	Example Value	Description
bus.node	$n.p$	652.1	bus and node identification for the worst case of violation
V:	$abs(\dot{V})_{n.p}$	0.926640	per unit voltage magnitude on the bus $n$ , node $p$
Ang:	$ang(\dot{V})_{n.p}$	-2.5	voltage angle on the bus $n$ , node $p$
Vvio:	$(V_{vio})_{n.p}$	8.07 V	voltage violation, in (V), on the bus $n$ , node $p$
phase id:	1, 2, or 3	$ph.\{1, 2, 3\}$	MG voltage phase identification by row
Mg1(V):	$\begin{bmatrix} (V_{drop}^{mg1})_{n.1} \\ (V_{drop}^{mg1})_{n.2} \\ (V_{drop}^{mg1})_{n.3} \end{bmatrix}$	$\begin{bmatrix} 18.90 \\ 6.82 \\ 15.31 \end{bmatrix}$	per-phase voltage contribution from an MG (MG1 in this example) to the voltage drop on bus $n$
MMG(V):	$\begin{bmatrix} (V_{drop}^{mmg})_{n.1} \\ (V_{drop}^{mmg})_{n.2} \\ (V_{drop}^{mmg})_{n.3} \end{bmatrix}$	$\begin{bmatrix} 159.61 \\ 276.42 \\ 127.41 \end{bmatrix}$	per-phase voltage contribution from the MMG to the voltage drop on bus $n$
Case_drop:	1, 2, 3, or 4	1	voltage drop case identification
kMmg:	$(k_{drop}^{mmg})_p$	0.856284	MMG load adjustment factor for phase $p$
kMg1:	$(k_{drop}^{mg1})_p$	0.855607	an individual MG (MG1 in this example) load adjustment factor for phase $p$
Loads that $\in \mathbb{U}_{in}$ :	from $(S_{mg1})_p$ to $(S'_{mg1})_p$	160+j110 136 + j94	the individual load adjustment (kW+jkvar) for MGs (MG1 in this example) that $\in \mathbb{U}_{in}$

Source: The author (2022).

## 6 Results and Discussion

This chapter presents the results and discussion for the simulations of the methodologies presented in Chapters 3 and 4. Section 6.1 present results and discussion for optimal day-ahead scheduling of MGs simulations, which are a reproduction of Sections 5 and 6 of the paper (SILVA; AOKI; LAMBERT-TORRES, 2020), and Section 6.2 presents results and discussion for the feeder voltage regulation simulations.

### 6.1 Optimal Day-Ahead Scheduling of MGs

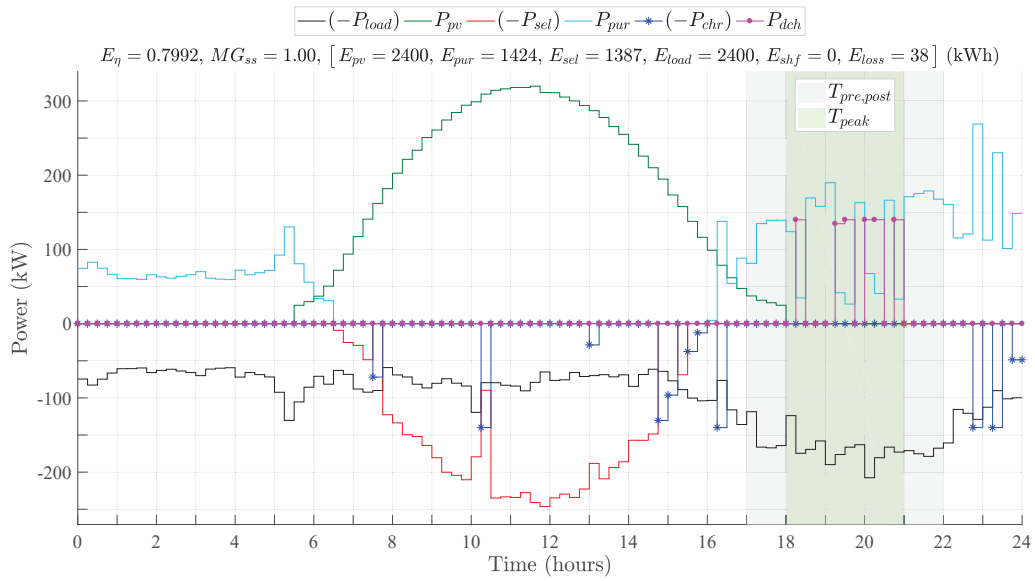
#### 6.1.1 Simulation Results

In power system buses with loads and generators connected, there is a convention in which the power generated is positive while the power consumed is negative (PONCE et al., 2017). Although in the modeling presented in this work all powers are positive, such a convention of signs was adopted in the figures throughout this section. This minimizes overlapping curves in the figures. Thus, the curves  $P_{load}$ ,  $P_{sel}$ ,  $P_{chr}$ , and  $P_{shf}$  are shown with negative values. Furthermore, these quantities are included in parentheses in the legends of the figures. Figure 6.1 presents the main findings of simulation 1. The pre and pos-peak, and on-peak time blocks are represented by  $T_{pre,pos}$  e  $T_{peak}$ , respectively. Figure 6.1a shows the curves that make up the balance of active powers in the microgrid. Figure 6.1b presents the BESS state of charge curve with its upper and lower bounds.

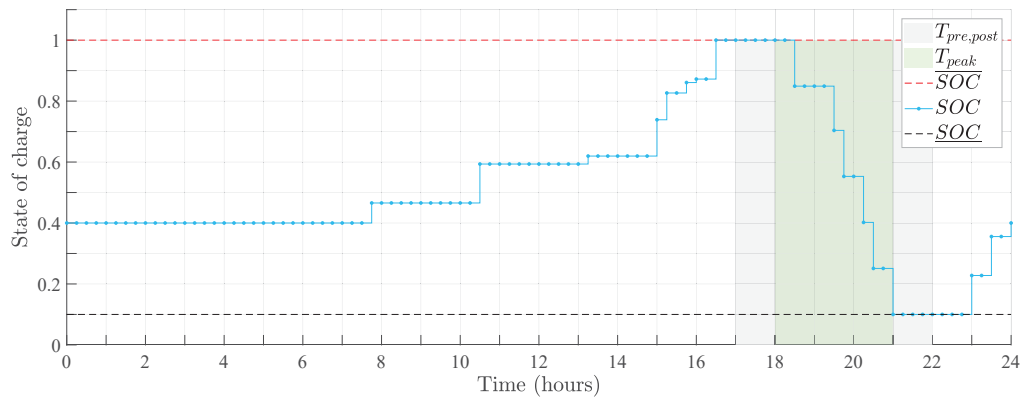
Results show that, before solar generation begins, the microgrid has to import the energy necessary to supply its load. On the other hand, during the period of sunlight, the microgrid exports the PV generation surplus in addition to storing energy to use it during the on-peak period. As expected for the energy arbitrage simulation, the storage system reaches its maximum state of charge during the off-peak period and then performs a complete discharge to the lower limit during the on-peak. At the end of the day, the BESS is recharged to reach its final state of charge. Furthermore, the BESS performs a complete cycle throughout the day and presents an energy loss ( $E_{loss}$ ) of 38 kWh, which is the loss per full cycle of the storage system.

Figure 6.2 shows the results of simulation 2. Two islanding periods  $T_{isl_1}$  and  $T_{isl_2}$  were added to the simulation. The storage system has the role of avoiding load shedding in the first islanding, minimizing curtailment in the second, and performing energy arbitrage during the on-peak period. Although the results show that BESS reaches its maximum state of charge before the first islanding and performs a complete discharge during the same (Figure 6.2b), the stored energy is not sufficient to supply 100% of the microgrid

Figure 6.1 – Results of simulation 1.



- (a) Results of simulation 1 for the power balance curves;  $E_{bill} = 249.36$  USD;  $E_{loss}$  represents energy losses throughout the day with BESS charging and discharging operations;  $T_{pre,post}$  stands for the pre and post-peak period;  $T_{peak}$  is the on-peak period.

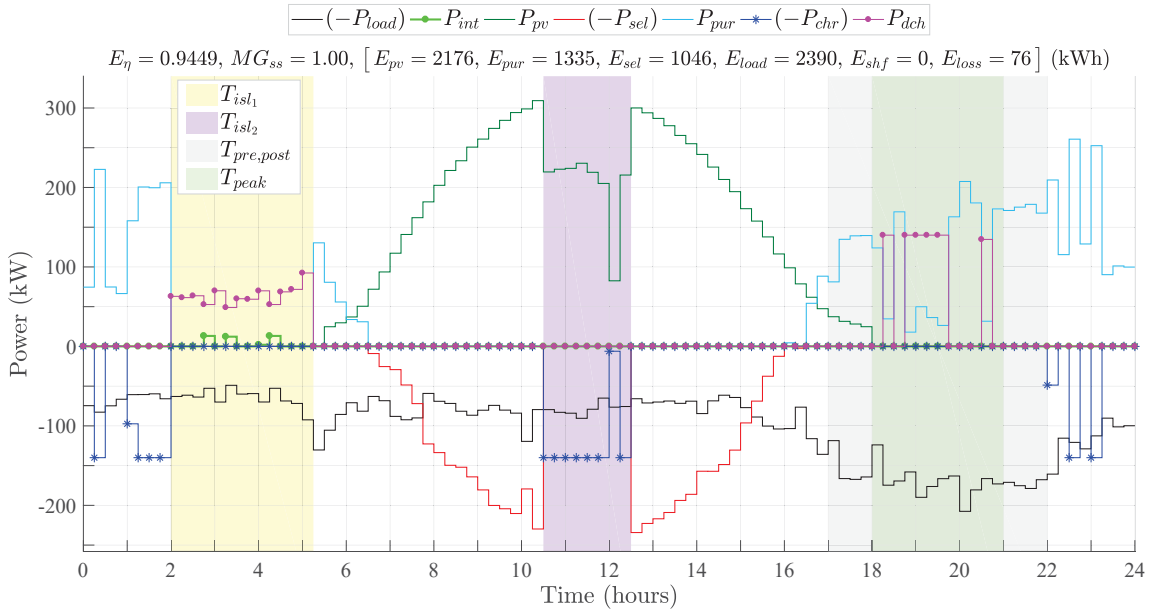


- (b) Results of simulation 1 for the BESS SOC.

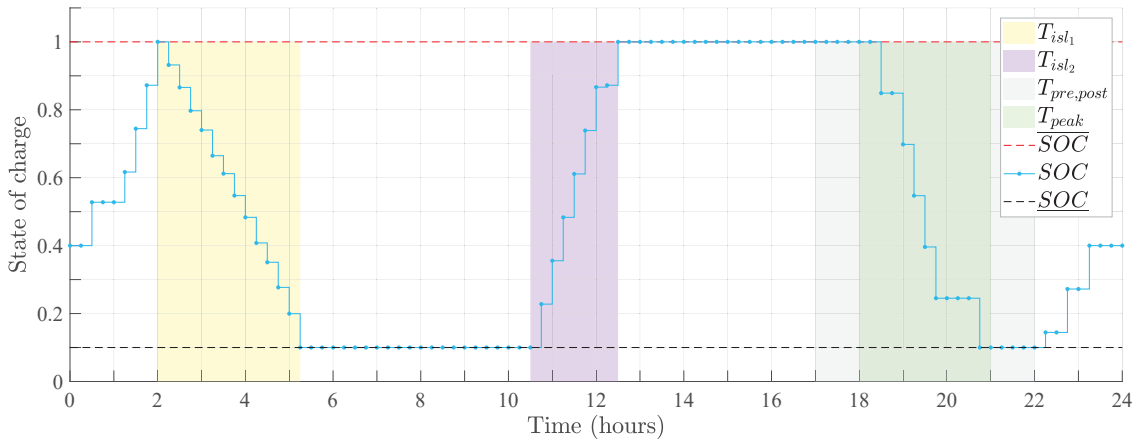
Source: Silva, Aoki and Lambert-Torres (2020).

load during that period. Thus, the interruptible load resource is required to complete the remaining energy and avoid load shedding, as illustrated in Figure 6.2a and expanded in Figure 6.2c;  $P_{int}$  presents four pulses of 15 min long, at 02:45, 03:15, 04:00, and 04:15, during the first islanding, which contributes approximately 10 kWh to the energy balance for that period. In practice, each pulse can represent a temporary power reduction or even shutdown of interruptible load groups, such as air conditioners and water heaters.

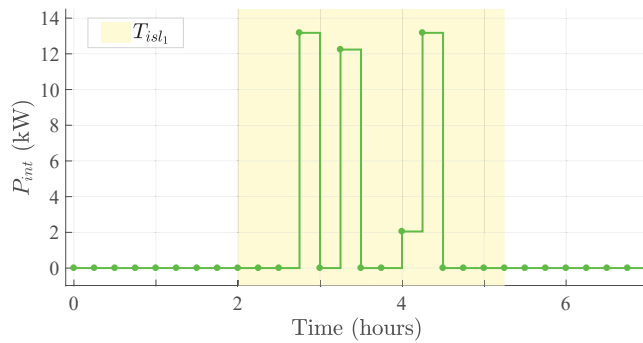
Figure 6.2 – Results of simulation 2.



(a) Power balance curves;  $[E_{pvc} = 223.85, E_{int} = 10.16]$  (kWh);  $E_{bill} = 294.82$  USD.



(b) Results of simulation 2 for the BESS SOC.



(c) Expanding the curve of interruptible loads during the first period of islanding.

According to results, during the second islanding period, the BESS performs a full charge in response to the surplus of solar generation that cannot be injected into the main grid. Even so, a curtailment of 223.85 kWh in the solar generation is expected for the next day. Besides, according to the optimal solution, all surplus energy produced outside the islanding must be exported to the main grid. Finally, BESS discharges during the on-peak period all energy stored during  $T_{isl_2}$ , performing the energy arbitrage, and then it returns to its initial state of charge.

Figure 6.3 illustrates the results of simulation 3, in which the first islanding period was increased by 45 min, and the shiftable load resource was added to the simulation. Results illustrated in Figure 6.3a show that although MG uses all its storage and interruptible loads resources (respecting the  $T_{int}$  limit), it will be necessary to perform 61.98 kWh of load shedding the next day, during the first islanding period.

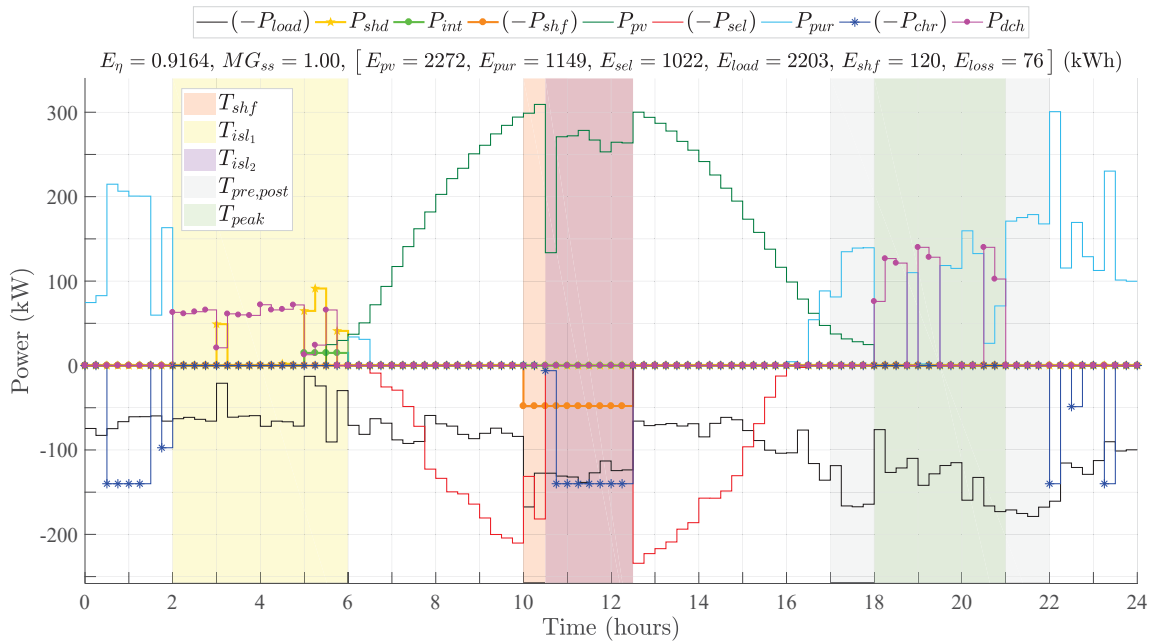
However, the use of shiftable loads allowed a drop in curtailment from 223.85 to 127.85 kWh during the second islanding. In the optimal solution, the optimizer reallocated 96 of the 120 kWh of shiftable loads taken from the on-peak period to the islanding period; the remaining 24 kWh were allocated in the half-hour before the second islanding. It is important to emphasize the optimizer performs the reallocation of shiftable loads in compliance with the continuous cycle requirement for this type of load. Finally, on this schedule (and the previous one), there should be a loss of 76 kWh due to the two full cycles to be performed by BESS the next day. In addition, the behavior of the BESS at the on-peak period is similar to simulations 1 and 2.

In the simulation 4, for a daily load of 2400 kWh (the same from previous simulations), the capacity of the PV system and the storage system were gradually increased. The storage system was configured as a percentage of the PV system capacity. Furthermore, the imported and exported energy at the microgrid PCC was limited by setting  $\bar{P}_{pcc} = 800$  kW in the model. A simulation was performed for each setting, and an optimal solution was reached in each case. Figure 6.4 shows the curves  $E_\eta \times MG_{ss}$  obtained from simulations. No directly controllable load resources were used in those simulations.

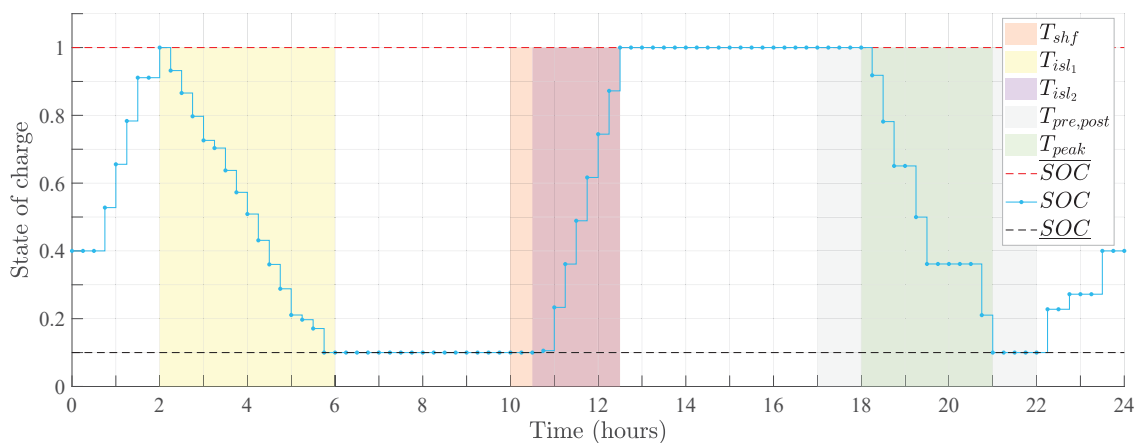
All the curves start in the increased energy bill area where  $E_\eta > 1$ , because the microgrid does not have sufficient distributed energy resources to make economically attractive the participation in the White Tariff. From  $MG_{ss} = 0.4$  onwards, the curves enter the reduced energy expenses area where  $0 < E_\eta < 1$ ; but only the curves of 16%, 20%, and 30% reach the profit or energy credit area ( $E_\eta < 0$ ), for  $MG_{ss}$  greater than or equal to 3.5, 3.3, and 3.1, respectively. In the light blue region ( $P_{sel} < \bar{P}_{pcc}$ ), the optimal use of the distributed energy resources is resulting in an energy export to the main grid whose power is less than the limit of 800 kW. On the other hand, the light green region contains the points for which this limit was reached. In that region, the generation surplus that cannot be exported must be stored by BESS. However, when the storage limit is reached, the curtailment process begins, which can be identified by the

turning point of curves of 12%, 16%, and 20%. Similar reasoning can be applied to the MG without BESS curve. From the turning point onwards, the higher the capacity of the PV system, the more energy will be wasted, and by consequence, the more will be the cost of the microgrid, as can be seen in the figure for those curves. The turning point of

Figure 6.3 – Results of simulation 3.



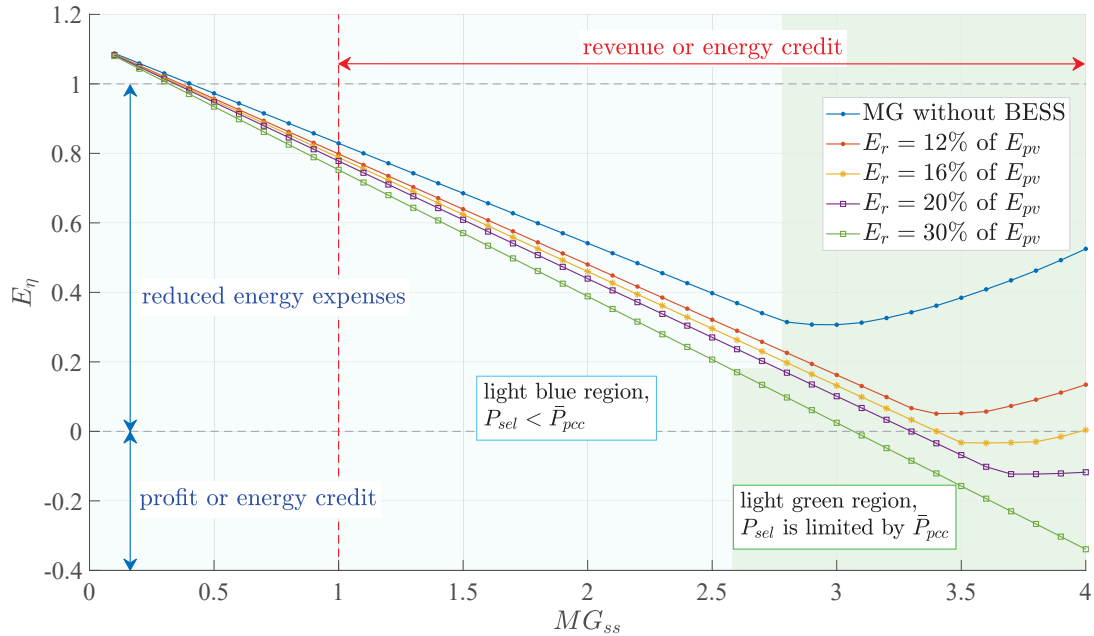
(a) Results of simulation 3 for the power balance curves;  $[E_{pvc} = 127.85, E_{shd} = 61.98, E_{int} = 14.92]$  (kWh);  $E_{bill} = 285.92$  USD.



(b) Results of simulation 3 for the BESS SOC.

Source: Silva, Aoki and Lambert-Torres (2020).

Figure 6.4 – Normalized energy bill for a sequence of simulations with increasing values of microgrid self-sufficiency; curves for BESS rated capacity ( $E_r$ ) from 12% to 30% of the average daily PV system capacity ( $E_{pv}$ );  $\bar{P}_{pcc} = 800$  kW;  $E_{load} = 2400$  kWh;  $E_{pv} := 2400 MG_{ss}$  kWh.



Source: Silva, Aoki and Lambert-Torres (2020).

the 30% curve is not shown in the figure as it must happen for  $MG_{ss} > 4.0$ .

Finally, although in this work, the MILP problem has thousands of variables and restrictions, the execution time in all simulations was less than 15 s on a personal computer of general use.

### 6.1.2 Discussion

Simulations presented in this work provide support to evaluate the proposed MG model. In general, results corroborate the consistency of the microgrid mathematical modeling proposed in this work. In practice, the MG used in the simulations can correspond to a medium to large industry, or to a residential area containing more than a hundred houses. Simulation 1 shows the Brazilian White Tariff can be economically attractive for a microgrid with solar generation and energy storage systems. In this example, a savings of 20% ( $E_\eta = 0.7992$ ) in the energy bill was observed. It is necessary to emphasize the energy arbitrage is directly related to the BESS costs. According to Equation 3.38,  $p_{bess}$  should be less than 0.0544 USD/kWh to enable energy arbitrage in the White Tariff; the value used in simulations, whose calculation is based on market data, was  $p_{bess} = 0.0339$  USD/kWh. Furthermore, the microgrid load profile used in this



study presents an increase in consumption during peak hours, which helps to reduce the costs of a microgrid with BESS and to perform energy arbitrage.

The results of the second simulation highlight the role of the storage system when the microgrid is disconnected from the main system. In the first islanding, for more than three hours, the BESS can supply the microgrid load without requiring load shedding; in the second, the storage system can reduce the PV curtailment from 450.65 to 223.85 kWh (50.33%) in the next day.

Results also show directly controllable loads can play a complementary role to that of the storage system. In the second simulation, the optimizer algorithm makes use of interruptible loads during the first islanding to avoid load shedding. In the third, although it is not possible to prevent shedding, the results show the optimizer first exhausts the resource of interruptible loads and then uses the load shedding one; the cost to use the former is less than the penalty for using the latter. Regarding shiftable loads, the results of the third simulation show their use can also help to minimize the PV curtailment, which was reduced from 450.65 to 127.85 kWh (71.63%). Thus, even with the penalties of load shedding, the costs in the third simulation are lower than in the second.

Results of simulation 4 show that a BESS system can reduce the energy costs of a microgrid with operational limits (as in practice) at the PCC bus, in addition to the reduction achieved by the PV system. In this model, the energy balance of a full day of operation must be zero when the MG self-sufficiency is unitary, even when there is no BESS. This is because the microgrid uses the main grid as a battery of infinite capacity and power limited by  $\bar{P}_{pcc}$  to exchange energy with the grid both when it generates surplus energy and when it only demands energy. Thus, from  $MG_{ss} > 1$  onwards, the region in which there is an energy credit or revenue for the microgrid begins. However, making a profit from the generation of energy requires the revenue must exceed the costs of operating the microgrid. Thus, the results show that in practice reaching the profit region for this microgrid may require self-sufficiency as high as  $MG_{ss} > 3$ . Furthermore, the size of the storage system must be adequate for this purpose; otherwise, such a region may not be hit, as illustrated in Figure 6.4.

It is necessary to emphasize that in Brazil, the current captive energy market does not allow customers to sell the surplus energy, even in the White Tariff; however, it allows the accumulation of energy credits. In this market, a scenario with  $MG_{ss} > 1$  may not be economically attractive, since day after day there will be an accumulation of energy credits that cannot be traded. However, the model presented in this work has the purpose of being generic enough to be applied in other types of markets, including a free energy market and future markets that include microgrids and renewable energy resources.

Considering that load and solar generation forecasts can vary considerably over the year in a microgrid, then addressing the day-ahead scheduling problem for a single day

may be a limitation of this work. A day-by-day analysis covering the four seasons as well as variations in load and solar generation forecasts could result in a richer set of simulation data. This type of analysis can be considered in future works. Furthermore, although in this work the decision variable for curtailment is continuous (a real number), in practice, it may be necessary to model this variable by ranges due to converter system technology limitations, which would make it an integer in the MILP problem. In addition, although the values used in this work are based on real market values, the results presented here must be interpreted with caution, as they are dependent on market prices for the PV system, the BESS, and the energy tariff.

## 6.2 Feeder Voltage Regulation

### 6.2.1 Simulation Results

Table 6.1 illustrates values for the weight  $w_{drop}$  (Equation 4.29) for nine ranges of  $k_{drop}^{in}$  values. These results were obtained through observation of several simulations with the feeder model adopted in the simulation platform. However, theoretically,  $w_{drop}$  does not depend on the feeder model being analyzed, but on the value of  $k_{drop}^{in}$  that this model is presenting during operation.

Table 6.1 – Simulation results for setting  $w_{drop}$  values.

Range of $k_{drop}^{in}$ values	$w_{drop}$
$0.0 < k_{drop}^{in} < 0.1$	4.00
$0.1 \leq k_{drop}^{in} < 0.3$	3.00
$0.3 \leq k_{drop}^{in} < 0.4$	2.00
$0.4 \leq k_{drop}^{in} < 0.5$	1.80
$0.5 \leq k_{drop}^{in} < 0.6$	1.40
$0.6 \leq k_{drop}^{in} < 0.7$	1.15
$0.7 \leq k_{drop}^{in} < 0.8$	1.10
$0.8 \leq k_{drop}^{in} < 0.9$	1.05
$0.9 \leq k_{drop}^{in} < 1.0$	1.00

Source: The author (2022).

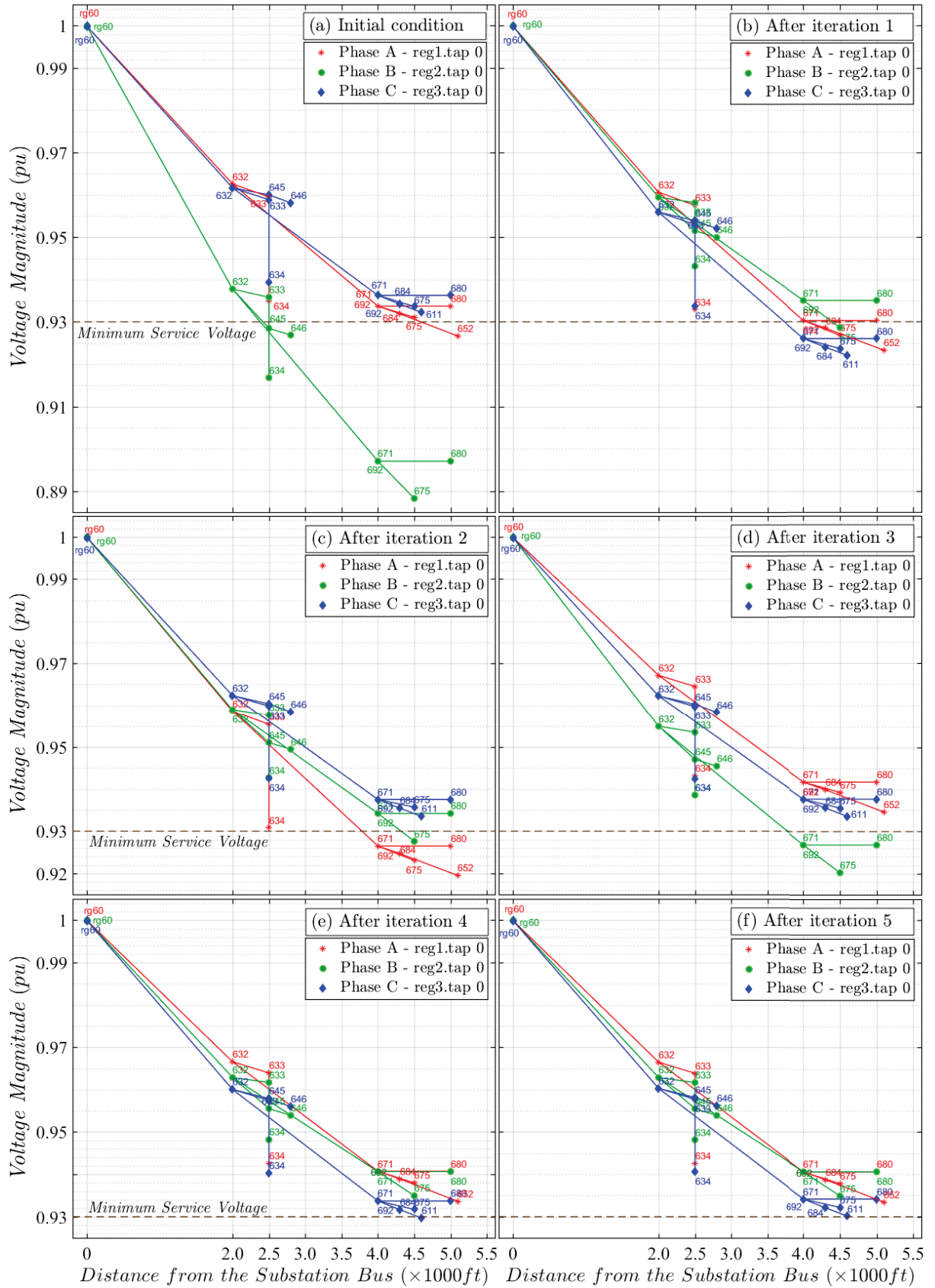
### 6.2.1.1 Voltage Drop Case 1

Simulation results for the voltage drop case 1, where  $V_{drop}^{mmg} > V_{vio}$ , are presented in Figures 6.5, 6.6, and 6.7. Figure 6.5 illustrates the evolution of the three-phase voltage profile along the feeder obtained from the simulation of voltage drop case 1. Each subplot shows the voltage magnitude of the three phases versus the distance of the buses from the substation bus. The buses, represented by markers, are identified by their names in the distribution feeder model. The lines joining the buses are following the feeder model topology, i.e., they compose a continuous path linking the rg60 source bus to the downstream buses. Subplots lines and markers are following the OpenDSS color pattern, where red, green, and blue represent the phases  $a$ ,  $b$ , and  $c$ , respectively. Also, a dashed line at 0.93 p.u., named Minimum Service Voltage, represents a minimum threshold that characterizes voltage violation when exceeded. Finally, as indicated in the legend of each subplot, the three voltage regulator taps are fixed at position 0. Figure 6.6 shows the output report frames for each iteration of the present voltage drop simulation case. Also, Figure 6.7 presents the final result report frames for the current simulation.

According to the initial condition of this simulation (Figure 6.5, upper left subplot), the green phase has six buses with voltage violation, the red phase only once, and the blue phase none. Also, node 675.2 presents the worst-case violation and therefore becomes the target of the voltage regulation algorithm in the first iteration. However, according to Figure 6.6, frame 1 (**## Iteration [1] ##**), the node under analysis is the mg4.2. In fact, according to the model presented in Figure 5.5, both nodes must present the same voltage phasor if the MG is connected to the main grid. Frame 1 also shows that there is a initial voltage violation of 100.24 V and all microgrids are actively contributing to the voltage drop at node mg4.2, which results in 299.87 V of MMG contribution. It further illustrates that the Matlab algorithm classified the first iteration as voltage drop case 1 since the MMG contribution voltage is greater than the violation voltage, which resulted in an MMG load adjustment factor (calculated from Equation 4.17) of 0.665730. This value was weighted by a  $w_{drop}$  of 1.15, resulting in 0.765590. For iteration 1, the set  $\mathbb{U}_{in}$  of MGs that must participate in the procedure is formed by all MGs since there was no negative contribution. The load adjustment factor for the  $\mathbb{U}_{in}$  group (calculated from Equation 4.22a) is 0.665722. However, as the weight  $w_{drop}$  described in Equation 4.29 must be applied in the first iteration, a load adjustment factor of 0.7656 for each MG can be verified in frame 1. In this case, the Matlab algorithm used a  $w_{drop}$  of 1.15, which is in accordance with the range of  $k_{drop}^{in}$  values from Table 6.1. Finally, frame 1 also presents the new load values to be used in the power flow calculation of the next iteration.

Figure 6.5 upper right subplot shows that, after iteration 1, the green phase is almost fully corrected, while the blue and red ones had a slight worsening. According to that figure, the worst case of violation is on node 611.3 now. On the other hand, the

Figure 6.5 – Three-phase voltage profile evolution along the feeder in simulation 1.



Source: The author (2022).

Figure 6.6 – Output report frames for the five iterations in simulation 1.

```

#####
Phase b, ## Iteration [ 1 ] ##
-----
[mg4.2] [V:0.888265] [Ang:-125.5] [Vvio: 100.24V]
-----
Vdrop-->  Mg1 (V)  Mg2 (V)  Mg3 (V)  Mg4 (V)  MMG (V)
ph.1      18.90    0.88    71.02   78.40   169.20
ph.2      6.82     31.69   52.24  209.13  299.87
ph.3     15.31   -12.10   84.13   50.05  137.40
-----
Case_drop: 1,      kMmg = 0.765590
kMg1:0.7656 kMg2:0.7656 kMg3:0.7656 kMg4:0.7656
-----
mg1b, from ( 120.00kW +j   90.00kvar)
         to (  91.87kW +j   68.90kvar)
mg2b, from ( 170.00kW +j  125.00kvar)
         to ( 130.15kW +j   95.70kvar)
mg3b, from ( 385.00kW +j  220.00kvar)
         to ( 294.75kW +j  168.43kvar)
mg4b, from ( 680.00kW +j  600.00kvar)
         to ( 520.60kW +j  459.35kvar)
-----
#####
Phase c, ## Iteration [ 2 ] ##
-----
[611.3] [V:0.922025] [Ang: 114.5] [Vvio: 19.15V]
-----
Vdrop-->  Mg1 (V)  Mg2 (V)  Mg3 (V)  Mg4 (V)  MMG (V)
ph.1     19.10    0.86    71.83   75.07   166.85
ph.2      2.13    24.64   28.24  131.24  186.26
ph.3     16.62   -9.54   90.15   53.40   150.64
-----
Case_drop: 1,      kMmg = 0.872845
kMg1:0.8804 kMg2:1.0000 kMg3:0.8804 kMg4:0.8804
-----
mg1c, from ( 120.00kW +j   90.00kvar)
         to ( 105.65kW +j   79.24kvar)
mg3c, from ( 385.00kW +j  220.00kvar)
         to ( 338.96kW +j  193.69kvar)
mg4c, from ( 290.00kW +j  212.00kvar)
         to ( 255.32kW +j  186.65kvar)
-----
#####
Phase a, ## Iteration [ 3 ] ##
-----
[652.1] [V:0.919483] [Ang:  -3.4] [Vvio: 25.26V]
-----
Vdrop-->  Mg1 (V)  Mg2 (V)  Mg3 (V)  Mg4 (V)  MMG (V)
ph.1     19.99    0.82    76.86   78.09   175.76
ph.2      2.25    24.69   28.66  132.30  187.91
ph.3     14.10   -9.53   76.58   41.98   123.14
-----
Case_drop: 1,      kMmg = 0.856284
kMg1:0.8556 kMg2:1.0000 kMg3:0.8556 kMg4:0.8556
-----
mg1a, from ( 160.00kW +j  110.00kvar)
         to ( 136.90kW +j   94.12kvar)
mg3a, from ( 385.00kW +j  220.00kvar)
         to ( 329.41kW +j  188.23kvar)
mg4a, from ( 485.00kW +j  190.00kvar)
         to ( 414.97kW +j  162.57kvar)
-----
#####
Phase b, ## Iteration [ 4 ] ##
-----
[mg4.2] [V:0.920227] [Ang:-124.3] [Vvio: 23.47V]
-----
Vdrop-->  Mg1 (V)  Mg2 (V)  Mg3 (V)  Mg4 (V)  MMG (V)
ph.1     16.21    0.85    60.79   70.74   148.59
ph.2      4.05    24.64   36.00  158.80  223.49
ph.3     14.20   -9.53   77.16   49.62   131.45
-----
Case_drop: 1,      kMmg = 0.894974
kMg1:0.8950 kMg2:0.8950 kMg3:0.8950 kMg4:0.8950
-----
mg1b, from (  91.87kW +j   68.90kvar)
         to (  82.22kW +j   61.67kvar)
mg2b, from ( 130.15kW +j   95.70kvar)
         to ( 116.48kW +j   85.65kvar)
mg3b, from ( 294.75kW +j  168.43kvar)
         to ( 263.80kW +j  150.74kvar)
mg4b, from ( 520.60kW +j  459.35kvar)
         to ( 465.92kW +j  411.11kvar)
-----
#####
Phase c, ## Iteration [ 5 ] ##
-----
[611.3] [V:0.929689] [Ang: 114.7] [Vvio:  0.75V]
-----
Vdrop-->  Mg1 (V)  Mg2 (V)  Mg3 (V)  Mg4 (V)  MMG (V)
ph.1     16.27    0.82    60.93   63.66   141.68
ph.2      2.39    21.91   27.41  120.81  172.52
ph.3     14.68   -8.52   79.51   46.11   131.78
-----
Case_drop: 1,      kMmg = 0.994332
kMg1:0.9947 kMg2:1.0000 kMg3:0.9947 kMg4:0.9947
-----
mg1c, from ( 105.65kW +j   79.24kvar)
         to ( 105.09kW +j   78.82kvar)
mg3c, from ( 338.96kW +j  193.69kvar)
         to ( 337.16kW +j  192.66kvar)
mg4c, from ( 255.32kW +j  186.65kvar)
         to ( 253.96kW +j  185.65kvar)
-----
#####

```

Source: The author (2022).

Figure 6.7 – Final result report frames for the simulation 1.

Phase a, Final Result:						Phase b, Final Result:					
[652.1] [V:0.926640] [Ang: -2.5] [Vvio: 8.07V]						[mg4.2] [V:0.888265] [Ang:-125.5] [Vvio: 100.24V]					
Vdrop-->	Mg1 (V)	Mg2 (V)	Mg3 (V)	Mg4 (V)	MMG (V)	Vdrop-->	Mg1 (V)	Mg2 (V)	Mg3 (V)	Mg4 (V)	MMG (V)
ph.1	18.90	0.88	71.02	68.81	159.61	ph.1	18.90	0.88	71.02	78.40	169.20
ph.2	6.82	31.69	52.24	185.67	276.42	ph.2	6.82	31.69	52.24	209.13	299.87
ph.3	15.31	-12.10	84.13	40.07	127.41	ph.3	15.31	-12.10	84.13	50.05	137.40
Case_drop: 1, kMmg = 0.856284						Case_drop: 1, kMmg = 0.685183					
kMg1	kMg2	kMg3	kMg4			kMg1	kMg2	kMg3	kMg4		
0.855607	1.000000	0.855607	0.855607			0.685183	0.685183	0.685183	0.685183		
mg1a, from ( 160.00kW +j 110.00kvar)						mg1b, from ( 120.00kW +j 90.00kvar)					
to ( 136.90kW +j 94.12kvar)						to ( 82.22kW +j 61.67kvar)					
mg3a, from ( 385.00kW +j 220.00kvar)						mg2b, from ( 170.00kW +j 125.00kvar)					
to ( 329.41kW +j 188.23kvar)						to ( 116.48kW +j 85.65kvar)					
mg4a, from ( 485.00kW +j 190.00kvar)						mg3b, from ( 385.00kW +j 220.00kvar)					
to ( 414.97kW +j 162.57kvar)						to ( 263.80kW +j 150.74kvar)					
						mg4b, from ( 680.00kW +j 600.00kvar)					
						to ( 465.92kW +j 411.11kvar)					
[652.1] [V:0.933458] [Ang: -3.1] [Vvio: -8.31V]						[mg4.2] [V:0.934900] [Ang:-123.9] [Vvio: -11.77V]					
Vdrop-->	Mg1 (V)	Mg2 (V)	Mg3 (V)	Mg4 (V)	MMG (V)	Vdrop-->	Mg1 (V)	Mg2 (V)	Mg3 (V)	Mg4 (V)	MMG (V)
ph.1	16.31	0.82	61.14	63.79	142.05	ph.1	16.31	0.82	61.14	73.55	151.81
ph.2	2.40	21.91	27.42	120.85	172.58	ph.2	2.40	21.91	27.42	137.25	188.98
ph.3	14.58	-8.52	78.97	45.66	130.69	ph.3	14.58	-8.52	78.97	53.96	138.99
Phase c, Final Result:											
[611.3] [V:0.932204] [Ang: 113.9] [Vvio: -5.29V]											
Vdrop-->	Mg1 (V)	Mg2 (V)	Mg3 (V)	Mg4 (V)	MMG (V)						
ph.1	18.90	0.88	71.02	68.81	159.61						
ph.2	6.82	31.69	52.24	185.67	276.42						
ph.3	15.31	-12.10	84.13	40.07	127.41						
Case_drop: 1, kMmg = 0.867897											
kMg1	kMg2	kMg3	kMg4								
0.875728	1.000000	0.875728	0.875728								
mg1c, from ( 120.00kW +j 90.00kvar)											
to ( 105.09kW +j 78.82kvar)											
mg3c, from ( 385.00kW +j 220.00kvar)											
to ( 337.16kW +j 192.66kvar)											
mg4c, from ( 290.00kW +j 212.00kvar)											
to ( 253.96kW +j 185.65kvar)											
[611.3] [V:0.930145] [Ang: 114.7] [Vvio: -0.35V]											
Vdrop-->	Mg1 (V)	Mg2 (V)	Mg3 (V)	Mg4 (V)	MMG (V)						
ph.1	16.31	0.82	61.14	63.79	142.05						
ph.2	2.40	21.91	27.42	120.85	172.58						
ph.3	14.58	-8.52	78.97	45.66	130.69						

Source: The author (2022).

results presented in Figure 6.6, frame 2, show that the node under analysis in the second iteration is really 611.3, with 19.15 V of violation. The values presented in each field of frame 2 can be computed in a similar way to that described for frame 1. Note that MG2 does not belong to the  $\mathbb{U}_{in}$  group since it does not have phase c and presents a negative contribution to that violation.

After iteration 2 (Figure 6.5, middle left subplot), the red phase has a slight worsening. The same happens after iteration 3 (middle right subplot) with the green one. After iteration 4 (lower left subplot), only node 611.3 is in a violation condition. Finally, after iteration 5 (lower right subplot), there is no more node with voltage violation.

In Figure 6.6, the results from frame 2 to 5 quantitatively illustrate the behavior observed in Figure 6.5, through the violations of 19.15 V, 25.26 V, 23.47 V, and 0.75 V, respectively.

Figure 6.7 illustrates the report with the final simulation results. It is possible to verify that phase *a* goes from a initial violation condition of 8.07 V to a final of  $-8.31$  V, phase *b* from 100.24 V to  $-11.77$  V, and phase *c* from  $-5.29$  V to  $-0.35$  V. The final load adjustment factors (in percentage) of the MGs is 85.56%, 68.52%, and 87.57% for phases *a*, *b*, and *c*, respectively.

Table 6.2 presents a list of intermediate load adjustment factor values taken from the results in Figure 6.6 and organized by iteration and by phase. Applying those values to Equation 4.30 it is possible to calculate the final adjustment factor values for each microgrid node, as shown in the last column of this table. Such values must be the same as those presented in the final simulation report in Figure 6.7.

Table 6.2 – Intermediate and final values of MG load adjustment factors in simulation 1.

buses	ph.	Intermediate $k_{drop}$ values					Final $k_{drop}$ value
		Iter. 1	Iter. 2	Iter. 3	Iter. 4	Iter. 5	
mg1, mg3, mg4	a	1.0	1.0	0.8556	1.0	1.0	0.8556
	b	0.7656	1.0	1.0	0.8950	1.0	0.6852
	c	1.0	0.8804	1.0	1.0	0.9947	0.8757
mg2	a	n.a	n.a	n.a	n.a	n.a	n.a
	b	0.7656	1.0	1.0	0.8950	1.0	0.6852
	c	n.a	n.a	n.a	n.a	n.a	n.a

Source: The author (2022).

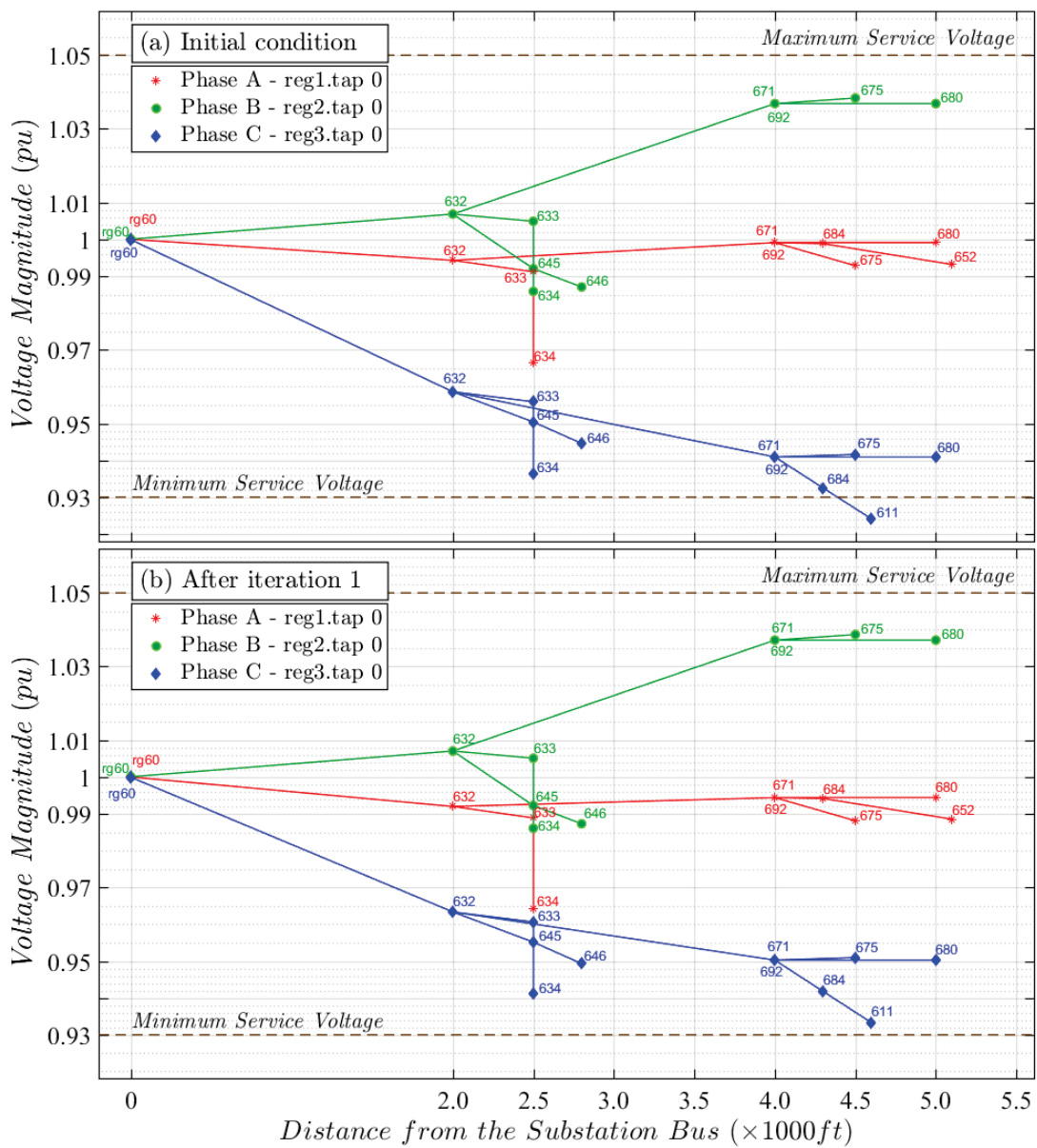


6.2.1.2 Voltage Drop Case 2

Simulation results for the voltage drop case 2, where  $V_{drop}^{mmg} \leq 0$ , are presented in Figure 6.8 and Figure 6.9. This simulation case required only one iteration for convergence to a violation-free state. Figure 6.8 shows that only node 611.3 presents voltage violation in the initial condition. Thus, after iteration 1, it is possible to verify that the non-violation condition has been reached.

According to the results presented in the final simulation report for phase *c* illus-

Figure 6.8 – Three-phase voltage profile evolution along the feeder in simulation 2.



Source: The author (2022).



Figure 6.9 – Final result report frames for the simulation 2.

```

#####
Phase a, Final Result:
-----
[634.1] [V:0.964170] [Ang: -2.2] [Vvio: -82.07V]
#####
Phase b, Final Result:
-----
[mg1.2] [V:0.986082] [Ang:-121.3] [Vvio:-134.70V]
#####
#####
Case_drop: 2, kMmg = 2.080540
kMg1          kMg2          kMg3          kMg4
1.000000      1.000000      1.179013      1.000000
-----
mg3c, from (-385.00kW +j -220.00kvar)
to (-453.92kW +j -259.38kvar)
-----
[611.3] [V:0.924111] [Ang: 116.6] [Vvio: 14.14V]
#####
Vdrop--> Mg1 (V)  Mg2 (V)  Mg3 (V)  Mg4 (V)  MMG (V)
ph.1      19.46    1.58   -74.56   96.22    42.69
ph.2       6.48    30.24  -46.50  -59.40   -69.17
ph.3      14.58   -12.15 -79.01   63.50   -13.09
#####
#####
Case_drop: 2, kMmg = 2.080540
kMg1          kMg2          kMg3          kMg4
1.000000      1.000000      1.179013      1.000000
-----
mg3c, from (-385.00kW +j -220.00kvar)
to (-453.92kW +j -259.38kvar)
-----
[611.3] [V:0.933312] [Ang: 117.1] [Vvio: -7.95V]
#####
Vdrop--> Mg1 (V)  Mg2 (V)  Mg3 (V)  Mg4 (V)  MMG (V)
ph.1      19.40    1.53   -62.97   96.17    54.13
ph.2       6.51    30.29  -47.98  -59.58   -70.76
ph.3      14.68   -12.13 -102.20   63.88   -35.78
#####
#####

```

Source: The author (2022).

trated in Figure 6.9, it is possible to confirm that the node under analysis is 611.3, with a violation voltage of 14.14 V. It is also possible to verify in that report the negative contribution ( $-13.09$  V) of the MMG to the voltage violation, which led the Matlab algorithm to classify this iteration as a voltage drop case 2.

The set of microgrids participating in the procedure  $\mathbb{U}_{in}$  is formed only by MG3, as it is the only one that presents both a negative contribution ( $-79.01$  V) and phase  $c$ .

The MMG load adjustment factor  $k_{drop}^{mmg}$  (calculated from Equation 4.17) is 2.08. Also, the load adjustment factor for each MG  $k_{drop}^{in}$  (calculated from Equation 4.22a) is 1.18. Thus, the MG3, which is already in supply mode, should increase its power injection on the MG3 bus, phase  $c$ , by 18%, i.e, from  $-385.00$  kW  $-j220.00$  kvar to  $-453.92$  kW  $-j259.38$  kvar, as illustrated in Figure 6.9.

Finally, the MMG contribution to the voltage drop at node 611.3 goes from  $-13.09$  V to  $-35.78$  V, and the violation voltage on that node goes from 14.14 V to  $-7.95$  V.

### 6.2.1.3 Voltage Drop Case 3

Simulation results for the voltage drop case 3, where  $0 < V_{drop}^{mmg} < V_{vio}$ , are presented in Figures 6.10, 6.11, and 6.12. In this simulation case, the Matlab algorithm achieves convergence to a violation-free condition after three iterations. Figure 6.10 illus-

trates the voltage profile along the feeder for the initial condition and after each iteration. Initially, the blue phase has six buses with voltage violations, the red phase only one bus, and the green none. The worst case is on node 611.3.

After the first iteration, the blue phase shows an improvement regarding the initial condition with only one node in the violation condition. The red phase shows a worsening in relation to the initial condition, although it continues with only one phase in violation. The worst case is on node 652.1. After the second iteration, only the blue phase remains in the violation condition with node 611.3. The last iteration fixes the blue phase entirely and keeps the others violation-free.

Figure 6.11 shows the output report frames for iterations 1, 2, and 3. In frame 1 (**## Iteration [1] ##**), the results show an initial voltage violation at node 611.3 of 36.65 V, and the MMG is contributing with 12.19 V to the voltage drop at that node. Under these conditions, the Matlab algorithm classifies this iteration as voltage drop case 3 ( $0 < V_{drop}^{mmg} < V_{vio}$ ).

The set of microgrids participating in the procedure  $\mathbb{U}_{in}$  is formed by MG1 and MG4, as they present a positive contribution (14.23 V and 86.40 V, respectively) and have the phase *c*.

As can be verified in frame 1, the MMG and MG load adjustment factors in this iteration are  $-2.0060$  and  $0.7312$ , respectively.

Results of frame 2 (**## Iteration [2] ##**) in Figure 6.11 show that 652.1 is the current node under analysis. Furthermore, the contribution of the MMG (37.93 V) is greater than the violation voltage (12.12 V), which drives the Matlab algorithm to classify this iteration as voltage drop case 1, as can be verified in that frame. MG1 and MG4 make up the set of microgrids  $\mathbb{U}_{in}$  participating in the procedure, as in iteration 1.

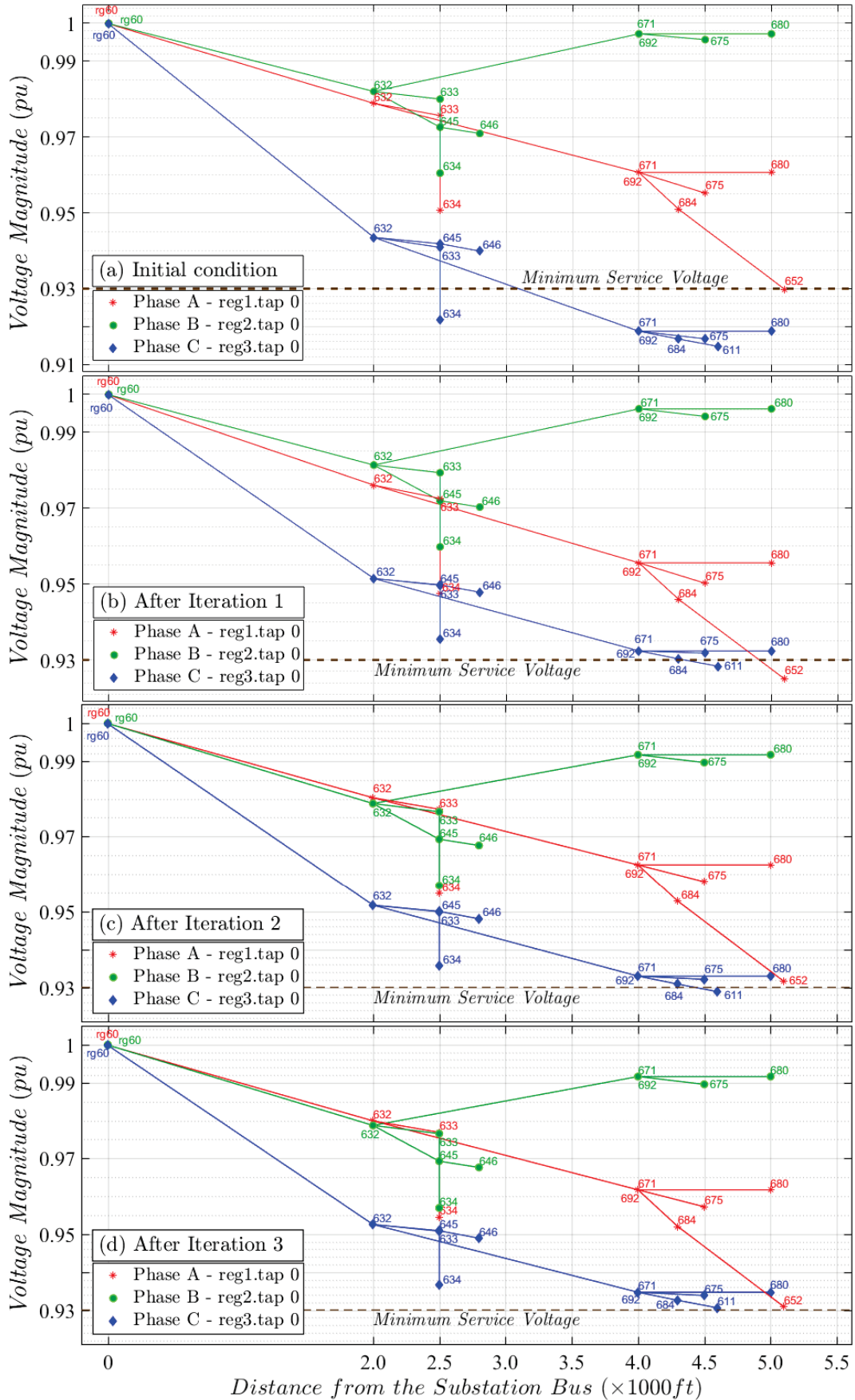
The load adjustment factors in iteration 2 are  $k_{drop}^{mmg} = 0.6805$  and  $k_{drop}^{in} = 0.8962$ , as can be verified in the results of frame 2.

In the next frame (**## Iteration [3] ##**), results show that 611.3 is again the node under analysis. Note that the Matlab algorithm classifies this iteration as voltage drop case 2 because  $V_{drop}^{mmg}$  is lower than zero ( $-24.69$  V). In addition, only MG3 is in the set of MGs participating in the procedure, as it is the only microgrid that has both the negative contribution feature ( $-78.30$  V) and the characteristic of having the *c* phase.

The load adjustment factors in this iteration are  $k_{drop}^{mmg} = 1.1102$  and  $k_{drop}^{in} = 1.0347$ , as can be verified in the results of frame 3.

A voltage drop case 2 with  $k_{drop}^{in} = 1.0347$  means that MG3 is in supply mode and must increase its power injection to node mg3.3 by 3.47%. The results of frame 3 show that, for the node mg3.3, there is an increase in modulus of the real power, from 385.00 kW to 398.36 kW, and of the reactive power, from 220.00 kvar to 227.63 kvar, i.e., 3.47%.

Figure 6.10 – Three-phase voltage profile evolution along the feeder in simulation 3.



Source: The author (2022).

Figure 6.11 – Output report frames for the three iterations in simulation 3.

<pre> ##### Phase c, ## Iteration [ 1 ] ## ----- [611.3] [V:0.914739] [Ang: 115.5] [Vvio: 36.65V] ----- Vdrop--&gt;  Mg1 (V)  Mg2 (V)  Mg3 (V)  Mg4 (V)  MMG (V) ph.1      20.27   1.51   -81.57   83.05   23.26 ph.2       6.79   30.97  -50.02   19.91    7.65 ph.3      14.23  -12.36  -76.08   86.40   12.19 ----- Case_drop: 3,    kMmg = -2.306806 kMg1:0.7311 kMg2:1.0000 kMg3:1.0000 kMg4:0.7311 ----- mg1c, from ( 120.00kW +j   90.00kvar)           to (  87.73kW +j   65.80kvar) mg4c, from ( 290.00kW +j  212.00kvar)           to ( 212.03kW +j  155.00kvar) ----- ##### </pre>						<pre> ##### Phase a, ## Iteration [ 2 ] ## ----- [652.1] [V:0.924954] [Ang: -3.7] [Vvio: 12.12V] ----- Vdrop--&gt;  Mg1 (V)  Mg2 (V)  Mg3 (V)  Mg4 (V)  MMG (V) ph.1      22.52    1.45  -80.30   94.26   37.93 ph.2       7.00   31.06  -50.76   20.49    7.79 ph.3       8.44  -12.34  -77.70   59.21  -22.39 ----- Case_drop: 1,    kMmg = 0.680502 kMg1:0.8962 kMg2:1.0000 kMg3:1.0000 kMg4:0.8962 ----- mg1a, from ( 160.00kW +j  110.00kvar)           to ( 143.40kW +j   98.58kvar) mg4a, from ( 485.00kW +j  190.00kvar)           to ( 434.67kW +j  170.28kvar) ----- ##### </pre>					
<pre> ##### Phase c, ## Iteration [ 3 ] ## ----- [611.3] [V:0.928869] [Ang: 115.7] [Vvio:  2.72V] ----- Vdrop--&gt;  Mg1 (V)  Mg2 (V)  Mg3 (V)  Mg4 (V)  MMG (V) ph.1      19.41    1.47  -79.00   79.74   21.62 ph.2       8.65   31.13  -51.25   30.51   19.04 ph.3       8.44  -12.38  -78.30   57.55  -24.69 ----- Case_drop: 2,    kMmg = 1.110019 kMg1:1.0000 kMg2:1.0000 kMg3:1.0347 kMg4:1.0000 ----- mg3c, from (-385.00kW +j -220.00kvar)           to (-398.36kW +j -227.63kvar) ----- ##### </pre>											

Source: The author (2022).

Figure 6.12 illustrates the final result report of this simulation. The results show that phases *a* and *c* have an initial voltage violation condition of 0.42 V and 36.65 V, respectively, and a final condition of  $-2.08$  V and  $-1.36$  V. Furthermore, only phases *a* and *c* experience load adjustment. While the MG1 and MG4 decrease their loads in phases *a* and *c*, the MG3 increases the power injection in phase *c*.

#### 6.2.1.4 Voltage Drop Case 4

Results for simulation 4, where  $V_{drop}^{mmg} = V_{vio}$ , are presented in Figures 6.13, 6.14, and 6.15. In this case, the Matlab algorithm reached a violation-free state after two iterations. Figure 6.13 illustrates the results for voltage profile along the feeder regarding the initial condition and after each iteration. According to results for initial condition, phase *c* presents all buses in the voltage violation zone except the source bus. On the other hand, phases *a* and *b* have all buses in violation-free condition. Again, the worst case is on node 611.3.

Figure 6.12 – Final result report frames for simulation 3.

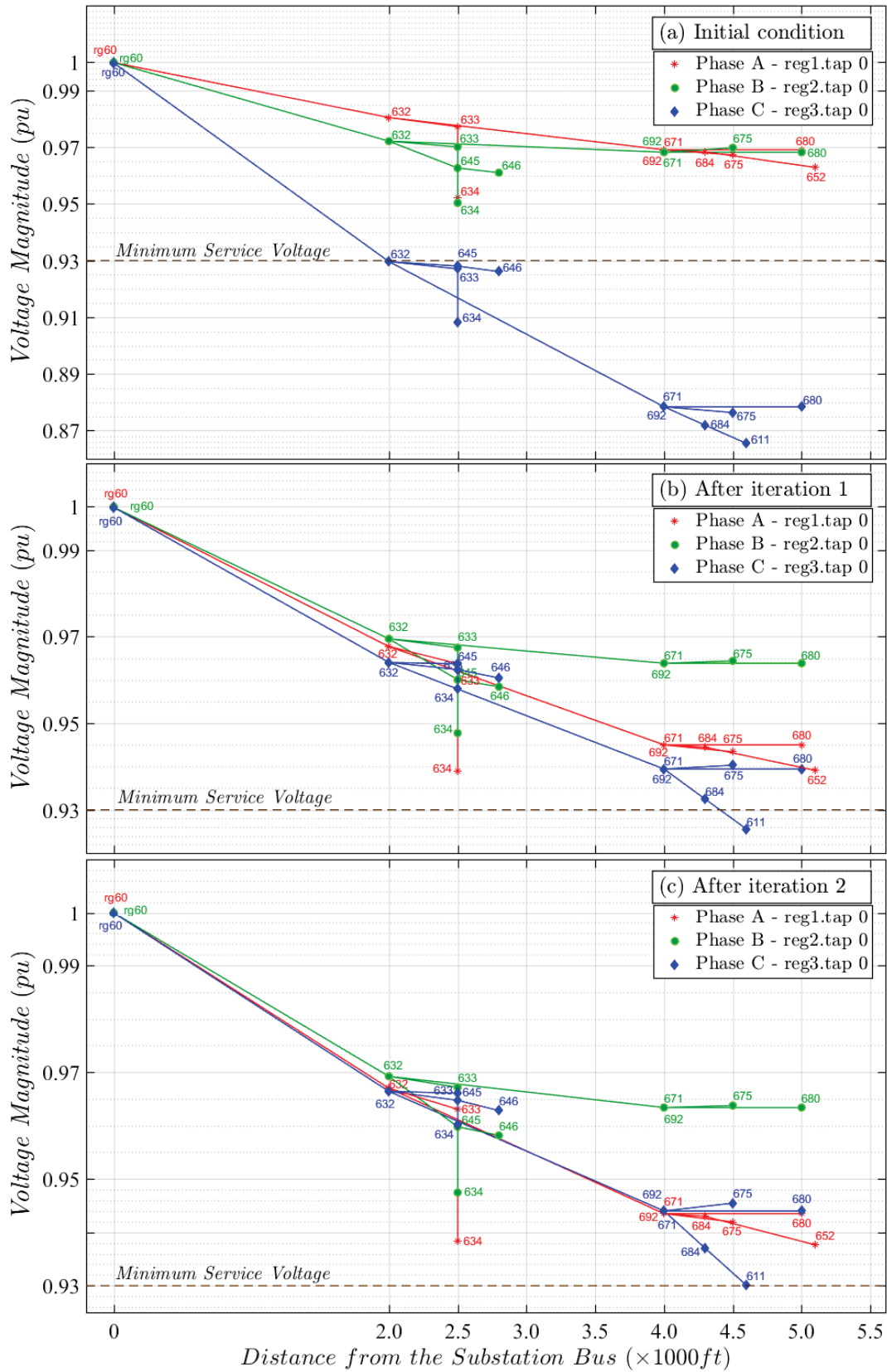
Phase a, Final Result:						Phase c, Final Result:					
[652.1] [V:0.929826] [Ang: -3.9] [Vvio: 0.42V]						[611.3] [V:0.914739] [Ang: 115.5] [Vvio: 36.65V]					
Vdrop-->	Mg1 (V)	Mg2 (V)	Mg3 (V)	Mg4 (V)	MMG (V)	Vdrop-->	Mg1 (V)	Mg2 (V)	Mg3 (V)	Mg4 (V)	MMG (V)
ph.1	20.27	1.51	-81.57	83.05	23.26	ph.1	20.27	1.51	-81.57	83.05	23.26
ph.2	6.79	30.97	-50.02	19.91	7.65	ph.2	6.79	30.97	-50.02	19.91	7.65
ph.3	14.23	-12.36	-76.08	86.40	12.19	ph.3	14.23	-12.36	-76.08	86.40	12.19
Case_drop: 1, kMmg = 0.680502						Case_drop: 3, kMmg = -2.560597					
kMg1		kMg2		kMg3		kMg1		kMg2		kMg3	
0.896221	1.000000	1.000000	0.896221	0.731121	1.000000	1.034691	0.731121	1.034691	0.731121	1.034691	0.731121
mg1a, from ( 160.00kW +j 110.00kvar)						mg1c, from ( 120.00kW +j 90.00kvar)					
to ( 143.40kW +j 98.58kvar)						to ( 87.73kW +j 65.80kvar)					
mg4a, from ( 485.00kW +j 190.00kvar)						mg3c, from (-385.00kW +j -220.00kvar)					
to ( 434.67kW +j 170.28kvar)						to (-398.36kW +j -227.63kvar)					
mg4c, from ( 290.00kW +j 212.00kvar)						to ( 212.03kW +j 155.00kvar)					
[652.1] [V:0.930868] [Ang: -3.3] [Vvio: -2.08V]						[611.3] [V:0.930566] [Ang: 115.8] [Vvio: -1.36V]					
Vdrop-->	Mg1 (V)	Mg2 (V)	Mg3 (V)	Mg4 (V)	MMG (V)	Vdrop-->	Mg1 (V)	Mg2 (V)	Mg3 (V)	Mg4 (V)	MMG (V)
ph.1	19.40	1.46	-76.80	79.64	23.71	ph.1	19.40	1.46	-76.80	79.64	23.71
ph.2	8.65	31.13	-51.43	30.52	18.87	ph.2	8.65	31.13	-51.43	30.52	18.87
ph.3	8.46	-12.38	-82.88	57.72	-29.08	ph.3	8.46	-12.38	-82.88	57.72	-29.08
Phase b, Final Result:						Phase b, Final Result:					
[634.2] [V:0.956950] [Ang:-122.0] [Vvio: -64.73V]						[634.2] [V:0.956950] [Ang:-122.0] [Vvio: -64.73V]					

Source: The author (2022).

It is possible to observe in the results of Figure 6.13 that after the first iteration, all nodes are in the violation-free zone, except for node 611.3, although the voltage profile in phases *a* and *b* presents an increase in the voltage drop of all nodes after the source node. Finally, the results show that after the third iteration all nodes are in the violation-free zone.

Figure 6.14 shows the output report frames for iterations 1 and 2. In frame 1 (## Iteration [1] ##), results show that the initial voltage violation at node 611.3 is equal to the MMG contribution (155.07 V). Under these conditions, the Matlab algorithm classifies this iteration as voltage drop case 4, which can be verified the results of frame 1. MG1, MG3, and MG4 make up the set of microgrids  $\mathbb{U}_{in}$  participating in the procedure, since they present a positive contribution to the voltage drop at the 611.3 node and, in addition, they have phase *c* connected to the distribution network. In this iteration, results show an MMG load adjustment factor of  $13 \times 10^{-6}$  and 0.2970 for the microgrids participating in the procedure, which represents a load reduction of 70.30% for each microgrid.

Figure 6.13 – Three-phase voltage profile evolution along the feeder in simulation 4.



Source: The author (2022).

Figure 6.14 – Output report frames for the two iterations in simulation 4.

Phase c, ## Iteration [ 1 ] ##						Phase c, ## Iteration [ 2 ] ##					
[611.3] [V:0.865437] [Ang: 112.3] [Vvio: 155.07V]						[611.3] [V:0.925551] [Ang: 114.6] [Vvio: 10.69V]					
Vdrop-->	Mg1 (V)	Mg2 (V)	Mg3 (V)	Mg4 (V)	MMG (V)	Vdrop-->	Mg1 (V)	Mg2 (V)	Mg3 (V)	Mg4 (V)	MMG (V)
ph.1	20.35	1.40	82.86	17.33	121.94	ph.1	25.96	1.14	118.08	38.86	184.04
ph.2	7.02	31.43	50.29	-9.62	79.12	ph.2	7.70	31.83	50.55	-6.90	83.18
ph.3	14.01	-12.44	72.34	81.16	155.07	ph.3	-1.26	-12.37	-9.10	24.51	1.78
Case_drop: 4, kMmg = 0.000053						Case_drop: 3, kMmg = -4.989077					
kMg1:0.2970 kMg2:1.0000 kMg3:0.2970 kMg4:0.2970						kMg1:1.0000 kMg2:1.0000 kMg3:1.0000 kMg4:0.5641					
mg1c, from ( 120.00kW +j 90.00kvar)						mg4c, from ( 68.92kW +j 50.38kvar)					
to ( 35.65kW +j 26.73kvar)						to ( 38.88kW +j 28.42kvar)					
mg3c, from ( 385.00kW +j 220.00kvar)											
to ( 114.36kW +j 65.35kvar)											
mg4c, from ( 232.00kW +j 169.60kvar)											
to ( 68.92kW +j 50.38kvar)											

Source: The author (2022).

Figure 6.15 – Final result report frames for simulation 4.

Phase a, Final Result:						Phase c, Final Result:					
[652.1] [V:0.937649] [Ang: -2.9] [Vvio: -18.37V]						[611.3] [V:0.865437] [Ang: 112.3] [Vvio: 155.07V]					
Phase b, Final Result:						Vdrop-->					
[634.2] [V:0.947449] [Ang:-123.1] [Vvio: -41.91V]						Mg1 (V) Mg2 (V) Mg3 (V) Mg4 (V) MMG (V)					
						ph.1 20.35 1.40 82.86 17.33 121.94					
						ph.2 7.02 31.43 50.29 -9.62 79.12					
						ph.3 14.01 -12.44 72.34 81.16 155.07					
						Case_drop: 4, kMmg = -0.000266					
						kMg1 kMg2 kMg3 kMg4					
						0.297049 1.000000 0.297049 0.167570					
						mg1c, from ( 120.00kW +j 90.00kvar)					
						to ( 35.65kW +j 26.73kvar)					
						mg3c, from ( 385.00kW +j 220.00kvar)					
						to ( 114.36kW +j 65.35kvar)					
						mg4c, from ( 232.00kW +j 169.60kvar)					
						to ( 38.88kW +j 28.42kvar)					
						[611.3] [V:0.930070] [Ang: 114.8] [Vvio: -0.17V]					
						Vdrop-->					
						Mg1 (V) Mg2 (V) Mg3 (V) Mg4 (V) MMG (V)					
						ph.1 25.92 1.12 117.46 43.38 187.88					
						ph.2 7.71 31.86 50.97 -6.56 83.98					
						ph.3 -1.27 -12.36 -8.87 13.13 -9.37					

Source: The author (2022).



Results of the next frame (**## Iteration [2] ##**) show that node 611.3 remains under analysis. However, in this iteration, the MMG contribution (1.78 V) is lower than the voltage violation (10.69 V). Therefore, the Matlab algorithm classifies this iteration as voltage drop case 3, which can be verified in the report. Only MG4 is part of the set of participating microgrids  $\mathbb{U}_{in}$  since it is the only one with a positive contribution. In this way, node mg4.c must experience an additional load reduction by a factor of 0.5641.

Figure 6.15 illustrates the final result report of this simulation. The results show that node 611.3 has an initial voltage violation of 155.07 V and a final condition of  $-1.17$  V. The final result shows that MG2 remains with its charge unchanged. MG1 and MG2 experience a load reduction in phase  $c$  of 70.30% while MG4 has a load reduction of 83.24% in phase  $c$ .

### 6.2.1.5 Feeder Operation Performance Indicators

Table 6.3 illustrates the MMG load adjustment and feeder operation performance indicators for the four simulations. In the first column is the identification of the simulation case (Sim. Case). The second column (Node) identifies the nodes whose initial condition represents the lowest voltage value for that phase along the feeder. The violation voltage ( $V_{vio}$ ) and the MMG contribution to the voltage drop ( $V_{drop}^{mmg}$ ) at the node under analysis before the adjustment procedure (Initial Voltages) are in columns 3 and 4. The following two columns (Final Voltages) present the same quantities with values after the procedure ( $V'_{vio}$  and  $V'_{drop}^{mmg}$ ). In the next column is the MMG load adjustment factor  $k_{drop}^{mmg}$ . Columns 8 and 11 show the initial MMG real ( $P_{mmg}$ ) and reactive ( $Q_{mmg}$ ) powers, which were calculated by applying the data from Table 5.2 to Equation 4.24a and Equation 4.24c, respectively. The final MMG load values,  $P'_{mmg}$  and  $Q'_{mmg}$  presented in columns 9 and 12, were calculated through Equation 4.24b and Equation 4.24d using the data from the final results reports of each simulation case (Figures 6.7, 6.9, 6.12, and 6.15). Finally, columns 10 and 13 illustrate the load variation of the MMG ( $\Delta P_{mmg}$  and  $\Delta Q_{mmg}$  calculated using Equation 4.25) required to overcome the voltage violation at the node under analysis.

Quantities in Table 6.3 show which nodes are in the voltage violation state; they quantify the voltage violation and the contribution of the MMG to the voltage drop on the bus under violation per phase; qualify the MMG as one of the loads that either contribute to the voltage drop on the bus or contribute to its voltage rise, and finally, it illustrates the amount of load that the MMG must place at the disposal of the DSO to use as a resource to reach the violation-free state. For all these reasons, the quantities in this table are considered to be feeder operation performance indicators and can be classified into voltage and power indicators, and load adjustment factor.



Table 6.3 – MMG load adjustment and feeder operation performance indicators; n.c. and unch. stand for “do not care” and “unchanged”, respectively.

Sim. Case	Node	Initial Voltages (V)			Final Voltages (V)			$k_{drop}^{mmg}$	MMG Load Adjustment $\{P \text{ (kW)}; Q \text{ (kvar)}\}$					
		$V_{vio}$	$V_{drop}^{mmg}$	$V'_{vio}$	$V'_{drop}^{mmg}$	$V_{vio}$	$V'_{drop}^{mmg}$		$P_{mmg}$	$P'_{mmg}$	$\Delta P_{mmg}$	$Q_{mmg}$	$Q'_{mmg}$	$\Delta Q_{mmg}$
1	652.1	8.07	159.61	-8.31	142.05	0.856	1030.00	881.28	148.72	520.00	444.92	75.08		
	mg4.2	100.24	299.87	-11.77	188.98	0.685	1355.00	928.42	426.58	1035.00	709.17	325.83		
	611.3	-5.29	127.41	-0.35	130.69	0.868	795.00	696.21	98.79	522.00	457.13	64.87		
2	634.1	-87.67	n.c.	-82.07	n.c.	n.c.	unch.	unch.	0	unch.	unch.	0		
	mg1.2	-134.13	n.c.	-134.70	n.c.	n.c.	unch.	unch.	0	unch.	unch.	0		
3	611.3	14.14	-13.09	-7.95	-35.78	2.081	-120.00	-188.92	68.92	-24.00	-63.38	39.38		
	652.1	0.42	23.26	-2.08	23.71	0.681	260.00	193.07	66.93	80.00	48.86	31.14		
	634.2	-73.14	n.c.	-64.73	n.c.	n.c.	unch.	unch.	0	unch.	unch.	0		
4	611.3	36.63	12.19	-1.36	-29.08	-2.561	25.00	-98.60	123.60	82.00	-6.83	88.83		
	652.1	-78.86	n.c.	-18.37	n.c.	n.c.	unch.	unch.	0	unch.	unch.	0		
	634.2	-48.84	n.c.	-41.91	n.c.	n.c.	unch.	unch.	0	unch.	unch.	0		
611.3	155.07	155.07	-0.17	-9.37	0.000	737.00	188.89	548.11	479.60	120.50	359.10			

Source: The author (2022).

In the simulation case 1, to overcome the voltage violation at node mg4.2, the MMG performs a load adjustment resulting in a contribution decrease of 63% from the initial value (from 299.87 V to 188.98 V). However, there is an adjustment of MMG load in all the phases, including phase  $c$ , that does not present a violation. This is because in a three-phase system, a load adjustment in one phase can affect the voltage drop in the other two phases as well. Thus, even if the voltage adjustment procedure is for a single or two phases, to account for available resources, it is necessary to consider the three-phase load provided by MMG, which in this case is 1271.51 kW.

In the case of simulation 2, the voltage indicators show that the MMG is initially in supply mode and increases its contribution to improve the voltage at node 611.3. This can also be verified in the load indicators where MMG makes available an additional load of 68.92 kW (from  $-120.00$  kW to  $-188.98$ ) to overcome the violation at that node.

In the simulation case 3, node 611.3, the power indicators show that the MMG switches from load mode (25 kW) to supply mode ( $-98.60$  kW) by making 123.60 kW available for this phase. On the other hand, in the adjustment performed for the phase  $a$  (node 652.1), the MMG remained in load mode. The same effect can be verified on voltage indicators.

In the case of simulation 4, the voltage indicators suggest that the MMG switches from initial load mode to supply mode at the end of the procedure (from 155.07 V to  $-9.37$  V). However, the power indicators suggest that the MMG is initially in load mode and remains in load mode at the end of the procedure (from 737.00 kW to 188.89 kW). In fact, the power indicators can be considered a reference to determine the operating mode (load mode at the end), while the voltage indicators show whether the MMG is contributing to the voltage drop or rise at the node under analysis (voltage rise in this case). This difference is due to the effect on the  $c$  phase of the loads in the other phases. Note for example in Figure 6.15, that MG2, even having no phase  $c$ , presents  $(V_{drop}^{mg2})_{611.3} = -12.27V$ .

Finally,  $k_{drop}^{mmg}$  in Table 6.3 precisely represents the load adjustment in the case of simulation 1 since for the three phases the relationship  $k_{drop}^{mmg} \times P_{mmg} = P'_{mmg}$  is valid. However, in simulation cases 2, 3, and 4, this relationship is not valid. Simulation 1 is a specific case in which all MGs participate in the procedure, and all are in load mode (initial and final condition). But, in the other simulation cases, this situation does not happen, as there are specific load adjustment factors for each MG that participates in the procedure. On the other hand, the value of  $k_{drop}^{mmg}$  can still be used to classify the voltage drop cases during the adjustment procedure.

## 6.2.2 Discussion

The simulation platform used in this work allowed performing a three-phase power flow of a highly loaded and unbalanced feeder, whose loading and unbalance are affected in different ways according to the operation of the MMG in a simulation case. It is a realistic representation of a typical distribution feeder with the addition of the multi-microgrids connection. Therefore, the simulation results provide an adequate basis to validate the methodology proposed in this work.

Results presented in the previous section support the validation of the methodology proposed in this study. All simulation cases start from an initial condition of voltage violation in one or more phases along the feeder and reach a final condition in which all buses are violation free, for any phase, after no more than five iterations. This characteristic of reaching an adequate load adjustment value (convergence) after a few iterations, stated in the results, is evidence that the values determined for  $w_{drop}$ , according to the  $k_{drop}^{in}$  range, are suitable for this purpose.

The operation performance indicators in Table 6.3 show the MMG contribution to a voltage violation through the indicators  $V_{drop}^{mmg}$  and  $V_{drop}^{mmg}$ . In addition, they illustrate through the power indicators the amount of load that the MMG must make available to meet a DSO's request. They also show that the load adjustment factor should not be used as a reference to determine this amount of load. Thus, voltage and power indicators from Table 6.3 can be used in practice to help classify a possible ancillary service provided by MMG.

The results presented in this work show how microgrids, whether operating associated or independently, can affect the operating performance of a distribution network in terms of voltage quality along a feeder. The numerous possible combinations of operating state of each microgrid connected to the main grid can result in voltage violation situations in one or more phases of the feeder, as the four cases presented in this work. On the other hand, the results also show that it is possible to take advantage of the distributed energy resources of microgrids to minimize this impact on the distribution network during the occurrence of a violation. Furthermore, from the standpoint of the DSO, it may be more advantageous to deal with only one entity that can concentrate the capacity of distributed energy resources (MMG) than to deal with each microgrid individually. From the point of view of microgrids, it can also be more advantageous to operate as a group since they can share resources to meet DSO adjustment requests. In addition, when microgrids are in an MMG, they can participate of optimized operating strategies to reduce MMG's operating costs according to the needs demanded by the DSO. Also, MGs may even join MMG to provide paid ancillary services to the DSO in the future when there is a regulatory framework for this service. According to the load curve characteristics of the feeder, such service can be requested for short periods of time throughout the day,

leaving the distributed energy resource available for the individual optimized operation of the MG during the rest of the day. This can be a way to add a new feature to a BESS inside an MG for example, which can add value to that product, reducing the overall investment cost of the system. Therefore, according to the results presented in this work, the second hypothesis in Section 1.1, item ii., “Microgrids operating in groups (MMG) have technical advantages that override the advantages of individual operation (IMG) in a scenario with operating restrictions” can be considered correct.

These statements can also validate the first hypothesis since a distribution network has operational limits that must not be exceeded. To minimize the operating costs of an MG, it may be necessary to mathematically consider the distribution network as an infinite capacity battery, which can store all the excess generation of an MG and fully supply any load demanded. However, the simulation results of this work show this cannot be possible. In addition, to the already known restrictions on the capacity of distribution lines and devices along this line, the issue of voltage quality on the distribution network must impose restrictions on the operation of MG DERs and the power flow at the PCC bus, as discussed in this section. Such constraints directly affect the optimization problem of each microgrid. Therefore, the first hypothesis in Section 1.1, item i., “A microgrid operator should not consider the distribution network an unrestricted source of resources to optimize its operating costs” can also be considered correct.

Compared with previous studies, as in (WANG et al., 2018; DOU et al., 2018; PAPPALARDO; CALDERARO; GALDI, 2022), the methodology presented in this work is different in the following main positive aspects:

- It is naturally designed for application in unbalanced three-phase distribution networks;
- It considers the effect of voltage variation on the phase of the bus under analysis due to power variations of the other phases along the feeder buses (cross-sensitivity);
- It does not require the computation of voltage sensitivity matrices;
- It is capable of jointly considering the real and reactive powers of the microgrids in the voltage level correction strategy;
- It addresses the operation of microgrids as a group (MMG) capable of negotiating with the DSO the necessary adjustments;
- It enables the MMG operator to strategically decide which microgrid should participate in the procedure;
- It presents operating performance indicators that emphasize the contribution of each microgrid to the voltage level on the bus under analysis, which is similar to

what the sensitivity matrix represents. Additionally, it presents such indicators grouped as MMG information, which contributes to the negotiations between the MMG operator and the DSO;

On the other hand, there are some limitations in the results of this work that can be addressed here. This methodology still does not address upper voltage limit violations as in (WANG et al., 2018; PAPPALARDO; CALDERARO; GALDI, 2022). In addition, it is not prepared for applications in mesh distribution networks as in (PAPPALARDO; CALDERARO; GALDI, 2022). Also, the simulations described in this section assume that the MMG can always meet the distributed energy resource request made by the DSO during a case of violation. On the one hand, if this condition is true in practice, by exhausting its DERs such as BESS and controllable loads, the MMG could also disconnect non-controllable loads. On the other hand, this is not a desirable action as it affects energy supply continuity rates and consumer well-being. Thus, in practical implementations, the DSO must consider a limit on the available resources of the MMG in the load adjustment algorithm. If this limit is reached, there may be only a partial correction of the voltage level on the bus under analysis, thus remaining the violation condition. In this case, the DSO can, among other things, trigger other voltage control methods such as voltage regulators and capacitor banks both in terms of real-time operation and operation planning. Regarding distribution system expansion planning, the DSO may consider installing new capacitor banks and voltage regulators in the distribution network. It can also determine optimal connection points for new MGs or BESS to access the distribution network to address such voltage problems. In addition, the DSO may identify the need to carry out works to expand the capacity of the distribution network. The optimal solution among such options may depend on several factors, and its analysis is outside the scope of this work.

This methodology was developed to be applied to different feeders, and is not limited to a specific topology (as long as the feeder is radial) or a particular circuit model, not even a specific number of buses or a specific number of MGs in an MMG, etc. Thus, theoretically it can be successfully applied to other feeder models. However, it has been tested for a single feeder, and this may be another limitation of the results in this work.

Finally, although not illustrated in the results of the present study, in theory, this methodology can be extended to a case where there is a BESS or other dispatchable energy resource along the feeder, outside an MMG or even an MG. Regarding the BESS, for example, the positive or negative load approach (supply mode and load mode) applies to battery charging and discharging operations, respectively. A BESS unit installed in a distribution network outside an MG may belong to a group of assets operated by an MMG. In this case, this unit can be included in the adjustment procedure as an additional MG with no conventional loads and no other DERs.

# 7 Conclusions and Final Considerations

## 7.1 Conclusions

In this work, the analysis of microgrids and multiple-microgrids modeling techniques was performed based on a systematic literature review on the subject. It resulted in the theoretical foundation presented in this thesis, which explores the concepts of distributed energy resources, control and protection of microgrids, and multiple microgrids. This analysis was essential to create a critical opinion on the subject and develop the formulation of both methodologies presented in this thesis.

A methodology for modeling the optimized day-ahead scheduling problem of microgrids was developed in this work. Distributed energy resources as battery energy storage system, photovoltaic system, and controllable loads were mathematically modeled, regarding their operation mode and operational cost. Although the microgrid resources have been modeled in detail, the linearity of the problem has been preserved, which contributes to simplifying its implementation in optimization software, and it helps to focus the work effort on modeling rather than optimization algorithms. Simulations were performed to validate this methodology and evaluate the optimal microgrid operation subject to the Brazilian White Tariff. Scenarios with scheduled intentional islanding, photovoltaic generation curtailment, shifting and interruption of controllable loads, shedding of conventional loads, and energy arbitrage were implemented in the simulations. The results validated the proposed mathematical model, showed the relevance of a BESS in reducing microgrid operating costs and gave rise to a publication in a scientific journal. The optimization modeling of microgrid DERs operation is an activity required to study the optimal operation of a feeder containing multiple microgrids.

The research carried out in this work also resulted in a development of a methodology for voltage regulation in a feeder through load adjustment in multi-microgrids. The entire theoretical basis for calculating the three-phase contribution of each microgrid and the MMG to the voltage drop on a bus in violation was presented. This methodology brings a different approach to computing the contribution of microgrids to voltage violation, although research in this area indicates the use of the voltage sensitivity matrix. A procedure describing the voltage control strategy for day-ahead and real-time applications was developed and proposed in this thesis. Simulations were performed on an unbalanced and highly loaded three-phase feeder model. The results validated the methodology and show in practice that microgrids can effectively provide ancillary services to assist the DSO in controlling the voltage quality of the distribution network. The methodology was also used to identify some performance indicators of the distribution network operation.

Both scientific hypotheses were validated by the results presented in this thesis. They show how the association of multiple microgrids, while subject to operating restrictions of a distribution system, affects the operating performance of a distribution network. The results enable to conclude that microgrids are subject to operational limits imposed by the distribution network, which must be taken into account when optimizing the operation of distributed energy resources, under the risk of affecting the voltage quality of the distribution network. In addition, by the results presented in this thesis, it is possible to conclude that the association of microgrids for operation purposes has technical advantages and can be beneficial both for the distribution grid operator and the microgrids.

Therefore, this thesis contributes scientifically to the area of power systems by presenting an optimization model for the operation of a microgrid, a voltage control methodology for feeders with multiple microgrids, the impact of these microgrids in an active distribution network, and their interaction with the distribution system operator through the formation of a multi-microgrid system.

## 7.2 Scientific Contributions

In general, this work produced two main scientific contributions: a methodology of mathematical modeling of an MG for the planning of the operation and a methodology of voltage adjustment in feeders with the active participation of microgrids providing ancillary services.

Specifically, in microgrid modeling, it was presented a practical methodology to compute the BESS availability cost, including an analytical development of a family of state of health curves to be applied in cost computing. To approximate the model to real systems, practical values of efficiency of all elements in a BESS were considered in the modeling, as batteries, converter, and coupling transformer. Unlike the works found in the literature, the BESS state of charge was modeled as a non-recursive constraint to the MILP problem to maintain the linearity of the problem. Furthermore, no works were found in the literature that addressed MG scheduled intentional islanding modeling presented in this work, which allowed the analysis of the possibility of the PV generation curtailment and the performing of load shedding. Additionally, in the works researched in the literature, there was no modeling of shiftable loads of continuous cycle in a non-interruptible way in the optimization problem, as presented in this work, which corresponds to the real behavior of these loads in practical applications. Finally, it was also noted in the works consulted in the literature the absence of a practical and detailed methodology to calculate the cost of the availability of a solar photovoltaic system as that presented in this work.

Regarding voltage regulation in feeders with microgrids, while some works in the



literature try to use the voltage sensitivity matrix as a voltage control strategy, in this work, a completely different methodology was proposed to solve the same problem. The contribution lies in the various positive and differentiated aspects of the proposed methodology. While in the literature consulted, the authors face some difficulties in applying their models to unbalanced three-phase feeders, that is, real feeders, the methodology proposed in this work was natively developed for this type of feeder. For this reason, in this work it was possible to verify the effect of the cross-sensitivity between phases by simulations, which is not possible in the models consulted in the literature. The proposed procedure does not require the calculation of the voltage sensitivity matrix, something that has been reported as a difficulty by the authors of the consulted works. The proposed model also addresses the adjustment of real and reactive power jointly in microgrids and in a three-phase way, which is still considered a challenge in the works consulted. In addition, there is a contribution related to the business layer of an active distribution network, as the proposed model technically allows an MMG operator to strategically decide which MG should participate in the proposed procedure. It also allows an MMG operator to negotiate with a DSO the provision of ancillary voltage control services considering the interests of the microgrids as a group due to the operation performance indicators that show the contribution of each microgrid to the voltage drop along the feeder.

### 7.3 Future Works

Concerning the optimal day-ahead scheduling of MGs, future works may examine the application of the model to an energy market with a framework of rules for free energy trading between entities, which can be multiple microgrids as well generation units distributed in an energy distribution network. Future work may also include an annual analysis of the optimal day-ahead scheduling problem.

Regarding the voltage adjustment methodology, future works may address the extension of the methodology in this work for both cases of upper voltage limit violation and cases of insufficient energy resources to meet adjustment requests. Also, they may address its application in feeders containing multiple MMGs, MGs, and DERs operating individually. Future work may also involve simulations considering the operation of voltage regulators in the substation and through the distribution network, as well simulations considering different models of feeders. Finally, future works can address the union of both methodologies present in this study by performing an optimal operation of microgrids considering the DSO requests for voltage regulation as an operational constraint.



## 7.4 Scientific Production

Main publications originated in this doctorate:

- Published journal paper: SILVA, V. A.; AOKI, A. R.; LAMBERT-TORRES, G. Optimal day-ahead scheduling of microgrids with battery energy storage system. *Energies*, MDPI AG, v. 13, n. 19, p. 5188, oct 2020, DOI: <https://doi.org/10.3390/en13195188>;
- Journal paper to be submitted: SILVA, V. A.; AOKI, A. R.; LAMBERT-TORRES, “A three-phase unbalanced feeder voltage control strategy for multi-microgrids in active distribution networks”. *Energies*, MDPI, “Optimization and Energy Management in Smart Grids” special issue (deadline 2022/09/20).

Other scientific productions carried out during this doctorate:

- Published journal paper: MACHADO, M.; SILVA, V. A.; BLASI, T. M.; KÜSTER, K. K.; AOKI, A. R.; FERNANDES, T. S. P.; LAMBERT-TORRES, G., Recent research and development of microgrids in Parana. *Brazilian Archives of Biology and Technology*, FapUNIFESP (SciELO), v. 64, n. spe, 2021, DOI: <https://doi.org/10.1590/1678-4324-75years-2021210177>;
- Published symposium paper: ETO, H. I.; VEIGA, E. C.; LEANDRO, M. G. R.; SILVA, V. A.; LACHOVICZ, F. J.; AOKI, A. R., Verifying potential impacts of microgrids by its modeling in power distribution system simulators. In: *Cigre Chengdu 2019 Symposium*. Chengdu: Proceedings of Cigre Chengdu 2019 Symposium, 2019. v. 1, p. 663–674, Paper repository: [Cigre Chendgu Paper 0156](#);
- ANEEL R&D project: [2020, Atual] - PD-02866-0511/2019, Programação diária de microgrids e redes ativas de distribuição considerando o gerenciamento pelo lado da demanda. Participation as doctoral scholarship student. Executing entity: UFPR. Contracting company: Copel. Coordinator: Alexandre R. Aoki, Dr.
- ANEEL R&D project: [2020, Atual] - PD-06491-0531/2019, Plataforma de Wide Area Control com Data Analytics e Machine Learning para Análise Distribuída de Controle. Participation as assistant researcher. Executing entities: UFPR and Gnarus Institute. Contracting company: Copel. Coordinator: Alexandre R. Aoki, Dr.
- ANEEL R&D project: [2022, Atual] - PD-06491-0563/2019, Inteligência Artificial Baseada em Automação Cognitiva e Similarity Matching Aplicada em Estudos

Elétricos de Transmissão e Geração Para Eficiência de Gestão de Obras. Participation as assistant researcher. Executing entities - UFPR and Gnarus Institute. Contracting company - Copel. Coordinator: Milton P. Ramos, Dr.

- Examination committee member: TORTELLI, O. L.; SILVA, V. A.; DEMONTI, R., Participação em banca de Leonardo Fuchs. Metodologia Para Otimização de uma Microrrede Conectada no Sistema de Distribuição de Energia Elétrica. 2019. Trabalho de Conclusão de Curso (Graduação em Engenharia Elétrica) - Universidade Federal do Paraná.
- Co-advising of specialization course of Guilherme Rojo Anzanello. Avaliação Técnico-Econômica de Tecnologias para Smart-Home. Curso de Pós-Graduação Latu Sensu Especialização em Eficiência Energética e Geração Distribuída. Advisor: Prof. Dr. Alexandre R. Aoki.
- Co-advising of undergraduate course of Raphael Marzalek Blasi. Avaliação de Requisitos e Alternativas para Projeto e Concepção de Microrredes. 2021. Trabalho de Conclusão de Curso. (Graduação em Engenharia Elétrica) - Universidade Federal do Paraná. Advisor: Prof. Dr. Alexandre R. Aoki.
- Co-advising of undergraduate course of Edson Cardoso Veiga and Matheus Gidalti Raimundo Leandro. Modelagem e simulação da operação de microrredes usando o OpenDSS e MatPower. 2018. Trabalho de Conclusão de Curso. (Graduação em Engenharia Elétrica) - Universidade Federal do Paraná. Advisor: Prof. Dr. Alexandre R. Aoki.

## REFERENCES

- ABB. *EssPro™ Energy Storage Power Conversion System (PCS): The power to control energy*. [S.l.], 2017. Available online: [https://new.abb.com/power-converters-inverters/energy-storage-grid-stabilization/energy-storage-power-conversion-system-\(pcs\)](https://new.abb.com/power-converters-inverters/energy-storage-grid-stabilization/energy-storage-power-conversion-system-(pcs)). Accessed on: 2020-02-22.
- ABB. *PVS800 Central Inverters*. [S.l.], 2018. Available online: <https://new.abb.com/power-converters-inverters/solar/central/pvs800>. Accessed on: 2018-06-25.
- AGÊNCIA NACIONAL DE ENERGIA ELÉTRICA. *Procedimentos de Distribuição de Energia Elétrica no Sistema Elétrico Nacional – PRODIST: Módulo 3 – Acesso ao Sistema de Distribuição*. rev. 7. Brasília, 2017. 61 p. Available online: <http://www.aneel.gov.br/prodist>. Accessed on: 2017-04-07.
- AGÊNCIA NACIONAL DE ENERGIA ELÉTRICA. *Procedimentos de Distribuição de Energia Elétrica no Sistema Elétrico Nacional – PRODIST: Módulo 1 – Introdução*. rev. 10. Brasília, 2018. 61 p. Available online: <http://www.aneel.gov.br/prodist>. Accessed on: 2020-02-19.
- AGÊNCIA NACIONAL DE ENERGIA ELÉTRICA. *Postos Tarifários*. Brasília: ANEEL, 2020. Available online: <https://www.aneel.gov.br/postos-tarifarios>. Accessed on: 2020-03-27.
- AGÊNCIA NACIONAL DE ENERGIA ELÉTRICA. *Procedimentos de Distribuição de Energia Elétrica no Sistema Elétrico Nacional – PRODIST: Módulo 8 – Qualidade de Energia Elétrica*. rev. 12. Brasília, 2021. 88 p. Available online: <http://www.aneel.gov.br/prodist>. Accessed on: 2022-01-28.
- ALAM, M. N.; CHAKRABARTI, S.; GHOSH, A. Networked microgrids: State-of-the-art and future perspectives. *IEEE Transactions on Industrial Informatics*, v. 15, n. 3, p. 1238–1250, mar 2019.
- ALPHAESS. *Energy Storage Systems ESS for commercial and industrial applications: Storion serires t50/t100*. [S.l.], 2019. Available online: [https://www.estenergy.pl/files/1958343234/file/t50\\_t100.pdf](https://www.estenergy.pl/files/1958343234/file/t50_t100.pdf). Accessed on: 2020-02-21.
- ALQUNUN, K.; GUESMI, T.; FARAH, A. Load shedding optimization for economic operation cost in a microgrid. *Electrical Engineering*, Springer Science and Business Media LLC, v. 102, n. 2, p. 779–791, jan 2020.
- ANEEL. *Resolução Normativa 697, de 16 de dezembro de 2015*. Brasília, 2015. Diário Oficial da União, 22/12/2015, Seção 1, página 229.
- ANTONIADOU-PLYTARIA, K. E. et al. Distributed and Decentralized Voltage Control of Smart Distribution Networks: Models, Methods, and Future Research. *IEEE Transactions on Smart Grid*, v. 8, n. 6, p. 2999–3008, nov 2017.
- ARGHANDEH, R. et al. On the definition of cyber-physical resilience in power systems. *Renewable and Sustainable Energy Reviews*, Elsevier BV, v. 58, p. 1060–1069, may 2016.

ARRIAGA, M.; NASR, E.; RUTHERFORD, H. Renewable energy microgrids in northern remote communities. *IEEE Potentials*, v. 36, n. 5, p. 22–29, sep 2017.

ATLANTIC CLEAN ENERGY SUPPLY LLC. *Customized ESS Solutions for Solar Farm & Micro Grid Application: ZLET - CIESS*. Beijing, 2019. Available online: <https://www.atlanticces.com/wp-content/uploads/2019/11/100KW-with-350KWH.pdf>. Accessed on: 2020-03-29.

BACKHAUS, S. N. et al. *Networked Microgrids Scoping Study*. Los Alamos, New Mexico, 2016. 54 p.

BAZIAR, A.; KAVOOSI-FARD, A.; ZARE, J. A novel self adaptive modification approach based on bat algorithm for optimal management of renewable MG. *Journal of Intelligent Learning Systems and Applications*, Scientific Research Publishing, Inc., v. 05, n. 01, p. 11–18, 2013.

BEN-TAL, A. et al. Adjustable robust solutions of uncertain linear programs. *Mathematical Programming*, Springer Nature, v. 99, n. 2, p. 351–376, mar 2004.

BEN-TAL, A. et al. Robust semidefinite programming. p. 1–21, 09 1998. Available online: [https://www.researchgate.net/publication/228477201\\_Robust\\_semidefinite\\_programming](https://www.researchgate.net/publication/228477201_Robust_semidefinite_programming). Accessed on: 2019-05-21.

BERTSIMAS, D.; SIM, M. The price of robustness. *Operations Research*, Institute for Operations Research and the Management Sciences (INFORMS), v. 52, n. 1, p. 35–53, feb 2004.

BLACKBURN, J. L.; DOMIN, T. J. *Protective Relaying: Principles and Applications*. 3th. ed. [S.l.]: CRC Press, 2006. 638 p. ISBN 1574447165.

BLOOM, A. et al. It's indisputable: Five facts about planning and operating modern power systems. *IEEE Power and Energy Magazine*, v. 15, n. 6, p. 22–30, nov 2017.

BOICEA, V. A. Energy storage technologies: The past and the present. *Proceedings of the IEEE*, v. 102, n. 11, p. 1777–1794, nov. 2014.

BRADLEY, S. P.; HAX, A. C.; MAGNANTI, T. L. *Applied Mathematical Programming*. [S.l.]: Addison-Wesley, 1977. ISBN 020100464X.

BULLICH-MASSAGUÉ, E. et al. Microgrid clustering architectures. *Applied Energy*, Elsevier BV, v. 212, p. 340–361, feb 2018.

CADE ELECTRONICS INC. *BU-908*:: Battery management system (bms). [S.l.], 2019. Available online: [https://batteryuniversity.com/learn/article/how\\_to\\_monitor\\_a\\_battery](https://batteryuniversity.com/learn/article/how_to_monitor_a_battery). Accessed on: 2020-02-21.

CLEAN COALITION. *Community Microgrids*. Denver, 2015. Available online: <https://clean-coalition.org/community-microgrids/>. Accessed on: 2019-05-18.

DENG, R. et al. A survey on demand response in smart grids: Mathematical models and approaches. *IEEE Transactions on Industrial Informatics*, Institute of Electrical and Electronics Engineers (IEEE), v. 11, n. 3, p. 570–582, jun 2015.

- DIVYA, K.; ØSTERGAARD, J. Battery energy storage technology for power systems—an overview. *Electric Power Systems Research*, Elsevier BV, v. 79, n. 4, p. 511–520, apr 2009.
- DORFLER, F.; SIMPSON-PORCO, J. W.; BULLO, F. Breaking the hierarchy: Distributed control and economic optimality in microgrids. *IEEE Transactions on Control of Network Systems*, v. 3, n. 3, p. 241–253, sep 2016.
- DOU, X. et al. A distributed voltage control strategy for multi-microgrid active distribution networks considering economy and response speed. *IEEE Access*, Institute of Electrical and Electronics Engineers (IEEE), v. 6, p. 31259–31268, 2018.
- EBRAHIMI, M. R.; AMJADY, N. Adaptive robust optimization framework for day-ahead microgrid scheduling. *International Journal of Electrical Power & Energy Systems*, Elsevier BV, v. 107, p. 213–223, may 2019.
- EID, B. M. et al. Control methods and objectives for electronically coupled distributed energy resources in microgrids: A review. *IEEE Systems Journal*, v. 10, n. 2, p. 446–458, jun 2016.
- EISELT, C.-L. S. H. *Linear Programming and its Applications*. [S.l.]: Springer-Verlag GmbH, 2007. 380 p. ISBN 3540736700.
- EL-HENDAWI, M. et al. Control and EMS of a grid-connected microgrid with economical analysis. *Energies*, MDPI AG, v. 11, n. 1, p. 129, jan 2018.
- ENSSLIN, L. et al. *ProKnow-C: Knowledge Development Process–Constructivist*. Brazil, 2010. Patent request pending at Brazil's patent office INPI.
- EPE, E. de P. E. *Brazilian Energy Balance 2021 Year 2020 - Final Report*. Brazil, 2021. Available online: <https://www.epe.gov.br/sites-pt/publicacoes-dados-abertos/publicacoes/PublicacoesArquivos/publicacao-601/topico-596/BEN2021.pdf>. Accessed on: 2022-05-01.
- ESMAEILI, S.; ANVARI-MOGHADDAM, A.; JADID, S. Optimal operation scheduling of a microgrid incorporating battery swapping stations. *IEEE Transactions on Power Systems*, Institute of Electrical and Electronics Engineers (IEEE), v. 34, n. 6, p. 5063–5072, nov 2019.
- EUROPEAN NETWORK OF TRANSMISSION SYSTEM OPERATORS FOR ELECTRICITY. *UCTE Operation Handbook: Policy 1 - Load-Frequency Control and Performance*. Brussels, Belgium, 2009. 32 p. Available online: [https://www.entsoe.eu/fileadmin/user\\_upload/\\_library/publications/entsoe/Operation\\_Handbook/Policy\\_1\\_final.pdf](https://www.entsoe.eu/fileadmin/user_upload/_library/publications/entsoe/Operation_Handbook/Policy_1_final.pdf). Accessed on: 2018-02-25.
- EXETER ASSOCIATES, INC. AND GE ENERGY. *PJM Renewable Integration Study: Review of industry practice and experience in the integration of wind and solar generation*. [S.l.], 2012. 193 p. Available online: <http://www.pjm.com/committees-and-groups/subcommittees/irs/pris.aspx>. Accessed on: 2017-03-26.
- FARUQUI, A.; BOURBONNAIS, C. The tariffs of tomorrow: Innovations in rate designs. *IEEE Power and Energy Magazine*, Institute of Electrical and Electronics Engineers (IEEE), v. 18, n. 3, p. 18–25, may 2020.

FEDERAL ENERGY REGULATORY COMMISSION - U.S. DEPARTMENT OF ENERGY. *Assessment of Demand Response and Advanced Metering*: Staff Report. Washington, DC, 2012. 130 p.

FITZGERALD, G. et al. *The Economics of Battery Energy Storage: How Multi-use, Customer-sited Batteries Deliver the Most Services and Value to Customers and the Grid*. Rocky Mountain Institute. Basalt, CO, 2015. 41 p. Available online: [http://www.rmi.org/electricity\\_battery\\_value](http://www.rmi.org/electricity_battery_value). Accessed on: 2017-04-15.

FOSSATI, J. P. et al. A method for optimal sizing energy storage systems for microgrids. *Renewable Energy*, Elsevier BV, v. 77, p. 539–549, may 2015.

GAO, H. et al. Decentralized energy management for networked microgrids in future distribution systems. *IEEE Transactions on Power Systems*, v. 33, n. 4, p. 3599–3610, jul 2018.

GOPALAN, S. A.; SREERAM, V.; IU, H. H. A review of coordination strategies and protection schemes for microgrids. *Renewable and Sustainable Energy Reviews*, v. 32, p. 222–228, abr. 2014.

GUERRERO, J. M. et al. Advanced Control Architectures for Intelligent Microgrids – Part I: Decentralized and Hierarchical Control. *IEEE Transactions on Industrial Electronics*, v. 60, n. 4, p. 1254–1262, abr. 2013. Available online: <https://doi.org/10.1109/tie.2012.2194969>.

GUI, E. M.; DIESENDORF, M.; MACGILL, I. Distributed energy infrastructure paradigm: Community microgrids in a new institutional economics context. *Renewable and Sustainable Energy Reviews*, Elsevier BV, v. 72, p. 1355–1365, may 2017.

HAN, H. et al. Review of power sharing control strategies for islanding operation of AC microgrids. *IEEE Transactions on Smart Grid*, v. 7, n. 1, p. 200–215, jan 2016.

HAN, Y. et al. Review of active and reactive power sharing strategies in hierarchical controlled microgrids. *IEEE Transactions on Power Electronics*, v. 32, n. 3, p. 2427–2451, mar 2017.

HAN, Y. et al. MAS-based distributed coordinated control and optimization in microgrid and microgrid clusters: A comprehensive overview. *IEEE Transactions on Power Electronics*, v. 33, n. 8, p. 6488–6508, aug 2018.

HEDERMAN, W. F. *IEEE Report to DOE QER on Priority Issues*: IEEE joint task force on quadriennial energy review. Washington, DC, 2014.

HUANG, C. et al. Optimal scheduling of microgrid with multiple distributed resources using interval optimization. *Energies*, MDPI AG, v. 10, n. 3, p. 339, mar 2017.

IEEE. *IEEE Standard for Interconnecting Distributed Resources with Electric Power Systems*: IEEE 1547-2003. New York, 2003. 27 p.

IEEE. *IEEE Guide for Design, Operation, and Integration of Distributed Resource Island Systems with Electric Power Systems*: IEEE 1547.4-2011. New York, 2011. 54 p.



- IEEE. *IEEE Guide for Conducting Distribution Impact Studies for Distributed Resource Interconnection*: IEEE 1547.7-2013. New York, 2014. 137 p.
- IEEE. *IEEE Recommended Practice for Electric Power Distribution System Analysis*: IEEE std 1729-2014. New York, 2014. 1-20 p.
- IEEE. *IEEE Standard for Interconnection and Interoperability of Distributed Energy Resources with Associated Electric Power Systems Interfaces*: IEEE 1547-2018. New York, 2018. 138 p.
- IEEE. *IEEE Guide for Design, Operation, and Maintenance of Battery Energy Storage Systems, both Stationary and Mobile, and Applications Integrated with Electric Power Systems*: IEEE std 2030.2.1-2019. New York, 2019. 44 p.
- ISO; IEC; IEEE. 21839 - ISO/IEC/IEEE draft international standard - systems and software engineering - systems of systems (SoS) considerations in life cycle stages of a system. *ISO/IEC/IEEE/P21839, 2019(E)*, p. 1–40, March 2019.
- JAMSHIDI, M. *System of Systems Engineering: Innovations for the 21st Century*. New Jersey: John Wiley & Sons, Inc., 2008. ISBN 9780470403501.
- JIMÉNEZ-ESTÉVEZ, G. A. et al. It Takes a Village: Social SCADA and Approaches to Community Engagement in Isolated Microgrids. *IEEE Power and Energy Magazine*, v. 12, n. 4, p. 60–69, jul. 2014.
- JORDAN, D. C.; KURTZ, S. R. *Photovoltaic Degradation Rates - An Analytical Review*. National Renewable Energy Laboratory - NREL, 2012. Available online: <https://www.nrel.gov/docs/fy12osti/51664.pdf>. Accessed on: 2020-04-17.
- KERSTING, W. H. Radial distribution test feeders. In: *2001 IEEE Power Engineering Society Winter Meeting. Conference Proceedings (Cat. No.01CH37194)*. Columbus, OH, USA: IEEE, 2001.
- KERSTING, W. H. *Distribution System Modeling and Analysis*. Boca Raton, Florida: CRC Press, 2002. 314 p. ISBN 0849308127.
- KIM, R.-K. et al. MILP-PSO combined optimization algorithm for an islanded microgrid scheduling with detailed battery ESS efficiency model and policy considerations. *Energies*, MDPI AG, v. 13, n. 8, p. 1898, apr 2020.
- KOUTSOUKIS, N. C. et al. Online reconfiguration of active distribution networks for maximum integration of distributed generation. *IEEE Transactions on Automation Science and Engineering*, Institute of Electrical and Electronics Engineers (IEEE), v. 14, n. 2, p. 437–448, apr 2017.
- KROPOSKI, B. et al. Achieving a 100% Renewable Grid: Operating Electric Power Systems with Extremely High Levels of Variable Renewable Energy. *IEEE Power and Energy Magazine*, [ieeexplore.ieee.org](http://ieeexplore.ieee.org), v. 15, n. 2, p. 61–73, 2017. ISSN 15407977. Available online: <http://ieeexplore.ieee.org/abstract/document/7866938/>.
- KUMAR, K. P.; SARAVANAN, B. Day ahead scheduling of generation and storage in a microgrid considering demand side management. *Journal of Energy Storage*, Elsevier BV, v. 21, p. 78–86, feb 2019.

- LAWDER, M. T. et al. Battery energy storage system (BESS) and battery management system (BMS) for grid-scale applications. *Proceedings of the IEEE*, Institute of Electrical and Electronics Engineers (IEEE), v. 102, n. 6, p. 1014–1030, jun 2014.
- LEE, G.-H. et al. Comparative study on optimization solvers for implementation of a two-stage economic dispatch strategy in a microgrid energy management system. *Energies*, MDPI AG, v. 13, n. 5, p. 1096, mar 2020.
- LI, B.; ROCHE, R.; MIRAOUI, A. Microgrid sizing with combined evolutionary algorithm and MILP unit commitment. *Applied Energy*, Elsevier BV, v. 188, p. 547–562, feb 2017.
- LI, Q. et al. MAS-based distributed control method for multi-microgrids with high-penetration renewable energy. *Energy*, Elsevier BV, v. 171, p. 284–295, mar 2019.
- LI, Y.; NEJABATKHAH, F. Overview of control, integration and energy management of microgrids. *Journal of Modern Power Systems and Clean Energy*, Springer Nature, v. 2, n. 3, p. 212–222, aug 2014.
- LIU, G. et al. Microgrid optimal scheduling with chance-constrained islanding capability. *Electric Power Systems Research*, Elsevier BV, v. 145, p. 197–206, apr 2017.
- LORUBIO, G.; SCHLOSSER, P. Euro mix: Current european energy developments and policy alternatives for 2030 and beyond. *IEEE Power and Energy Magazine*, v. 12, n. 2, p. 65–74, mar 2014.
- MAHMOUD, M. S.; ALYAZIDI, N. M.; ABOUHEAF, M. I. Adaptive intelligent techniques for microgrid control systems: A survey. *International Journal of Electrical Power & Energy Systems*, Elsevier BV, v. 90, p. 292–305, sep 2017.
- MAIER, M. W. Architecting principles for systems-of-systems. *Systems Engineering*, Wiley, v. 1, n. 4, p. 267–284, 1998.
- MANZ, D.; PIWKO, R.; MILLER, N. Look Before You Leap: The Role of Energy Storage in the Grid. *IEEE Power and Energy Magazine*, v. 10, n. 4, p. 75–84, jul. 2012.
- MANZ, D. et al. The Grid of the Future: Ten Trends That Will Shape the Grid Over the Next Decade. *IEEE Power and Energy Magazine*, v. 12, n. 3, p. 26–36, maio 2014.
- MARNAY, C. et al. Microgrid Evolution Roadmap. In: *2015 International Symposium on Smart Electric Distribution Systems and Technologies (EDST)*. Vienna: Proceedings..., 2015. p. 139–144.
- MARNAY, C. et al. *Microgrids 1, Engineering, Economics, & Experience - WG C6.22 Microgrids Evolution Roadmap*: WG C6.22 microgrids evolution roadmap. Paris, France: CIGRE, 2015. ISBN 978-2-85873-338-5.
- MATHWORKS. *Optimization Toolbox™ User's Guide*. Natick, MA, USA: The MathWorks, Inc., 2019. 1658 p.
- MEMON, A. A.; KAUHANIEMI, K. A critical review of AC microgrid protection issues and available solutions. *Electric Power Systems Research*, Elsevier BV, v. 129, p. 23–31, dec 2015.



- MENGELKAMP, E. et al. Designing microgrid energy markets: A case study: The brooklyn microgrid. *Applied Energy*, Elsevier BV, v. 210, p. 870–880, jan 2018.
- MICROGRID KNOWLEDGE. *Here comes the future: Bronzeville ‘microgrid cluster’ set to begin operating this year*. Newbury, USA., 2022. (<https://microgridknowledge.com/bronzeville-microgrid-cluster-lessons-comed/>). Accessed on: 2022-04-10.
- NEHME, B. F. et al. Real-time thermoelectrical model of PV panels for degradation assessment. *IEEE Journal of Photovoltaics*, Institute of Electrical and Electronics Engineers (IEEE), v. 7, n. 5, p. 1362–1375, sep 2017.
- NGUYEN, A.-D. et al. Impact of demand response programs on optimal operation of multi-microgrid system. *Energies*, MDPI AG, v. 11, n. 6, p. 1452, jun 2018.
- NGUYEN, T. A.; CROW, M. L. Stochastic optimization of renewable-based microgrid operation incorporating battery operating cost. *IEEE Transactions on Power Systems*, Institute of Electrical and Electronics Engineers (IEEE), v. 31, n. 3, p. 2289–2296, may 2016.
- NOSRATABADI, S. M.; HOOSHMAND, R.-a.; GHOLIPOUR, E. A comprehensive review on microgrid and virtual power plant concepts employed for distributed energy resources scheduling in power systems. *Renewable and Sustainable Energy Reviews*, Elsevier, v. 67, p. 341–363, jan 2017. ISSN 1364-0321. Available online: (<http://dx.doi.org/10.1016/j.rser.2016.09.025>).
- NREL. *PVWatts Calculator - NREL*. [S.l.]: National Renewable Energy Laboratory - NREL, 2020. (<https://pvwatts.nrel.gov/pvwatts.php>). Accessed on: 2020-04-17.
- OLIVAL, P.; MADUREIRA, A.; MATOS, M. Advanced voltage control for smart microgrids using distributed energy resources. *Electric Power Systems Research*, Elsevier BV, v. 146, p. 132–140, may 2017.
- PALIZBAN, O.; KAUHANIEMI, K. Energy storage systems in modern grids—matrix of technologies and applications. *Journal of Energy Storage*, Elsevier BV, v. 6, p. 248–259, may 2016.
- PAPPALARDO, D.; CALDERARO, V.; GALDI, V. Microgrids-based approach for voltage control in distribution systems by an efficient sensitivity analysis method. *IEEE Systems Journal*, Institute of Electrical and Electronics Engineers (IEEE), p. 1–12, 2022.
- PARHIZI, S. et al. State of the Art in Research on Microgrids: A Review. *IEEE Access*, v. 3, p. 890–925, jun. 2015.
- PONCE, P. et al. *Power System Fundamentals*. 1st. ed. [S.l.]: CRC Press, 2017. 445 p. ISBN 9781315148991.
- PRUDHVIRAJ, D.; KIRAN, P. B. S.; PINDORIYA, N. M. Stochastic energy management of microgrid with nodal pricing. *Journal of Modern Power Systems and Clean Energy*, Journal of Modern Power Systems and Clean Energy, v. 8, n. 1, p. 102–110, 2020.
- PVOUTPUT.ORG. PVOUTPUT.ORG, 2020. Available online: (<https://pvoutput.org/ladder.jsp>). Accessed on: 2020-01-17.

- RAMLI, M. A.; BOUCHEKARA, H.; ALGHAMDI, A. S. Efficient energy management in a microgrid with intermittent renewable energy and storage sources. *Sustainability*, MDPI AG, v. 11, n. 14, p. 3839, jul 2019.
- REBOURS, Y. G. et al. A survey of frequency and voltage control ancillary services—part i: Technical features. *IEEE Transactions on Power Systems*, v. 22, n. 1, p. 350–357, feb 2007.
- REPO, S. et al. The IDE4I project: Defining, designing, and demonstrating the ideal grid for all. *IEEE Power and Energy Magazine*, Institute of Electrical and Electronics Engineers (IEEE), v. 15, n. 3, p. 41–51, may 2017.
- RODRIGUES, E. et al. Energy storage systems supporting increased penetration of renewables in islanded systems. *Energy*, Elsevier BV, v. 75, p. 265–280, oct 2014.
- SAMSUNG SDI. *Smart Battery Systems for Energy Storage*. [S.l.], 2016. Available online: [http://www.samsungsdi.com/upload/ess\\_brochure/Samsung%20SDI%20brochure.EN.pdf](http://www.samsungsdi.com/upload/ess_brochure/Samsung%20SDI%20brochure.EN.pdf). Accessed on: 2020-02-24.
- SANDIA NATIONAL LABORATORIES. *DOE/EPRI 2013 Electricity Storage Handbook in Collaboration with NRECA*. [S.l.], 2013. 166 p. Available online: <https://energy.gov/sites/prod/files/2013/08/f2/ElecStorageHndbk2013.pdf>. Accessed on: 2017-04-04.
- SHAHIDEHPOUR, M. et al. Networked microgrids: Exploring the possibilities of the IIT-bronzeville grid. *IEEE Power and Energy Magazine*, Institute of Electrical and Electronics Engineers (IEEE), v. 15, n. 4, p. 63–71, jul 2017.
- SIEBERT, L. C. *Sistema de Otimização de Resposta à Demanda para Redes Elétricas Inteligentes*. 135 p. Master Thesis (Mestrado em Engenharia Elétrica) — Universidade Federal do Paraná, Curitiba, 2013. Available online: <http://acervodigital.ufpr.br/handle/1884/35731>. Accessed on: 2017-04-14.
- SILVA, V. A.; AOKI, A. R.; LAMBERT-TORRES, G. Optimal day-ahead scheduling of microgrids with battery energy storage system. *Energies*, MDPI AG, v. 13, n. 19, p. 5188, oct 2020.
- SMITH, M.; TON, D. Key connections: The U.S. department of energy’s microgrid initiative. *IEEE Power and Energy Magazine*, Institute of Electrical and Electronics Engineers (IEEE), v. 11, n. 4, p. 22–27, jul 2013.
- SOARES, A.; GOMES, A.; ANTUNES, C. H. Domestic load characterization for demand-responsive energy management systems. In: *2012 IEEE International Symposium on Sustainable Systems and Technology (ISSST)*. [S.l.]: IEEE, 2012.
- STRBAC, G. et al. Microgrids: Enhancing the resilience of the european megagrid. *IEEE Power and Energy Magazine*, v. 13, n. 3, p. 35–43, may 2015.
- TAYAB, U. B. et al. A review of droop control techniques for microgrid. *Renewable and Sustainable Energy Reviews*, Elsevier BV, v. 76, p. 717–727, sep 2017.
- TON, D. T.; SMITH, M. A. The U.S. Department of Energy's Microgrid Initiative. *The Electricity Journal*, Elsevier BV, v. 25, n. 8, p. 84–94, out. 2012.

- VAAHEDI, E. et al. The emerging transactive microgrid controller: Illustrating its concept, functionality, and business case. *IEEE Power and Energy Magazine*, v. 15, n. 4, p. 80–87, jul 2017.
- VARDAKAS, J. S.; ZORBA, N.; VERIKOUKIS, C. V. A survey on demand response programs in smart grids: Pricing methods and optimization algorithms. *IEEE Communications Surveys & Tutorials*, v. 17, n. 1, p. 152–178, 2015.
- WANG, B.; ZHANG, C.; DONG, Z. Interval optimization based coordination of demand response and battery energy storage system considering SoC management in a microgrid. *IEEE Transactions on Sustainable Energy*, Institute of Electrical and Electronics Engineers (IEEE), p. 1–1, 2020.
- WANG, X. et al. Optimal voltage regulation for distribution networks with multi-microgrids. *Applied Energy*, Elsevier BV, v. 210, p. 1027–1036, jan 2018.
- WARNER, J. *Handbook of Lithium-Ion Battery Pack Design - Chemistry, Components, Types and Terminology*. Elsevier Inc., 2015. 239 p. ISBN 0128014563. Available online: <https://www.ebook.de/product/24143299/john.t.warner.handbook.of.lithium.ion.battery.pack.design.html>.
- XU, B. et al. Modeling of lithium-ion battery degradation for cell life assessment. *IEEE Transactions on Smart Grid*, Institute of Electrical and Electronics Engineers (IEEE), v. 9, n. 2, p. 1131–1140, mar 2018.
- YAMAKAWA, E. K. *Sistema de Controle Nebuloso Para Bancos de Capacitores Automáticos Aplicados em Alimentadores de Distribuição de Energia Elétrica*. Thesis (Master Thesis) — Federal University of Parana, Curitiba, ago. 2007. Available online: <https://acervodigital.ufpr.br/bitstream/handle/1884/14076/Dissertacao%20Final%20Eduardo.pdf?sequence=1>.
- YAZDANIAN, M.; MEHRIZI-SANI, A. Distributed control techniques in microgrids. *IEEE Transactions on Smart Grid*, v. 5, n. 6, p. 2901–2909, nov 2014.
- ZHANG, B. et al. Robust optimization for energy transactions in multi-microgrids under uncertainty. *Applied Energy*, Elsevier BV, v. 217, p. 346–360, may 2018.
- ZHANG, Z.; WANG, J.; WANG, X. An improved charging/discharging strategy of lithium batteries considering depreciation cost in day-ahead microgrid scheduling. *Energy Conversion and Management*, Elsevier BV, v. 105, p. 675–684, nov 2015.
- ZHAO, B. et al. Energy management of multiple microgrids based on a system of systems architecture. *IEEE Transactions on Power Systems*, Institute of Electrical and Electronics Engineers (IEEE), v. 33, n. 6, p. 6410–6421, nov 2018.
- ZHOU, Q.; BIALEK, J. W. Simplified calculation of voltage and loss sensitivity factors in distribution networks. *16th PSCC*, Institute of Electrical and Electronics Engineers (IEEE), p. 6, jul. 2008.

# Appendix

# Appendix A – Linear Programming

This appendix addresses the concepts and definitions of linear programming related to the subject of this work. The main objective is to present the technical language of LP used throughout the main text.

## A.1 Introduction

According to Bradley, Hax and Magnanti (1977), “management science is characterized by the use of mathematical models in providing guidelines to managers for making effective decisions within the state of the current information...”. Mathematical programming is a part of the management science that deals with problems which require the optimal allocation of limited and competing resources, which are subject to a set of constraints imposed by the nature of the problem. Here, the term “programming” is a synonym for optimization (EISELT, 2007).

Tertiary control of microgrids requires the optimal dispatch of limited and distributed energy resources. Such resources are competing with each other; decisions as buying or selling energy, charging or discharging the battery, work at the maximum power point tracking or making curtailment, meeting the entire load or carrying out load shedding, must be made at any time. Also, this control is subject to physical constraints such as nominal power limits on devices, power balance, among others. So, tertiary control of microgrids can be handled as a mathematical programming problem.

Linear programming is a specific case of mathematical programming in which all the relationships involved in the problem are linear. On the other words, LP is the problem of finding a vector  $\mathbf{x}$  that minimizes (or maximizes) a linear function subject to linear constraints,

$$\begin{aligned} & \underset{\mathbf{x}}{\text{minimize}} && f(\mathbf{x}) = \mathbf{f}^T \mathbf{x} \\ & \text{subject to} && \begin{cases} \mathbf{A}\mathbf{x} \leq \mathbf{b} \\ \mathbf{A}_{eq}\mathbf{x} = \mathbf{b}_{eq} \\ \mathbf{l}_b \leq \mathbf{x} \leq \mathbf{u}_b \end{cases} \end{aligned} \quad (\text{A.1})$$

where  $f(\mathbf{x})$  is the objective function,  $\mathbf{x} \in \mathbb{R}^{s_x}$  is the vector of decision variables,  $s_x$  (size of  $\mathbf{x}$ ) is the number of decision variables,  $\mathbf{f} \in \mathbb{R}^{s_x}$  is the vector of parameters,  $\mathbf{A} \in \mathbb{R}^{s_a \times s_x}$  is the matrix of inequality constraints,  $s_a$  (number of rows of  $\mathbf{A}$ ) is the number of inequality constraints,  $\mathbf{b} \in \mathbb{R}^{s_a}$  is the vector of inequality constraints,  $\mathbf{A}_{eq} \in \mathbb{R}^{s_e \times s_x}$  is the matrix of equality constraints,  $s_e$  (number of rows of  $\mathbf{A}_{eq}$ ) is the number of equality constraints,  $\mathbf{b}_{eq} \in \mathbb{R}^{s_e}$  is the vector of equality constraints,  $\mathbf{l}_b \in \mathbb{R}^{s_x}$  is the lower bound vector, and  $\mathbf{u}_b \in \mathbb{R}^{s_x}$  is the upper bound vector.

If the LP problem requires an integer solution  $\mathbf{x}$ , then it is called Integer Linear Programming (ILP), i.e.,

$$\begin{aligned} & \underset{\mathbf{x}}{\text{minimize}} && f(\mathbf{x}) = \mathbf{f}^T \mathbf{x} \\ & \text{subject to} && \begin{cases} \mathbf{A}\mathbf{x} \leq \mathbf{b} \\ \mathbf{A}_{eq}\mathbf{x} = \mathbf{b}_{eq} \\ \mathbf{l}_b \leq \mathbf{x} \leq \mathbf{u}_b \\ \mathbf{x} \in \mathbb{Z}^{s_x} \end{cases} \end{aligned} \quad (\text{A.2})$$

On the other hand, if the LP problem requires a solution  $\mathbf{x} = [\mathbf{x}_{st}, \mathbf{x}_p]^T$  that is a mix of integers ( $\mathbf{x}_{st} \in \mathbb{Z}^{s_{st}}$ ) and real numbers ( $\mathbf{x}_p \in \mathbb{R}^{s_p}$ ), then it is called Mixed-Integer Linear Programming, i.e.,

$$\begin{aligned} & \underset{\mathbf{x}}{\text{minimize}} && f(\mathbf{x}) = \mathbf{f}^T \mathbf{x} \\ & \text{subject to} && \begin{cases} \mathbf{A}\mathbf{x} \leq \mathbf{b} \\ \mathbf{A}_{eq}\mathbf{x} = \mathbf{b}_{eq} \\ \mathbf{l}_b \leq \mathbf{x} \leq \mathbf{u}_b \\ \mathbf{x}_{st} \in \mathbb{Z}^{s_{st}} \end{cases} \end{aligned} \quad (\text{A.3})$$

where  $s_{st}$  is the size of  $\mathbf{x}_{st}$ ,  $s_p$  is the size of  $\mathbf{x}_p$ , and  $s_{st} + s_p = s_x$ .

## A.2 Mixed-Integer Linear Programming with Matlab

Matlab software has an optimization toolbox with a group of solvers to address problems of linear, non-linear, quadratic, and multi-objective programming. Among them are the `linprog()` function, to deal with LP problems as in Equation A.1, and the `intlinprog()` to solve ILP and MILP problems as in Equation A.2 and Equation A.3.

The microgrid modeling performed in this work results in an MILP problem. Therefore, the simulation results were obtained using the function `intlinprog()`, i.e.,

$$[\mathbf{x}_s, fval, exitflag, output] = \text{intlinprog}(\mathbf{f}, \text{intcon}, \mathbf{A}, \mathbf{b}, \mathbf{A}_{eq}, \mathbf{b}_{eq}, \mathbf{l}_b, \mathbf{u}_b, \text{options}) \quad (\text{A.4})$$

where

- $\mathbf{x}_s$  is a feasible solution (optimal or not) for the problem;
- $fval$  is the value of the objective function for the feasible solution,  $f(\mathbf{x}_s)$  ;
- $\{\mathbf{f}, \mathbf{A}, \mathbf{b}, \mathbf{A}_{eq}, \mathbf{b}_{eq}, \mathbf{l}_b, \mathbf{u}_b\}$  are illustrated in (A.3);
- $\text{intcon}$  is a vector with the indexes of the integer elements in the decision vector  $\mathbf{x}$ ;
- $\text{exitflag}$  is an integer that identifies the algorithm stopping condition, as illustrated in Table A.1.

- *output* is a structure with information about the optimization process, as illustrated in Table A.2.
- *option* is a structure that allows the user to set up the solving algorithm, as illustrated in Table A.3.

Table A.1 – Identifying the reasons why the algorithm stopped.

Exit Flag	Description
2	intlinprog stopped prematurely. Integer feasible point found
1	intlinprog converged to the solution $\mathbf{x}$
0	intlinprog stopped prematurely. No integer feasible point found
-1	intlinprog stopped by an output function or plot function
-2	No feasible point found
-3	Root LP problem is unbounded

Source: Adapted from MathWorks (2019).

The `intlinprog` algorithm can use at least six stages to solve the MILP problem (MATHWORKS, 2019):

- i. Initial preprocessing - according to MathWorks (2019) usually it is possible to reduce the size of the problem eliminating redundant decision variables and constraints. This can decrease the overall algorithm run time and can make the solution numerically more stable. Also, such a preprocessing step can detect an infeasible problem.
- ii. Linear programming - this stage solves an initial relaxed problem (the original problem without integers constraints) using LP solution techniques. According to MathWorks (2019), if  $\mathbf{x}_{LP}$  is a solution to the relaxed LP problem, then  $\mathbf{f}^T \mathbf{x}_{LP} \leq \mathbf{f}^T \mathbf{x}$  is valid because  $\mathbf{x}_{LP}$  minimizes the same function with fewer constraints. As a consequence,  $\mathbf{f}^T \mathbf{x}_{LP}$  is an initial lower bound for the MILP problem, and is called Root LB.
- iii. Mixed-Integer program preprocessing - this stage can determine whether the MILP problem is infeasible, remove redundancies and tighten the LP relaxation of the MILP problem;

Table A.2 – Information about the optimization process.

<i>output</i>	Description
<i>.relativegap</i>	$= (U - L)/( U  + 1) \times 100(\%)$ is the relative difference (%) between upper $U$ and lower $L$ bounds of the objective function.
<i>.absolutegap</i>	$= (U - L)$ is the absolute difference between upper and lower bounds of the objective function.
<i>.numfeaspoints</i>	is the number of integer feasible points found.
<i>.numnodes</i>	is the number of nodes in branch-and-bound algorithm.
<i>.constrviolation</i>	$= \max([0; \max( \mathbf{A}_{eq}\mathbf{x} - \mathbf{b}_{eq} ); [\mathbf{l}_b - \mathbf{x}]; [\mathbf{x} - \mathbf{u}_b]; [\mathbf{A}\mathbf{x} - \mathbf{b}]])$ is a flag to identify violation of constraints; 0 stands for no violated constraint; any positive value represents at least one violated constraint.
<i>.message</i>	is the exit message

Source: Adapted from MathWorks (2019).

- iv. Cut Generation - cuts are additional linear inequality constraints that `intlinprog` adds to the problem. These inequalities can restrict the feasible region of the LP relaxations so that their solutions are closer to integers (further tightening the LP relaxation). At this stage points are called Cuts LB.
- v. Heuristics to find feasible solutions - the algorithm uses heuristic techniques to search for feasible points (called Heuristics UB) and set them as an upper bound (UB) on the objective function;
- vi. Branch and Bound - an branch and bound algorithm is used to search systematically for the optimal solution. This algorithm solves LP relaxations with restricted ranges of possible values of the integer variables. It attempts to generate a sequence of updated bounds on the optimal objective function value. At this stage points are called Branch/bound UB and Branch/bound LB.

Figure A.1 shows a graphical output from a simulation with the `intlingprog` function. It presents the algorithm output at each stage of processing and uses Matlab’s terminology, as previously mentioned. As the interactions occurred, the difference between the upper and lower limits decreased until it was null (relative gap equal to 0), which indicates that the algorithm has converged to an optimal value (165448).

On the other hand, there are simulations in which the relative gap does not reach the value 0, but the algorithm stops if it reaches the “`options.RelativGapTolerance`”



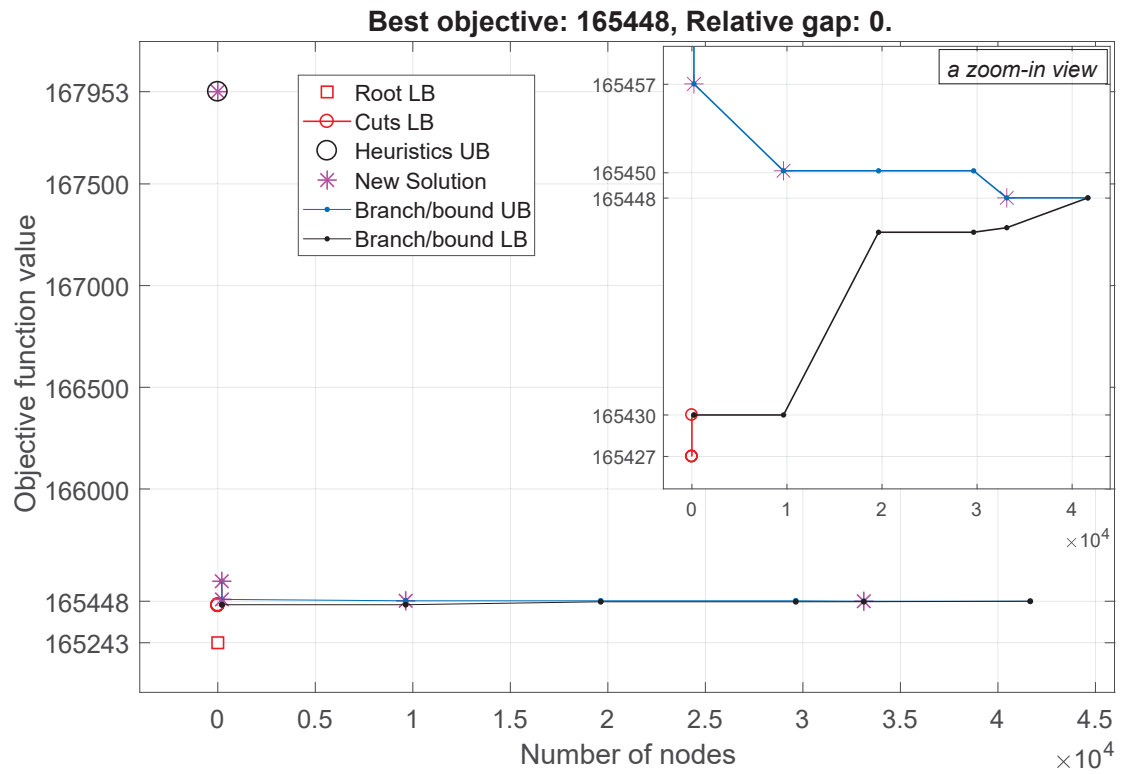
Table A.3 – A short list of options to set up the solving algorithm.

<i>options</i>	Description
<i>.AbsoluteGapTolerance</i>	<code>intlinprog</code> stops if $U - L \leq \textit{AbsoluteGapTolerance}$ ; default value is 0.
<i>.ConstraintTolerance</i>	is a tolerance to consider constraint satisfied. Values should range from 1e-9 to 1e-3; default is 1e-4.
<i>.Heuristics</i>	is an option to select the algorithm to search for feasible points: 'basic', 'intermediate', and 'advanced'. Default is 'basic'.
<i>.IntegerTolerance</i>	is a tolerance to consider an element from the solution $\mathbf{x}_s$ an integer. Values should range from 1e-6 to 1e-3; default is 1e-5.
<i>.LPOptimalityTolerance</i>	is a nonnegative real where reduced costs must exceed <code>LPOptimalityTolerance</code> for a variable to be taken into the basis.
<i>.MaxTime</i>	<code>intlinprog</code> prematurely stops if <i>MaxTime</i> seconds is reached; default value is 7200.
<i>.OutputFcn</i>	is an option to specify one or more custom function that <code>intlinprog</code> calls during the optimization.
<i>.PlotFcn</i>	is an option to specify functions that plot the progress of the optimization while the algorithm executes.
<i>.RelativeGapTolerance</i>	<code>intlinprog</code> stops if $(U - L)/( U  + 1) \leq \textit{RelativeGapTolerance}$ . Values should range from 0 to 1; default is 1e-4.
<i>.RootLPAlgorithm</i>	algorithm for solving linear programs: 'dual-simplex' algorithm or 'primal-simplex' algorithm. Default is 'dual-simplex'.

Source: Adapted from MathWorks (2019).

criterion as illustrated in Table A.3. Otherwise, it will continue to run until it reaches the “*options.MaxTime*” time. Although there was a numerical convergence that respects a previously established tolerance, it is possible to exist a mathematically better solution than the one found. But from an engineering point of view, it makes no difference as long as “*options.RelativeGapTolerance*” is acceptable.

Finally, choosing default values for the parameters listed in Table A.3 can be a good strategy. However, tolerances may require a fine-tuning according to the problem

Figure A.1 – Graphical output from a simulation with the `intlingprog` function.

Source: The author (2022).

to be solved.

# Appendix B – Literature Review

## Methodology

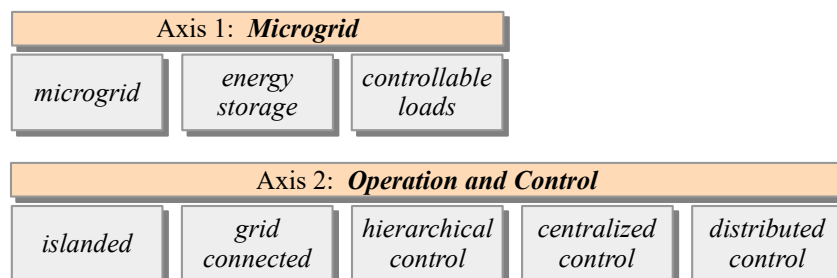
### B.1 Literature Review on MG Operation and Control

The literature review on operation and control of microgrid was carried out using the methodology developed by Ensslin et al. (2010). The main purpose of Ensslin’s method is to select from thousands of papers only a few dozens to be read. Basically, the method consists of two steps: performing an initial search for articles from keywords to form a primary list of articles and then filtering it in a successive way in order to reduce the number of papers until reaching the final result.

Figure B.1 shows two research axes and the keywords chosen for each one. A keyword can be composed of one or more words, as in “energy storage”. In order to form a single search option, a keyword from axis 1 was associated with another from axis 2. Then, considering all keywords of both axes, 15 search options were formed. The software Publish or Perish (PoP) was used to carry out the searches, considering only the last 10 years. One possible search option is “islanded mode” & “controllable loads”. According to the syntax of PoP, the quotation marks mean that the occurrence of the entire group of words must be considered, in that order, as well as the symbol & stands for the occurrence of both group of words in a single paper must be considered.

The number of matched results for each one of the 15 queries carried out by the Publish or Perish are illustrated in Table B.1. The number of results for a query is limited to the 1 000 most relevant ones by Google Scholar. A set of 14 131 results (papers, reports, and books) was obtained by merging the 15 queries, thus forming the primary

Figure B.1 – Defining the searches parameters: research axes and its keywords



Source: The author (2022).

list of articles.

Table B.1 – Number of matched results for each query.

Operation and Control	Microgrid		
	microgrid	“energy storage”	“controllable loads”
“islanded”	1000	999	1000
“grid connected”	1000	999	1000
“hierarchical control”	999	997	538
“centralized control”	1000	999	766
“distributed control”	1000	1000	834
<b>Total</b>		<b>14 131</b>	

Source: The author (2022).

As a next step, redundant titles were removed from the primary list, resulting in a new list with 7608 titles. Then, the selection process was started:

- i. select by publisher: considering only journal papers, in addition to considering only the most relevant publishers, namely: IEEE, Elsevier and Springer, a new list with 3012 papers was obtained (see Table B.2);
- ii. select by title: considering only those titles with adherence to the main subject it was obtained a new list with 604 papers (see Table B.2), called here Raw Set of Papers;
- iii. order the list: the list of title was ordered according to the number of citations;
- iv. establish the representativeness: it was considered a minimum of 14 citation by year ( $R_{min} := 14$  cites/year);
- v. make use of the flowchart illustrated in Figure B.2:
  - by making use of the flowchart, 374 titles were selected for further reading the abstract section .
  - select by abstract: 135 papers were selected after reading the abstract section, forming the Papers Database illustrated in Figure B.2.

Ensslin et al. (2010) states that a final list of papers should contain less than 40 papers. Thus, it was applied an additional filtering in order to decrease the current list

Table B.2 – The main publishers and the number of general and selected titles

Publisher	General Result		Selected Titles	
	Titles	Proportion (%)	Titles	Proportion (%)
IEEE	1 949	64.71	386	12.81
Elsevier	943	31.31	197	6.54
Springer	120	3.98	21	0.70
<b>Total</b>	<b>3 012</b>	100	<b>604</b>	20.05

Source: The author (2022).

from 135 to a number next to 40 papers. Thus, subjective classes were created in order to classify all the papers after reading both the introduction and conclusion sections:

- $[A+]$  : I must read this paper;
- $[A-]$  : I should read this paper;
- $[B+]$  : I would like to read this paper;
- $[B-]$  : I can read this paper;
- $[C]$  : I could read this paper if necessary;
- $[D]$  : I will not read this paper;
- $[E]$  : Paper not available.

Table B.3 lists the final classification. Although the first class  $[A+]$  already contains a sufficient number of papers, those ones from other classes can also be consulted if necessary. According to the Ensslin's method, all papers in the final list ( $[A+]$ ) must be fully read to verify the adherence to the work. Papers selected in this stage will form the final bibliographic portfolio of the research, which is expected to contain approximately 20 scientific articles (ENSSLIN et al., 2010).

Table B.3 – Results from the classification step.

Classes	$A+$	$A-$	$B+$	$B-$	$C$	$D$	$E$
Number of Papers	40	25	1	20	27	23	1

Source: The author (2022).

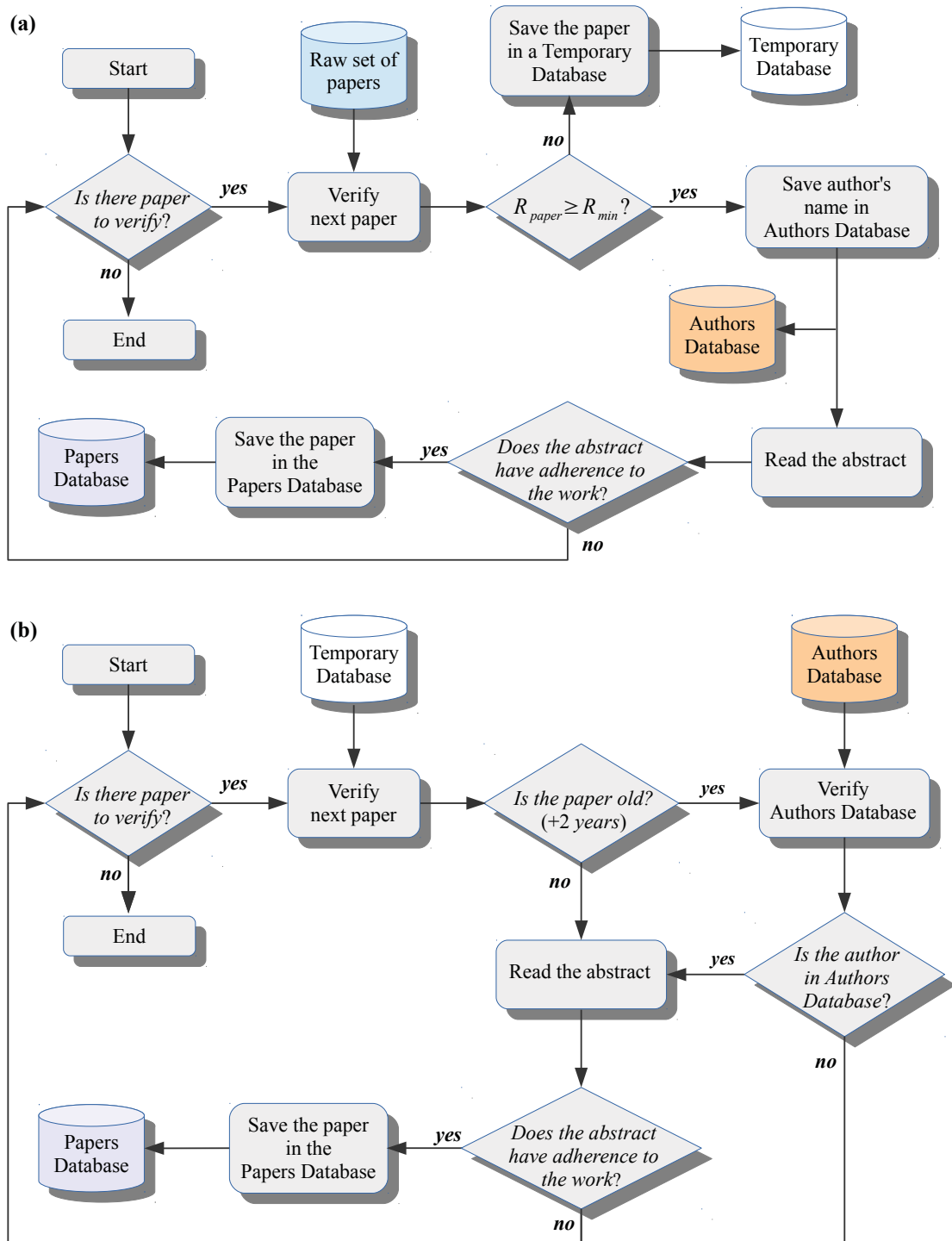
## B.2 Literature Review on Multi-Microgrids

The literature review on multi-microgrids was carried out using the methodology developed by Ensslin et al. (2010), as presented in Appendix B.1. A primary search for scientific articles considering a subject of interest and using a web search engine usually returns thousands of titles in response. The primary purpose of Ensslin’s method is to select from these thousands of papers only a few dozens to form a bank of papers. The technique consists of performing an initial search for articles from keywords to form the first list of titles and then filtering it successively to reduce the number of papers until reaching the final result.

Figure B.3 shows two axes of research and the keywords chosen for each one. A keyword can be composed of one or more words, as in “community microgrid”. In order to form a single search option (a query), keywords from axis 1 were associated with the keyword from axis 2, forming two queries options: {“multi-microgrid” & “distributed control”} and {“community microgrid” & “distributed control”}. The software Publish or Perish was used to carry out the queries, considering only the last 10 years. According to the syntax of PoP, the quotation marks mean that the occurrence of the entire group of words must be considered, in that order, as well as the symbol & stands for the occurrence of both group of words in a single paper must be considered.

A set of 1 770 results (papers, reports, and books) was obtained after merging the 2 queries and then forming a primary list. Then, it was made a selection by the most relevant publishers, namely IEEE, Elsevier, and Springer, resulting in a new list with 964 papers. As a next step, redundant titles were removed from the list, resulting in a new one with 928 titles. Then, a new list with 507 considering only journal papers was obtained. So, the process of selecting by titles was started considering only those titles with adherence to the main subject, and it was obtained a new list with 126 papers, called here Raw Set of Papers. So, it was established the minimum representativeness of 5 citation by year ( $R_{min} := 5$  cites/year), and making use of the flowchart illustrated in Figure B.2, 39 titles were selected by representativeness, 68 by year of publication (the recent ones), and 19 by authors bank. After reading the abstract section, 45 papers were selected to form the final bank of papers.

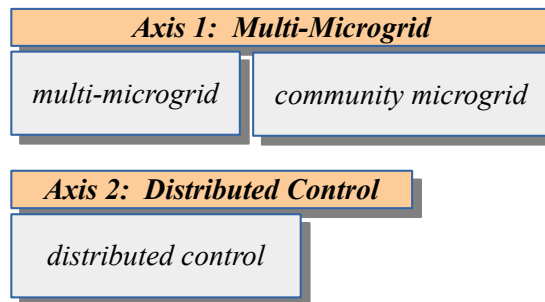
Figure B.2 – Flowchart representing the Ensslin’s raw set of papers filtering; (a) Selecting papers and authors by representativeness; (b) Selecting both recent papers and those whose authors have representativeness



Legend :  $\begin{cases} R_{min} & = \text{minimum representativeness} \\ R_{paper} & = \text{current paper representativeness} \end{cases}$

Source: Adapted from Ensslin et al. (2010).

Figure B.3 – Axes of research and its keywords



Source: The author (2022).



## Appendix C – Repository

Matlab files used to produce the simulation results of Section 6.1 are available in the following repository:

- [〈https://github.com/vander-silva/thesis2022\\_paper01〉](https://github.com/vander-silva/thesis2022_paper01)

Matlab files used to produce the simulation results of Section 6.2 will be available in the following repository:

- [〈https://github.com/vander-silva/thesis2022\\_paper02〉](https://github.com/vander-silva/thesis2022_paper02)

after the publication of these results in a scientific journal.


# **Annex**

# Annex A – BESS Technical Data

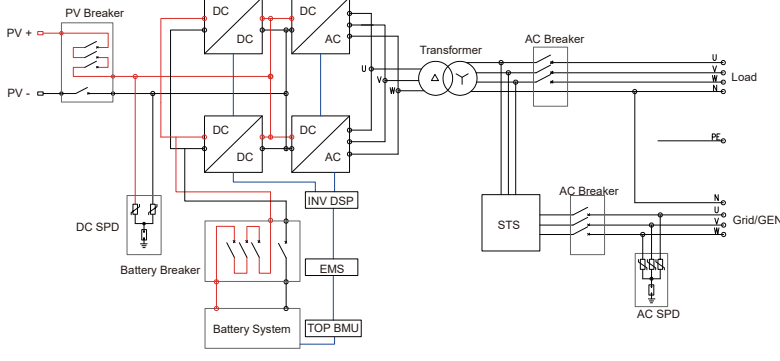
Figure A.1 – Datasheet of a BESS for commercial and industrial applications.

System Specification			
Model	Storion-T50		Storion-T100
Nominal Output Power	50 kW		100 kW
Max. PV Input Power	100 kW		200 kW
Capacity Range	28.7 kWh ~ 1032.2 kWh (90% DoD)		
Battery Chemistry	LFP (LiFePO4)		
IP Protection	IP21/IP65 (in Container)		
Warranty	3 Year Product Warranty, 10 Year Performance Warranty		
Inverter Technical Specification			
Max. PV Input Current	110 A	220 A	Phase
PV Input Voltage Range	520 ~ 900 V		Three-Phase
MPPT Number	1		Nominal AC Current
Battery Voltage Range	250 ~ 520 V		72 A
Max. Charging/Discharging Current	150 A	300 A	144A
Max. Charging/Discharging Power	50 kW	100 kW	Off-grid Voltage Range
Rated Voltage	400 V		360 ~ 440 V
Grid Voltage Range	340 ~ 460 V		Rated Frequency
Power Factor Range	1 (lagging) ~ 1 (leading)		50/60 Hz
			Backup
			UPS (With STS Module)
			Dimension (W x D x H)
			800 x 800 x 2160 mm
			Weight
			520 kg
			750 kg
			Grid Regulation
			AS 4777.2/3
			Safety
			IEC 62109-1&-2
Battery Technical Specification			
Module Model	M48112-S		Module Capacity
Module Weight	65 kg		5.7 kWh
Module Dimension (W x D x H)	450 x 580 x 165 mm		Module Nominal Voltage
Max. Charging/Discharging Current	112 A (1C)		51.2 V
			Cycle Life
			≥ 6000
			Operating Temperature Range
			-10 °C ~ 50 °C*
High Voltage Control Box Technical Specification			
BMU Model	HV900112 (TOP BMU required with more than one cluster)		
DC Voltage Range	200 ~ 900 V		
Nominal Output Current	112 A		
Battery Modules Connection	5 ~ 9 M48112-S in series in one cluster		
Clusters Connection	Max. 20 clusters in parallel		

\*When the temperature is below 0 °C or above 40 °C, the performance will be limited.



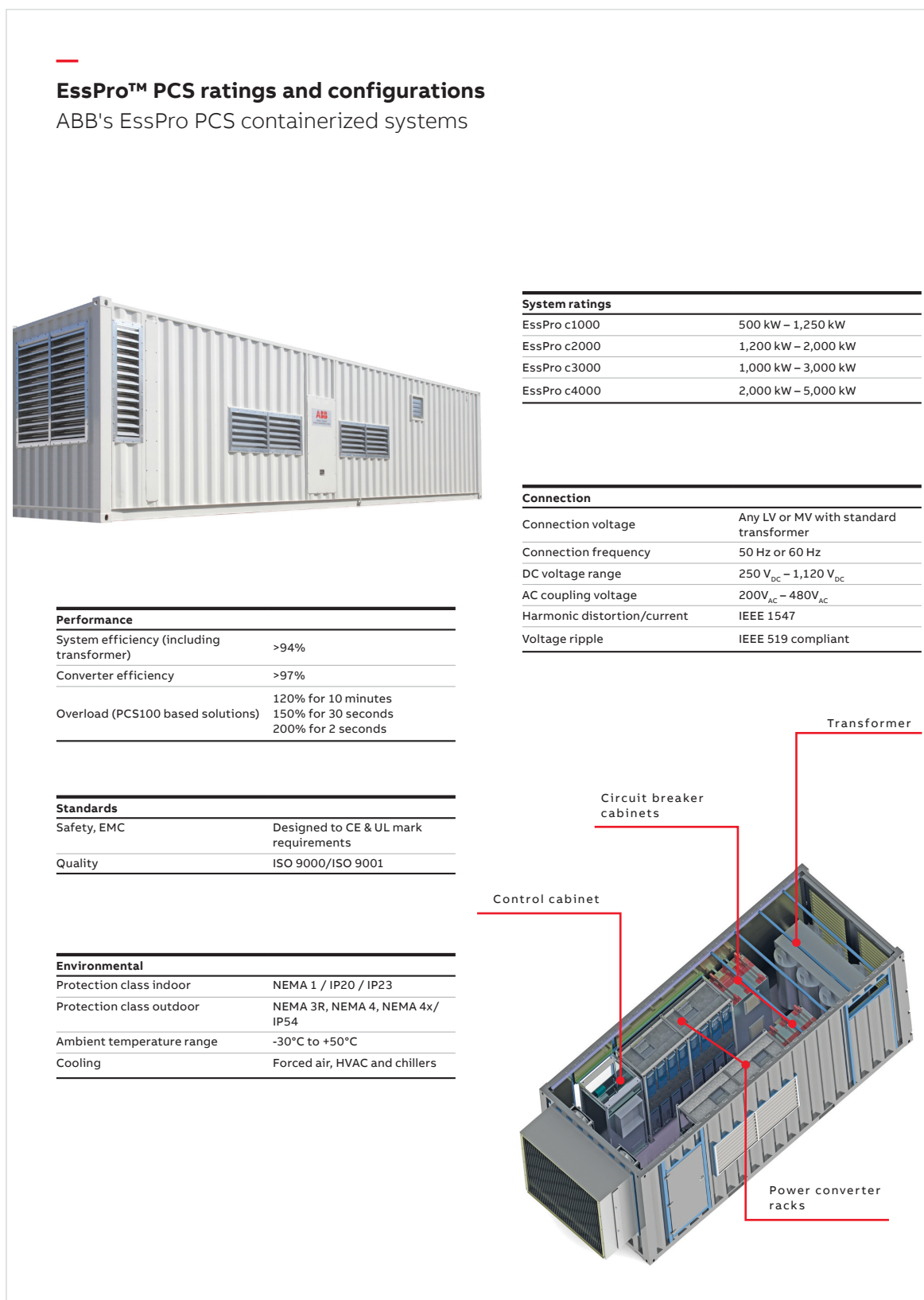
**T50/T100 System Diagram**



Alpha-ESS / Alpha ESS Co., Ltd.

Source: (ALPHAESS, 2019).

Figure A.2 – Datasheet of a power converter for grid applications with battery energy storage.



Source: (ABB, 2017).

Figure A.3 – Datasheet of ESS solution for solar farm and microgrid application.



ZLET-CIESS gives commercial and industrial power consumer an optimal solution to achieve reliable power supply at low cost, enable the islands without power and remote area where power grid is hard to establish to enjoy lights. It also improves solar energy generate integration.

**Compatibility**  
On-grid and off-grid operation. Compatible to different voltage level and frequency demand via changing transformer

**Various Application**  
Demand Response  
Micro-grid  
Power Distribution Extension  
Renewable Energy Integration  
Maximization

**High Efficiency**  
Complicated BMS and EMS, thermal management and balancing function enable the whole system's round trip efficiency reaches to 90%

**Reliability**  
Modular design  
Reduce power consumption  
Independent air tunnel for cooling system  
Easy maintenance & fast replacement

**Outdoor Installation**  
The outdoor cabinet is made of a vandalism-proof double wall aluminum structure and state-of-the-art thermal insulation material.

**5 years warranty**  
Real time after service

Customized ESS Solution for Solar Farm & Micro Grid Application

Item	CIESS100
Nominal Power	100 kW
Nominal Capacity	350 kWh
Connection voltage	380 V
Nominal Charge/Discharge Power	100kW
Max. Charge/Discharge Power	110kW (0.33C)
Rated Frequency	50/60 Hz
Total Harmonic distortion	< 3%
Power Factor	-1 ~ +1
Round-trip Battery Efficiency	> 0.95
Round-trip System Efficiency	> 0.88
Cell chemistry	LFP
DC Voltage Range	570-832 V
Specified Cycles(@ nominal C-rate)	> 5000
Supported Communication Interfaces	Inner Interface: CAN
Control and Monitoring Via external interface	External Interface: CAN, Ethernet, RS485
Touch Screen	Touch
Remote Monitoring	Optional data collection duration: 1~15 minute Real-time data monitoring & 15 years historic data record
Dimensions (L x W x H)	2,991 * 2,438 * 2,896 mm
Weight	7,000 kg
Protection class	IP54
Temperature Range	-20 ~ 55 °C
Humidity	10 %~90 %

Source: (ATLANTIC CLEAN ENERGY SUPPLY LLC, 2019).

# Annex B – Central Inverter for Solar PV Power Plants Technical Data

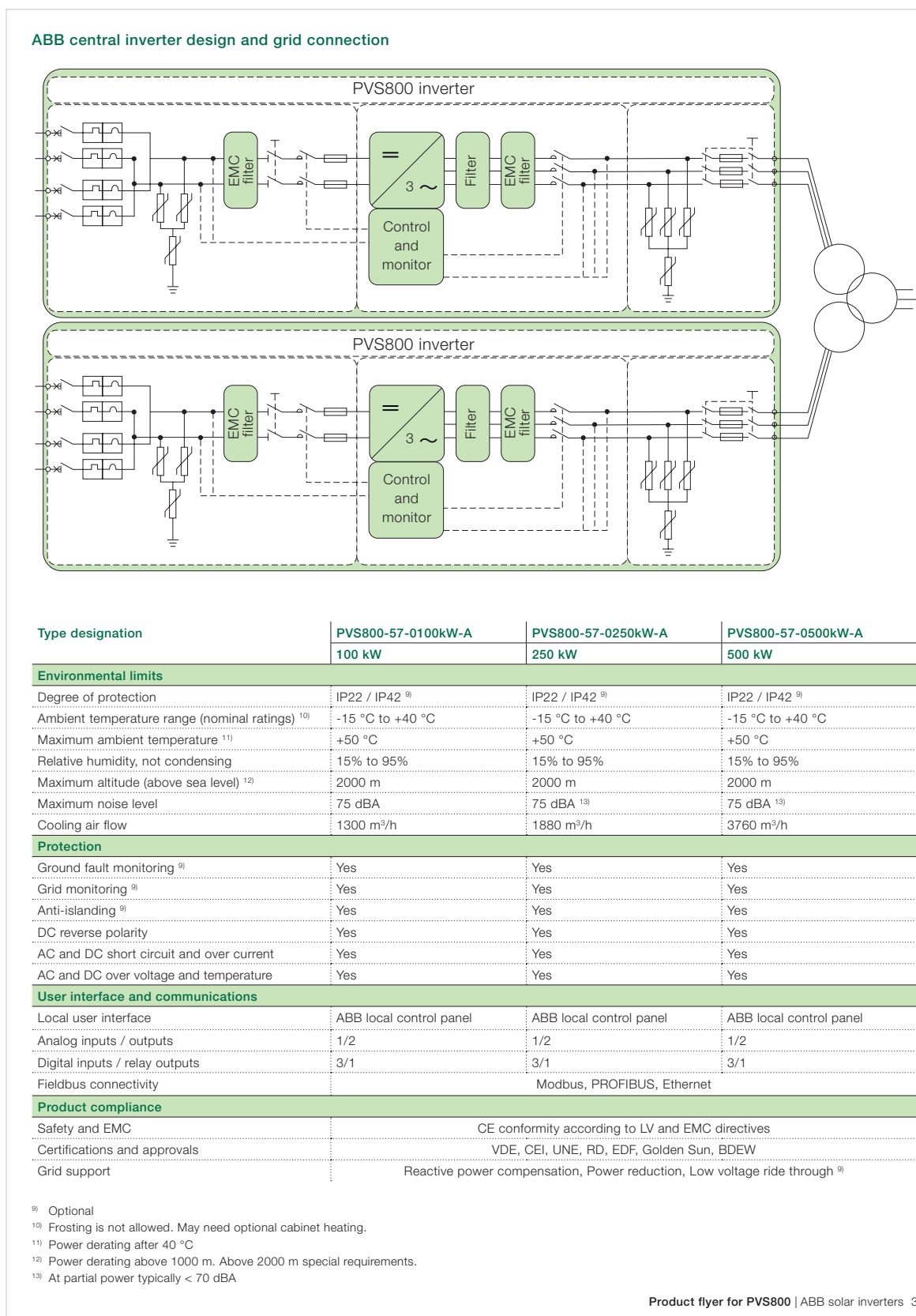
This annex contains technical data of central inverters for solar PV power plants from the manufacturer ABB (ABB, 2018). One for power plants of 100 kW, 250 kW, and 500 kW and another for large power plants (1.7 MW). Graphical symbols are in accordance with the International Electrotechnical Commission (IEC) 60617 database, named Graphical Symbols for (electrotechnical) Diagrams.

Figure B.4 – PVS800-57 central inverter for 100, 250, and 500 kW solar PV power plants; technical datasheet part 1.

Technical data and types			
Type designation	PVS800-57-0100kW-A 100 kW	PVS800-57-0250kW-A 250 kW	PVS800-57-0500kW-A 500 kW
<b>Input (DC)</b>			
Recommended max input power ( $P_{PV}$ ) <sup>1)</sup>	120 kW <sub>p</sub>	300 kW <sub>p</sub>	600 kW <sub>p</sub>
DC voltage range, mpp ( $U_{DC}$ )	450 to 750 V (- 825 V*)	450 to 750 V (- 825 V*)	450 to 750 V (- 825 V*)
Maximum DC voltage ( $U_{max(DC)}$ )	900 V (1000 V*)	900 V (1000 V*)	900 V (1000 V*)
Maximum DC current ( $I_{max(DC)}$ )	245 A	600 A	1145 A
Voltage ripple	< 3%	< 3%	< 3%
Number of protected DC inputs (parallel)	1 (+/-) / 4 <sup>2)</sup>	2 (+/-) / 8 <sup>2)</sup>	4 (+/-) / 16 <sup>2)</sup>
<b>Output (AC)</b>			
Nominal AC output power ( $P_{N(AC)}$ )	100 kW	250 kW	500 kW
Nominal AC current ( $I_{N(AC)}$ )	195 A	485 A	965 A
Nominal output voltage ( $U_{N(AC)}$ ) <sup>3)</sup>	300 V	300 V	300 V
Output frequency <sup>4)</sup>	50 / 60 Hz	50 / 60 Hz	50 / 60 Hz
Harmonic distortion, current <sup>5)</sup>	< 3%	< 3%	< 3%
Power factor compensation (cosφ)	Yes	Yes	Yes
Distribution network type <sup>6)</sup>	TN and IT	TN and IT	TN and IT
<b>Efficiency</b>			
Maximum <sup>7)</sup>	98.0%	98.0%	98,6%
Euro-eta <sup>7)</sup>	97,5%	97,6%	98,2%
<b>Power consumption</b>			
Own consumption in operation	< 350 W	< 300 W	< 600 W
Standby operation consumption	< appr. 55 W	< appr. 55 W	< appr. 55 W
External auxiliary voltage <sup>8)</sup>	230 V, 50 Hz	230 V, 50 Hz	230 V, 50 Hz
<b>Dimensions and weight</b>			
Width / Height / Depth, mm (W / H / D)	1030 / 2130 / 644	1830 / 2130 / 644	3030 / 2130 / 644
Weight appr.	550 kg	1100 kg	1800 kg
<sup>1)</sup> Inverter limits the power to a safe level	<sup>5)</sup> At nominal power	<sup>*</sup> Max 1000 V <sub>DC</sub> input voltage as an option with mppt range 450 to 825 V. If DC is > 1000 V <sub>DC</sub> inverter is not damaged, but will not start.	
<sup>2)</sup> Optional MCB inputs, 80 A each	<sup>6)</sup> 300 V output must be IT type		
<sup>3)</sup> Grid voltage (+/- 10%)	<sup>7)</sup> Without auxiliary power consumption at 450 V U <sub>DC</sub>		
<sup>4)</sup> Grid frequency (48 to 63 Hz)	<sup>8)</sup> 115 V, 60 Hz optional		
2 ABB solar inverters   Product flyer for PVS800			

Source: (ABB, 2018).

Figure B.5 – PVS800-57 central inverter for 100, 250, and 500 kW solar PV power plants; technical datasheet part 2.



Source: (ABB, 2018).

Figure B.6 – PVS800-57B central inverter for 1, 645, and 1, 732 kW solar PV power plants; technical datasheet part 1.

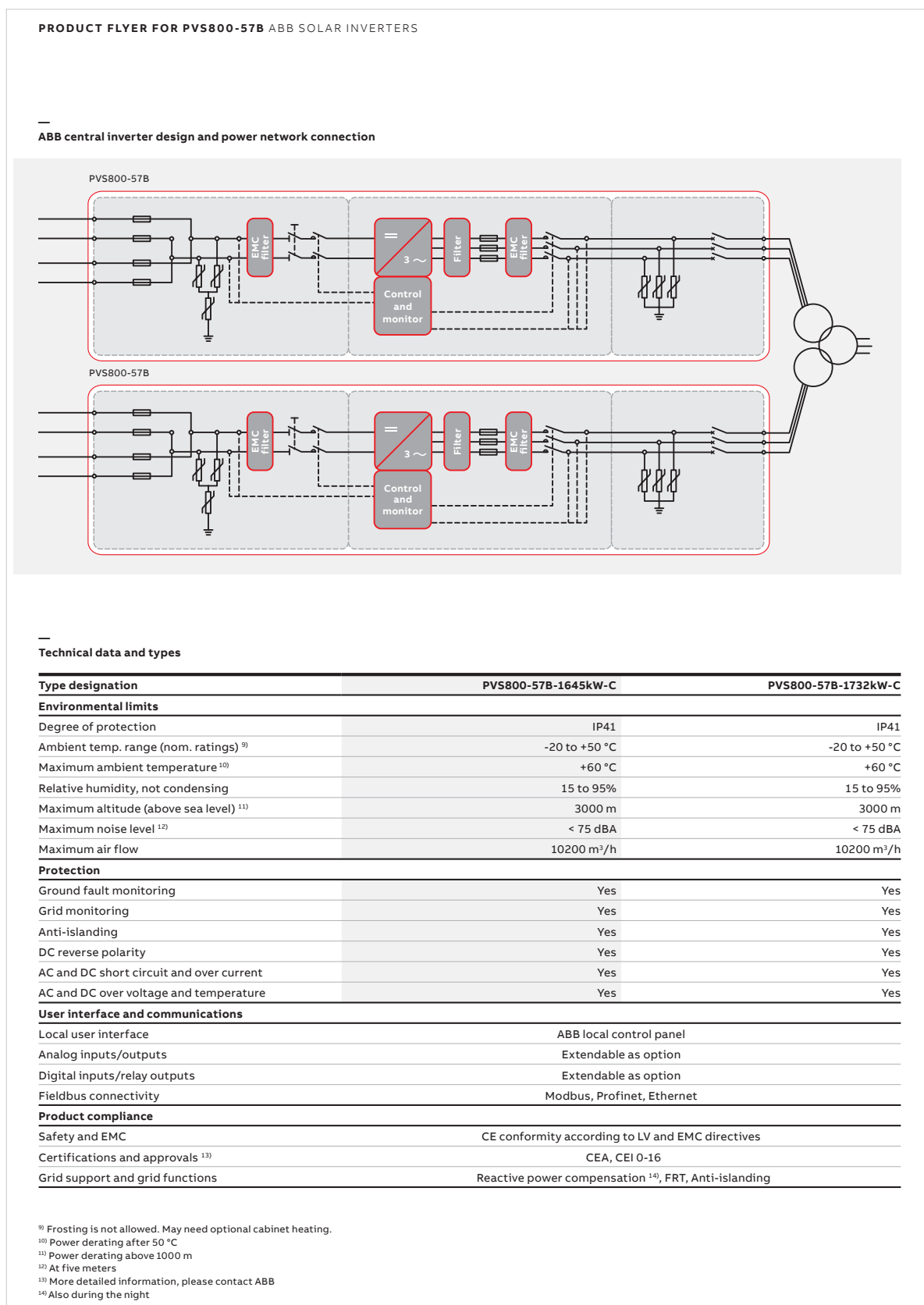
— Technical data and types		
Type designation	PVS800-57B-1645kW-C	PVS800-57B-1732kW-C
<b>Input (DC)</b>		
Maximum input power ( $P_{PV,max}$ ) <sup>1)</sup>	2468 kWp	2598 kWp
DC voltage range, mpp ( $U_{DC,mpp}$ )	550 to 850 V	580 to 850 V
Maximum DC voltage ( $U_{max(DC)}$ )	1000 V	1000 V
Maximum DC current ( $I_{max(DC)}$ )	3700 A	3700 A
Number of protected DC inputs	16 to 24	16 to 24
<b>Output (AC)</b>		
Nominal power ( $P_{N(AC)}$ ) <sup>2)</sup>	1645 kW	1732 kW
Maximum output power <sup>3)</sup>	1975 kW	2078 kW
Power at $\cos\phi = 0.95$ <sup>2)</sup>	1562 kW	1645 kW
Nominal AC current ( $I_{N(AC)}$ )	2500 A	2500 A
Nominal output voltage ( $U_{N(AC)}$ ) <sup>4)</sup>	380 V	400 V
Output frequency	50/60 Hz	50/60 Hz
Harmonic distortion, current <sup>5)</sup>	< 3%	< 3%
Distribution network type <sup>6)</sup>	TN and IT	TN and IT
<b>Efficiency</b>		
Maximum <sup>7)</sup>	98.5%	98.5%
Euro-eta <sup>7)</sup>	98.3%	98.4%
<b>Power consumption</b>		
Own consumption in operation	1800 W	1800 W
Standby operation consumption	60 W	60 W
External auxiliary voltage	400 V	400 V
<b>Dimensions and weight</b>		
Width/Height/Depth, mm (W/H/D)	4030/2150/720	4030/2150/720
Weight appr. <sup>8)</sup>	3000 kg	3000 kg

<sup>1)</sup> Recommended maximum input power  
<sup>2)</sup> At 50 °C. See the user manual for details.  
<sup>3)</sup> At 25 °C. See the user manual for details.  
<sup>4)</sup> +/-10%  
<sup>5)</sup> At nominal power  
<sup>6)</sup> Inverter side must be IT type  
<sup>7)</sup> Without auxiliary power consumption at min  $U_{DC}$   
<sup>8)</sup> For the smallest number of protected inputs. See the user manual for details.

Source: (ABB, 2018).



Figure B.7 – PVS800-57B central inverter for 1,645, and 1,732 kW solar PV power plants; technical datasheet part 2.



Source: (ABB, 2018).